2012

# Experimental investigation of cavitation instability through a circular orifice

Matthew A. Hitt

# EXPERIMENTAL INVESTIGATION OF CAVITATION INSTABILITY THROUGH A CIRCULAR ORIFICE

**by**

**MATTHEW A. HITT**

**A THESIS**

**Submitted in partial fulfillment of the requirements**
**for the degree of Master of Science in Engineering**
**in**
**The Department of Mechanical and Aerospace Engineering**
**to**
**The School of Graduate Studies**
**of**
**The University of Alabama in Huntsville**

**HUNTSVILLE, ALABAMA**

**2012**

In presenting this thesis in partial fulfillment of the requirements for a master's degree from The University of Alabama in Huntsville, I agree that the Library of this University shall make it freely available for inspection. I further agree that permission for extensive copying for scholarly purposes may be granted by my advisor or, in his/her absence, by the Chair of the Department or the Dean of the School of Graduate Studies. It is also understood that due recognition shall be given to me and to The University of Alabama in Huntsville in any scholarly use which may be made of any material in this thesis.

Matthew A. Hitt — 3/14/2012

Matthew A. Hitt (date)

## THESIS APPROVAL FORM

Submitted by Matthew A. Hitt in partial fulfillment of the requirements for the degree of Master of Science in Engineering in Aerospace Engineering and accepted on behalf of the Faculty of the School of Graduate Studies by the thesis committee.

We, the undersigned members of the Graduate Faculty of The University of Alabama in Huntsville, certify that we have advised and/or supervised the candidate of the work described in this thesis. We further certify that we have reviewed the thesis manuscript and approve it in partial fulfillment of the requirements for the degree of Master of Science in Engineering in Aerospace Engineering.

Robert A Frederick Jr 3/14/12 Committee Chair
Dr. Robert A. Frederick (date)

David M Lineberry 3/14/2012 Advisor
Dr. David M. Lineberry (date)

3/14/12 Committee Chair
Dr. Francis C. Wessling (date)

3/14/12 Department Chair
Dr. Keith Hollingsworth (date)

03/14/12 College Dean
Dr. Shankar Mahalingam (date)

Rhonda Kay Gaede 3/15/12 Graduate Dean
Dr. Rhonda Gaede (date)

**ABSTRACT**
School of Graduate Studies
The University of Alabama in Huntsville

Degree Master of Science in Engineering College/Dept. Engineering/Mechanical and Aerospace Engineering

Name of Candidate Matthew A. Hitt

Title Experimental Investigation of Cavitation Instability through a Circular Orifice

This thesis details the results of an experimental investigation into the cavitation instabilities created by a circular orifice. This experiment was conducted in concert with a computational simulation to serve as a reference point for the simulation. Testing was conducted using liquid nitrogen as a cryogenic propellant simulant. A 1.06 cm diameter thin orifice with a rounded inlet was tested in an approximately 1.25 kg/s flow with inlet pressures ranging from 504.1 kPa to 829.3 kPa. Shedding resulted in a primary frequency with a cavitation related subharmonic frequency. For this experiment, the cavitation instability ranged from 153 Hz to 275 Hz. Additionally, the strength of the cavitation occurred as a function of cavitation number. At lower cavitation numbers, the strength of the cavitation instability ranged from 2.4 % to 7 % of the inlet pressure. However, at higher cavitation numbers, the strength of the cavitation instability ranged from 0.6 % to 1 % of the inlet pressure.

Abstract Approval: Committee Chair Robert G. Frederick Jr.

Department Chair

Graduate Dean Rhonda Kay Saede 3/15/12

## ACKNOWLEDGMENTS

I have been blessed with the ability to work on this project and with all the people who have made this experiment possible. First, I would like to thank Dr. Robert Frederick for his guidance as my Committee Chair. His advice and support both for this project and for keeping me supported as a graduate student is greatly appreciated. Also, I would like to thank Dr. David Lineberry for his assistance and advice. His expertise with Labview and excellence with figures is greatly appreciated. In addition, I would like to thank Dr. Francis Wessling for his instruction. The achievements that I have made as an engineer are very much due to the teachings of Dr. Wessling.

Also, I would like to thanks several others who have assisted with this project. I would like to thank Mr. Vineet Ahuja for his explanations of cavitation and his providing the simulation results for comparison. I would like to thank Mr. Tony Hall and Mr. Ethan Wilson for their help with assembling the system and conducting tests. In addition, the help of Mr. Anthony Edmondson with ordering components is greatly appreciated. The assistance and advice of Mr. Royal Ritchie with his machining work and Mr. William Bush with his welding work are greatly appreciated. Without their help, this project would not have been possible.

In addition, I appreciate the help and encouragement of all the PRC faculty and students with whom I have had the opportunity to work. In particular, I would like to thank Mr. Henry Mulkey for his encouragement to pursue further work with cryogens and Dr. Marlow Moser for his instruction in performing experimental research. Also, I would like to thank Mr. Chad Eberhart and Mr. Brian Sweeney for their help with asking questions to help me consider various aspects of my project.

Finally, I would like to thank my family for their support and encouragement throughout my studies. The support from my father and mother has been invaluable. I could not have made it this far without them.

## TABLE OF CONTENTS

Page

## LIST OF FIGURES

Figure Page

## LIST OF TABLES

Table Page

## LIST OF SYMBOLS

| | |
|---|---|
| B | Systematic expanded uncertainty |
| $\beta$ | Venturi beta ratio |
| $C_d$ | Venturi discharge coefficient |
| D | Tube inner diameter |
| $d_v$ | Venturi throat diameter |
| f | Frequency |
| $LN_2$ | Liquid nitrogen |
| $\dot{m}$ | Mass flow rate |
| $\mu$ | Dynamic viscosity |
| P | Pressure |
| $P_v$ | Vapor pressure |
| Re | Reynolds number |
| $\rho$ | Density |
| $\sigma$ | Cavitation number |
| St | Strouhal number |
| t | Orifice thickness |
| U | Expanded uncertainty |
| V | Velocity |

*Subscripts*

| | |
|---|---|
| 1 | Orifice inlet |
| vent | Venturi |

*To my brother Jonathan who set a high standard of academic achievement*

*"The works of the LORD are great, sought out of all them that have pleasure therein."*
*- Psalm 111:2*

# CHAPTER 1

## INTRODUCTION

Orifices are used in several different fluid applications including rocket propulsion systems. In particular, they are frequently used to control the mass flow rate in a system, reduce the pressure in a system, or to dampen pressure oscillations in a system.[1-3] However, orifices are particularly vulnerable to cavitation due to the high jet velocities at the orifice throat.[2] As the flow cavitates in the orifice, pressure instabilities are generated which can have negative effects on the system. In a launch vehicle, low frequency instabilities in a feed system can lead to a pogo instability in the vehicle. Pogo instability is caused by the coupling of the feed system instability with the natural harmonics of the launch vehicle. This coupling leads to the expansion and contraction of the vehicle. Rockets that have experienced pogo instabilities include the Titan II and the Saturn V.[4]

Cavitation induced instabilities in launch vehicle feed systems can lead to thrust oscillations. Due to the lower density and high volume of cavitation bubbles, the mass flow rate downstream of the cavitation point can vary. Since thrust is a function of the propellant flow rates, the mass flow rate oscillations lead to thrust oscillations in the engine.[5]

Due to the several negative effects of cavitation, the existence of cavitation is eliminated as much as possible. To better remove cavitation in a feedline system, computational models are developed to predict the existence of cavitation and determine means of eliminating it. In order to improve the effectiveness of the computational models, experimental tests are conducted to validate the results from the models.

## 1.1 Literature Review

To gain a better understanding of the phenomena occurring during testing, a literature review of similar testing was conducted. The literature review focused on combustion instability, cavitation, and orifice flow. This division helped provide an understanding of the phenomena occurring in the experiment and how the experiment related to the greater field of rocket propulsion.

### 1.1.1 Combustion Instability

Combustion instability is when significant pressure oscillations occur in the combustion chamber of an engine. These instabilities may or may not be detrimental to the engine. In general, combustion instability can be divided into three different categories depending upon the frequency range and source of the instability. A summary of the types of instabilities, their frequency ranges, causes, and effects on the system can be found in Table 1.1.

**Table 1.1: Combustion Instability Modes[3]**

| Instability | Frequency | Cause |
|---|---|---|
| Chugging | < 400 Hz | Feedline |
| Buzzing | 400 Hz – 1000 Hz | Feedline or Combustion |
| Acoustic | > 1000 Hz | Combustion |

Low frequency instability, also known as “chug,” typically occurs at frequencies less than 400 Hz. This type of instability is typically generated by oscillations created by feed system components. While this type does not typically couple with the combustion chamber, large volume combustion chambers with low frequency responses can couple with chugging instability. While not strictly combustion instability, a chugging instability can couple with the structural resonance of the launch vehicle resulting in a “pogo” instability. Pogo is when the coupling of the launch resonance with the chugging instability causes the vehicle structure to expand and contract. Chugging instabilities typically do not result in damage to the engine. However, chugging instabilities reduce engine efficiency and create thrust oscillations.

High frequency instabilities, also known as acoustic instabilities, are typically generated by combustion phenomena. Acoustic instabilities are considered to occur above 1000 Hz. These instabilities are typically the most damaging to the engine and can result in catastrophic failures. High frequency oscillations in a combustion chamber can greatly increase the heat transfer from the combustion gasses to the chamber. This can be a significant hazard around the throat and can result in the physical separation of the nozzle especially at the throat.

Intermediate frequency instabilities, also known as “buzz,” are considered to occur in the range of 400 to 1000 Hz. Buzzing instability can be generated by either feedline or combustion chamber instabilities. As such, buzzing instabilities are often better considered as higher frequency chugging instabilities or lower frequency acoustic instabilities rather than their own class of instability. As with chugging instabilities,

buzzing instabilities tend to be less damaging to the launch vehicle than acoustic instabilities.[3, 6]

### 1.1.2 Cavitation

The formation and collapse of bubbles in a flowing liquid is called cavitation.[7] Cavitation occurs when the velocity of a liquid causes the local static pressure to drop below the local vapor pressure. However, some studies have indicated that viscous shear stresses can influence the formation of cavitation.[8] In rocket engines, the necessary velocities for cavitation can be easily produced by an orifice[2] or by a rotating blade.[9] When the velocity reaches levels capable of producing cavitation, a vapor cavity starts to grow on a solid surface in contact with the liquid.[8] As the vapor cavity grows, the cavity starts to elongate into the system, and disturbances in the system cause the cavity to split forming a vapor bubble.[10] The bubble travels downstream until it reaches a point in the flow where the local static pressure returns above the vapor pressure. When the bubble reaches a high pressure point, the bubble collapses. While cryogens follow the same pattern in cavitation development as other liquids, cryogenic liquids form smaller bubbles than other liquids due to thermodynamic effects from vaporization.[5] As the cryogen vaporizes, a thermal depression is created in the flow which reduces the size of the bubble because more energy is required to form a bubble in a colder area.[5] An illustration of the pressure formation requirements of cavitation is shown in Figure 1.1.

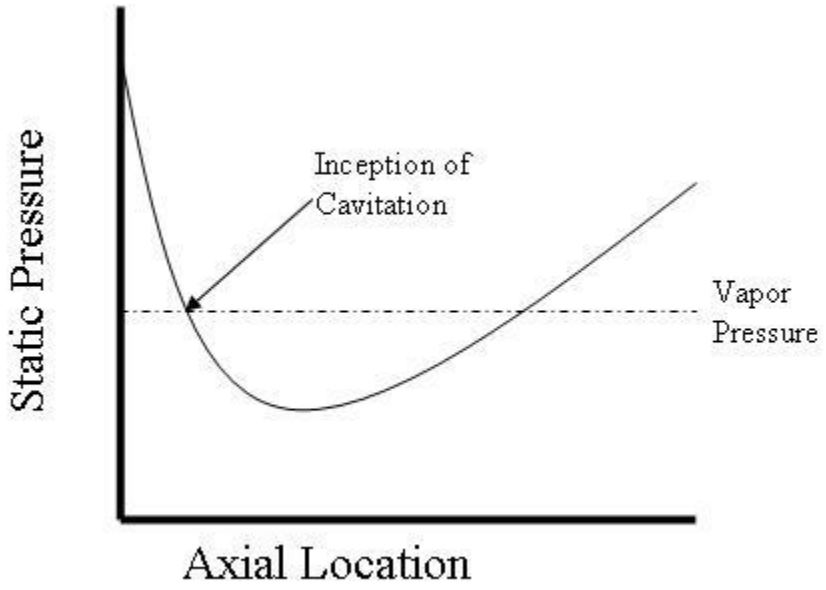


**Figure 1.1: Cavitation in an Orifice[7]**

To characterize the type and severity of the cavitation in a system, the nondimensional cavitation number is used. Several different versions of the cavitation number exist. Due to the type of component tested and the location of the sensors, the cavitation number used in this experiment is given by the equation

$$\sigma = \frac{P_1 - P_v}{\frac{1}{2} \cdot \rho \cdot V_1^2}, \tag{1.1}$$

where σ is the cavitation number, where $P_1$ is the upstream pressure, $P_v$ is the vapor pressure based on the temperature at the $P_1$ measurement location, ρ is the density based on the temperature at the $P_1$ measurement location, and $V_1$ is the velocity at the orifice throat. The cavitation number indicates the relative strength of cavitation at the test point. As the cavitation number decreases, the relative strength of the cavitation increases.[7, 11-12]

Cavitation in a system generally occurs in two main types. These two types are "incipient" and "choked." Incipient cavitation is when cavitation first begins to occur in the system. During incipient cavitation, the flow rate of the fluid still increases with increasing pressure drop. As cavitation continues to develop, it eventually reaches the point termed choked cavitation. Once choked cavitation occurs, the flow rate of the fluid through the component is fixed and no longer increases with increasing pressure drop.[7] Typically, incipient cavitation occurs at a cavitation number on the order of 1.[11] However, in some cases, cavitation has been observed to occur at a higher cavitation number than 1.[12]

Cavitation in a system can have several negative effects in the system. These effects range from minor difficulties such as increased noise level to damage of system components. When the cavitation bubbles reach a region of higher pressure, they collapse violently. This violent collapse can create significant localized pressure spikes. These bubble implosions and pressure spikes can cause erosion and damage of components in the system as the cavitation collapse leads to material from a component's being stripped away. This erosion is particularly serious if the bubbles collapse next to the surface of a component. Erosion of a system component can lead to structural fatigue and failure or can remove protective coatings from the component resulting in potential corrosion damage.[7, 13] In addition to system damage, cavitation can cause an efficiency loss in a system. As the system cavitates, the local fluid density fluctuates due to the lower density of vapor and the high volume of the bubbles produced. These fluctuations in the fluid density cause the mass flow rate in the system to fluctuate. This in turn results in a fluctuation of the thrust of the launch vehicle. In addition to thrust

fluctuations, as previously stated, cavitation can also produce a pogo instability in the rocket.

Cavitation has had negative effects on actual launch vehicles. Specifically, cavitation instabilities in the Delta 4 oxidizer feed line are considered to have been contributory to erroneous pressure readings leading to an early shutdown of the RS-68 engine.[14] Also, large pressure fluctuations have contributed to structural cracks in the liquid hydrogen lines in the space shuttle.[14]

### 1.1.3 Orifice Flow

As stated in previous sections, the use of an orifice in a cryogenic flow can lead to cavitation in the flow resulting in feedline instabilities. In addition to cavitation instabilities, the use of an orifice in a flow can also result in additional fluid dynamic instabilities. These instabilities can result from such phenomena as turbulence or vortex shedding.[14]

One significant example of fluid dynamic instability is orifice whistling. Orifice whistling occurs when the acoustic power scattered from an orifice is greater than the power incident to the orifice. To estimate at what frequency the orifice whistling will occur, the Strouhal number is used. The Strouhal number is given by

$$St = \frac{f \cdot t}{V_1}, \tag{1.2}$$

where $St$ is the Strouhal number, $f$ is the orifice shedding frequency, $t$ is the orifice thickness, and $V_1$ is the orifice throat velocity. The Strouhal number is a function of Reynolds number and generally lies in the range of 0.2 to 0.3.[15-17] If whistling occurs in an orifice, acoustic feedback can occur and cause instabilities to exist upstream of the orifice.[11]

## 1.2 Computational Model

This experiment was performed in conjunction with Combustion Research and Flow Technology, Inc. (CRAFT Tech). CRAFT Tech created a computation modeling of the flow of liquid nitrogen ($LN_2$) through a single-hole orifice. The modeling was conducted using a three-dimensional with half-plane symmetry approximation RANS-LES model.[20] The purpose of the model of the single-hole orifice was to provide baseline results to better determine the effect of cavitation in a system and possible ways to eliminate the cavitation instabilities.

In order to match conditions able to be produced in the experimental system, the simulation was based on an orifice inlet pressure of 551.6 kPa (80 psia), an orifice inlet temperature of 88.75 K, and a mass flow rate of 1.36 kg/s (3 lbm/s). These conditions are summarized in Table 1.2. An image of the simulation showing the formation of cavitation bubbles in the flow is shown in Figure 1.2.

**Table 1.2: Simulation Conditions[20]**

| | |
|---|---|
| Orifice Inlet Pressure | 551.6 kPa |
| Orifice Inlet Temperature | 88.75 K |
| Mass Flow Rate | 1.36 kg/s |

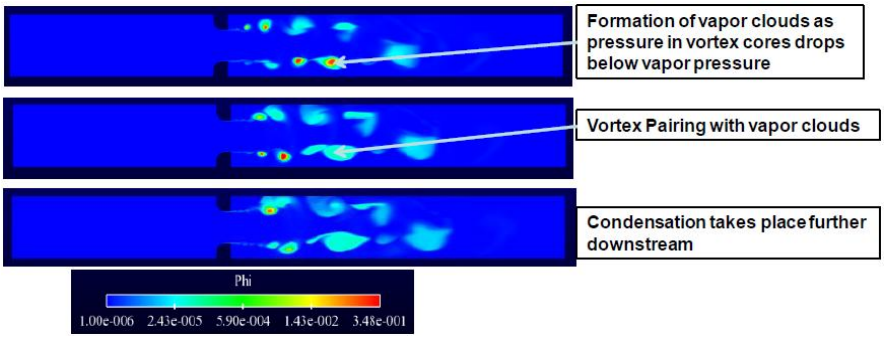


**Figure 1.2: Image of Model Showing Vapor Formation[20]**

An image illustrating the pressure fluctuations in the flow created by the orifice is shown in Figure 1.3. As can be seen in the image, the vortex core localized with the cavitation bubbles provides a localized pressure depression. As the bubbles collapse, the fluid surrounding the collapse region increases in pressure as shown in the condensation shock. The pressure spike is then convected downstream resulting in a pressure wave propagating downstream.

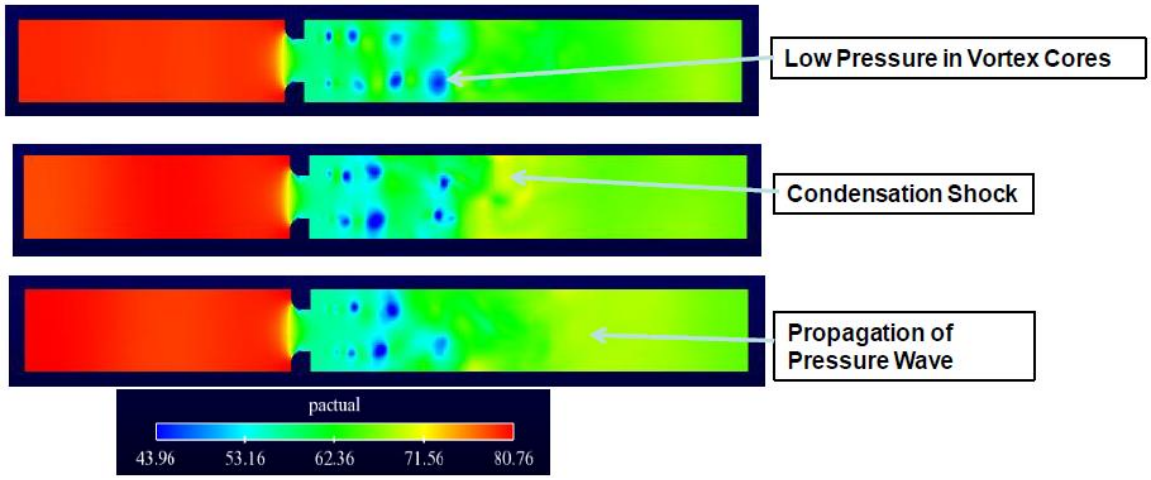


**Figure 1.3: CFD Model Demonstrating Pressure Fluctuations in Flow[20]**

As can be seen in Figure 1.4 in the graph in the upper left corner, several dominant frequencies emerged in the computational simulation. These include 386 Hz, 650 Hz, and 750 Hz instabilities. Also, not marked in the figure, is an additional peak occurring in the 1200 Hz to 1400 Hz range.

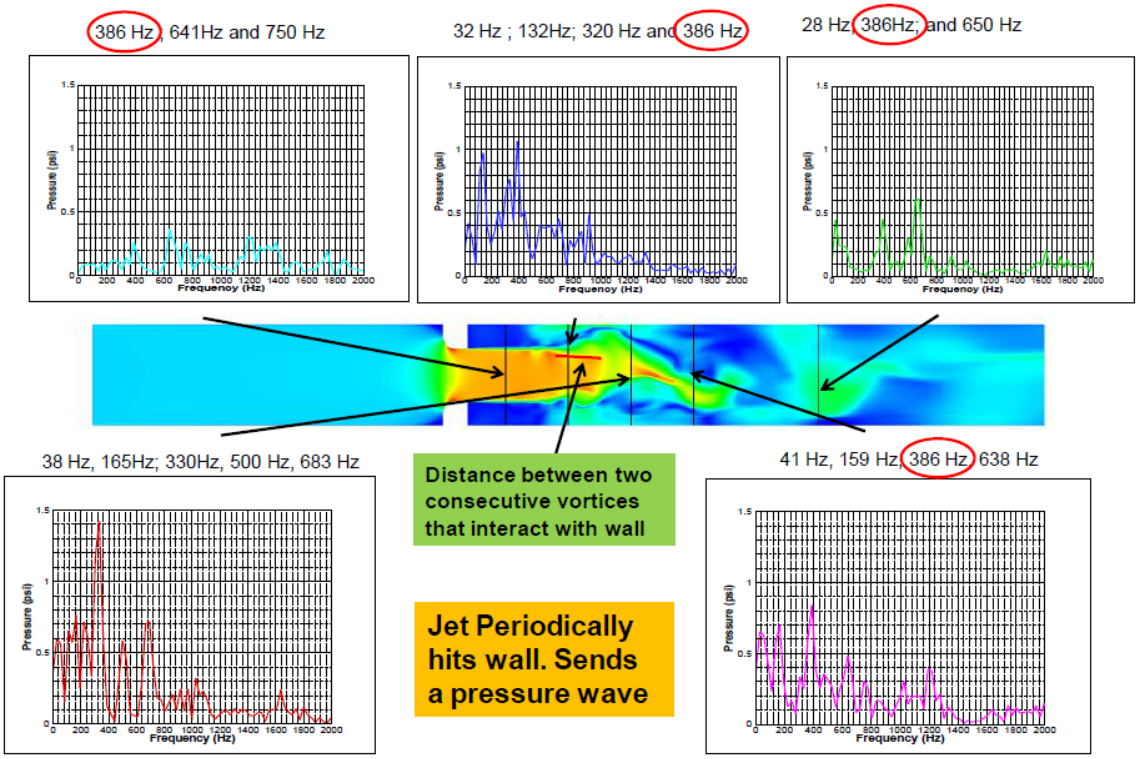


**Figure 1.4: FFT's from the Computational Model[20]**

## 1.3 Objective

The objective of this experiment is to quantify the instabilities induced by the use of a cryogen through a rounded-inlet, circular orifice. The particular test conditions were selected to provide an experimental comparison for a CFD model. To provide the comparison, multiple tests were conducted at the same mass flow rate and Reynolds number but with a variable orifice inlet pressure.

# CHAPTER 2

# EXPERIMENTAL APPROACH

To evaluate the cavitation instabilities created by an orifice, a test system was developed for using $LN_2$. To characterize the flow conditions, the system was equipped with thermocouples and static pressure transducers. A high frequency pressure sensor was used to measure the frequency and amplitude of the instabilities downstream of the orifice. To determine the effect of the cavitation related instabilities, a test matrix was planned to test at conditions with a stronger cavitation response and at conditions with a weaker cavitation response.

## 2.1 PRC Cryogenic Test Facility

Testing for the project was conducted at the University of Alabama in Huntsville (UAH) Propulsion Research Center (PRC) using the PRC Cryogenic Test Facility.[18] The PRC cryogenic test facility was originally designed to deliver single phase liquid oxygen to a rocket hot-fire test stand at flow rates of up to 1.36 kg/s (3 lbm/s). The facility is capable of handling inert or oxidizing cryogenic liquids in the temperature range of atmospheric $LN_2$ or warmer. The main propellant lines of the cryogenic facility are plumbed with 1.27 cm (0.5 in.) outer diameter stainless steel seamless tubing. The propellant lines are jacketed with 2.54 cm (1 in.) Teflon tubing for $LN_2$ cooling flow. In

rocket testing the cooling jackets help to maintain single phase liquid oxygen from the run tank to the test article.

The facility was modified from the hot-fire rocket testing configuration in order to better accommodate the $LN_2$ flow testing conducted in this experiment. The schematic for the experimental setup is shown in Figure 2.1. The revised flow path consisted of 2.54 cm (1 in.) OD tubing without teflon nitrogen jacket. The existing 1.27 cm (0.5 in.) valves and fittings were replaced with 2.54 cm (1 in.) components or eliminated where possible. The overall flow path length from the run tank to the test article was shortened and simplified as much as possible to minimize heat losses and pressure losses through the system. These changes allowed for testing at an increased flow rate while maintaining a lower operating pressure in order to allow for cavitation in the test orifice without having cavitation occur in the system. For this experiment, the facility is divided into subsystems of the run tank, flow path, test orifice, and instrumentation. Each subsystem is described below.

### 2.1.1 Run Tank

The PRC Cryogenic Test Facility is designed for the use of LOX. As such, all components connected to the oxygen system are oxygen cleaned even when used with $LN_2$. The facility uses an 87 L (23 gal.) run tank with a $LN_2$ jacket used for chilling the working fluid. The tank is pressurized using gaseous nitrogen ($GN_2$) provided by k-bottles that are attached to a manifold. The pressure of the $GN_2$ pressurant is regulated by a dome loaded pressure regulator controlled by a remotely actuated pressure shutoff valve.

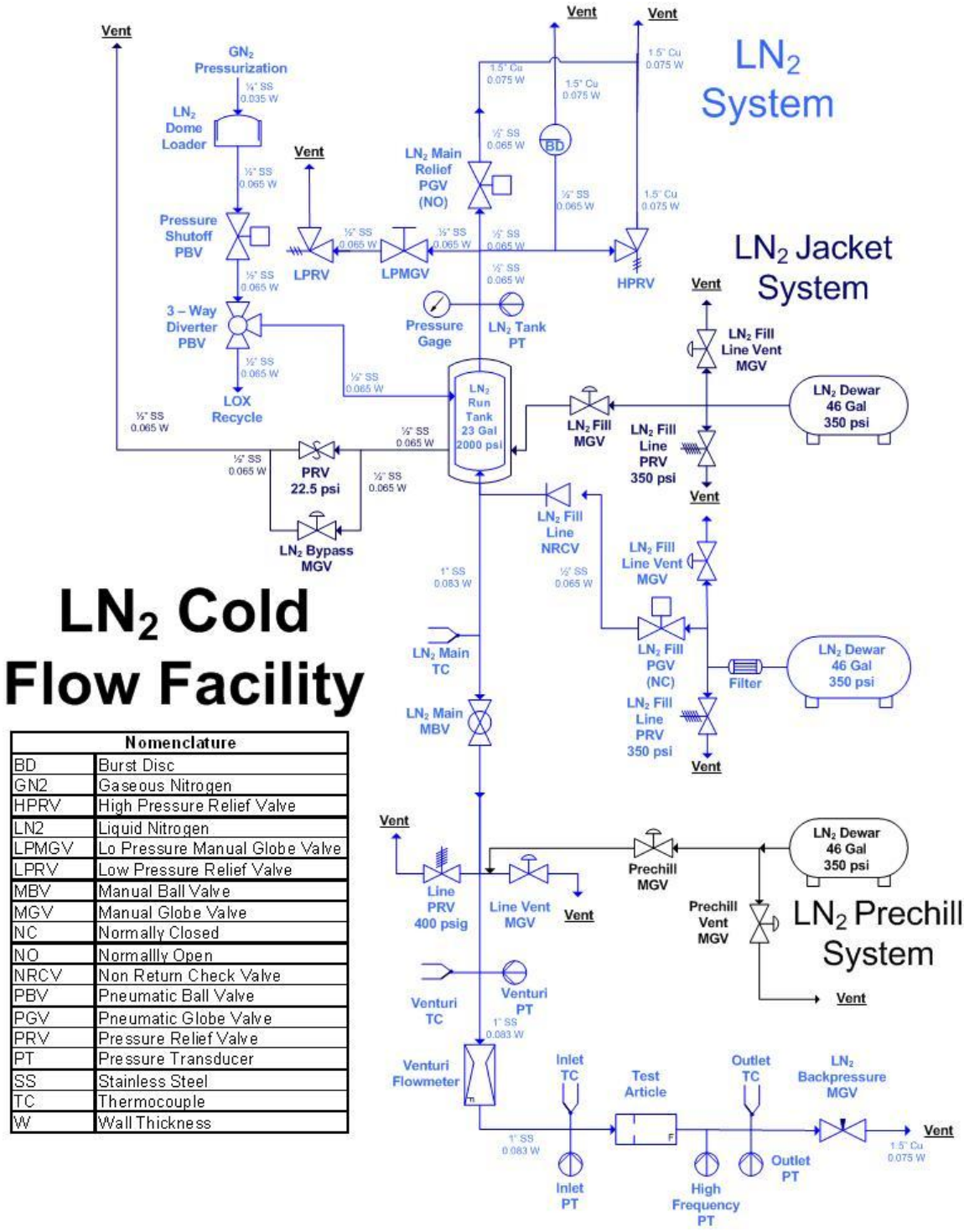


| Nomenclature | |
|---|---|
| BD | Burst Disc |
| GN2 | Gaseous Nitrogen |
| HPRV | High Pressure Relief Valve |
| LN2 | Liquid Nitrogen |
| LPMGV | Lo Pressure Manual Globe Valve |
| LPRV | Low Pressure Relief Valve |
| MBV | Manual Ball Valve |
| MGV | Manual Globe Valve |
| NC | Normally Closed |
| NO | Normallly Open |
| NRCV | Non Return Check Valve |
| PBV | Pneumatic Ball Valve |
| PGV | Pneumatic Globe Valve |
| PRV | Pressure Relief Valve |
| PT | Pressure Transducer |
| SS | Stainless Steel |
| TC | Thermocouple |
| W | Wall Thickness |

**Figure 2.1: Flowpath Schematic**

The facility is vented using a remotely actuated pneumatic globe valve (PGV). As a safety precaution, the system has both a high pressure relief valve (HPRV) and a burst disc (BD), both of which are designed for 16.5 MPa (2400 psi), to prevent overpressurization of the run tank. Additionally, the system contains a low pressure relief valve (LPV) designed for 1034 kPa (150 psi) that is isolated from the tank by a manual globe valve. The LPV maintains a low pressure in the tank when a cryogen is present in the tank before and after system pressurization for testing.

The inner core of the LOX tank is filled from a dewar that is connected to the inner core of the LOX tank. All cryogens used in the LOX tank pass through a filter at the system inlet to prevent any particulate matter from entering the system. The filling of the inner core is controlled by a remotely actuated PGV.

Similar to the inner core, the outer jacketing of the LOX tank is filled from a dewar which is connected to the outer jacket. The filling of the tank is controlled by a manual fill valve. The temperature in the outer jacket is controlled by regulating the boil-off pressure of the fluid in the outer jacket. The outer jacket is connected to a 151.7 kPa (22 psig) relief valve and a manual bypass valve. This enables the pressure of the $LN_2$ to be set to a gage pressure ranging from 0 kPa to 151.7 kPa (0 psig to 22 psig). The resulting temperature of the $LN_2$ is the saturation temperature for the set pressure.

### 2.1.2 Orifice Test Flow Path

The flow path for the orifice testing consisted of 2.54 cm (1 in.) outer diameter 316 stainless steel tubing with 0.21 cm (0.083 in.) wall thickness resulting in a 2.12 cm (0.834 in.) inner diameter flow path. The tubing and components in the system were insulated using Cryogel®Z insulation to minimize the heat transfer from the surroundings

into the $LN_2$. The flow through the system was initiated by opening a manually actuated, quarter turn, cryogenic ball valve. The mass flow rate was controlled by a fixed diameter, cavitating venturi. The governing equation used for calculating the flow rate was

$$\dot{m} = C_d \cdot (\frac{\pi}{4} \cdot d_v^2) \cdot \sqrt{\frac{2 \cdot (p_{vent} - p_v) \cdot \rho_{vent}}{1 - \beta^4}}, \quad (2.1)$$

where $\dot{m}$ is the mass flow rate, $C_d$ is the discharge coefficient, $d_v$ is the throat diameter of the venturi, $p_1$ is the venturi inlet pressure, $p_{vent}$ is the venturi inlet vapor pressure, $\rho_{vent}$ is the density of the $LN_2$ at the venturi inlet, and $\beta$ is the ratio of the venturi throat diameter to the tubing inner diameter. The discharge coefficient was not specified by the manufacturer but was calculated using the manufacturer specified mass flow rate and fluid properties.

The initial test loop design utilized a tee-type filter with a 250 micron sintered bronze filter element after the venturi. The purpose of the filter was to remove cavitation induced instabilities created by the cavitating venturi. Due to the large thermal mass of the filter and difficulties reaching the required orifice inlet conditions, the filter was removed from the system for testing.

The inlet pressure of the test orifice was controlled using a backpressure valve downstream of the test orifice. The throttling valve used was a cryogenic globe valve with a maximum $C_v$ of 11.6. The test orifice inlet pressure was set by adjusting the position of the backpressure valve, increasing the pressure drop across the backpressure valve thus raising the orifice inlet pressure

After the backpressure valve, the flowpath expanded to 1-1/2 in. copper pipe and was plumbed into the test stand oxygen vent and vented to atmosphere. A photo of the

PRC cryogenic test facility used in the experiment is shown in Figure 2.2. Details regarding system hardware are shown in Appendix A.

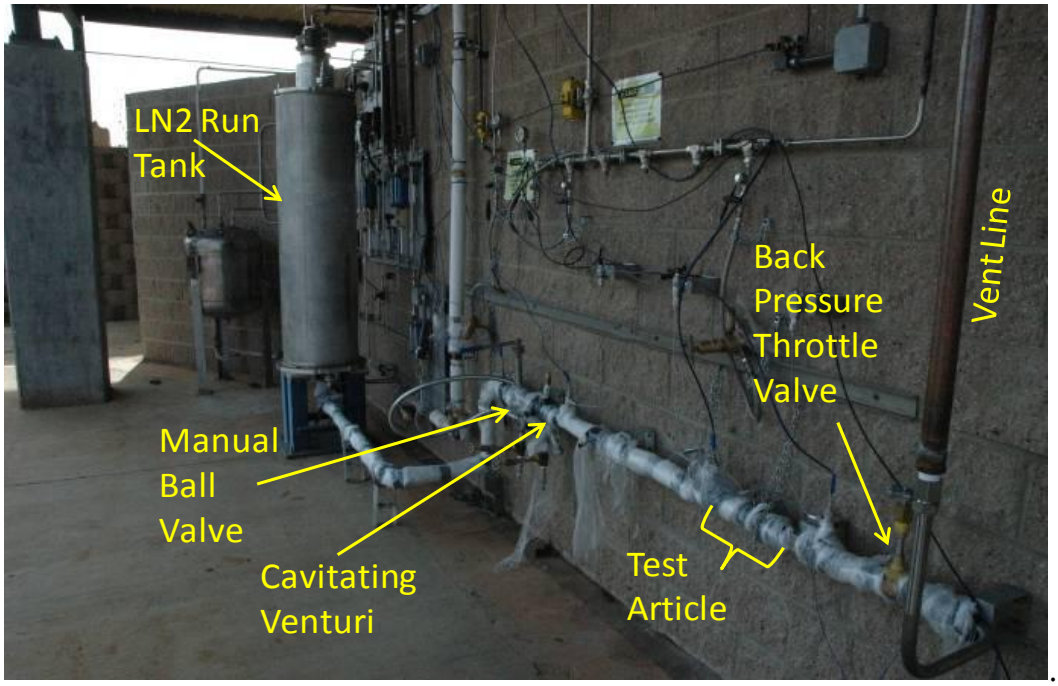


**Figure 2.2: Cryogenic Test Facility**

### 2.1.3 Test Orifice

The test orifice used in this experiment was a single element, circular orifice. The orifice had a throat diameter of 1.06 cm (0.417 in.) and a beta ratio of 0.5. The test orifice had a smooth inlet with a 0.26 cm (0.104 in.) radius and was 0.53 cm (0.209 in.) thick. This thickness yields a thickness to diameter ratio of 0.5 which falls within the range for a thin orifice.[11] The test orifice component was fabricated from 316 stainless steel. In addition to the orifice, the component included a high frequency measurement port 1.32 cm (0.521 in. or 0.625 tubing diameters) downstream of the orifice. Tube

fittings were welded using smooth welds to the component to connect the component to the flow path. A picture of the test orifice component is shown in Figure 2.3.

**Figure 2.3: Test Orifice Component**

### 2.1.4 Instrumentation and Uncertainty

The primary instrumentation locations can be seen in the facility flow schematic shown in Figure 2.1. Manufacturer information about instrumentation and curvefits for the static pressure transducers are in Appendix A. Temperature measurements were taken upstream of the main ball valve, upstream of the cavitating venturi, upstream of the orifice and downstream of the orifice. Each location had an Omega TMQSS-125U-6 T-type thermocouple. The thermocouples had a minimum temperature measurement range of -200 °C. Ungrounded thermocouple junctions were selected to prevent the occurrence of a ground loop. The thermocouples were not calibrated on site for the temperature

range expected in testing, thus the uncertainty for the thermocouples was taken as the larger of 1.0 °C or 1.5% of measurement, as per the manufacturer specifications.

In addition to system static pressure measurements necessary for establishing flow from the run tank, static pressure measurements were taken upstream of the venturi and upstream and downstream of the orifice. These static pressure measurements were made using Omega pressure transducers. Each of the static pressure transducers used a 0.32 cm (0.125 in.) OD tubing standoff which positioned the transducer approximately 76.2 cm (30 in.) away from the main tubing to protect the transducers from the cryogenic temperatures. The venturi inlet pressure was measured using an Omega PX309 transducer with a range of 0 to 3448 kPa (0 to 500 psig) and an output of 0 to 5 V DC. The orifice inlet and outlet pressures were measured using Omega PX209 transducers each with a range of 0 to 2069 kPa (0 to 300 psig) and an output of 0 to 5 V DC. Each static pressure transducer was connected to the DAQ and calibrated over the range 0 to 1965 kPa (0 to 285 psig) using a deadweight pressure tester. The transducers were assumed to have a linear pressure-voltage relationship and a $2^{nd}$ order regression analysis was performed to determine calibration uncertainty for each transducer. The calibration uncertainties for each static pressure transducer are shown in Table . The uncertainty curvefits for the transducers are a second order equation and are of the form $U = a \cdot V^2 + b \cdot V + c$ where U is the uncertainty of the pressure transducer in psi, V is the output voltage of the transducer in volts, and a, b, and c are the constants given in Table 2.1. Results from the uncertainty curvefit are in units of psi.

**Table 2.1: Static Pressure Transducer Uncertainties**

| Transducer | a | b | c | Uncertainty at (125 psi) |
|---|---|---|---|---|
| Omega 96607 | 0.109 | -0.532 | 2.705 | 14.27 kPa (2.07 psi) |
| Omega 96611 | 0.11 | -0.54 | 2.734 | 14.41 kPa (2.09 psi) |
| Omega 103110D854 | 0.045 | -0.116 | 1.14 | 7.38 kPa (1.07 psi) |

A single high frequency dynamic pressure measurement was taken downstream of the orifice to measure pressure fluctuations resulting from flow instabilities. The measurement was made using a PCB 112A05 pressure sensor with a PCB 422E51 in-line charge converter. The pressure sensor had a minimum operating temperature of -240 °C and a sensitivity of 1.1 pC/psi. The inline charge converter had a 100 mV/pC conversion factor and a ±5 V output. The pressure sensor and charge converter combination had a ±296.5 kPa (±43 psi) output.

The locations of the orifice associated measurements are shown in Figure 2.4. The orifice inlet static pressure and temperature were measured at the same location approximately 17.8 cm (7 in. or 8.4 tube diameters) upstream of the test orifice. The orifice outlet pressure and temperature were measured at the same location approximately 26.4 cm (10.4 in. or 12.5 tube diameters) downstream of the orifice. The thermocouples were immersed into the flow, and, as stated previously, the transducers were connected via a standoff. The high frequency pressure sensor was flush mounted tangentially to the inner surface of the tubing 1.32 cm (0.52 in. or 0.64 tube diameters) downstream of the orifice.

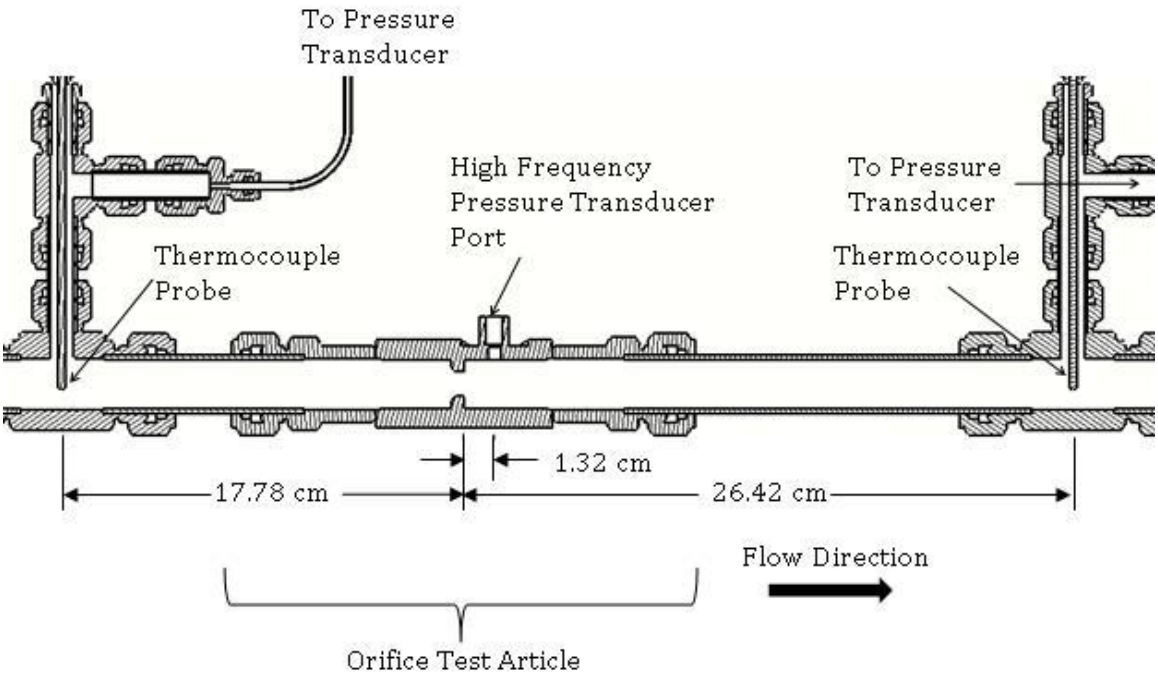


**Figure 2.4: Orifice Instrumentation Layout**

The venturi had a manufacturer specified uncertainty of 5% at the design conditions without any associated uncertainties specified for the inlet conditions. As such, this uncertainty was assumed to be associated with the $C_d$ of the venturi. The total uncertainty in mass flow rate used this assumption along with the uncertainties of the upstream static pressure and temperature to determine a mass flow rate uncertainty.

## 2.2 Data Acquisition

Experimental data was taken using a National Instruments PXI-1052 chassis. The chassis is capable of supporting both NI PXI and NI SCXI cards. Thermocouple data was taken using a NI-SCXI 1102 card with a 2 Hz low-pass filter. Static pressure was taken using a NI-SCXI 1102B card with a 200 Hz low-pass filter. Both the thermocouple and static pressure measurements were sampled at 500 Hz with 250 samples taken at a

time. The high frequency pressure measurements were taken using a NI-SCXI 1143 data card paired with a NI-SCXI 1305 terminal block. For this experiment, the filter was not programmed with a cutoff frequency. The high frequency pressure measurements were sampled at 50,000 Hz with 5,000 samples taken at a time.

Data was taken using a LabVIEW code which sampled the data and output the data into *.lvm files. The thermocouple and static pressure measurements were grouped together and termed "low speed data" while the high frequency measurements were termed "high speed data." During data recording, LabVIEW would alternate between sampling low speed and high speed data and would output the low speed data and the high speed data into separate files. In addition, each time data was output, the file number for that type would be incremented by 1. This incrementing allowed for ease of matching low speed and high speed data for each test.

### 2.3 Data Analysis

The experiment consisted of different flow conditions through the orifice, some at a low inlet pressure and some at a high inlet pressure in order to assess cavitation response through the orifice. With a high inlet pressure, the fluid is well below the saturation curve thus the probability of cavitation across the orifice is reduced. At lower inlet pressures, the pressure drop from the inlet to the throat of the orifice can exceed the drop required to reach the vapor pressure and strong cavitation can occur. The low frequency test data was used to determine the test conditions of the orifice for each data set collected. The key parameters used to characterize the flow conditions were the orifice inlet pressure, orifice inlet temperature, mass flow rate, Reynolds number, and cavitation number.

The Reynolds number is given by the equation

$$\mathrm{Re} = \frac{4 \cdot \dot{m}}{\pi \cdot \mu_1 \cdot D}, \tag{2.2}$$

where Re is the Reynolds number, $\dot{m}$ is the mass flow rate of the $LN_2$, $D$ is the inner diameter of the tubing, and $\mu_1$ is the kinematic viscosity of the $LN_2$ at the orifice inlet. The Reynolds number indicates the flow similarity among the different inlet conditions.

Fast Fourier Transforms (FFT) of the high frequency data were performed to analyze the pressure fluctuations downstream of the orifice. The FFT's were then used to determine the cavitation response. This determination was performed by identifying the dominant instability and visually examining each FFT for subharmonics of this dominant frequency.

## 2.4 Test Method

Testing was conducted adjacent to the PRC test cell as shown in Figure 2.5. On test day, the outer jacket of the run tank was initially filled to chill the tank. After the outer jacket was filled, the inner core was filled. To maintain liquid in the tank before testing and to prevent overpressurization, the inner core was maintained at approximately 1103 kPa (160 psig) by using the low pressure relief valve on the tank. To better serve as a temperature control for the test nitrogen, the outer jacket was maintained at atmospheric pressure throughout the experiment by opening the atmospheric bypass valve in order to lower the saturation temperature of the jacketing nitrogen. Prior to testing, an $LN_2$ dewar was connected to the system, and $LN_2$ was bled through the system to chill the system lines. After the system was considered to be sufficiently chilled from the prechill dewar, the prechill flow was stopped, and the run tank was pressurized. The pressurization of the run tank led to an increase in the saturation temperature for the nitrogen in the inner

core. For testing, the backpressure valve was opened to ensure that the backpressure was sufficiently low to allow the cavitating venturi to choke the flow. Immediately prior to the flow's being initiated, data recording was started. Once recording was confirmed, the run valve was opened to start the flow. During testing, the backpressure valve was adjusted to obtain the desired orifice inlet pressures. After the tank's inner core was emptied of $LN_2$, the run valve was closed, and data recording was stopped. The tank jacket and inner core were then refilled as needed to conduct further tests. Further information regarding the method of testing can be found in the experimental test procedure shown in Appendix E.

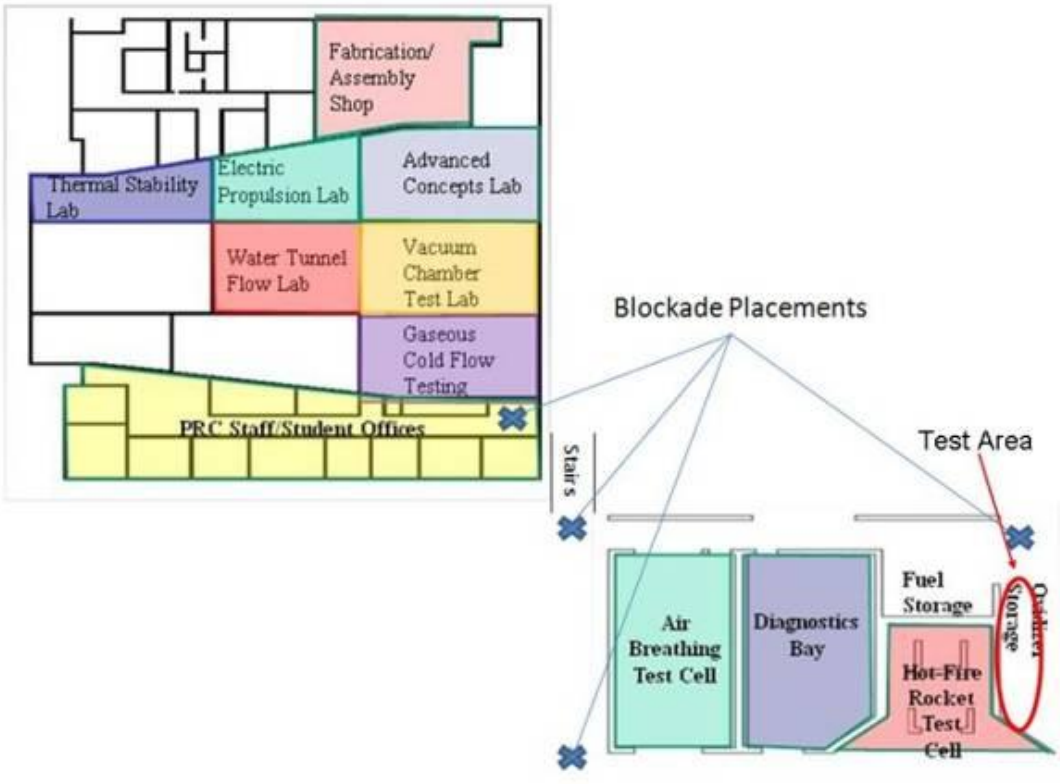


**Figure 2.5: JRC Footprint**

# CHAPTER 3

# RESULTS AND ANALYSIS

Data from both the checkout and the comparison test are presented in this chapter. Checkout data were used to ensure system functionality and verify that the required test conditions could be achieved. After the checkout data was evaluated, changes were made to the system to improve orifice inlet conditions, and testing was conducted.

## 3.1 Checkout Test

Three different test runs were conducted during the checkout test. Since data were not taken continuously, the checkout test resulted in 39 different data points. Each of the 39 checkout data points were analyzed to determine whether the test conditions were reached. A plot of orifice inlet conditions from checkout testing compared against the $LN_2$ saturation curve is shown in Figure 3.1.

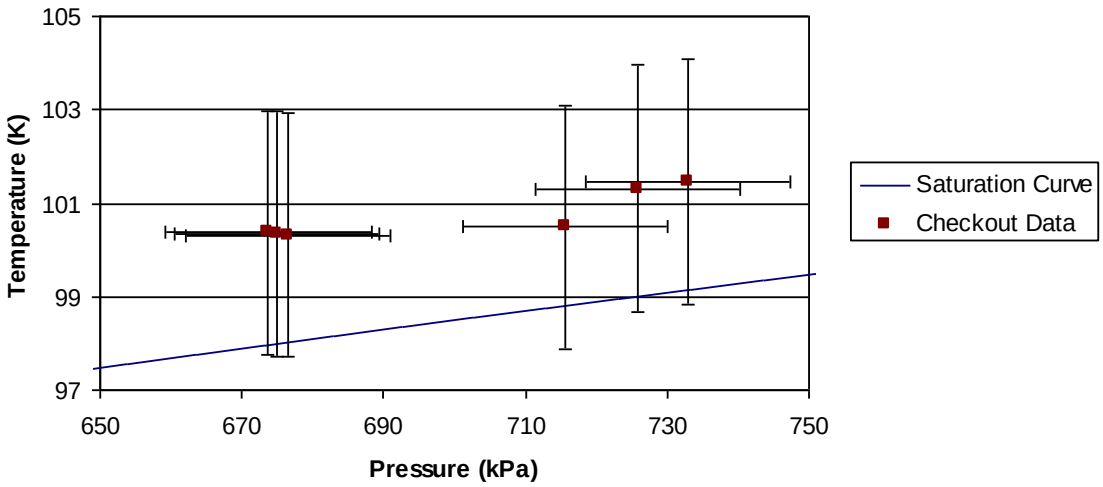


**Figure 3.1: Sample Checkout Data vs. Saturation Curve**

As shown, the data points from checkout testing lie slightly on the vapor side of the saturation curve. This inability to reach liquid conditions at the orifice inlet was considered to be due to either high $LN_2$ temperatures in the tank, heating from cooling the filter and from ambient air, or inaccurate readings from the orifice inlet thermocouple. During the system checkout, the jacketing on the tank was not replenished during testing and the jacket was maintained at a slight positive pressure. The thermocouple readings were considered to be possibly inaccurate due to the thermocouple's being inserted into the boundary layer instead of the fluid freestream. This insertion depth was initially chosen to mitigate any instabilities created by the thermocouple. However, calculations indicated that a potential difference in the thermal boundary layer could exist.

These temperature concerns were addressed through various changes to the system and test method. The heating concerns were addressed by removing the filter from the system and by insulating the line coming out of the tank. The tank temperature

concern was addressed by replenishing the $LN_2$ in the jacket during testing and by leaving the jacket at ambient pressure to lower the saturation temperature of the jacket $LN_2$. The thermocouple concern was addressed by removing the thermocouple and replacing it with one that was inserted into the fluid freestream.

### 3.2 Comparison Test Results

The orifice testing was conducted in seven different test runs. Since data was taken continuously throughout each run, a large number of data points were collected. These data points included start-up and shut-down data. To select the test data, any data point that appeared to fall within or close to a time during which the orifice inlet pressure was being changed were neglected. In addition, the remaining data points were analyzed, and the cavitation numbers for the remaining data points were calculated. To determine the frequency response of cavitation, the analysis was limited to the data points with an average cavitation number between 0.5 and 2.5. Finally, an FFT was performed for each set of test data, and the maximum amplitude and the associated frequency were determined. To remove the effect of a non-zero mean in the pressure data, the first two FFT bins were set equal to zero. The FFT results were then examined, and several data points were noticed to have strong instantaneous pressure spikes which resulted in the FFT's not having an accurate result. These data points and graphs are shown in Appendix I. These criteria resulted in 15 data points for the orifice testing. The following sections detail the results of a few representative tests and provide a summary of all the test points.

### 3.2.1 Test Matrix

The planned test matrix for the experiment is shown in Table 3.1. Plans for testing focused on achieving two different test conditions, one at a lower orifice inlet pressure and another at a higher orifice inlet pressure. These conditions were chosen to provide a test point with a stronger cavitation response and a test point with a weaker cavitation response. The planned test matrix was modified during testing. This modification was because original goals called for moving the high frequency pressure sensor to a different location during testing which was deemed to be unfeasible due to the thermal contraction of the system. As such the test matrix was modified to achieve a variety of inlet conditions.

**Table 3.1: Test Matrix**

| | Condition 1 | Condition 2 |
|---|---|---|
| Orifice Inlet Pressure (kPa) | 551.6 | 827.4 |
| Orifice Inlet Temperature (K) | 88.75 | 88.75 |
| Mass Flow Rate (kg/s) | 1.36 | 1.36 |

### 3.2.2 Test Block Summary

The summary of the orifice and venturi conditions and uncertainty for the testing data points are shown in Table 3.2. The three highlighted data points are those discussed in detail later in this chapter. These data points were chosen to show a variety of cavitation numbers. High frequency plots of the other data points are shown in Appendix G. The average inlet conditions for all 15 data points versus the saturation curve are shown in Figure 3.2. As can be seen in the figure, most of the data points lie well within the saturation curve and can be classified as single-phase liquid. However,

the uncertainty bars on some of the data points extend beyond the saturation curve into the vapor region. As such, those data points are classified as two-phase liquid.

**Table 3.2: Testing Conditions Summary**

| | | Venturi Pressure | | Venturi Temp | | Inlet Pressure | | Inlet Temp | | Outlet Pressure | | Outlet Temp | |
|---|---|---|---|---|---|---|---|---|---|---|---|---|---|
| Set | Test | [kPa] | Uncertainty [%] | [K] | Uncertainty [%] | [kPa] | Uncertainty [%] | [K] | Uncertainty [%] | [kPa] | Uncertainty [%] | [K] | Uncertainty [%] |
| 164499 | 103 | 1682.9 | 0.5 | 93.1 | 2.9 | 617.0 | 2.5 | 94.7 | 2.8 | 516.6 | 3.0 | 109.4 | 2.2 |
| 165099 | 33 | 1640.7 | 0.5 | 90.5 | 3.0 | 601.2 | 2.6 | 92.2 | 2.9 | 498.1 | 3.2 | 107.2 | 2.3 |
| 165099 | 34 | 1637.4 | 0.5 | 90.4 | 3.0 | 601.2 | 2.6 | 92.2 | 2.9 | 499.3 | 3.2 | 107.3 | 2.3 |
| 166178 | 41 | 1665.0 | 0.5 | 93.6 | 2.9 | 650.5 | 2.3 | 94.9 | 2.8 | 551.3 | 2.8 | 109.6 | 2.2 |
| 166178 | 42 | 1662.5 | 0.5 | 93.6 | 2.9 | 649.0 | 2.3 | 95.0 | 2.8 | 550.4 | 2.8 | 109.7 | 2.2 |
| 166178 | 43 | 1660.7 | 0.5 | 93.6 | 2.9 | 649.1 | 2.3 | 95.0 | 2.8 | 550.4 | 2.8 | 109.7 | 2.2 |
| 167223 | 39 | 1673.3 | 0.5 | 92.2 | 2.9 | 634.8 | 2.4 | 93.8 | 2.9 | 530.2 | 3.0 | 108.6 | 2.3 |
| 167223 | 41 | 1668.0 | 0.5 | 92.2 | 2.9 | 829.3 | 1.8 | 93.4 | 2.9 | 721.0 | 2.1 | 108.9 | 2.3 |
| 167223 | 42 | 1665.1 | 0.5 | 92.2 | 2.9 | 826.6 | 1.8 | 93.4 | 2.9 | 718.8 | 2.1 | 108.9 | 2.3 |
| 167223 | 43 | 1662.2 | 0.5 | 92.3 | 2.9 | 824.1 | 1.8 | 93.4 | 2.9 | 715.8 | 2.1 | 108.8 | 2.3 |
| 167223 | 44 | 1659.5 | 0.5 | 92.3 | 2.9 | 824.2 | 1.8 | 93.3 | 2.9 | 715.8 | 2.1 | 108.7 | 2.3 |
| 167223 | 54 | 1632.7 | 0.5 | 92.4 | 2.9 | 765.0 | 1.9 | 93.3 | 2.9 | 660.4 | 2.3 | 108.6 | 2.3 |
| 167223 | 55 | 1630.7 | 0.5 | 92.4 | 2.9 | 766.4 | 1.9 | 93.2 | 2.9 | 662.7 | 2.3 | 108.5 | 2.3 |
| 167223 | 56 | 1628.7 | 0.5 | 92.4 | 2.9 | 765.6 | 1.9 | 93.2 | 2.9 | 662.1 | 2.3 | 108.6 | 2.3 |
| 167223 | 59 | 1621.6 | 0.5 | 92.9 | 2.9 | 650.8 | 2.3 | 94.0 | 2.9 | 551.6 | 2.8 | 108.8 | 2.3 |

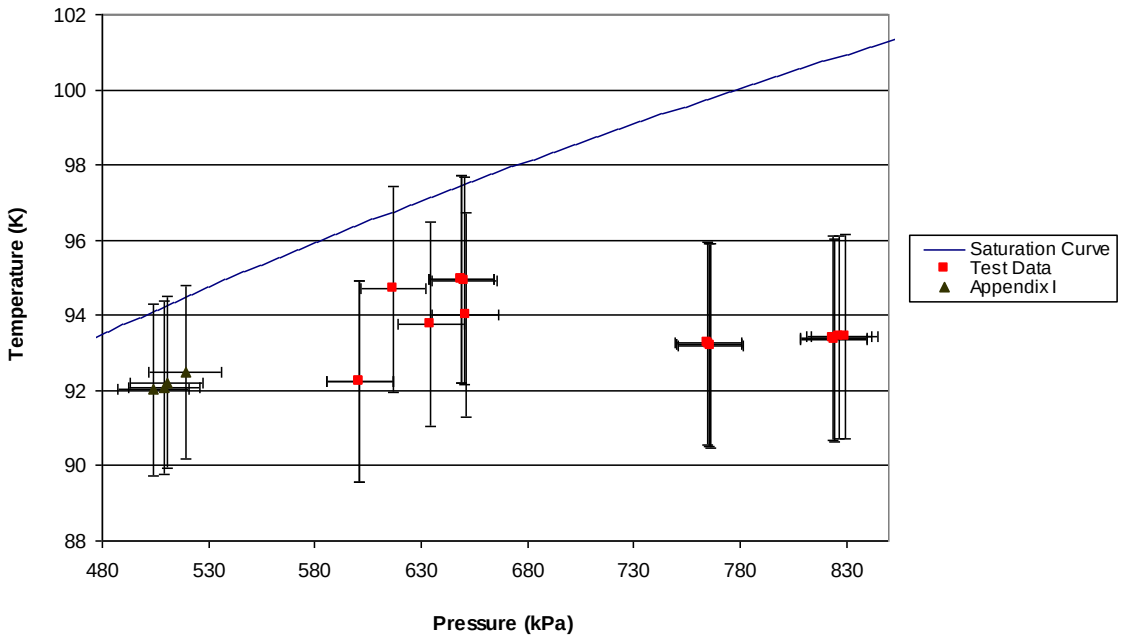


**Figure 3.2: Orifice Inlet Conditions vs. Saturation Curve**

The temperature and pressure data were used to calculate the mass flow rate, pressure drop, Reynolds number, cavitation number, and Strouhal number. The results of these calculations are shown in Table 3.3. An important note regarding the uncertainties provided in this table is that the cavitation number uncertainty is presented as the absolute value while the other uncertainties provided are percentages of the nominal value. This presentation was selected due to the small values of the cavitation number.

Results from the test data show that the orifice inlet pressure ranged from 601.2 kPa (87.2 psia) to 829.5 kPa (120.3 psia). The inlet conditions were non-dimensionalized using the cavitation number for comparison. The cavitation number data show two distinct groupings. One group had cavitation numbers ranging from 0.6 to 1.1, and another group had cavitation numbers ranging from 2.1 to 2.5. The mass flow rate was relatively constant over the data points with average flow rates ranging from 1.22 kg/s to 1.29 kg/s (2.69 lbm/s to 2.83 lbm/s) with approximately 8 % uncertainty. Also, the pressure drop was fairly constant with an approximate value of 103.4 kPa (15 psid) across the data conditions. The average Reynolds number for the data points ranged from 789,300 to 833,800 with 11 % to 12 % uncertainty. These Reynolds numbers indicate that the flow was fully turbulent for all data points. The relative constancy of these parameters indicates that the inlet flow conditions for each of the data points were similar. The Strouhal numbers all fell within the expected range of 0.2 to 0.3. This indicated that the measured wake instabilities were correctly identified. The process of classifying instabilities is explained in the following section.

**Table 3.3: Test Conditions Results**

| | | Mass Flow Rate | | Orifice Pressure Drop | | Cavitation Number | | Reynold's Number | | Strouhal Number | |
|---|---|---|---|---|---|---|---|---|---|---|---|
| Set | Test | [kg/s] | Uncertainty [%] | [kPa] | Uncertainty % | | Uncertainty | | Uncertainty % | | Uncertainty % |
| 164499 | 103 | 1.25 | 8.1 | 100.3 | 0.2 | 0.6 | 0.8 | 833800 | 12 | 0.24 | 10 |
| 165099 | 33 | 1.29 | 7.7 | 103.1 | 0.2 | 1.1 | 0.7 | 795800 | 11 | 0.28 | 10 |
| 165099 | 34 | 1.29 | 7.7 | 101.9 | 0.2 | 1.1 | 0.7 | 795300 | 11 | 0.29 | 10 |
| 166178 | 41 | 1.23 | 8.3 | 99.2 | 0.2 | 0.8 | 0.8 | 825900 | 12 | 0.27 | 11 |
| 166178 | 42 | 1.23 | 8.3 | 98.5 | 0.3 | 0.8 | 0.9 | 826100 | 12 | 0.27 | 10 |
| 166178 | 43 | 1.23 | 8.3 | 98.7 | 0.3 | 0.8 | 0.9 | 825500 | 12 | 0.27 | 11 |
| 167223 | 39 | 1.26 | 8.0 | 104.6 | 0.2 | 1.0 | 0.8 | 820200 | 11 | 0.27 | 10 |
| 167223 | 41 | 1.26 | 8.0 | 108.3 | 0.4 | 2.5 | 0.9 | 810200 | 12 | 0.27 | 10 |
| 167223 | 42 | 1.26 | 8.0 | 107.8 | 0.5 | 2.4 | 0.9 | 809000 | 12 | 0.22 | 10 |
| 167223 | 43 | 1.26 | 8.0 | 108.3 | 0.5 | 2.4 | 0.9 | 807200 | 12 | 0.27 | 10 |
| 167223 | 44 | 1.26 | 8.0 | 108.4 | 0.4 | 2.5 | 0.9 | 804900 | 12 | 0.26 | 10 |
| 167223 | 54 | 1.24 | 8.1 | 104.6 | 0.4 | 2.1 | 0.9 | 792500 | 12 | 0.21 | 10 |
| 167223 | 55 | 1.24 | 8.1 | 103.7 | 0.3 | 2.1 | 0.9 | 790000 | 12 | 0.20 | 10 |
| 167223 | 56 | 1.24 | 8.1 | 103.5 | 0.3 | 2.1 | 0.9 | 789300 | 12 | 0.21 | 10 |
| 167223 | 59 | 1.22 | 8.2 | 99.2 | 0.3 | 1.1 | 0.8 | 799700 | 12 | 0.27 | 10 |

### 3.2.3 Set 165099-Test 33

Plots of the orifice inlet and outlet conditions for Set 165099-Test 33 will be presented in this section. Due to similarity, plots of the inlet and outlet conditions for other data points will not be presented in this chapter. The static plots of all other data points are shown in Appendix F.

The orifice inlet pressure and inlet temperature are shown in Figure 3.3 and Figure 3.4 respectively. As shown in Figure 3.3, the orifice inlet pressure had strong fluctuations about a mean pressure of approximately 601.2 kPa. The instabilities in the inlet pressure possibly came from either instabilities generated by the cavitating venturi or from shedding instabilities generated by the thermocouple. Due to the low sampling frequency of 500 Hz, any instability over 250 Hz would be aliased. As such, the true frequency of the instability in the orifice inlet pressure was unable to be confidently determined from the collected data.

The orifice inlet temperature was fairly steady throughout the data point. As shown in the plot, the inlet temperature increased by 0.25 K during the experiment. This increase was well below the uncertainty of 2.7 K associated with the measurement.

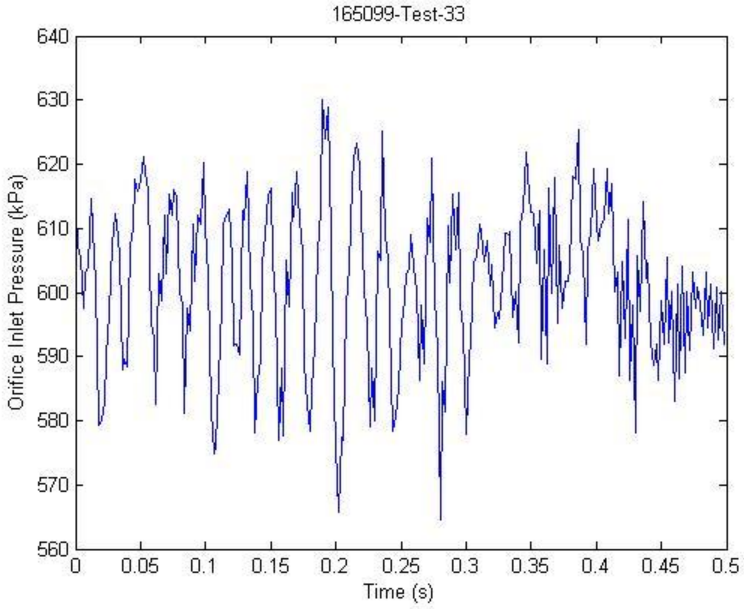


**Figure 3.3: Set 165099-Test 33 Orifice Inlet Pressure**

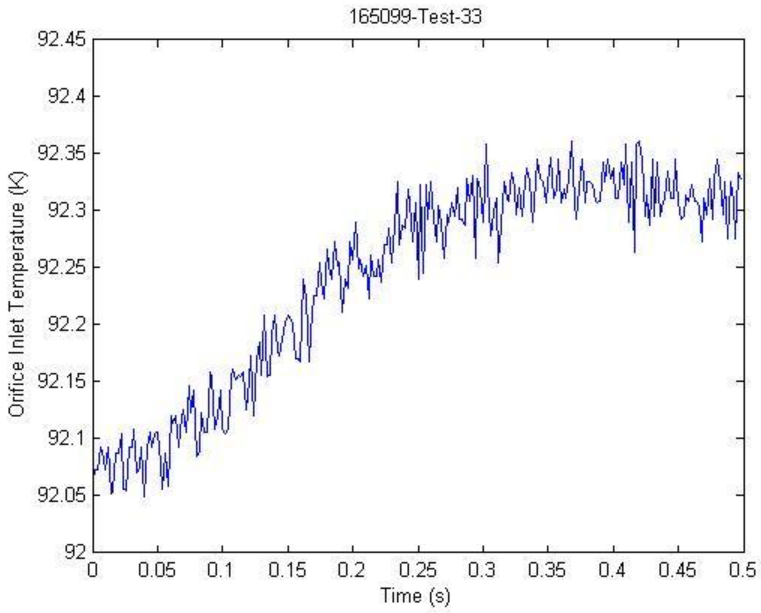


**Figure 3.4: Set 165099-Test 33 Orifice Inlet Temperature**

The orifice outlet pressure and temperature are shown in Figure 3.5 and Figure 3.6 respectively. As can be seen in Figure 3.5, the orifice outlet pressure shows instabilities similar to those seen in the inlet pressure measurement. For the orifice outlet, the pressure had a mean of approximately 500 kPa with fluctuations around the mean.

The orifice outlet temperature was constant throughout the data point. As can be seen in the plot, the rise in inlet temperature was not reflected in the outlet temperature. This constancy of temperature downstream of the orifice is thought to be caused by the boiling of the $LN_2$. As the pressure of the $LN_2$ drops as it flows through the orifice, the liquid starts to boil. Since the nitrogen saturation temperature is a relatively weak function of pressure in the tested range, the liquid would boil at a relatively constant temperature leading to a constant temperature downstream of the orifice.

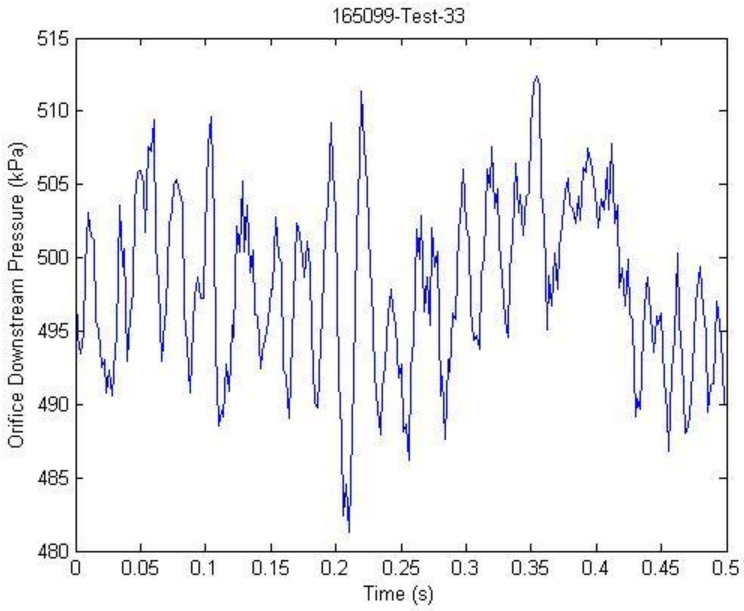


**Figure 3.5: Set 165099-Test 33 Orifice Outlet Pressure**

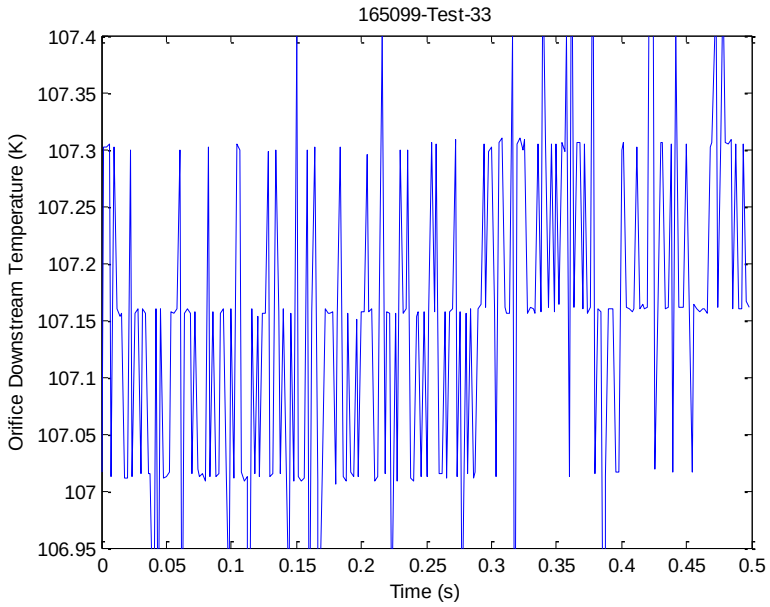


**Figure 3.6: Set 165099-Test 33 Orifice Outlet Temperature**

The high frequency test data from Set 165099-Test 33 are shown in Figure 3.7. A magnified section of these data is shown in Figure 3.8. As can be seen in the plots, the data include several sharp spikes in the pressure trace. These spikes are likely due to the occurrence of cavitation in the flow. Since this data point had a cavitation number of 1.1, the presence of cavitation was expected. In addition, another observable feature in the data is that the data are slightly attenuated due to saturation. Saturation of a sensor occurs when what is measured exceeds the output capability of the sensor. For the high frequency pressure sensor and charge converter used in this experiment, saturation occurred when the pressure spikes exceeded ±296.5 kPa (±43 psi). Saturation of the transducer was exacerbated due to the fluctuations' of the dynamic transducer resulting in a non-zero mean. For a saturated signal, the absolute magnitudes of the instability peaks are not quite accurate. However, the relative strengths of the peaks are considered to be accurate. This view is due to the fact that when saturation occurs in a measurement, the measured signal appears as a square wave due to the attenuation. As such, when an FFT is conducted for a saturated sensor, harmonics of the frequency can appear as the FFT is trying to match the signals comprised in a square wave.

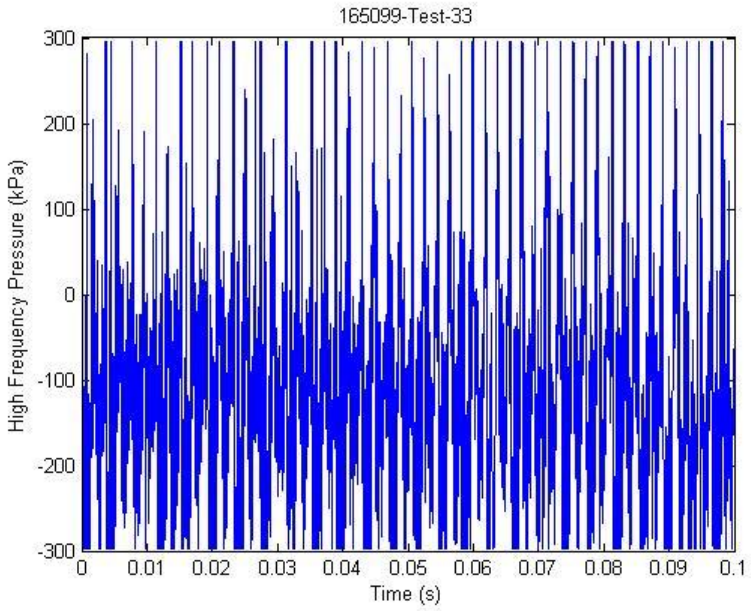


**Figure 3.7: Set 165099-Test 33 High Frequency Raw Signal**

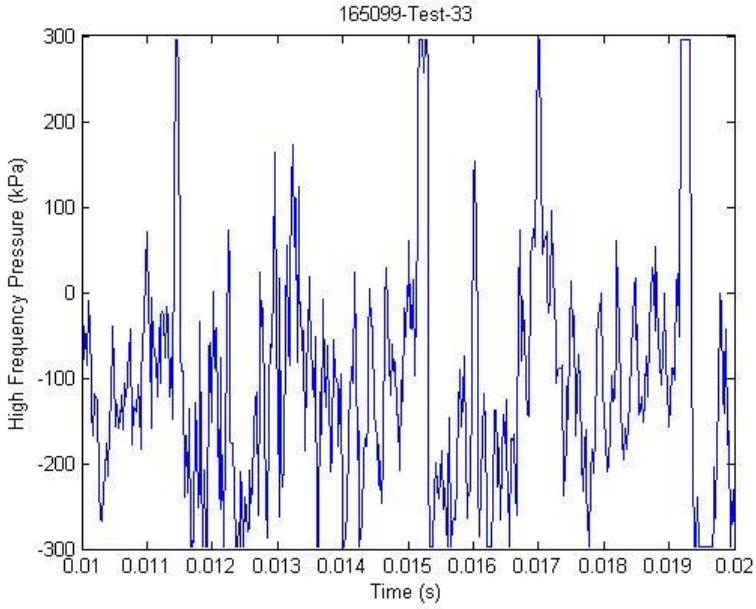


**Figure 3.8: Set 165099-Test 33 Magnified High Frequency Raw Signal**

The FFT of Set 165099-Test 33 as shown in Figure 3.9 indicated the presence of three dominant instability frequencies. For this particular data point, the pressure sensor was not significantly saturated. As can be seen in the FFT, there were three dominant instability peaks. The dominant peak occurred at approximately 520 Hz with an amplitude of approximately 80 kPa. The second largest instability peak was a harmonic of the dominant peak and occurred at 1044 Hz with an amplitude of approximately 35 kPa. The third largest instability was a subharmonic of the dominant instability and occurred at approximately 255 Hz with an amplitude of approximately 31 kPa. The subharmonic frequency was suspected to be due to the cavitation response as the primary disturbance in the orifice flow would be caused by the vortex shedding from the instability thus being the most likely phenomena to cause the split in the cavitation bubble. This would indicate that the cavitation response would be related to the orifice shedding frequency.

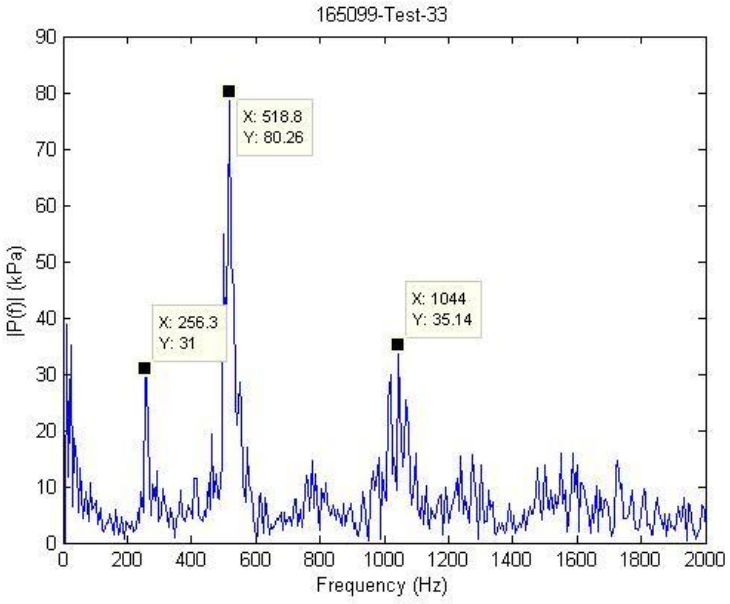


**Figure 3.9: Set 165099-Test 33 FFT**

### 3.2.4 Set 166178-Test 42

The high frequency test data from Set 166178-Test 42 is shown in Figure 3.10. A magnified section of this data is shown in Figure 3.11. As can be seen in the plots, the data includes several sharp spikes in the pressure trace. These spikes are likely due to the occurrence of cavitation in the flow. As with Set 165099-Test 33, the pressure sensor was slightly saturated during this data point.

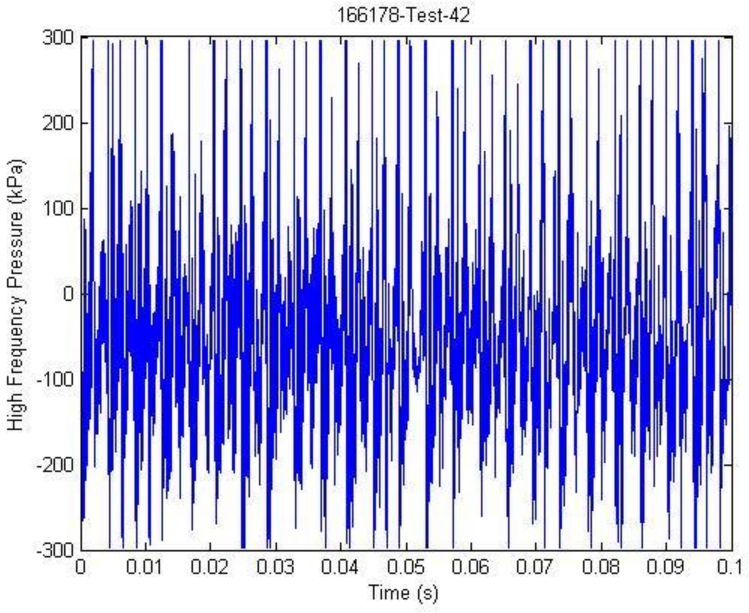


**Figure 3.10: Set 166178-Test 42 High Frequency Raw Signal**

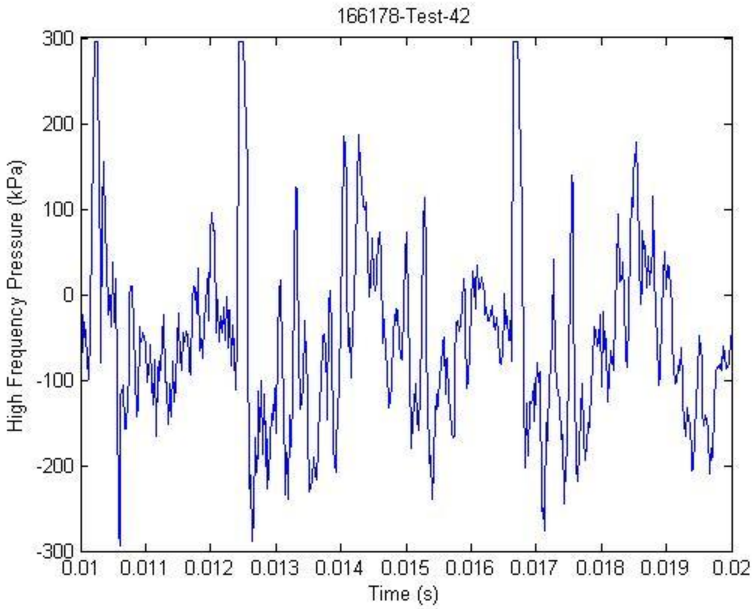


**Figure 3.11: Set 166178-Test 42 Magnified High Frequency Raw Signal**

The FFT of Set 166178-Test 42 is shown in Figure 3.12. For this particular data point, the pressure sensor was not significantly saturated. However, since the pressure sensor did experience saturation, the effects of saturation mentioned previously are considered to be present. As can be seen in the FFT, there were three dominant instability peaks. The dominant peak occurred at approximately 490 Hz with an amplitude of approximately 73 kPa. The second largest instability peak was a harmonic of the dominant peak and occurred at 975 Hz with an amplitude of approximately 27 kPa. The third largest instability was a subharmonic of the dominant instability and occurred at approximately 245 Hz with an amplitude of approximately 17 kPa.

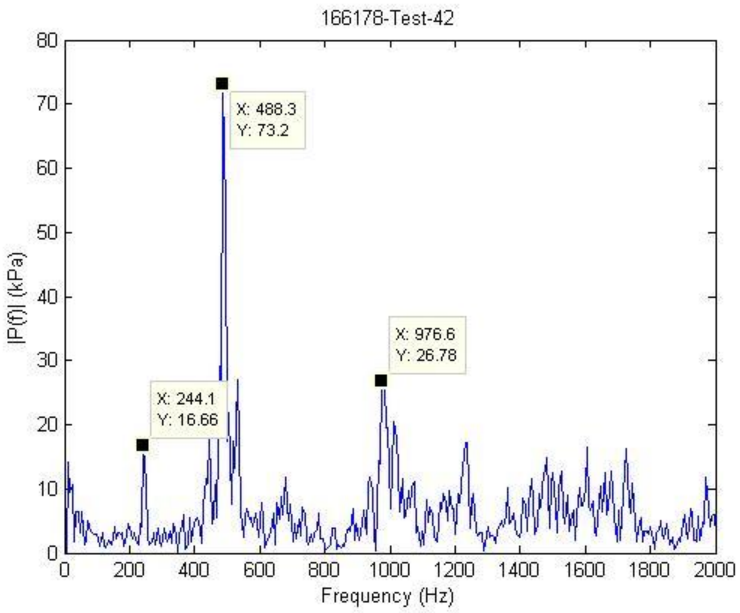


**Figure 3.12: Set 166178-Test 42 FFT**

### 3.2.5 Set 167223-Test 42

The high frequency test data from Set 167223-Test 42 is shown in Figure 3.13. A magnified section of this data is shown in Figure 3.14. As can be seen in the plots, the sharp spikes which appeared in the two previously discussed data points are absent for this data point. Since this data point had a cavitation number of 2.4 indicating a weaker cavitation response, the absence of the sharp spikes was expected. Also, the pressure sensor was significantly saturated during this data point leading to the previously discussed conclusions regarding the accuracy of the FFT of this data point.

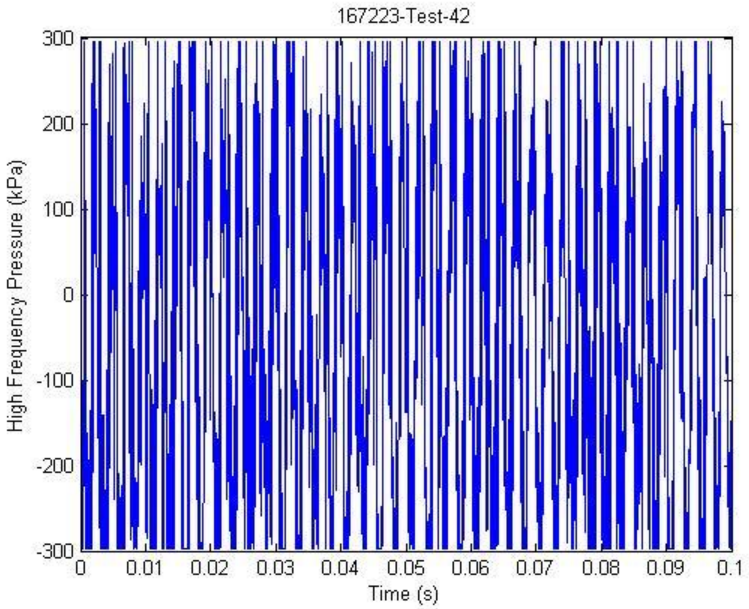


**Figure 3.13: Set 167223-Test 42 High Frequency Raw Signal**

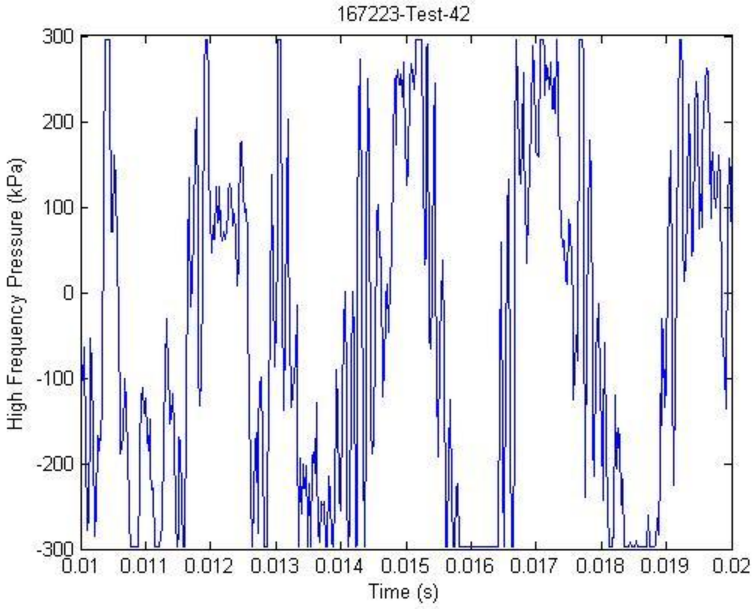


**Figure 3.14: Set 167223-Test 42 Magnified High Frequency Raw Signal**

The FFT of Set 167223-Test 42 is shown in Figure 3.15. As seen in the figure, two dominant instability frequencies were present. The dominant peak occurred at approximately 400 Hz with an amplitude of approximately 195 kPa. The second largest instability peak was a harmonic of the dominant peak and occurred at 805 Hz with an amplitude of approximately 41 kPa. Unlike the previous two data points, the subharmonic response during this test was negligible. As shown in the figure, the subharmonic instability occurred at approximately 215 Hz with an amplitude of approximately 7 kPa. Since the cavitation response as observed in the high frequency raw data plot was present in the first two data points and absent in this one and the subharmonic instability was also present in the first two data points and absent in this one, the subharmonic instability was considered to be linked to the presence of cavitation in the flow.

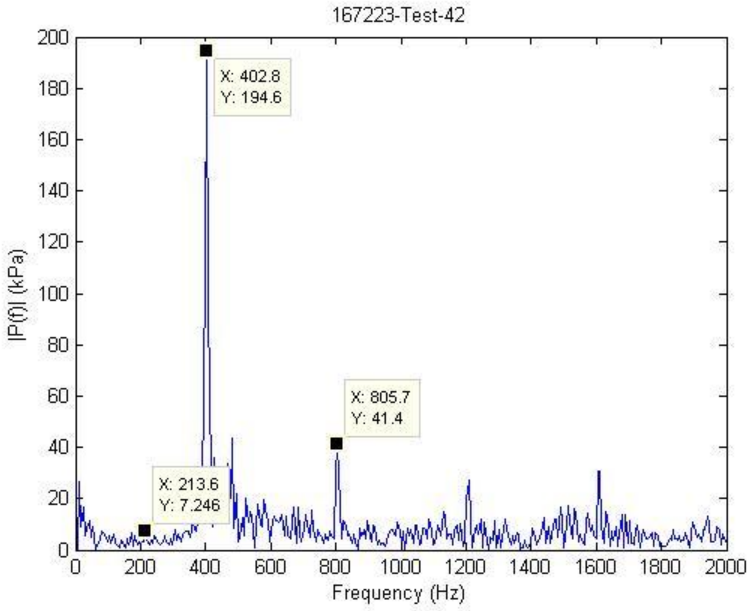


**Figure 3.15: Set 167223-Test 42 FFT**

### 3.2.6 Instability Analysis

For this analysis, these three instabilities were categorized as the primary instability, the subharmonic instability, and the harmonic instability. The primary instability was typically the instability with the largest amplitude and was typically in the range of 400 to 500 Hz. The harmonic instability was the first harmonic of the primary instability. The subharmonic instability was the first subharmonic of the primary instability. The three instabilities for each data point are shown in Table 3.4.

**Table 3.4: Instability Responses**

| Set | Test | Primary Frequency (Hz) | Primary Instability (% inlet) | Sub Frequency (Hz) | Sub Inst. (% inlet) | Harmonic Frequency (Hz) | Harm Inst. (% inlet) |
|---|---|---|---|---|---|---|---|
| 164499 | 103 | 439.5 | 5.3% | 219.7 | 2.77% | 872.8 | 3.8% |
| 165099 | 33 | 518.8 | 13.3% | 256.3 | 5.16% | 1044 | 5.8% |
| 165099 | 34 | 543.2 | 21.3% | 274.7 | 6.95% | 1086 | 8.8% |
| 166178 | 41 | 500.5 | 11.2% | 250.2 | 3.01% | 994.9 | 4.8% |
| 166178 | 42 | 488.3 | 11.3% | 244.1 | 2.57% | 976.6 | 4.1% |
| 166178 | 43 | 500.5 | 11.2% | 250.2 | 2.51% | 994.9 | 6.2% |
| 167223 | 39 | 518.8 | 8.6% | 250.2 | 3.26% | 1019 | 5.8% |
| 167223 | 41 | 494.4 | 15.3% | 250.2 | 0.57% | 1001 | 3.7% |
| 167223 | 42 | 402.8 | 23.5% | 213.6 | 0.88% | 805.7 | 5.0% |
| 167223 | 43 | 494.4 | 15.8% | 195.3 | 0.74% | 988.8 | 2.9% |
| 167223 | 44 | 482.2 | 14.4% | 244.1 | 0.78% | 952.1 | 3.1% |
| 167223 | 54 | 372.3 | 20.0% | 189.2 | 1.02% | 744.6 | 5.9% |
| 167223 | 55 | 372.3 | 16.3% | 207.5 | 0.91% | 738.5 | 6.2% |
| 167223 | 56 | 372.3 | 21.5% | 152.6 | 0.90% | 744.6 | 7.0% |
| 167223 | 59 | 488.3 | 15.5% | 244.1 | 2.44% | 976.6 | 4.4% |

The harmonic instability was hypothesized to be a product of the wake instability caused by the whistling of the orifice. This was tested by using the harmonic frequency as the shedding frequency when calculating the Strouhal number. For this test, the Strouhal number was calculated to be $0.28 \pm 10$ %. This value fell within the expected range of 0.2 to 0.3 verifying the hypothesis. The primary instability was considered to be a result of the same shedding phenomena that caused the harmonic instability. Since the high frequency pressure measurements were made only on one side of the orifice, the pressure sensor would be influenced by some vortexes more than others due to the

rotating shedding of vortices from the orifice. The subharmonic instability is the instability considered to be primarily produced from cavitation.

The primary frequency of each data point plotted against cavitation number and against Reynolds number is shown in Figure 3.16 and Figure 3.17 respectively. As can be seen in Figure 3.16, the primary frequency is relatively constant with a potential slight decrease at higher cavitation number. Also, as shown in Figure 3.17, the primary frequency is relatively constant over the range of Reynolds numbers tested. The relative constancy of the primary frequency with both Reynolds number and cavitation number indicates that the primary frequency is a function of the shedding frequency which was relatively constant over the test conditions.

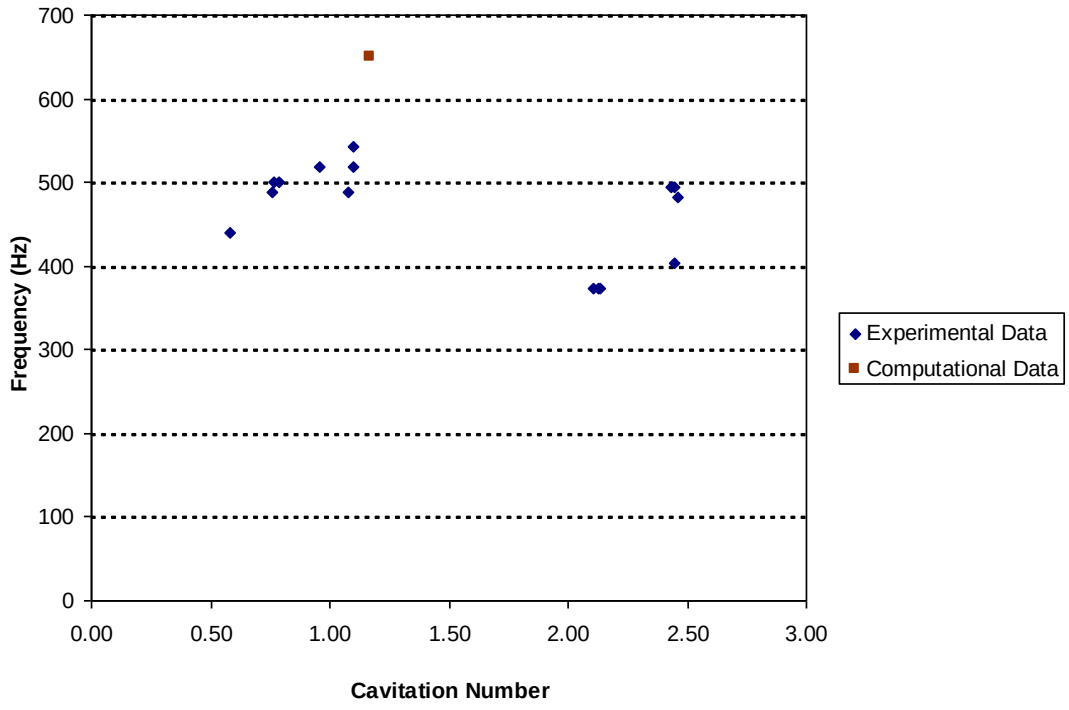


**Figure 3.16: Primary Frequency vs. Cavitation Number**

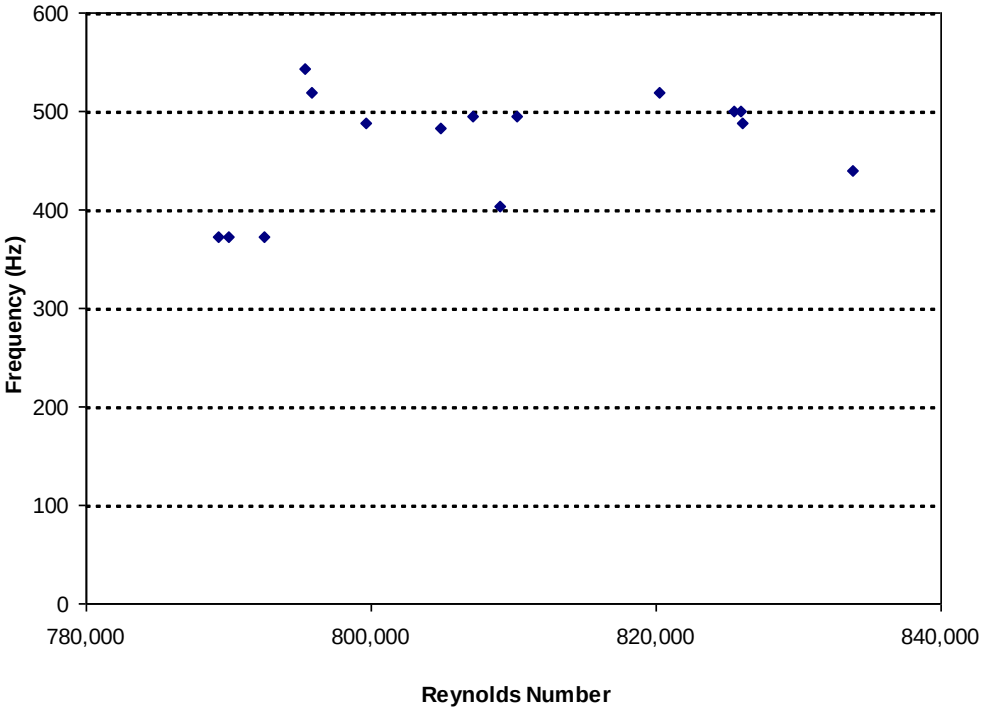


**Figure 3.17: Primary Frequency vs. Reynolds Number**

The subharmonic frequency and subharmonic frequency amplitude are shown plotted against cavitation number in Figure 3.18 and Figure 3.19 respectively. As shown in Figure 3.18, the subharmonic frequency decreases slightly with increasing cavitation number. This decrease matches the decrease seen in the primary frequency. This decrease is expected since as it matches the decrease in the primary frequency.

As can be seen in Figure 3.19, the subharmonic frequency amplitude as a percentage of the orifice inlet pressure decreases with cavitation number. However, there is an increase around a cavitation number of 1. Due to the lack of data in the cavitation number range of 1 to 2, it is unknown whether the increase is significant or whether it is an aberration. Also, it is unknown whether the decrease in amplitude shown from a cavitation number of 1 to a cavitation number of 2 is a step decrease or a gradual

decrease. This decrease in the strength of the stability suggests that the subharmonic response is the cavitation response because the cavitation response should decrease with increasing cavitation number.

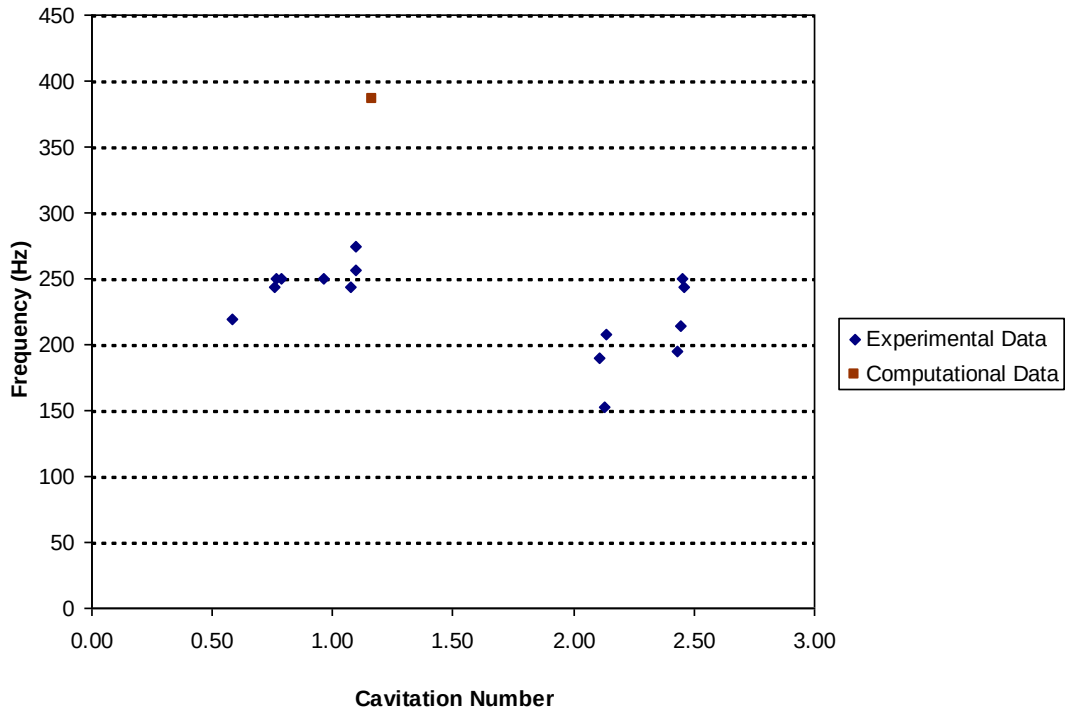


**Figure 3.18: Subharmonic Frequency vs. Cavitation Number**

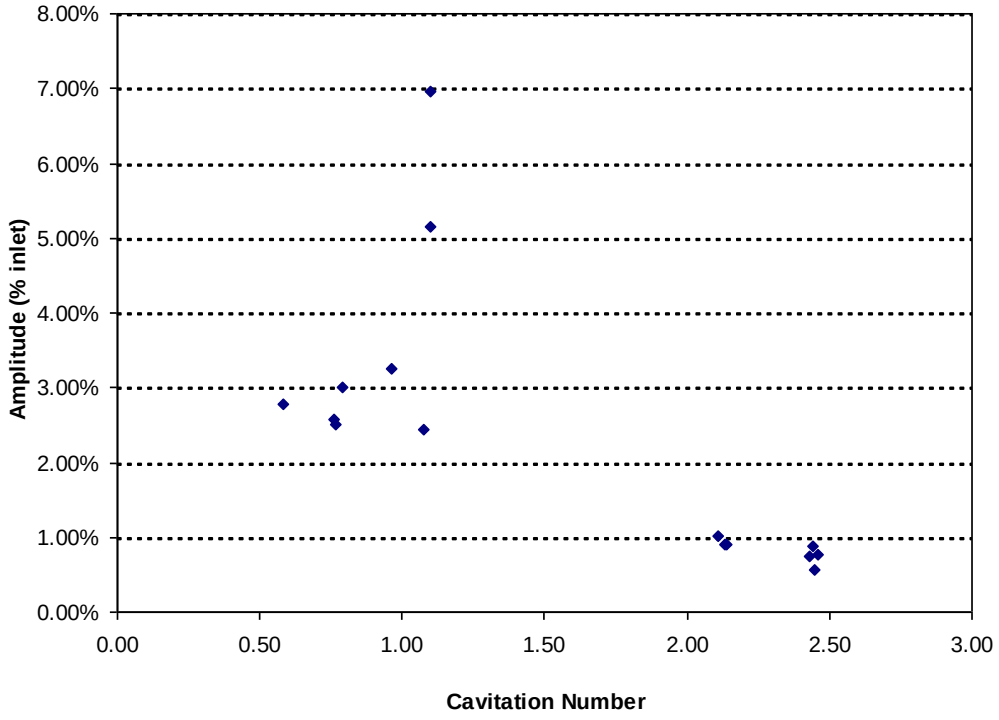


**Figure 3.19: Subharmonic Frequency Amplitude vs. Cavitation Number**

## 3.3 General Uncertainty Analysis

To better understand the causes of the uncertainty in the calculated parameters, a Taylor Series Method (TSM) uncertainty analysis was conducted for one of the test conditions.[19] A TSM analysis was selected due to the simplicity of taking the necessary derivatives. For a TSM analysis, the uncertainty for a measurement with uncorrelated errors is calculated using the equation

$$U_r = \sqrt{\sum \left( \frac{\partial r}{\partial x_i} \cdot U_{i_i} \right)^2} \quad , \tag{3.1}$$

where $U_r$ is the uncertainty of the calculated parameter, $r$ is the calculated parameter, $x_i$ is the contributing parameter, and $U_i$ is the uncertainty of the contributing parameter. If the errors in a calculation are correlated, the equation used is

$$U_r = \sqrt{\sum \left( \frac{\partial r}{\partial x_i} \cdot U_i \right)^2 + 2 \cdot \sum \left( \left( \frac{\partial r}{\partial x_i} \right) \cdot \left( \frac{\partial r}{\partial x_j} \right) \cdot \right) \cdot B_i \cdot B_j}, \quad (3.2)$$

where $B_i$ and $B_j$ are the systematic uncertainties of the correlated errors and the other parameters are defined similarly as before.

For density, viscosity, and vapor pressure data, curvefits were developed as a function of temperature only. A second order curvefit was used for the venturi inlet density; a third order curvefit was used for the orifice inlet density; and a fourth order curvefit was used for viscosity and vapor pressure. The necessary data for creating the curvefits were taken from National Institute of Standards and Technology (NIST). Due to the large uncertainty in the temperature measurements, the uncertainty of the NIST data and the curvefit was assumed to be negligible. Thus, wherever density, viscosity, or vapor pressure appeared in an equation, the appropriate curvefit was substituted for the parameter in the equation, and the uncertainty in the property was then determined as a propagation of temperature uncertainty using Equation 3.1.

The test condition selected for the general uncertainty analysis was Set 166178-Test 42. For the analysis, the uncertainty magnification factors (UMFs) and the uncertainty percent contributors (UPCs) were calculated for the mass flow rate, Reynolds number and cavitation number of the test condition. The UMFs indicate the sensitivity of the result uncertainty to each elemental uncertainty. If the absolute value of the UMF is greater than 1, the propagated uncertainty is magnified. If the absolute value of the UMF is less than 1, the propagated uncertainty is minimized. The equation for calculating UMFs is

$$UMF_i = \left(\frac{\partial r}{\partial x_i}\right) \cdot \left(\frac{X_i}{r}\right), \tag{3.3}$$

where $UMF_i$ is the UMF of the contributing parameter, $X_i$ is the value of the contributing parameter, and $r$ is the calculated result.

The UPCs for a value indicate the relative portion of the uncertainty of a result that comes from each elemental uncertainty source. The equation for calculating the UPCs is

$$UPC_i = \frac{\left(UMF_i\right)^2 \cdot \left(\frac{U_i}{X_i}\right)^2}{\left(\frac{U_r}{r}\right)^2} \cdot 100, \tag{3.4}$$

where $UPC_i$ is the UPC of the contributing parameter. As can be seen in the equation, the UPCs are calculated based on the uncertainty squared. As such, the UPCs do not provide a true percent contribution from each parameter.

A summary of the nominal values and associated uncertainties for the test condition is shown in Table 3.5. Details for the uncertainty calculations can be found in Appendix C. In determining the uncertainty for each measurement, the systematic uncertainty was calculated and then compared to the random uncertainty in the measurement. For each measured parameter, the systematic uncertainty was significantly larger than the random uncertainty so that the random uncertainty could be neglected. The exception to this was the uncertainty of the pressure drop across the orifice. Since the upstream and downstream pressure measurements were calibrated against the same standard, their associated errors were correlated thus reducing the systematic uncertainty

of the calculation. As such, the random error of the pressure drop was not able to be neglected.

**Table 3.5: Set 166178-Test 42 Uncertainty Summary**

| Parameter | Nominal | Units | Uncertainty | Units | % Nominal |
|---|---|---|---|---|---|
| Venturi Inlet Pressure | 1662.5 | kPa | 7.6 | kPa | 0.5 |
| Venturi Inlet Temperature | 93.6 | K | 2.7 | K | 2.9 |
| Orifice Inlet Pressure | 649.0 | kPa | 15.2 | kPa | 2.3 |
| Orifice Inlet Temperature | 95.0 | K | 2.7 | K | 2.8 |
| Orifice Outlet Pressure | 550.4 | kPa | 15.5 | kPa | 2.8 |
| Orifice Outlet Temperature | 109.7 | K | 2.5 | K | 2.2 |
| Pressure Drop | 98.5 | kPa | 0.3 | kPa | 0.3 |
| Mass Flow Rate | 1.2 | kg/s | 0.1 | kg/s | 8.3 |
| Reynolds Number | 826100 | - | 94120 | - | 11.4 |
| Strouhal Number | 0.3 | - | 0.03 | - | 10.4 |
| Cavitation Number | 0.8 | - | 0.9 | - | 111.6 |

Results for the UMF and UPC calculations for the mass flow rate, Reynolds number, and cavitation number are shown in Tables 3.6 through 3.8. For the cavitation number, the UMFs are shown graphically in Figure , and the UPCs are shown in Figure . Charts showing the UMFs and UPCs for the mass flow rate and Reynolds number are presented in Appendix D.

As can be seen in Table 3.6, the largest contributor to the mass flow rate uncertainty is the venturi inlet temperature measurement. Other significant contributors to the uncertainty are the venturi discharge coefficient and the venturi throat diameter. The effect of the uncertainties for each of those parameters on the overall uncertainty is

increased due to the fact that none of the uncertainties from those parameters are minimized.

**Table 3.6: Mass Flow Rate Uncertainty Analysis**

| Base Line Orifice | 166178-42 | |
|---|---|---|
| | UMF | UPC |
| Venturi Discharge Coeff. | 1 | 36.32 |
| Venturi Throat Diameter | 2.019 | 21.9 |
| Venturi Inlet Pressure | 0.71 | 0.15 |
| Venturi Inlet Temperature | 1.86 | 41.62 |
| Tube Inner Diameter | 0.019 | 0.00 |

From Table 3.7, the largest contributor to the Reynolds number is uncertainty is the orifice inlet temperature. Other significant contributing parameters are the venturi inlet temperature, venturi discharge coefficient, and the venturi throat diameter. As with the mass flow rate uncertainties, none of the uncertainties significant contributors are minimized.

**Table 3.7: Reynolds Number Uncertainty Analysis**

| Base Line Orifice | 166178-42 | |
|---|---|---|
| | UMF | UPC |
| Venturi Discharge Coeff. | 1 | 18.54 |
| Venturi Throat Diameter | 2.019 | 11.18 |
| Venturi Inlet Pressure | 0.71 | 0.079 |
| Venturi Inlet Temperature | 1.86 | 21.25 |
| Tube Inner Diameter | 1.019 | 0.28 |
| Orifice Inlet Temperature | 2.879 | 48.68 |

As can be seen in Table 3.8 and Figures 3.20 and 3.21, the single most significant contributor to the cavitation number uncertainty is the orifice inlet temperature. Due to

the large UMF and UPC of the orifice inlet temperature, the other contributing factors to the cavitation number uncertainty are essentially insignificant. The significance of the orifice inlet temperature is expected since $p_v$, $\rho$, and $\mu$ are all functions of the orifice inlet temperature

**Table 3.8: Cavitation Number Uncertainty Analysis**

| Base Line Orifice | 166178-42 | |
|---|---|---|
| | UMF | UPC |
| Venturi Discharge Coeff. | -2 | 0.807 |
| Venturi Throat Diameter | -4.038 | 0.487 |
| Venturi Inlet Pressure | -1.42 | 0.003435 |
| Venturi Inlet Temperature | 3.719 | 0.925 |
| Orifice Throat Diameter | 4 | 0.186 |
| Tube Inner Diameter | 0.038 | 0.00 |
| Orifice Inlet Temperature | -39.064 | 97.59 |

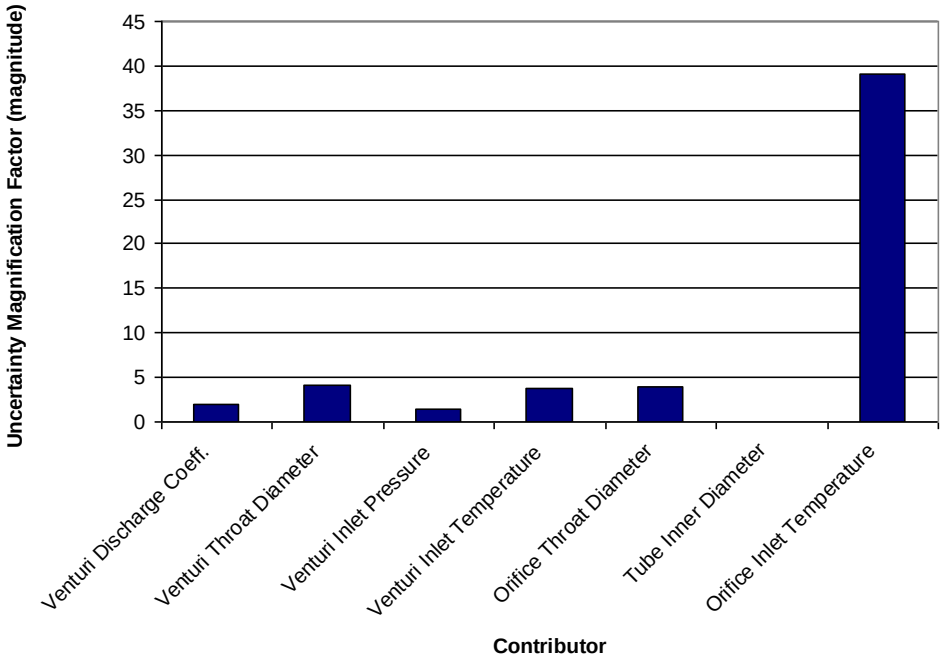


**Figure 3.20: Cavitation Number Uncertainty Magnification Factors**

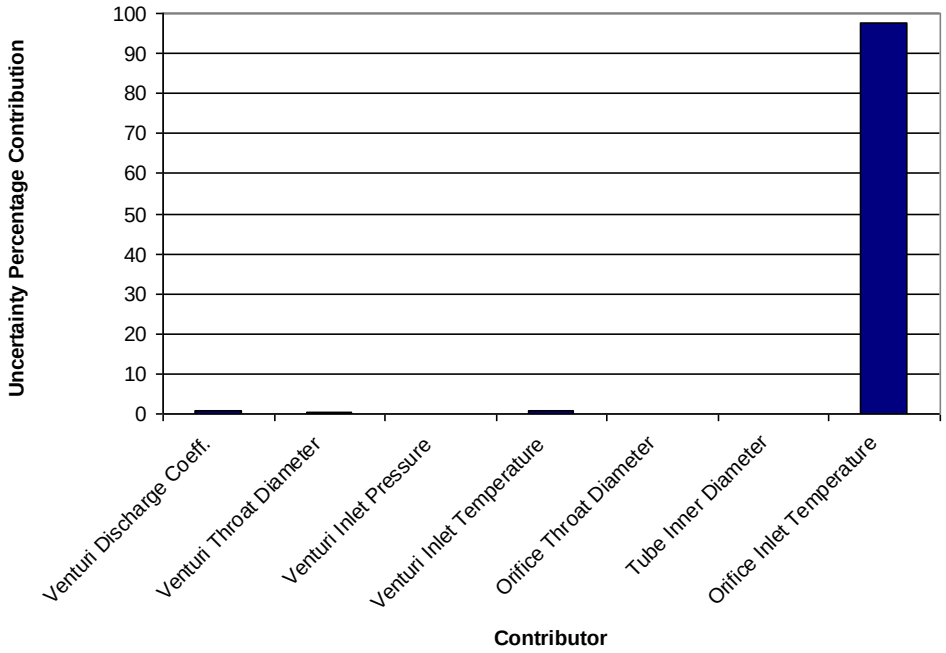


**Figure 3.21: Cavitation Number Uncertainty Percent Contributors**

## 3.4 Computational Results

Due to the significance of vapor pressure and the lack of similarity between the simulation and the experimental tests at the orifice inlet temperature, it was determined to use the cavitation number as the similarity parameter as it incorporated both the orifice inlet pressure and temperature. Due to the similarity in cavitation number, Set 165099-Test 33 was used for comparison. As can be seen in the description of the model in Chapter 1, the pattern predicted in the model matches with the observed pattern of a primary frequency, subharmonic frequency, and harmonic frequency. In the simulation, the primary frequency appears to occur in the 650 Hz to 750 Hz range with the subharmonic frequency's occurring at 386 Hz, and the harmonic frequency's occurring in the 1200 Hz to 1400 Hz range. While the overall pattern in the simulation matches that

found in the experimental results, the frequency values are not an exact match. A comparison between the experimental and computational frequencies is shown in Table 3.9.

**Table 3.9: Frequency Response Comparison**

| | Set 165099-Test 33 | Simulation |
|---|---|---|
| Primary | 256 Hz | 386 Hz |
| Subharmonic | 519 Hz | 650 to 750 Hz |
| Harmonic | 1044 Hz | 1200 to 1400 Hz |

As can be seen in the table, the subharmonic frequency response differs by around 125 Hz, the primary frequency differs by around 200 Hz, and the harmonic frequency differs by around 250 Hz. Since the experimental inlet conditions did not quite match the simulation conditions, an analysis was conducted to predict what the frequency would have been assuming a constant Strouhal number. Details of the calculation are shown in Appendix H. The prediction calculation indicated that the harmonic frequency would occur at 1180 Hz. This predicted frequency is relatively close to the simulation result of 1200 Hz to 1400 Hz. This indicates that the discrepancy between the experimental and computational frequency results was partly due to the differences in inlet flow conditions. However, the cause of the differences in amplitude is unknown. Differences in the experimental and computational results could also be due to assumptions used in the computational model such as no heat transfer from the system to the $LN_2$. Another possible cause for the difference between the results is that the computational results may have had similar pressure traces to the data shown in Appendix I. As such, an FFT would not accurately reflect the amplitudes of the instabilities.

# CHAPTER 4

# CONCLUSIONS

A summary of the test results and recommendations for system improvements and future testing are presented in this chapter. Recommendations for future changes focus on improving conditioning of the $LN_2$ and reducing system uncertainty. Future work focuses on testing over the range of cavitation numbers not tested in this experiment and testing other orifice geometries.

## 4.1 Summary

Results from the experimental testing indicated that the cavitation instability induced by an orifice is a subharmonic of the wake instability of the orifice. For this experiment, the cavitation instability occurred around 250 Hz. In general, the pattern of instabilities in both the experimental and simulation results was similar. However, the particular frequencies predicted by the computational model did not exactly match the experimental results. As indicated by the frequency prediction based on the simulation conditions, the difference in the frequency results could be due to differences in the inlet conditions between the experiment and the simulation. In addition, the difference in results could also be due to assumptions used in the computational modeling such as no heat transfer from the system to the $LN_2$.

Also results from the experimental testing indicate that the strength of the cavitation response decreases with increasing cavitation number. This result was expected as higher cavitation numbers indicate that the cavitation occurring is not as strong. Results indicate a more significant response at flow conditions with a cavitation number of approximately 1 or less. The cavitation response diminishes at flow conditions with a cavitation number of 2 or greater.

## 4.2 Recommendations

Recommendations for future work center around improving measurement accuracy and increasing the control of test conditions. Implementing these changes would increase the accuracy of the experiment and better enable achieving the desired inlet conditions to match the computational models.

Regarding improving measurement accuracy, the main focus would be to lower the uncertainty in the mass flow rate and the temperature measurements. Ideally, a coriolis meter or optical meter could be added to the system to make a direct measurement of the flow rate rather than relying upon calculating a value from a cavitating venturi. However, immediate ways to improve the current system would be to perform an accurate measurement of the venturi throat diameter using measurement cylinders. This could lower the uncertainty of the measurement by an order of magnitude. Also, the mass flow rate measurement could be improved by performing a calibration of the venturi to reduce the uncertainty of the discharge coefficient.

In addition to the reducing the uncertainty in the venturi discharge coefficient and the venturi throat diameter, a key part of reducing the uncertainties in the calculated parameters is to reduce the uncertainties in the temperature measurements. This is

particularly important for the venturi inlet and orifice inlet temperature measurements. For future work, it is recommended that the T-type thermocouples used in the system be replaced by RTD's. With a proper calibration of the RTD's, the uncertainty in each temperature measurement could be reduced by 80 %.

Simply implementing the temperature probe change could lower the mass flow uncertainty by 20 %, the Reynolds number uncertainty by 40 %, and the cavitation number uncertainty by 75 %. If all the recommended reductions to the uncertainties of the various parameters were implemented, it could lead to an 85 % reduction in the mass flow uncertainty, an 80 % reduction in the Reynolds number uncertainty and the cavitation number uncertainty.

For improving control of the test conditions, it is recommended that a trough be constructed and filled with $LN_2$. The system lines and test article would then be immersed in the trough. While the tank jacketing provides initial temperature conditioning and the system insulation prevents heat transfer to the tubing, the temperature of the $LN_2$ does not quite reach the desired value. By immersing the system and test article in a cooling trough, the $LN_2$ could be chilled to the required temperature and the orifice downstream temperature could be reduced resulting in a closer match to the simulations.

Other recommendations for improving the experiment are to increase the sampling rate of the static pressure transducers to 1,000 Hz, to switch to a charge converter with a lower sensitivity, and to add additional high frequency pressure sensors to the system. By increasing the sampling rate of the static pressure transducers to 1000 Hz, the Nyquist frequency of the static transducers would be increased to 500 Hz.

This would help with acquiring useful frequency response data from the static pressure transducers as both the primary and subharmonic frequencies tended to fall below 500 Hz. FFT's could be performed on the static data to determine a frequency response which could then be compared to the frequency response determined from the high frequency pressure sensor to check for similarity between the two responses.

Reducing the sensitivity of the charge converter would lower the voltage output per pressure input. This would reduce the risk of saturation in either the charge converter or the DAQ. This would enable more accurate measurements from the high frequency pressure sensor of the pressure fluctuations in the flow which would yield more accurate results from the FFT's of the high frequency data.

Adding additional high frequency pressure sensors would allow for a better understanding of the instabilities occurring in the system. It is recommended that a high frequency pressure sensor be placed upstream of the orifice to measure the instabilities at the orifice inlet. Additional pressure sensors could be placed at different positions downstream of the orifice to gather additional data. In particular, it is recommended that additional pressure sensors be placed at different angles at the same axial location used in the experiment. This would allow for determining phase data from the frequency response to better understand the instability occurring in the flow and the vortex shedding from the orifice. Also, a high frequency pressure sensor could be placed further downstream from the orifice to measure the pressure fluctuations further from the orifice.

### 4.3 Future Work

Recommended future work related to this project would be to run more tests to better characterize the cavitation response induced by the orifice. Potential future work

would focus on three main areas. The first area would be to determine the effect of cavitation number on the cavitation response. Further testing could be conducted to fill the gap in inlet cavitation numbers tested during this experiment. The amplitudes measured in the additional testing could be plotted against cavitation number to evaluate the variation of the cavitation response with cavitation number. The second area of future testing would be the effect of orifice shape on the frequency response. Orifices of same thickness and diameter so as to have the same Strouhal number but different inlet and outlet geometries could be tested to determine whether the shape of an orifice affects the shedding and cavitation responses. Also, orifices with different thicknesses could be tested to determine the effect of varying geometry on the shedding and cavitation responses. The third area of future testing would be optical measurements. This could be performed by either using a transparent test article section to see and image the bubble sizes and shapes generated by the orifice or using a gamma ray or x ray technique. The measured bubble sizes could then be compared to the cavitation number to determine the effect of cavitation number on the cavitation bubbles.

# APPENDICES

# APPENDIX A

## Hardware Sheets

| Model Number 112A05 | CHARGE OUTPUT PRESSURE SENSOR | | | Revision H ECN #: 29520 |
|---|---|---|---|---|
| | ENGLISH | SI | | |
| **Performance** | | | | |
| Sensitivity (-10 to +25 %) | 1.1 pC/psi | 0.160 pC/kPa | | |
| Measurement Range | 5 kpsi | 34475 kPa | | |
| Maximum Pressure (static) | 10 kpsi | 68950 kPa | | |
| Resolution | 4 mpsi | 0.028 kPa | | |
| Resonant Frequency | ≥200 kHz | ≥200 kHz | | |
| Rise Time (Reflected) | ≤2.0 µ sec | ≤2.0 µ sec | | |
| Non-Linearity | ≤1.0 % FS | ≤1.0 % FS | [2] | |
| **Environmental** | | | | |
| Acceleration Sensitivity | ≤0.003 psi/g | ≤0.0021 kPa/(m/s²) | | |
| Temperature Range (Operating) | -400 to +600 °F | -240 to +316 °C | | |
| Temperature Coefficient of Sensitivity | ≤0.03 %/°F | ≤0.054 %/°C | | |
| Maximum Flash Temperature | 3000 °F | 1649 °C | | |
| Maximum Shock | 10000 g pk | 98070 m/s² pk | | |
| **Electrical** | | | | |
| Output Polarity (Positive Pressure) | Negative | Negative | | |
| Capacitance | 18 pF | 18 pF | | |
| Insulation Resistance (at room temp.) | ≥$10^{12}$ ohm | ≥$10^{12}$ ohm | | |
| **Physical** | | | | |
| Sensing Element | Quartz | Quartz | | |
| Sensing Geometry | Compression | Compression | | |
| Housing Material | 17-4 Stainless Steel | 17-4 Stainless Steel | | |
| Diaphragm | 316L Stainless Steel | 316L Stainless Steel | | |
| Sealing | Welded Hermetic | Welded Hermetic | | |
| Electrical Connector | 10-32 Coaxial Jack | 10-32 Coaxial Jack | | |
| Weight | 0.212 oz | 6.0 gm | | |

**Optional Versions** (Optional versions have identical specifications and accessories as listed for standard model except where noted below. More than one option maybe used.)

**E** - Emralon coating

| | Emralon | Emralon |
|---|---|---|
| Coating | | |
| Electrical Isolation (Case) | $10^8$ ohm | $10^8$ ohm |

Supplied Accessory: Model 065A08 Isolation ring, 0.250" OD x 0.218" ID x 0.027" thk, anodized aluminum [1]

Supplied Accessory: Model 065A22 Isolation Seal, .250" OD x .218" ID x .015", Torlon or Vespel [2]

**P** - Positive Output Polarity

**W** - Water Resistant Cable

Supplied Accessory: Model 060A03 Clamp nut, 5/16-24-2A thd, 1/4" hex, stainless steel (for Series 111, 112 and 113) [3]

**WM** - Water Resistant Cable

Supplied Accessory: Model 060A05 Clamp nut, M7 x 0.75-6G thd (for Series M111, M112 and M113) [3]

**Notes**

[1] Resolution dependent on range setting and cable length used in charge system.
[2] Zero-based, least-squares, straight line method.
[3] Clamp nut installed prior to cable attachment

**Supplied Accessories**

060A03 Clamp nut, 5/16-24-2A thd, 1/4" hex, stainless steel (1)
060A05 Clamp nut M7 x 0.75-6g thd (1)
065A02 Seal ring, sensor flush mount, 0.248" OD x 0.219" ID x 0.015" thk, brass (3)
065A05 Seal sleeve sensor recess mount 0.248" OD x 0.221" ID x 0.240" thk 17-7 (1)

*All specifications are at room temperature unless otherwise specified.*
In the interest of constant product improvement, we reserve the right to change specifications without notice.
ICP® is a registered trademark of PCB group, Inc.

| Entered: BLS | Engineer: NJL | Sales: RWM | Approved: RPF | Spec Number: |
|---|---|---|---|---|
| Date: 10/17/2008 | Date: 10/02/2008 | Date: 10/03/2008 | Date: 10/02/2008 | 7304 |

PCB PIEZOTRONICS PRESSURE DIVISION
3425 Walden Avenue
Depew, NY 14043
UNITED STATES
Phone: 888-684-0011
Fax: 716-686-9129
E-mail: pressure@pcb.com
Web site: www.pcb.com

| Model Number 422E51 | IN-LINE CHARGE CONVERTER | Revision E ECN #: 37900 |
|---|---|---|

| | ENGLISH | SI | |
|---|---|---|---|
| **Performance** | | | |
| Sensitivity (±5.0 %) (Charge Conversion) | 100 mV/pC | 100 mV/pC | |
| Input Range | ±50 pC | ±50 pC | |
| Overrange | ±8 V | ±8 V | |
| Low Frequency Response (-5 %) | 5 Hz | 5 Hz | |
| High Frequency Response (-5 %) | 100 kHz | 100 kHz | [3] |
| Non-Linearity | ≤1.0 % FS | ≤1.0 % FS | |
| **Environmental** | | | |
| Temperature Range (Operating) | -65 to +250 °F | -54 to +121 °C | |
| Maximum Shock | 5000 g pk | 49050 m/s² pk | |
| Maximum Vibration (5 to 2000 Hz) | 100 g pk | 981 m/s² pk | |
| **Electrical** | | | |
| Excitation Voltage | 18 to 28 VDC | 18 to 28 VDC | |
| Constant Current Excitation | 2 to 20 mA | 2 to 20 mA | |
| Output Voltage | ±5.0 V | ±5.0 V | |
| Output Polarity | Inverted | Inverted | |
| Output Impedance | 100 ohm | 100 ohm | |
| Output Bias Voltage | 9 to 13 VDC | 9 to 13 VDC | |
| Maximum Input Voltage | 40 V | 40 V | |
| Broadband Electrical Noise (1 to 10000 Hz) | 49 µV | -86 dB | [1] |
| Spectral Noise (1 Hz) | 19 µV/√Hz | -94 dB | [1] |
| Spectral Noise (10 Hz) | 5.1 µV/√Hz | -106 dB | [1] |
| Spectral Noise (100 Hz) | 1.5 µV/√Hz | -116 dB | [1] |
| Spectral Noise (1 kHz) | 0.6 µV/√Hz | -124 dB | [1] |
| Spectral Noise (10 kHz) | 0.2 µV/√Hz | -134 dB | [1] |
| Capacitance (Feedback) | 10 pF | 10 pF | |
| Overload Recovery Time | 10 µsec | 10 µsec | |
| Discharge Time Constant | >0.1 sec | >0.1 sec | |
| Resistance (Feedback) | $1.2x10^{10}$ ohm | $1.2x10^{10}$ ohm | [2] |
| Source Capacitance Loading | 0.0005 %/pF | 0.0005 %/pF | |
| **Physical** | | | |
| Housing Material | Stainless Steel | Stainless Steel | |
| Sealing | Epoxy | Epoxy | |
| Electrical Connector (Input) | 10-32 Coaxial Jack | 10-32 Coaxial Jack | |
| Electrical Connector (Output) | BNC Jack | BNC Jack | |
| Size (Diameter x Length) | 0.52 in x 3.4 in | 13 mm x 86 mm | |
| Weight | 1.15 oz | 32.7 gm | |

CE[4]

*All specifications are at room temperature unless otherwise specified.*
In the interest of constant product improvement, we reserve the right to change specifications without notice.
ICP® is a registered trademark of PCB group, Inc.

**Optional Versions** (Optional versions have identical specifications and accessories as listed for standard model except where noted below. More than one option maybe used.)

**Notes**

[1] Tested using voltage source and input capacitor equal to the feedback capacitor, to simulate a charge output sensor.
[2] Effective feedback resistance for time constant is 3 times tested value due to circuitry (i.e 1x10E9 = 3x10E9 ohm)
[3] High frequency response may be limited by supply current and output cable length.
[4] See PCB Declaration of Conformance PS024 for details. A low impendance connection from case to earth ground is required to maintain CE compliance.

| Entered: DMW | Engineer: KL | Sales: JJM | Approved: BAM | Spec Number: |
|---|---|---|---|---|
| Date: 12/14/2011 | Date: 12/14/2011 | Date: 12/14/2011 | Date: 12/14/2011 | 25577 |

PCB PIEZOTRONICS
ELECTRONICS DIVISION

3425 Walden Avenue
Depew, NY 14043
UNITED STATES
Phone: 888-684-0015
Fax: 716-684-0987
E-mail: electronics@pcb.com
Web site: www.pcb.com

# Quick Disconnect Thermocouples

## with Miniature Connectors
## Standard and Metric Dimensions

Starts at **$24**

- Glass Filled Nylon Connector Body Rated to 220°C (425°F)
- 304, 310, 316, 321 SS, Inconel, or Super OMEGACLAD® XL Sheath
- Standard 6 and 12" Lengths Available†
- Sheath Diameters from 0.010 to 0.125"
- Grounded, Ungrounded, or Exposed Junction
- Mating Connector, Cable Clamp, and Locking Clip Included FREE!
- Color-Coded SMP Miniature Connector Termination
- Custom Lengths Available

Available as SUPER OMEGACLAD™XL

See Section W

See page A-43 to A-48.

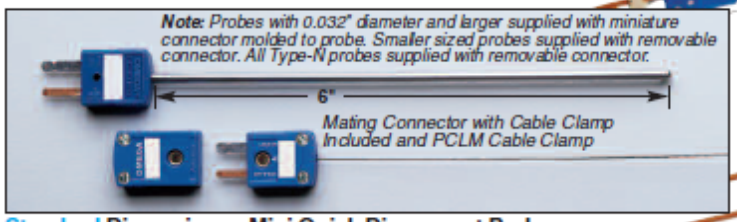


Shown smaller than actual size.

**MOST POPULAR MODELS HIGHLIGHTED!**

### Standard Dimensions - Mini Quick Disconnect Probes

**To Order** *(Specify Model Number)*

| Alloy/ANSI Color Code | Sheath Dia. inches | Model No. 6" Length | Price G*/E* | Price U* | Model No. 12" Length | Price G*/E* | Price U* | Price/Add'l 6" |
|---|---|---|---|---|---|---|---|---|
| Iron-Constantan 304 SS Sheath J | 0.010 | JMQSS-010(*)-6 | $48.00 | $68.00 | JMQSS-010(*)-12 | $49.25 | $69.25 | $1.25 |
| | 0.020 | JMQSS-020(*)-6 | 28.00 | 30.00 | JMQSS-020(*)-12 | 28.65 | 30.65 | 0.65 |
| | 0.032 | JMQSS-032(*)-6 | 28.00 | 30.00 | JMQSS-032(*)-12 | 28.65 | 30.65 | 0.65 |
| | 0.040 | JMQSS-040(*)-6 | 28.00 | 30.00 | JMQSS-040(*)-12 | 28.65 | 30.65 | 0.65 |
| | 0.062 | JMQSS-062(*)-6 | 24.00 | 26.00 | JMQSS-062(*)-12 | 24.80 | 26.80 | 0.80 |
| | 0.125 | JMQSS-125(*)-6 | 24.00 | 26.00 | JMQSS-125(*)-12 | 24.95 | 26.95 | 0.95 |
| CHROMEGA®-ALOMEGA® 304 SS Sheath K | 0.010 | KMQSS-010(*)-6 | $48.00 | $68.00 | KMQSS-010(*)-12 | $49.25 | $69.25 | $1.25 |
| | 0.020 | KMQSS-020(*)-6 | 28.00 | 30.00 | KMQSS-020(*)-12 | 28.65 | 30.65 | 0.65 |
| | 0.032 | KMQSS-032(*)-6 | 28.00 | 30.00 | KMQSS-032(*)-12 | 28.65 | 30.65 | 0.65 |
| | 0.040 | KMQSS-040(*)-6 | 28.00 | 30.00 | KMQSS-040(*)-12 | 28.65 | 30.65 | 0.65 |
| | 0.062 | KMQSS-062(*)-6 | 24.00 | 26.00 | KMQSS-062(*)-12 | 24.80 | 26.80 | 0.80 |
| | 0.125 | KMQSS-125(*)-6 | 24.00 | 26.00 | KMQSS-125(*)-12 | 24.95 | 26.95 | 0.95 |
| CHROMEGA®-ALOMEGA® Super OMEGACLAD® XL Sheath K | 0.010 | KMQXL-010(*)-6 | $51.00 | $71.00 | KMQXL-010(*)-12 | $52.20 | $72.35 | $2.50 |
| | 0.020 | KMQXL-020(*)-6 | 31.00 | 33.00 | KMQXL-020(*)-12 | 31.65 | 33.65 | 2.50 |
| | 0.032 | KMQXL-032(*)-6 | 31.00 | 33.00 | KMQXL-032(*)-12 | 31.65 | 33.65 | 2.50 |
| | 0.040 | KMQXL-040(*)-6 | 31.00 | 33.00 | KMQXL-040(*)-12 | 31.65 | 33.65 | 0.85 |
| | 0.062 | KMQXL-062(*)-6 | 27.00 | 29.00 | KMQXL-062(*)-12 | 27.80 | 29.80 | 1.05 |
| | 0.125 | KMQXL-125(*)-6 | 27.00 | 29.00 | KMQXL-125(*)-12 | 27.95 | 29.80 | 2.10 |
| OMEGA-P®-OMEGA-N® Super OMEGACLAD® XL Sheath N | 0.020 | NMQXL-020(*)-6 | $31.00 | $33.00 | NMQXL-020(*)-12 | $31.65 | $33.65 | $2.50 |
| | 0.032 | NMQXL-032(*)-6 | 31.00 | 33.00 | NMQXL-032(*)-12 | 31.65 | 33.65 | 2.50 |
| | 0.040 | NMQXL-040(*)-6 | 31.00 | 33.00 | NMQXL-040(*)-12 | 31.65 | 33.65 | 0.85 |
| | 0.062 | NMQXL-062(*)-6 | 27.00 | 29.00 | NMQXL-062(*)-12 | 27.80 | 29.80 | 1.05 |
| | 0.125 | NMQXL-125(*)-6 | 27.00 | 29.00 | NMQXL-125(*)-12 | 27.95 | 29.80 | 2.10 |
| CHROMEGA®-Constantan 304 SS Sheath E | 0.010 | EMQSS-010(*)-6 | $48.00 | $68.00 | EMQSS-010(*)-12 | $49.25 | $69.80 | $1.25 |
| | 0.020 | EMQSS-020(*)-6 | 28.00 | 30.00 | EMQSS-020(*)-12 | 28.65 | 30.65 | 0.65 |
| | 0.032 | EMQSS-032(*)-6 | 28.00 | 30.00 | EMQSS-032(*)-12 | 28.65 | 30.65 | 0.65 |
| | 0.040 | EMQSS-040(*)-6 | 28.00 | 30.00 | EMQSS-040(*)-12 | 28.65 | 30.65 | 0.65 |
| | 0.062 | EMQSS-062(*)-6 | 24.00 | 26.00 | EMQSS-062(*)-12 | 24.80 | 26.80 | 0.80 |
| | 0.125 | EMQSS-125(*)-6 | 24.00 | 26.00 | EMQSS-125(*)-12 | 24.95 | 26.95 | 0.95 |
| Copper-Constantan 304 SS Sheath T | 0.020 | TMQSS-020(*)-6 | $28.00 | $30.00 | TMQSS-020(*)-12 | $28.65 | $30.65 | $0.65 |
| | 0.032 | TMQSS-032(*)-6 | 28.00 | 30.00 | TMQSS-032(*)-12 | 28.65 | 30.65 | 0.65 |
| | 0.040 | TMQSS-040(*)-6 | 28.00 | 30.00 | TMQSS-040(*)-12 | 28.65 | 30.65 | 0.65 |
| | 0.062 | TMQSS-062(*)-6 | 24.00 | 26.00 | TMQSS-062(*)-12 | 24.80 | 26.95 | 0.80 |
| | 0.125 | TMQSS-125(*)-6 | 24.00 | 26.00 | TMQSS-125(*)-12 | 24.95 | 26.95 | 0.95 |
| OMEGALLOY® Inconel 600 Sheath N | 0.010 | NMQIN-010(*)-6 | $48.00 | $68.00 | NMQIN-010(*)-12 | $49.25 | $69.25 | $1.25 |
| | 0.020 | NMQIN-020(*)-6 | 28.00 | 30.00 | NMQIN-020(*)-12 | 29.00 | 30.80 | 0.65 |
| | 0.032 | NMQIN-032(*)-6 | 28.00 | 30.00 | NMQIN-032(*)-12 | 29.00 | 30.80 | 0.65 |
| | 0.040 | NMQIN-040(*)-6 | 28.00 | 30.00 | NMQIN-040(*)-12 | 29.00 | 30.80 | 0.65 |
| | 0.062 | NMQIN-062(*)-6 | 24.00 | 26.00 | NMQIN-062(*)-12 | 24.80 | 26.95 | 0.80 |
| | 0.125 | NMQIN-125(*)-6 | 24.00 | 26.00 | NMQIN-125(*)-12 | 24.95 | 26.95 | 0.95 |

** Specify junction type: E (exposed), G (grounded), or U (ungrounded). † Other lengths available, consult Sales Department. **To order with Inconel Sheath**, Change "SS" in model no. to "IN". No additional charge. Type J is not available in Inconel 0.010 diameter. Example: **KMQIN-125G-6, $24.***

*For metric probe configurations with glass filled nylon connector body refer to page A-54 and remove the "H" from the model number, and $3 from price.*

***To Order with 310, 316, or 321 SS Sheath**, change "SS" in model no. to "310SS", "316SS", or "321SS", respectively. No add'l charge. Example: **TMQ321SS-125G-6, $24.***

***Ordering Example: KMQSS-125G-6**, subminiature quick-disconnect probe, Type K, 0.125" OD stainless steel sheath, 6" length, grounded junction, **$24.***

***KMQSS-M300U-300**, subminiature quick-disconnect probe, Type K, stainless steel sheath, 3 mm OD, 300 mm length, ungrounded junction, **$26.95.***

# RUGGED SOLID STATE TRANSDUCERS
## WITH AMPLIFIED OUTPUTS
## STANDARD AND METRIC MODELS

EXCLUSIVE!



### PX209 Series
**0-15 to 0-300 psi-Standard Units**
**0-1 to 0-20 bar-Metric Units**
**Gage, Absolute, and Compound Ranges**

Starts at $215


Standard

- Stainless Steel Fitting and Body
- 5-Point NIST-Traceable Calibration Included
- Solid State Media Isolation (Suitable for Use with Many Industrial Liquids and Gases)
- Broad Temperature-Compensated Range of -20 to 80°C (-4 to 176°F) Yields High Stability with Changing Temperatures
- Electrical Isolation to 100 MΩ Ensures Long-Term Reliability
- Rugged High Shock and Vibration Design for Tough OEM Applications
- 100,000 Hr MTBF Typical

Based on proprietary sensor technology developed by OMEGA to meet the high reliability and accuracy demanded by aerospace applications, the PX209/PXM209 Series voltage and current output pressure transducer offers superior performance in non-corrosive applications, including: engine/powertrain testing, well monitoring, and ground and race water monitoring. The transducer uses a 4-active-arm bridge sensor with a micro-machined diffused silicon diaphragm and proprietary thin-film media, plus dielectric isolation barriers.

This same core sensing element technology, which includes multiple types of signal conditioning and the ability to survive extremes of shock and vibration, provides a modular building block for OMEGA's revolutionary family of pressure-sensing instruments.

### SPECIFICATIONS

**Voltage Output**

**Excitation:** 24 Vdc @ 15 mA
**5 Vdc Output:** 7 to 35 Vdc
**10 Vdc Output:** 12 to 35 Vdc
**Output:** 0 to 5 Vdc or 0 to 10 Vdc, ±1.5% FSO, 3-wire
**Zero Balance:** 0 Vdc ±2% FSO

**4 to 20 mA Output**

**Excitation:** 24 Vdc (7 to 35 Vdc) reverse polarity protected
**Output:** 4 to 20 mA (2-wire) ±1% FSO
**Zero Balance:** 4 mA ±2% FSO

**Max Loop Resistance:** 50 x (supply voltage - 10) Ω

**Common Specifications**

**Accuracy:** 0.25% FS (including linearity, hysteresis and repeatability)
**Operating Temperature:** -54 to 121°C (-65 to 250°F)
**Compensated Temperature:** -20 to 80°C (-4 to 176°F)
**Thermal Effects:** 0.04% FS/°C (0.02% FS/°F)
**Proof Pressure:** 150%
**Burst Pressure:** 300% range max
**Response Time:** 2 ms typical
**Vibration Sensitivity:** At 20 g peak sinusoidal vibration from 10 Hz to 2000 Hz (⅛" D.A.), the output shall not exceed 0.04% FS/g for 15 psi range to 0.005% FS/g for 100 psi and above
**Natural Frequency:** >35 kHz for 100 psi range
**Gage Type:** Diffused silicon strain gage
**Wetted Parts:** 316 SS, borosilicate glass, silicon nitride, epoxy
**Pressure Port:** See dimensional drawing on page B-150
**Electrical Connections:**
**PX209/PXM209:** 1 m (36") shielded 4-conductor cable
**PX219/PXM219:** DIN 40050 plug connector supplied
**Weight:** 128 g (4.5 oz)

## STANDARD MODELS

**AVAILABLE FOR FAST DELIVERY!**

**To Order (Specify Model Number)**

| psi | bar | CABLE STYLE | PRICE | CONN. STYLE | PRICE | COMPATIBLE METERS* |
|---|---|---|---|---|---|---|
| **GAGE PRESSURE RANGES (psig) WITH 0 TO 5 Vdc OUTPUT** | | | | | | |
| 0 to 15 | 0 to 1.0 | PX209-015G5V | $215 | PX219-015G5V | $215 | DP18, DP41-E, DP25B-E |
| 0 to 30 | 0 to 2.1 | PX209-030G5V | 215 | PX219-030G5V | 215 | DP18, DP41-E, DP25B-E |
| 0 to 60 | 0 to 4.1 | PX209-060G5V | 215 | PX219-060G5V | 215 | DP18, DP41-E, DP25B-E |
| 0 to 100 | 0 to 6.9 | PX209-100G5V | 215 | PX219-100G5V | 215 | DP18, DP41-E, DP25B-E |
| 0 to 200 | 0 to 13.8 | PX209-200G5V | 215 | PX219-200G5V | 215 | DP18, DP41-E, DP25B-E |
| 0 to 300 | 0 to 20.7 | PX209-300G5V | 215 | PX219-300G5V | 215 | DP18, DP41-E, DP25B-E |
| **ABSOLUTE PRESSURE RANGES (psia) WITH 0 TO 5 Vdc OUTPUT** | | | | | | |
| 0 to 15 | 0 to 1.0 | PX209-015A5V | $235 | PX219-015A5V | $235 | DP18, DP41-E, DP25B-E |
| 0 to 30 | 0 to 2.1 | PX209-030A5V | 235 | PX219-030A5V | 235 | DP18, DP41-E, DP25B-E |
| 0 to 60 | 0 to 4.1 | PX209-060A5V | 235 | PX219-060A5V | 235 | DP18, DP41-E, DP25B-E |
| 0 to 100 | 0 to 6.9 | PX209-100A5V | 235 | PX219-100A5V | 235 | DP18, DP41-E, DP25B-E |
| 0 to 200 | 0 to 13.8 | PX209-200A5V | 235 | PX219-200A5V | 235 | DP18, DP41-E, DP25B-E |
| 0 to 300 | 0 to 20.7 | PX209-300A5V | 235 | PX219-300A5V | 235 | DP18, DP41-E, DP25B-E |
| **VACUUM AND COMPOUND RANGES WITH 0 TO 5 Vdc OUTPUT** | | | | | | |
| -14.7 to 0 | -1 to 0 | PX209-30VAC5V | $235 | PX219-30VAC5V | $235 | DP18, DP41-E, DP25B-E |
| -14.7 to 15 | -1 to 1.0 | PX209-30V15G5V | 235 | PX219-30V15G5V | 235 | DP18, DP41-E, DP25B-E |
| -14.7 to 45 | -1 to 3.1 | PX209-30V45G5V | 235 | PX219-30V45G5V | 235 | DP18, DP41-E, DP25B-E |
| -14.7 to 85 | -1 to 5.9 | PX209-30V85G5V | 235 | PX219-30V85G5V | 235 | DP18, DP41-E, DP25B-E |
| -14.7 to 135 | -1 to 9.3 | PX209-30V135G5V | 235 | PX219-30V135G5V | 235 | DP18, DP41-E, DP25B-E |

*Comes complete with 5-point NIST calibration certificate.* ** See section D for compatible meters.*

*See pages B-149 and B-150 for PX209 units with 4 to 20 mA output.*

***Note:** To order 0 to 10 Vdc output, replace "5V" suffix with "10V" (no extra charge).*

***Ordering Example:** PX219-015G5V, 0 to 5 Vdc output transducer for gage pressure with a 0 to 15 psia range, PS-4G snubber for gasses and TX4-100 shielded wire, $215 + 12.75 + 35.00 = $262.75.*

## STANDARD ACCESSORIES

| MODEL | PRICE | DESCRIPTION |
|---|---|---|
| PS-4G | $12.75 | ¼ NPT pressure snubber for gaseous media |
| PS-4E | 12.75 | ¼ NPT pressure snubber for water and light oils |
| PS-4D | 12.75 | ¼ NPT pressure snubber for dense liquids (motor oil) |
| TX4-100 | 35.00 | 30 m (100') of 4-conductor shielded wire |

## METRIC ACCESSORIES

| MODEL | PRICE | DESCRIPTION |
|---|---|---|
| PS-4G-MG | $12.75 | G¼ pressure snubber for gaseous media |
| PS-4E-MG | 12.75 | G¼ pressure snubber for water and light oils |
| PS-4D-MG | 12.75 | G¼ pressure snubber for dense liquids (motor oil) |
| TX4-100 | 35.00 | 30 m (100') of 4-conductor shielded wire |

**Order a snubber to protect your pressure transducer!**

**PS-4G, $12.75, shown smaller than actual size.**

## METRIC MODELS

**AVAILABLE FOR FAST DELIVERY!**

**To Order (Specify PXM209 for Cable or PXM219 for DIN Connector)**

| bar | psi | CABLE STYLE | PRICE | CONN. STYLE | PRICE | COMPATIBLE METERS* |
|---|---|---|---|---|---|---|
| **GAGE PRESSURE RANGES (bar) WITH 0 to 10 Vdc OUTPUT** | | | | | | |
| 0 to 1.0 | 0 to 15 | PXM209-001G10V | $215 | PXM219-001G10V | $215 | DP18, DP41-E, DP25B-E |
| 0 to 1.6 | 0 to 23 | PXM209-1.60G10V | 215 | PXM219-1.60G10V | 215 | DP18, DP41-E, DP25B-E |
| 0 to 2.5 | 0 to 36 | PXM209-2.50G10V | 215 | PXM219-2.50G10V | 215 | DP18, DP41-E, DP25B-E |
| 0 to 4.0 | 0 to 58 | PXM209-004G10V | 215 | PXM219-004G10V | 215 | DP18, DP41-E, DP25B-E |
| 0 to 6.0 | 0 to 87 | PXM209-006G10V | 215 | PXM219-006G10V | 215 | DP18, DP41-E, DP25B-E |
| 0 to 10.0 | 0 to 145 | PXM209-010G10V | 215 | PXM219-010G10V | 215 | DP18, DP41-E, DP25B-E |
| 0 to 16.0 | 0 to 232 | PXM209-016G10V | 215 | PXM219-016G10V | 215 | DP18, DP41-E, DP25B-E |
| 0 to 20.0 | 0 to 290 | PXM209-020G10V | 215 | PXM219-020G10V | 215 | DP18, DP41-E, DP25B-E |
| **ABSOLUTE PRESSURE RANGES (bar) WITH 0 to 10 Vdc OUTPUT** | | | | | | |
| 0 to 1.0 | 0 to 15 | PXM209-001A10V | $235 | PXM219-001A10V | $235 | DP18, DP41-E, DP25B-E |
| 0 to 1.6 | 0 to 23 | PXM209-1.60A10V | 235 | PXM219-1.60A10V | 235 | DP18, DP41-E, DP25B-E |
| 0 to 2.5 | 0 to 36 | PXM209-2.50A10V | 235 | PXM219-2.50A10V | 235 | DP18, DP41-E, DP25B-E |
| 0 to 4.0 | 0 to 58 | PXM209-004A10V | 235 | PXM219-004A10V | 235 | DP18, DP41-E, DP25B-E |
| 0 to 6.0 | 0 to 87 | PXM209-006A10V | 235 | PXM219-006A10V | 235 | DP18, DP41-E, DP25B-E |
| 0 to 10.0 | 0 to 145 | PXM209-010A10V | 235 | PXM219-010A10V | 235 | DP18, DP41-E, DP25B-E |
| 0 to 16.0 | 0 to 232 | PXM209-016A10V | 235 | PXM219-016A10V | 235 | DP18, DP41-E, DP25B-E |
| 0 to 20.0 | 0 to 290 | PXM209-020A10V | 235 | PXM219-020A10V | 235 | DP18, DP41-E, DP25B-E |
| **VACUUM AND COMPOUND RANGES (bar) WITH 0 to 10 Vdc OUTPUT** | | | | | | |
| VAC to 0 | VAC to 0 | PXM209-VAC000C10V | $235 | PXM219-VAC000C10V | $235 | DP18, DP41-E, DP25B-E |
| VAC to 1 | VAC to 15 | PXM209-VAC001C10V | 235 | PXM219-VAC001C10V | 235 | DP18, DP41-E, DP25B-E |
| VAC to 3 | VAC to 45 | PXM209-VAC003C10V | 235 | PXM219-VAC003C10V | 235 | DP18, DP41-E, DP25B-E |
| VAC to 6 | VAC to 87 | PXM209-VAC006C10V | 235 | PXM219-VAC006C10V | 235 | DP18, DP41-E, DP25B-E |
| VAC to 9 | VAC to 131 | PXM209-VAC009C10V | 235 | PXM219-VAC009C10V | 235 | DP18, DP41-E, DP25B-E |

*Comes complete with 5-point calibration.* ** See section D for compatible meters.*

***Note:** The voltage output versions of the vacuum and compound sensors generate 0 Vdc at vacuum and 5Vdc or 10 Vdc at full scale.*

***Ordering Example:** PXM219-001G10V, 0 to 10 Vdc output transducer for gage pressure with a 0 to 1 bar range, PS-4G-MG snubber and TX4-100 shielded wire, $215 + 12.75 + 35 = $262.75.*

# RUGGED SOLID STATE TRANSDUCERS
## WITH AMPLIFIED OUTPUTS
## STANDARD AND METRIC MODELS

EXCLUSIVE!



## PX209/PXM209 Series

***0-15 to 0-300 psi-Standard Units***
***0-1 to 0-20 bar-Metric Units***
***Gage, Absolute, and Compound Ranges***

Starts at
**$235**

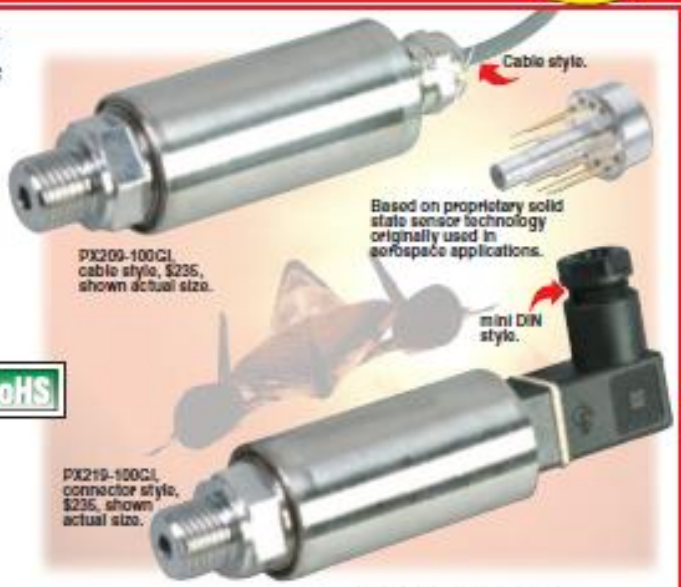


Standard

- Stainless Steel Fitting and Body
- 5-Point NIST-Traceable Calibration Included
- Solid State Media Isolation (Suitable for Use with Many Industrial Liquids and Gases)
- Broad Temperature-Compensated Range of -20 to 80°C (-4 to 176°F) Yields High Stability with Changing Temperatures
- Electrical Isolation to 100 MΩ Ensures Long-Term Reliability
- Rugged High Shock and Vibration Design for Tough OEM Applications
- 100,000 Hr MTBF Typical

Based on proprietary sensor technology developed by OMEGA to meet the high reliability and accuracy demanded by aerospace applications, the PX209/PXM209 Series voltage and current output pressure transducer offers superior performance in non-corrosive applications, including: engine/powertrain testing, well monitoring, and ground and race water monitoring. The transducer uses a 4-active-arm bridge sensor with a micro-machined diffused silicon diaphragm and proprietary thin-film media, plus dielectric isolation barriers.

This same core sensing element technology, which includes multiple types of signal conditioning and the ability to survive extremes of shock and vibration, provides a modular building block for OMEGA's revolutionary family of pressure-sensing instruments.

### SPECIFICATIONS

**Voltage Output**

**Excitation:** 24 Vdc @ 15 mA
**5 Vdc Output:** 7 to 35 Vdc
**10 Vdc Output:** 12 to 35 Vdc
**Output:** 0 to 5 Vdc or 0 to 10 Vdc, ±1.5% FSO, 3-wire
**Zero Balance:** 0 Vdc ±2% FSO

**4 to 20 mA Output**

**Excitation:** 24 Vdc (7 to 35 Vdc) reverse polarity protected
**Output:** 4 to 20 mA (2-wire) ±1% FSO
**Zero Balance:** 4 mA ±2% FSO

**Max Loop Resistance:**
50 x (supply voltage - 10) Ω

**Common Specifications**

**Accuracy:** 0.25% FS (including linearity, hysteresis and repeatability)
**Operating Temperature:** -54 to 121°C (-65 to 250°F)
**Compensated Temperature:** -20 to 80°C (-4 to 176°F)
**Thermal Effects:** 0.04% FS/°C (0.02% FS/°F)
**Proof Pressure:** 150%
**Burst Pressure:** 300% range max
**Response Time:** 2 ms typical
**Vibration Sensitivity:** At 20 g peak sinusoidal vibration from 10 Hz to 2000 Hz (⅛" D.A.), the output shall not exceed 0.04% FS/g for 15 psi range to 0.005% FS/g for 100 psi and above
**Natural Frequency:** >35 kHz for 100 psi range
**Gage Type:** Diffused silicon strain gage
**Wetted Parts:** 316 SS, borosilicate glass, silicon nitride, epoxy
**Pressure Port:** See dimensional drawing on page B-91
**Electrical Connections:**
**PX209/PXM209:** 1 m (36") shielded 4-conductor cable
**PX219/PXM219:** DIN 40050 plug connector supplied
**Weight:** 128 g (4.5 oz)

## STANDARD MODELS

**AVAILABLE FOR FAST DELIVERY!**

### To Order (Specify PX209 for Cable or PX219 for DIN Connector)

| psi | bar | CABLE STYLE | PRICE | CONN. STYLE | PRICE | COMPATIBLE METERS* |
|---|---|---|---|---|---|---|
| **GAGE PRESSURE RANGES (psig) WITH 4 TO 20 mA OUTPUT** | | | | | | |
| 0 to 15 | 0 to 1.0 | PX209-015GI | $235 | PX219-015GI | $235 | DP8, DP41-E, DP25B-E |
| 0 to 30 | 0 to 2.1 | PX209-030GI | 235 | PX219-030GI | 235 | DP8, DP41-E, DP25B-E |
| 0 to 60 | 0 to 4.1 | PX209-060GI | 235 | PX219-060GI | 235 | DP8, DP41-E, DP25B-E |
| 0 to 100 | 0 to 6.9 | PX209-100GI | 235 | PX219-100GI | 235 | DP8, DP41-E, DP25B-E |
| 0 to 200 | 0 to 13.8 | PX209-200GI | 235 | PX219-200GI | 235 | DP8, DP41-E, DP25B-E |
| 0 to 300 | 0 to 20.7 | PX209-300GI | 235 | PX219-300GI | 235 | DP8, DP41-E, DP25B-E |
| **ABSOLUTE PRESSURE RANGES (psia) WITH 4 TO 20 mA OUTPUT** | | | | | | |
| 0 to 15 | 0 to 1.0 | PX209-015AI | $235 | PX219-015AI | $235 | DP8, DP41-E, DP25B-E |
| 0 to 30 | 0 to 2.1 | PX209-030AI | 235 | PX219-030AI | 235 | DP8, DP41-E, DP25B-E |
| 0 to 60 | 0 to 4.1 | PX209-060AI | 235 | PX219-060AI | 235 | DP8, DP41-E, DP25B-E |
| 0 to 100 | 0 to 6.9 | PX209-100AI | 235 | PX219-100AI | 235 | DP8, DP41-E, DP25B-E |
| 0 to 200 | 0 to 13.8 | PX209-200AI | 235 | PX219-200AI | 235 | DP8, DP41-E, DP25B-E |
| 0 to 300 | 0 to 20.7 | PX209-300AI | 235 | PX219-300AI | 235 | DP8, DP41-E, DP25B-E |
| **VACUUM AND COMPOUND RANGES WITH 4 TO 20 mA OUTPUT** | | | | | | |
| -14.7 to 0 | -1 to 0 | PX209-30VACI | $235 | PX219-30VACI | $235 | DP8, DP41-E, DP25B-E |
| -14.7 to 15 | -1 to 1.0 | PX209-30V15CI | 235 | PX219-30V15CI | 235 | DP8, DP41-E, DP25B-E |
| -14.7 to 45 | -1 to 3.1 | PX209-30V45CI | 235 | PX219-30V45CI | 235 | DP8, DP41-E, DP25B-E |
| -14.7 to 85 | -1 to 5.9 | PX209-30V85CI | 235 | PX219-30V85CI | 235 | DP8, DP41-E, DP25B-E |
| -14.7 to 135 | -1 to 9.3 | PX209-30V135CI | 235 | PX219-30V135CI | 235 | DP8, DP41-E, DP25B-E |

*Comes complete with 5-point NIST traceable calibration. * See section D for compatible meters.*

***Ordering Example:** PX219-015AI, 4 to 20 mA output transducer for absolute pressure with a 0 to 15 psia range, PS-4G snubber and TX4-100 shielded wire, $235 + 12.75 + 35 = $282.75.*

Cable style.

STANDARD
PX209-100GI, $215, shown smaller than actual size.

**Order a snubber to protect your pressure transducer!**

PS-4G, $12.75, shown actual size.

## STANDARD ACCESSORIES

| MODEL | PRICE | DESCRIPTION |
|---|---|---|
| PS-4G | $12.75 | ¼ NPT pressure snubber for gaseous media |
| PS-4E | 12.75 | ¼ NPT pressure snubber for water and light oils |
| PS-4D | 12.75 | ¼ NPT pressure snubber for dense liquids (motor oil) |
| TX4-100 | 35.00 | 30 m (100') of 4-conductor shielded wire |

## METRIC ACCESSORIES

| MODEL | PRICE | DESCRIPTION |
|---|---|---|
| PS-4G-MG | $12.75 | G¼ pressure snubber for gaseous media |
| PS-4E-MG | 12.75 | G¼ pressure snubber for water and light oils |
| PS-4D-MG | 12.75 | G¼ pressure snubber for dense liquids (motor oil) |
| TX4-100 | 35.00 | 30 m (100') of 4-conductor shielded wire |

Recommended Reference Video: Pressure, Industrial Measurement Series, **VT-1005-DVD, $100.** Visit omega.com/bobl for Additional Books

## METRIC MODELS

**AVAILABLE FOR FAST DELIVERY!**

### To Order (Specify PXM209 for Cable or PXM219 for DIN Connector)

| bar | CABLE STYLE | PRICE | CONN. STYLE | PRICE | COMPATIBLE METERS* |
|---|---|---|---|---|---|
| **GAGE PRESSURE RANGES (bar) WITH 4 to 20 mA OUTPUT** | | | | | |
| 0 to 1.0 | PXM209-001GI | $235 | PXM219-001GI | $235 | DP8, DP41-E, DP25B-E |
| 0 to 1.6 | PXM209-1.60GI | 235 | PXM219-1.60GI | 235 | DP8, DP41-E, DP25B-E |
| 0 to 2.5 | PXM209-2.50GI | 235 | PXM219-2.50GI | 235 | DP8, DP41-E, DP25B-E |
| 0 to 4.0 | PXM209-004GI | 235 | PXM219-004GI | 235 | DP8, DP41-E, DP25B-E |
| 0 to 6.0 | PXM209-006GI | 235 | PXM219-006GI | 235 | DP8, DP41-E, DP25B-E |
| 0 to 10.0 | PXM209-010GI | 235 | PXM219-010GI | 235 | DP8, DP41-E, DP25B-E |
| 0 to 16.0 | PXM209-016GI | 235 | PXM219-016GI | 235 | DP8, DP41-E, DP25B-E |
| 0 to 20.0 | PXM209-020GI | 235 | PXM219-020GI | 235 | DP8, DP41-E, DP25B-E |
| **ABSOLUTE PRESSURE RANGES (bar) WITH 4 to 20 mA OUTPUT** | | | | | |
| 0 to 1.0 | PXM209-001AI | $215 | PXM219-001AI | $215 | DP8, DP41-E, DP25B-E |
| 0 to 1.6 | PXM209-1.60AI | 235 | PXM219-1.60AI | 235 | DP8, DP41-E, DP25B-E |
| 0 to 2.5 | PXM209-2.50AI | 235 | PXM219-2.50AI | 235 | DP8, DP41-E, DP25B-E |
| 0 to 4.0 | PXM209-004AI | 235 | PXM219-004AI | 235 | DP8, DP41-E, DP25B-E |
| 0 to 6.0 | PXM209-006AI | 235 | PXM219-006AI | 235 | DP8, DP41-E, DP25B-E |
| 0 to 10.0 | PXM209-010AI | 235 | PXM219-010AI | 235 | DP8, DP41-E, DP25B-E |
| 0 to 16.0 | PXM209-016AI | 235 | PXM219-016AI | 235 | DP8, DP41-E, DP25B-E |
| 0 to 20.0 | PXM209-020AI | 235 | PXM219-020AI | 235 | DP8, DP41-E, DP25B-E |
| **VACUUM AND COMPOUND RANGES (bar) WITH 4 to 20 mA OUTPUT** | | | | | |
| VAC to 0 | PXM209-VAC000CI | $235 | PXM219-VAC000CI | $235 | DP8, DP41-E, DP25B-E |
| VAC to 1 | PXM209-VAC001CI | 235 | PXM219-VAC001CI | 235 | DP8, DP41-E, DP25B-E |
| VAC to 3 | PXM209-VAC003CI | 235 | PXM219-VAC003CI | 235 | DP8, DP41-E, DP25B-E |
| VAC to 6 | PXM209-VAC006CI | 235 | PXM219-VAC006CI | 235 | DP8, DP41-E, DP25B-E |
| VAC to 9 | PXM209-VAC009CI | 235 | PXM219-VAC009CI | 235 | DP8, DP41-E, DP25B-E |

*Comes complete with 5-point NIST traceable calibration. * See section D for compatible meters.*

***Note:** The current output versions of the vacuum and compound sensors generate 4 mA at vacuum and 20 mA at full scale.*

***Ordering Example:** PXM219-001AI, 4 to 20 mA output transducer for absolute pressure with a 0 to 1 bar range, PS-4G-MG snubber and TX4-100 shielded wire, $235 + 12.75 + 35 = $282.75.*

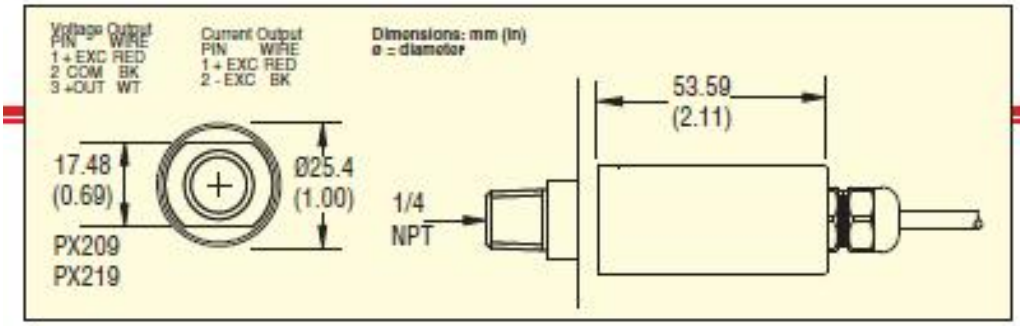


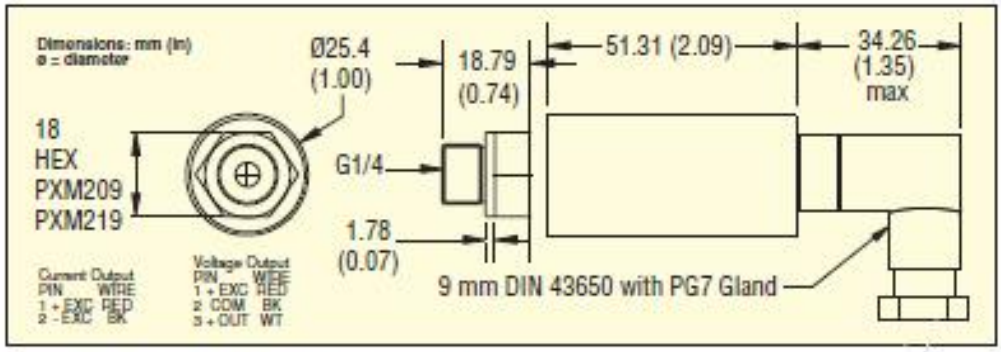


# MAKE IT WIRELESS!

## ADD WIRELESS CAPABILITY TO YOUR PROCESS MEASUREMENT SYSTEM!

**Wireless Connections From Your Sensor to Your Instrumentation:**

- Thermocouple, RTD, Infrared Temperature, Humidity, pH, as well as Process Voltage/Current
- Easy to Install and Use
- Capable of Distances up to 120 m (400')


WRS232-USB wireless transmitter, $159, shown close to actual size.

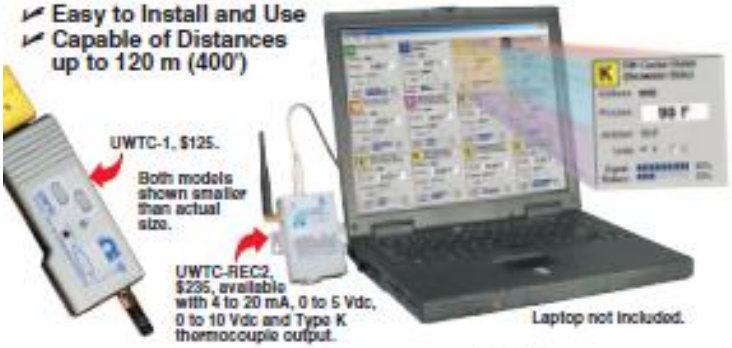


**Wireless Communications From Your Instrument to a PC:**

- Convert the RS232 Signal on Your Meter, Controller or PLC
- Works with any PC with a USB Port
- Easy to Install with Seamless Operation
- Capable of Distances up to 120 m (400')

B-150

# ALL STAINLESS STEEL TRANSDUCER MULTIMEDIA COMPATIBILITY

## HIGH-PERFORMANCE SILICON TECHNOLOGY

LARGE INVENTORY Fast Shipment!



### PX309 Series

*0-1 to 0-10,000 psi*
*0-0.07 to 0-690 bar*
*100 mV, 0 to 5 V,*
*and 4 to 20 mA Outputs*

Starts at $175

NIST CE RoHS

- 1, 2 & 5 psi Low Pressure Ranges!
- All Stainless Steel Construction
- Gage or Absolute Pressure
- Rugged Solid State Design
- High Stability, Low Drift
- 0.25% Static Accuracy
- IP 65 Protection Class



All models shown actual size.

We provide a complete range of services—from product inception, through design and prototypes, to manufacturing and testing. Our application engineers work closely with our customers to **customize**, **design** or create entirely **new products**. Call us—whether you're an OEM, manufacturer, or end user.

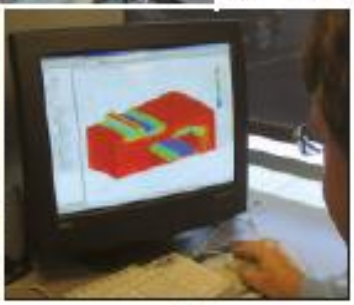

Now Available with M12 Connector

Engineered from 1 to 10,000 psi. Low Pressure Ranges: 1, 2 & 5 psi.

# RUGGED, GENERAL PURPOSE TRANSDUCER

## COMMON SPECIFICATIONS

**mV Output Wiring**

| Wiring | Cable | M12 and mini DIN | Twist-Lock |
|---|---|---|---|
| Excitation (+) | Red | Pin 1 | Pin A |
| Output (+) | White | Pin 3 | Pin C |
| Output (-) | Green | Pin 4 | Pin D |
| Excitation (-) | Black | Pin 2 | Pin B |
| Spare | | | Pin E |
| Vent | | | Pin F |

**5 Vdc Output Wiring**

| Wiring | Cable | M12 and mini DIN | Twist-Lock |
|---|---|---|---|
| Excitation (+) | Red | Pin 1 | Pin A |
| Excitation (-) | Black | Pin 2 | Pin B |
| Output (+) | White | Pin 3 | Pin C |
| N/C[1] | | Pin 4 | Pin D |
| Spare | | | Pin E |
| Vent | | | Pin F |

**mA Output Wiring**

| Wiring | Cable | M12 and mini DIN | Twist-Lock |
|---|---|---|---|
| Supply (+) | Red | Pin 1 | Pin A |
| Supply (-) | Black | Pin 2 | Pin B |
| N/C[1] | | Pin 3 | Pin C |
| N/C[1] | | Pin 4 | Pin D |
| Spare | | | Pin E |
| Vent | | | Pin F |

[1] *N/C: Do not connect any wires to this pin.*

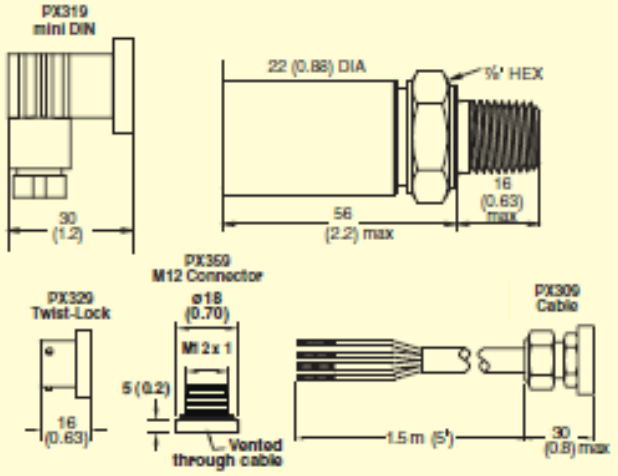


### SPECIFICATIONS

OMEGA's PX309 Series models below 100 psi use a high-accuracy silicon sensor protected by an oil-filled stainless steel diaphragm. Units 100 psi and above use silicon strain gages molecularly bonded to the stainless steel diaphragm

**Long-Term Stability (1 Year):** ±0.25% typical

**Typical Life:** 10 million cycles typical

**Operating Temperature:** -40 to 85°C (-40 to 185°F)

**Proof Pressure:**

**All psia and ≤50 psig Ranges:** 3x capacity or 20 psi, whichever is greater

**100 psig Ranges:** 2x capacity

**Burst Pressure:** 500% of capacity or 25 psi, whichever is greater

**Response Time:** <1 ms

**Shock:** 50 g, 11 ms half-sine

**Vibration:** ±20 g

**Protection Class:** IP 65

**Wetted Parts:**

316 SS for all psia and 1 to 50 psig ranges; 17-4 PH stainless steel for ranges 100 to 10,000 psig

**Pressure Port:** ¼-18 MNPT

**Electrical Connections:**

**PX309:** 1.5 m (5') 2-, 3-, or 4-conductor cable (mA, 5V, mV outputs, respectively)

**PX319:** mini DIN connector with mating connector included

**PX329:** Twist-lock connector, vented mating connector sold separately (PT06V-10-6S)

**PX359:** M12, 4-pin connector

**Weight:**

**PX309:** 154 g (5.4 oz)

**PX319, PX329, PX359:** 100 g (3.5 oz)

### 100 mV OUTPUT

**Excitation:**

**0 to 50 psig and All psia Ranges:** 10 Vdc (ratiometric), (5 to 12 Vdc limits)

**100 to 10,000 psig Ranges:** 5 Vdc (ratiometric), (3 to 10 Vdc limits)

**Output:** 0 to 100 mV, except 2 psi = 40 mV and 1 psi = 20 mV

**Accuracy:** ±0.25% FS BSL at 25°C; includes linearity, hysteresis and repeatability

**Zero Offset:** ±2% FSO; ±4% for 1 and 2 psi ranges

**Span Setting:** ±2% FSO; ±4% for 1 and 2 psi ranges

**Compensated Temperature:** 0 to 50°C (32 to 122°F)

**Thermal Zero and Span Effects (Over Compensated Range):**

**15 to 10,000 psi Ranges:** ±2% FSO

**5 psi Range:** ±3% FSO

**2 psi Range:** ±4% FSO

**1 psi Range:** ±5% FSO

PX329 Mating Connector PT06V-10-6S $26.50

### 5V OUTPUT

**Excitation:** 9 to 30 Vdc (reverse polarity and overvoltage protected)

**Output:** 0 to 5 Vdc or 4 to 20 mA

**Static Accuracy 5 to 10,000 psi:** ±0.25% FS BSL at 25°C; includes linearity, hysteresis and repeatability

**Zero Offset:** ±2% FSO; ±4% for 1 and 2 psi ranges

**Span Setting:** ±2% FSO; ±4% for 1 and 2 psi ranges

**Compensated Temperature:**

**>5 psi Range:** -20 to 85°C (-4 to 185°F)

**≤5 psi Range:** 0 to 50°C (32 to 122°F)

**Total Error Band:** ±2% FSO; includes linearity, hysteresis, repeatability, thermal hysteresis and thermal errors (except 2 psi = ±3% and 1 psi = ±4.5%)

Order a snubber to protect your pressure transducer!

PS-4G, $12.75, shown actual size.

*Snubbers protect sensors from fluid hammers/spikes.*

# HOW TO ORDER PX309 SERIES
## WITH 100 mV OUTPUTS

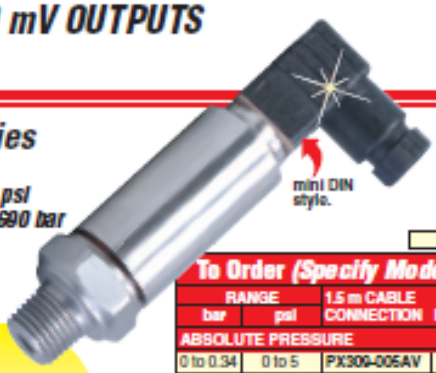


PX319-050GV, $175, mini DIN connector included, shown smaller than actual size.

Metric thread adaptors available, see section C.

### PX309 Series
**100 mV Output**
**0-1 to 0-10,000 psi**
**0-70 mbar to 0-690 bar**

Starts at $175

Standard

- Gage or Absolute Pressure
- Low Pressure to 1 psig
- Rugged Solid State Design
- All Stainless Steel Construction
- High Stability, Low Drift
- 0.25% Accuracy

### 100 mV OUTPUT SPECIFICATIONS

**Excitation:**
**0 to 50 psig and All psia Ranges:** 10 Vdc (ratiometric), (5 to 12 Vdc limits)
**100 to 10,000 psig Ranges:** 5 Vdc (ratiometric), (3 to 10 Vdc limits)
**Output:** 0 to 100 mV, except 2 psi = 40 mV and 1 psi = 20 mV
**Accuracy:** ±0.25% FS BSL at 25°C; includes linearity, hysteresis and repeatability
**Zero Offset:** ±2% FSO; ±4% for 1 and 2 psi ranges
**Span Setting:** ±2% FSO; ±4% for 1 and 2 psi ranges
**Compensated Temperature:** 0 to 50°C (32 to 122°F)
**Thermal Zero and Span Effects (Over Compensated Range):**
**15 to 10,000 psi Ranges:** ±2% FSO
**5 psi Range:** ±3% FSO
**2 psi Range:** ±4% FSO
**1 psi Range:** ±5% FSO

LOW-PRESSURE RANGES HIGHLIGHTED

### To Order (Specify Model Number)

| RANGE bar | RANGE psi | 1.5 m CABLE CONNECTION | PRICE | MINI DIN CONNECTION | PRICE | TWIST-LOCK CONNECTION | PRICE |
|---|---|---|---|---|---|---|---|
| **ABSOLUTE PRESSURE** | | | | | | | |
| 0 to 0.34 | 0 to 5 | PX309-005AV | $300 | PX319-005AV | $300 | PX329-005AV | $300 |
| 0 to 1 | 0 to 15 | PX309-015AV | 195 | PX319-015AV | 215 | PX329-015AV | 235 |
| 0 to 2.1 | 0 to 30 | PX309-030AV | 195 | PX319-030AV | 215 | PX329-030AV | 235 |
| 0 to 3.4 | 0 to 50 | PX309-050AV | 195 | PX319-050AV | 215 | PX329-050AV | 235 |
| 0 to 6.9 | 0 to 100 | PX309-100AV | 195 | PX319-100AV | 215 | PX329-100AV | 235 |
| 0 to 14 | 0 to 200 | PX309-200AV | 195 | PX319-200AV | 215 | PX329-200AV | 235 |
| 0 to 21 | 0 to 300 | PX309-300AV | 195 | PX319-300AV | 215 | PX329-300AV | 235 |
| **GAGE PRESSURE** | | | | | | | |
| 0 to 0.07 | 0 to 1 | PX309-001GV | $300 | PX319-001GV | $300 | PX329-001GV | $300 |
| 0 to 0.14 | 0 to 2 | PX309-002GV | 300 | PX319-002GV | 300 | PX329-002GV | 300 |
| 0 to 0.34 | 0 to 5 | PX309-005GV | 300 | PX319-005GV | 300 | PX329-005GV | 300 |
| 0 to 1 | 0 to 15 | PX309-015GV | 175 | PX319-015GV | 175 | PX329-015GV | 215 |
| 0 to 2.1 | 0 to 30 | PX309-030GV | 175 | PX319-030GV | 175 | PX329-030GV | 215 |
| 0 to 3.4 | 0 to 50 | PX309-050GV | 175 | PX319-050GV | 175 | PX329-050GV | 215 |
| 0 to 6.9 | 0 to 100 | PX309-100GV | 175 | PX319-100GV | 175 | PX329-100GV | 215 |
| 0 to 10 | 0 to 150 | PX309-150GV | 175 | PX319-150GV | 175 | PX329-150GV | 215 |
| 0 to 14 | 0 to 200 | PX309-200GV | 175 | PX319-200GV | 175 | PX329-200GV | 215 |
| 0 to 21 | 0 to 300 | PX309-300GV | 175 | PX319-300GV | 175 | PX329-300GV | 215 |
| 0 to 34 | 0 to 500 | PX309-500GV | 175 | PX319-500GV | 175 | PX329-500GV | 215 |
| 0 to 69 | 0 to 1000 | PX309-1KGV | 175 | PX319-1KGV | 175 | PX329-1KGV | 215 |
| 0 to 138 | 0 to 2000 | PX309-2KGV | 175 | PX319-2KGV | 175 | PX329-2KGV | 215 |
| 0 to 207 | 0 to 3000 | PX309-3KGV | 175 | PX319-3KGV | 175 | PX329-3KGV | 215 |
| 0 to 345 | 0 to 5000 | PX309-5KGV | 175 | PX319-5KGV | 175 | PX329-5KGV | 215 |
| 0 to 517 | 0 to 7500 | PX309-7.5KGV | 175 | PX319-7.5KGV | 175 | PX329-7.5KGV | 215 |
| 0 to 690 | 0 to 10,000 | PX309-10KGV | 175 | PX319-10KGV | 175 | PX329-10KGV | 215 |

*Comes complete with 5-point NIST-traceable calibration.*

*Notes: 1. Units 100 psig and above may be subjected to vacuum on the pressure port without damage. 2. For alternative performance specifications to suit your application, contact Engineering.*

*Ordering Examples: PX309-100GV, 100 psi gage pressure transducer with 100 mV output at 5 Vdc excitation and 1.5 m cable termination, $175. PX319-015AV, 15 psi absolute pressure transducer with 100 mV output @ 10 Vdc excitation and mini DIN termination, $215.*

*PX329-3KGV, 3000 psi gage pressure transducer with 100 mV output @ 5 Vdc excitation and twist-lock termination, $215. Mating connector sold separately; order PT06V-10-6S, $26.50. Consult Sales for OEM pricing.*

### ACCESSORIES

| MODEL NO. | PRICE | DESCRIPTION |
|---|---|---|
| CAL-3 | $150.00 | Recalibration: 5-point NIST traceable |
| PT06V-10-6S | 26.50 | Mating connector for PX329 |
| CA-39-4PC22-5 | 90.00 | 4-conductor mating twist-lock connector with 1.5 m (5') cable for PX329 |
| CX5302 | 15.00 | Extra mini DIN connector for PX319 |

# HOW TO ORDER PX309 SERIES
## WITH 0 TO 5 Vdc OUTPUT

### PX309 Series
**0 to 5 Vdc Output**
**0-1 to 0-10,000 psi**
**0-70 mbar to 0-690 bar**

Twist-lock style.

PX329-015G5V, $275, shown actual size.

Metric thread adaptors available, see section C.

Starts at $225

NIST Standard CE RoHS

- Gage or Absolute Pressure
- Low Pressure to 1 psig
- Rugged Solid State Design
- All Stainless Steel Construction
- High Stability, Low Drift
- 0.25% Static Accuracy

### 5V OUTPUT SPECIFICATIONS

**Excitation:** 9 to 30 Vdc (reverse polarity and overvoltage protected)

**Output:** 0 to 5 Vdc or 4 to 20 mA

**Static Accuracy 5 to 10,000 psi:** ±0.25% FS BSL at 25°C; includes linearity, hysteresis and repeatability

**Zero Offset:** ±2% FSO; ±4% for 1 and 2 psi ranges

**Span Setting:** ±2% FSO; ±4% for 1 and 2 psi ranges

**Compensated Temperature:**
- >5 psi Range: -20 to 85°C (-4 to 185°F)
- ≤5 psi Range: 0 to 50°C (32 to 122°F)

**Total Error Band:** ±2% FSO; includes linearity, hysteresis, repeatability, thermal hysteresis and thermal errors (except 2 psi = ±3% and 1 psi = ±4.5%)

LOW-PRESSURE RANGES HIGHLIGHTED

**To Order (Specify Model Number)**

| RANGE bar | RANGE psi | 1.5 m CABLE CONNECTION | PRICE | MINI DIN CONNECTION | PRICE | TWIST-LOCK CONNECTION | PRICE |
|---|---|---|---|---|---|---|---|
| **ABSOLUTE PRESSURE** | | | | | | | |
| 0 to 0.34 | 0 to 5 | PX309-005A5V | $325 | PX319-005A5V | $325 | PX329-005A5V | $350 |
| 0 to 1 | 0 to 15 | PX309-015A5V | 245 | PX319-015A5V | 245 | PX329-015A5V | 295 |
| 0 to 2.1 | 0 to 30 | PX309-030A5V | 245 | PX319-030A5V | 245 | PX329-030A5V | 295 |
| 0 to 3.4 | 0 to 50 | PX309-050A5V | 245 | PX319-050A5V | 245 | PX329-050A5V | 295 |
| 0 to 6.9 | 0 to 100 | PX309-100A5V | 245 | PX319-100A5V | 245 | PX329-100A5V | 295 |
| 0 to 14 | 0 to 200 | PX309-200A5V | 245 | PX319-200A5V | 245 | PX329-200A5V | 295 |
| 0 to 21 | 0 to 300 | PX309-300A5V | 245 | PX319-300A5V | 245 | PX329-300A5V | 295 |
| **GAGE PRESSURE** | | | | | | | |
| 0 to 0.07 | 0 to 1 | PX309-001G5V | $345 | PX319-001G5V | $345 | PX329-001G5V | $370 |
| 0 to 0.14 | 0 to 2 | PX309-002G5V | 325 | PX319-002G5V | 325 | PX329-002G5V | 350 |
| 0 to 0.34 | 0 to 5 | PX309-005G5V | 300 | PX319-005G5V | 300 | PX329-005G5V | 325 |
| 0 to 1 | 0 to 15 | PX309-015G5V | 225 | PX319-015G5V | 225 | PX329-015G5V | 275 |
| 0 to 2.1 | 0 to 30 | PX309-030G5V | 225 | PX319-030G5V | 225 | PX329-030G5V | 275 |
| 0 to 3.4 | 0 to 50 | PX309-050G5V | 225 | PX319-050G5V | 225 | PX329-050G5V | 275 |
| 0 to 6.9 | 0 to 100 | PX309-100G5V | 225 | PX319-100G5V | 225 | PX329-100G5V | 275 |
| 0 to 10 | 0 to 150 | PX309-150G5V | 225 | PX319-150G5V | 225 | PX329-150G5V | 275 |
| 0 to 14 | 0 to 200 | PX309-200G5V | 225 | PX319-200G5V | 225 | PX329-200G5V | 275 |
| 0 to 21 | 0 to 300 | PX309-300G5V | 225 | PX319-300G5V | 225 | PX329-300G5V | 275 |
| 0 to 34 | 0 to 500 | PX309-500G5V | 225 | PX319-500G5V | 225 | PX329-500G5V | 275 |
| 0 to 69 | 0 to 1000 | PX309-1KG5V | 225 | PX319-1KG5V | 225 | PX329-1KG5V | 275 |
| 0 to 138 | 0 to 2000 | PX309-2KG5V | 225 | PX319-2KG5V | 225 | PX329-2KG5V | 275 |
| 0 to 207 | 0 to 3000 | PX309-3KG5V | 225 | PX319-3KG5V | 225 | PX329-3KG5V | 275 |
| 0 to 345 | 0 to 5000 | PX309-5KG5V | 225 | PX319-5KG5V | 225 | PX329-5KG5V | 275 |
| 0 to 517 | 0 to 7500 | PX309-7.5KG5V | 225 | PX319-7.5KG5V | 225 | PX329-7.5KG5V | 275 |
| 0 to 690 | 0 to 10,000 | PX309-10KG5V | 225 | PX319-10KG5V | 225 | PX329-10KG5V | 275 |

*Comes complete with 5-point NIST-traceable calibration.*

*Notes: 1. Units 100 psig and above may be subjected to vacuum on the pressure port without damage. 2. For alternative performance specifications to suit your application, contact Engineering.*

*Ordering Examples: PX309-100G5V, 100 psi gage pressure transducer with 0 to 5 Vdc output and 1.5 m cable termination, $225.*

*PX319-015A5V, 15 psi absolute pressure transducer with 0 to 5 Vdc output and mini DIN termination, $245.*

*PX329-3KG5V, 3000 psi gage pressure transducer with 0 to 5 Vdc output and twist-lock termination, $275.*

*Mating connector sold separately; order PT06V-10-6S, $26.50. Consult Sales for OEM pricing.*

**ACCESSORIES**

| MODEL NO. | PRICE | DESCRIPTION |
|---|---|---|
| CAL-3 | $150.00 | Recalibration: 5-point NIST traceable |
| PT06V-10-6S | 26.50 | Mating connector for PX329 |
| CA-39-4PC22-5 | 90.00 | 4-conductor mating twist-lock connector with 1.5 m (5') cable for PX329 |
| CX5302 | 15.00 | Extra mini DIN connector for PX319 |

# HOW TO ORDER PX309 SERIES
## WITH 4 TO 20 mA OUTPUT

### PX309 Series
**4 to 20 mA Output**
**0-1 to 0-10,000 psi**
**0-70 mbar to 0-690 bar**


Starts at $225

Standard

- Gage or Absolute Pressure
- Low Pressure to 1 psig
- Rugged Solid State Design
- All Stainless Steel Construction
- High Stability, Low Drift
- 0.25% Static Accuracy

### 4 to 20 mA OUTPUT SPECIFICATIONS

**Excitation:** 9 to 30 Vdc (reverse polarity and overvoltage protected)
**Output:** 4 to 20 mA
**Static Accuracy 5 to 10,000 psi:** ±0.25% FS BSL at 25°C; includes linearity, hysteresis and repeatability
**Zero Offset:** ±2% FSO; ±4% for 1 and 2 psi ranges
**Span Setting:** ±2% FSO; ±4% for 1 and 2 psi ranges
**Compensated Temperature:**
≥5 psi Range: -20 to 85°C (-4 to 185°F)
≤5 psi Range: 0 to 50°C (32 to 122°F)
**Total Error Band:** ±2% FSO; Includes linearity, hysteresis, repeatability, thermal hysteresis and thermal errors (except 2 psi = ±3% and 1 psi = ±4.5%)

Metric thread adaptors available, see section C.

LOW-PRESSURE RANGES HIGHLIGHTED

### To Order (Specify Model Number)

| RANGE bar | RANGE psi | 1.5 m CABLE CONNECTION | PRICE | MINI DIN CONNECTION | PRICE | TWIST-LOCK CONNECTION | PRICE |
|---|---|---|---|---|---|---|---|
| **ABSOLUTE PRESSURE** | | | | | | | |
| 0 to 0.34 | 0 to 5 | PX309-005AI | $325 | PX319-005AI | $325 | PX329-005AI | $350 |
| 0 to 1 | 0 to 15 | PX309-015AI | 245 | PX319-015AI | 245 | PX329-015AI | 295 |
| 0 to 2.1 | 0 to 30 | PX309-030AI | 245 | PX319-030AI | 245 | PX329-030AI | 295 |
| 0 to 3.4 | 0 to 50 | PX309-050AI | 245 | PX319-050AI | 245 | PX329-050AI | 295 |
| 0 to 6.9 | 0 to 100 | PX309-100AI | 245 | PX319-100AI | 245 | PX329-100AI | 295 |
| 0 to 14 | 0 to 200 | PX309-200AI | 245 | PX319-200AI | 245 | PX329-200AI | 295 |
| 0 to 21 | 0 to 300 | PX309-300AI | 245 | PX319-300AI | 245 | PX329-300AI | 295 |
| **GAGE PRESSURE** | | | | | | | |
| 0 to 0.07 | 0 to 1 | PX309-001GI | $345 | PX319-001GI | $345 | PX329-001GI | $370 |
| 0 to 0.14 | 0 to 2 | PX309-002GI | 325 | PX319-002GI | 325 | PX329-002GI | 350 |
| 0 to 0.34 | 0 to 5 | PX309-005GI | 300 | PX319-005GI | 300 | PX329-005GI | 300 |
| 0 to 1 | 0 to 15 | PX309-015GI | 225 | PX319-015GI | 225 | PX329-015GI | 275 |
| 0 to 2.1 | 0 to 30 | PX309-030GI | 225 | PX319-030GI | 225 | PX329-030GI | 275 |
| 0 to 3.4 | 0 to 50 | PX309-050GI | 225 | PX319-050GI | 225 | PX329-050GI | 275 |
| 0 to 6.9 | 0 to 100 | PX309-100GI | 225 | PX319-100GI | 225 | PX329-100GI | 275 |
| 0 to 10 | 0 to 150 | PX309-150GI | 225 | PX319-150GI | 225 | PX329-150GI | 275 |
| 0 to 14 | 0 to 200 | PX309-200GI | 225 | PX319-200GI | 225 | PX329-200GI | 275 |
| 0 to 21 | 0 to 300 | PX309-300GI | 225 | PX319-300GI | 225 | PX329-300GI | 275 |
| 0 to 34 | 0 to 500 | PX309-500GI | 225 | PX319-500GI | 225 | PX329-500GI | 275 |
| 0 to 69 | 0 to 1000 | PX309-1KGI | 225 | PX319-1KGI | 225 | PX329-1KGI | 275 |
| 0 to 138 | 0 to 2000 | PX309-2KGI | 225 | PX319-2KGI | 225 | PX329-2KGI | 275 |
| 0 to 207 | 0 to 3000 | PX309-3KGI | 225 | PX319-3KGI | 225 | PX329-3KGI | 275 |
| 0 to 345 | 0 to 5000 | PX309-5KGI | 225 | PX319-5KGI | 225 | PX329-5KGI | 275 |
| 0 to 517 | 0 to 7500 | PX309-7.5KGI | 225 | PX319-7.5KGI | 225 | PX329-7.5KGI | 275 |
| 0 to 690 | 0 to 10,000 | PX309-10KGI | 225 | PX319-10KGI | 225 | PX329-10KGI | 275 |

*Comes complete with 5-point NIST-traceable calibration.*
*Notes: 1. Units 100 psig and above may be subjected to vacuum on the pressure port without damage. 2. For alternative performance specifications to suit your application, contact Engineering.*
***Ordering Examples:** PX309-100GI, 100 psi gage pressure transducer with 4 to 20 mA output and 1.5 m cable termination, $225. PX319-015AI, 15 psi absolute pressure transducer with 4 to 20 mA output and mini DIN termination, $300. PX329-3KGI, 3000 psi gage pressure transducer with 4 to 20 mA output and twist-lock termination, $275. Mating connector sold separately; order PT06V-10-6S, $26.50. Consult Sales for OEM pricing.*

**ACCESSORIES**

| MODEL NO. | PRICE | DESCRIPTION |
|---|---|---|
| CAL-3 | $150.00 | Recalibration: 5-point NIST traceable |
| PT06V-10-6S | 26.50 | Mating connector for PX329 |
| CA-39-4PC22-5 | 90.00 | 4-conductor mating twist-lock connector with 1.5 m (5') cable for PX329 |
| CX5302 | 15.00 | Extra mini DIN connector for PX319 |

# HOW TO ORDER PX309 SERIES
## CABLE TERMINATION TRANSDUCERS WITH 100 mV, 0 TO 5 Vdc, or 4 to 20 mA OUTPUTS

### PX309 Models
*1.5 m (5') Cable Termination*
*0-1 to 0-10,000 psia*
*0-70 mbar to 0-690 bar*

Metric thread adaptors available, see section C.

MOST POPULAR MODELS HIGHLIGHTED!

NIST Standard CE RoHS

Starts at $175

Cable style.

PX309-100GV, $175, cable termination, shown actual size.

- 5-Point NIST Traceable Calibration
- Gage or Absolute Pressure
- All Stainless Steel Construction
- Rugged Solid State Design
- High Stability, Low Drift
- 0.25% Accuracy

**To Order (Specify Model Number)**

| RANGE bar | RANGE psi | 10 mV/V OUTPUT MODEL NO. | mV PRICE | 0 to 5 Vdc OUTPUT MODEL NO. | 4 to 20 mA OUTPUT MODEL NO. | Amp PRICE |
|---|---|---|---|---|---|---|
| **ABSOLUTE PRESSURE** | | | | | | |
| 0 to 5 | 0 to 0.34 | PX309-005AV | $300 | PX309-005A5V | PX309-005AI | $325 |
| 0 to 15 | 0 to 1 | PX309-015AV | 195 | PX309-015A5V | PX309-015AI | 245 |
| 0 to 30 | 0 to 2.1 | PX309-030AV | 195 | PX309-030A5V | PX309-030AI | 245 |
| 0 to 50 | 0 to 3.4 | PX309-050AV | 195 | PX309-050A5V | PX309-050AI | 245 |
| 0 to 100 | 0 to 6.9 | PX309-100AV | 195 | PX309-100A5V | PX309-100AI | 245 |
| 0 to 200 | 0 to 14 | PX309-150AV | 195 | PX309-150A5V | PX309-150AI | 245 |
| 0 to 300 | 0 to 21 | PX309-200AV | 195 | PX309-200A5V | PX309-200AI | 245 |
| **GAGE PRESSURE** | | | | | | |
| 0 to 1 | 0 to 0.07 | PX309-001GV | $300 | PX309-001G5V | PX309-001GI | $345 |
| 0 to 2 | 0 to 0.14 | PX309-002GV | 300 | PX309-002G5V | PX309-002GI | 325 |
| 0 to 5 | 0 to 0.34 | PX309-005GV | 300 | PX309-005G5V | PX309-005GI | 300 |
| 0 to 15 | 0 to 1 | PX309-015GV | 175 | PX309-015G5V | PX309-015GI | 225 |
| 0 to 30 | 0 to 2.1 | PX309-030GV | 175 | PX309-030G5V | PX309-030GI | 225 |
| 0 to 50 | 0 to 3.4 | PX309-050GV | 175 | PX309-050G5V | PX309-050GI | 225 |
| 0 to 100 | 0 to 6.9 | PX309-100GV | 175 | PX309-100G5V | PX309-100GI | 225 |
| 0 to 150 | 0 to 10.3 | PX309-150GV | 175 | PX309-150G5V | PX309-150GI | 225 |
| 0 to 200 | 0 to 14 | PX309-200GV | 175 | PX309-200G5V | PX309-200GI | 225 |
| 0 to 300 | 0 to 21 | PX309-300GV | 175 | PX309-300G5V | PX309-300GI | 225 |
| 0 to 500 | 0 to 34 | PX309-500GV | 175 | PX309-500G5V | PX309-500GI | 225 |
| 0 to 1000 | 0 to 69 | PX309-1KGV | 175 | PX309-1KG5V | PX309-1KGI | 225 |
| 0 to 2000 | 0 to 138 | PX309-2KGV | 175 | PX309-2KG5V | PX309-2KGI | 225 |
| 0 to 3000 | 0 to 207 | PX309-3KGV | 175 | PX309-3KG5V | PX309-3KGI | 225 |
| 0 to 5000 | 0 to 345 | PX309-5KGV | 175 | PX309-5KG5V | PX309-5KGI | 225 |
| 0 to 7500 | 0 to 517 | PX309-7.5KGV | 175 | PX309-7.5KG5V | PX309-7.5KGI | 225 |
| 0 to 10,000 | 0 to 690 | PX309-10KGV | 175 | PX309-10KG5V | PX309-10KGI | 225 |

*Comes complete with 5-point NIST-traceable calibration.*

*Note: Ranges 100 psi and above may be subjected to a vacuum on the process port without damage.*

*Ordering Examples: PX309-100GV, 100 psi gage pressure transducer 10 mV/V output and 1.5 m (5') cable termination, $175.*
*PX309-030A5V, 30 psi absolute pressure transducer with 0 to 5 Vdc output and 1.5 m (5') cable termination, $245.*
*PX309-3KGI, 3000 psi gage pressure transducer with 4 to 20 mA output and 1.5 m (5') cable termination, $225.*

ACCESSORIES

| MODEL NO. | PRICE | DESCRIPTION |
|---|---|---|
| DP25B-S | $245 | 4-digit strain meter for mV/V models |
| DP25B-E | 245 | 4-digit process meter for amplified models |
| CAL-3 | 150 | Recalibration with 5-pt NIST traceable documentation |

B-35

# HOW TO ORDER PX309 SERIES

## mini DIN CONNECTOR WITH 100 mV, 0 TO 5 Vdc, or 4 to 20 mA OUTPUTS



### PX319 Models

*mini DIN Connector Series*
*0-1 to 0-10,000 psia*
*0-70 mbar to 0-690 bar*

Starts at $175

NIST CE RoHS

Standard

PX319-100GV, $175, mini DIN connector style, shown actual size.

- 5-Point NIST Traceable Calibration
- Gage or Absolute Pressure
- All Stainless Steel Construction
- Rugged Solid State Design
- High Stability, Low Drift
- 0.25% Accuracy

Metric thread adaptors available, see section C.

MOST POPULAR MODELS HIGHLIGHTED!

**To Order (Specify Model Number)**

| RANGE psi | RANGE bar | 10 mV/V OUTPUT MODEL NO. | mV PRICE | 0 to 5 Vdc OUTPUT MODEL NO. | 4 to 20 mA OUTPUT MODEL NO. | Amp PRICE |
|---|---|---|---|---|---|---|
| **ABSOLUTE PRESSURE** | | | | | | |
| 0 to 5 | 0 to 0.34 | PX319-005AV | $300 | PX319-005A5V | PX319-005AI | $325 |
| 0 to 15 | 0 to 1 | PX319-015AV | 195 | PX319-015A5V | PX319-015AI | 245 |
| 0 to 30 | 0 to 2.1 | PX319-030AV | 195 | PX319-030A5V | PX319-030AI | 245 |
| 0 to 50 | 0 to 3.4 | PX319-050AV | 195 | PX319-050A5V | PX319-050AI | 245 |
| 0 to 100 | 0 to 6.9 | PX319-100AV | 195 | PX319-100A5V | PX319-100AI | 245 |
| 0 to 200 | 0 to 14 | PX319-150AV | 195 | PX319-150A5V | PX319-150AI | 245 |
| 0 to 300 | 0 to 21 | PX319-200AV | 195 | PX319-200A5V | PX319-200AI | 245 |
| **GAGE PRESSURE** | | | | | | |
| 0 to 1 | 0 to 0.07 | PX319-001GV | $300 | PX319-001G5V | PX319-001GI | $345 |
| 0 to 2 | 0 to 0.14 | PX319-002GV | 300 | PX319-002G5V | PX319-002GI | 325 |
| 0 to 5 | 0 to 0.34 | PX319-005GV | 300 | PX319-005G5V | PX319-005GI | 300 |
| 0 to 15 | 0 to 1 | PX319-015GV | 175 | PX319-015G5V | PX319-015GI | 225 |
| 0 to 30 | 0 to 2.1 | PX319-030GV | 175 | PX319-030G5V | PX319-030GI | 225 |
| 0 to 50 | 0 to 3.4 | PX319-050GV | 175 | PX319-050G5V | PX319-050GI | 225 |
| 0 to 100 | 0 to 6.9 | PX319-100GV | 175 | PX319-100G5V | PX319-100GI | 225 |
| 0 to 150 | 0 to 10.3 | PX319-150GV | 175 | PX319-150G5V | PX319-150GI | 225 |
| 0 to 200 | 0 to 14 | PX319-200GV | 175 | PX319-200G5V | PX319-200GI | 225 |
| 0 to 300 | 0 to 21 | PX319-300GV | 175 | PX319-300G5V | PX319-300GI | 225 |
| 0 to 500 | 0 to 34 | PX319-500GV | 175 | PX319-500G5V | PX319-500GI | 225 |
| 0 to 1000 | 0 to 69 | PX319-1KGV | 175 | PX319-1KG5V | PX319-1KGI | 225 |
| 0 to 2000 | 0 to 138 | PX319-2KGV | 175 | PX319-2KG5V | PX319-2KGI | 225 |
| 0 to 3000 | 0 to 207 | PX319-3KGV | 175 | PX319-3KG5V | PX319-3KGI | 225 |
| 0 to 5000 | 0 to 345 | PX319-5KGV | 175 | PX319-5KG5V | PX319-5KGI | 225 |
| 0 to 7500 | 0 to 517 | PX319-7.5KGV | 175 | PX319-7.5KG5V | PX319-7.5KGI | 225 |
| 0 to 10,000 | 0 to 690 | PX319-10KGV | 175 | PX319-10KG5V | PX319-10KGI | 225 |

*Comes complete with 5-point NIST traceable calibration and mating mini DIN connector*

*Note: Ranges 100 psi and above may be subjected to a vacuum on the process port without damage.*

*Ordering Examples: PX319-100GV, 100 psi gage pressure transducer 10 mV/V output and mini DIN connector termination, $175.*

*PX319-030A5V, 30 psi absolute pressure transducer 0 to 5 Vdc output and mini DIN connector termination, $245.*

*PX319-3KGI, 3000 psi gage pressure transducer 4 to 20 mA output and mini DIN connector termination, $225.*

ACCESSORIES

| MODEL NO. | PRICE | DESCRIPTION |
|---|---|---|
| DP2SB-S | $245 | 4-digit strain meter for mV/V models |
| DP2SB-E | 245 | 4-digit process meter for amplified models |
| CX5302 | 15 | Spare mini DIN connector for PX319 |
| CAL-3 | 150 | Recalibration with 5-pt NIST traceable documentation |

B-36

# HOW TO ORDER PX309 SERIES
## TWIST-LOCK CONNECTOR WITH 100 mV, 0 TO 5 Vdc, OR 4 TO 20 mA OUTPUTS

### PX329 Models
**Twist-Lock Connector Series**
**0-1 to 0-10,000 psia**
**0-70 mbar to 0-690 bar**

Starts at $215

NIST CE RoHS

Standard

PX329-100GV, $215, twist-lock connector, show actual size.

PX329 Mating Connector PT06V-10-6S $26.50

- 5-Point NIST Traceable Calibration
- Gage or Absolute Pressure
- All Stainless Steel Construction
- Rugged Solid State Design
- High Stability, Low Drift
- 0.25% Accuracy

Metric thread adaptors available, see section C.

☐ MOST POPULAR MODELS HIGHLIGHTED!

**To Order (Specify Model Number)**

| RANGE psi | RANGE bar | 10 mV/V OUTPUT MODEL NO. | mV PRICE | 0 to 5 Vdc OUTPUT MODEL NO. | 4 to 20 mA OUTPUT MODEL NO. | Amp PRICE |
|---|---|---|---|---|---|---|
| **ABSOLUTE PRESSURE** | | | | | | |
| 0 to 5 | 0 to 0.34 | PX329-005AV | $300 | PX329-005A5V | PX329-005AI | $325 |
| 0 to 15 | 0 to 1 | PX329-015AV | 235 | PX329-015A5V | PX329-015AI | 245 |
| 0 to 30 | 0 to 2.1 | PX329-030AV | 235 | PX329-030A5V | PX329-030AI | 245 |
| 0 to 50 | 0 to 3.4 | PX329-050AV | 235 | PX329-050A5V | PX329-050AI | 245 |
| 0 to 100 | 0 to 6.9 | PX329-100AV | 235 | PX329-100A5V | PX329-100AI | 245 |
| 0 to 200 | 0 to 14 | PX329-150AV | 235 | PX329-150A5V | PX329-150AI | 245 |
| 0 to 300 | 0 to 21 | PX329-200AV | 235 | PX329-200A5V | PX329-200AI | 245 |
| **GAGE PRESSURE** | | | | | | |
| 0 to 1 | 0 to 0.07 | PX329-001GV | $300 | PX329-001G5V | PX329-001GI | $370 |
| 0 to 2 | 0 to 0.14 | PX329-002GV | 300 | PX329-002G5V | PX329-002GI | 350 |
| 0 to 5 | 0 to 0.34 | PX329-005GV | 300 | PX329-005G5V | PX329-005GI | 325 |
| 0 to 15 | 0 to 1 | PX329-015GV | 215 | PX329-015G5V | PX329-015GI | 275 |
| 0 to 30 | 0 to 2.1 | PX329-030GV | 215 | PX329-030G5V | PX329-030GI | 275 |
| 0 to 50 | 0 to 3.4 | PX329-050GV | 215 | PX329-050G5V | PX329-050GI | 275 |
| 0 to 100 | 0 to 6.9 | PX329-100GV | 215 | PX329-100G5V | PX329-100GI | 275 |
| 0 to 150 | 0 to 10.3 | PX329-150GV | 215 | PX329-150G5V | PX329-150GI | 275 |
| 0 to 200 | 0 to 14 | PX329-200GV | 215 | PX329-200G5V | PX329-200GI | 275 |
| 0 to 300 | 0 to 21 | PX329-300GV | 215 | PX329-300G5V | PX329-300GI | 275 |
| 0 to 500 | 0 to 34 | PX329-500GV | 215 | PX329-500G5V | PX329-500GI | 275 |
| 0 to 1000 | 0 to 69 | PX329-1KGV | 215 | PX329-1KG5V | PX329-1KGI | 275 |
| 0 to 2000 | 0 to 138 | PX329-2KGV | 215 | PX329-2KG5V | PX329-2KGI | 275 |
| 0 to 3000 | 0 to 207 | PX329-3KGV | 215 | PX329-3KG5V | PX329-3KGI | 275 |
| 0 to 5000 | 0 to 345 | PX329-5KGV | 215 | PX329-5KG5V | PX329-5KGI | 275 |
| 0 to 7500 | 0 to 517 | PX329-7.5KGV | 215 | PX329-7.5KG5V | PX3297.5KGI | 275 |
| 0 to 10,000 | 0 to 690 | PX329-10KGV | 215 | PX329-10KG5V | PX329-10KGI | 275 |

*Comes complete with 5-point NIST traceable calibration. Mating connector sold separately, see accessories.*

*Note: Ranges 100 psi and above may be subjected to a vacuum on the process port without damage.*

*Ordering Examples: PX329-100GV, 100 psi gage pressure transducer 10 mV/V output and twist-lock connector termination, $215.*

*PX329-030A5V, 30 psi absolute pressure transducer 0 to 5 Vdc output and twist-lock connector termination, $245.*

*PX329-3KGI, 3,000 psi gage pressure transducer 4 to 20 mA output and twist-lock connector termination, $275.*

*Mating connector sold separately, specify model PT06V-10-6S, $26.50.*

ACCESSORIES

| MODEL NO. | PRICE | DESCRIPTION |
|---|---|---|
| DP25B-S | $245.00 | 4-digit strain meter for mV/V models |
| DP25B-E | 245.00 | 4-digit process meter for amplified models |
| PT06V-10-6S | 26.50 | Mating twist-lock connector for PX329 |
| CA-39-4-PC22-5 | 90.00 | 1.5 m (5'), 4-conductor cable with mating twist-lock connector for PX329 |
| CAL-3 | 150.00 | Recalibration with 5 pt NIST traceable documentation |

B-37

# HOW TO ORDER PX309 SERIES

## M12 CONNECTOR WITH 100 mV, 0 TO 5 Vdc, OR 4 TO 20 mA OUTPUTS



### PX359 Models

*M12 Connector Series*
*0-1 to 0-10,000 psia*
*0-70 mbar to 0-690 bar*

Starts at $195

Standard


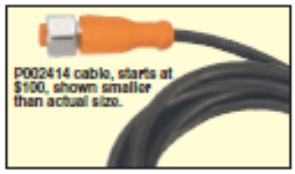


- 5-Point NIST Traceable Calibration
- Gage or Absolute Pressure
- All Stainless Steel Construction
- Rugged solid State Design
- High Stability, Low Drift
- 0.25% Accuracy

MOST POPULAR MODELS HIGHLIGHTED!

**To Order (Specify Model Number)**

| RANGE psi | RANGE bar | 10 mV/V OUTPUT MODEL NO. | mV PRICE | 0 to 5 Vdc OUTPUT MODEL NO. | 4 to 20 mA OUTPUT MODEL NO. | Amp PRICE |
|---|---|---|---|---|---|---|
| **ABSOLUTE PRESSURE** | | | | | | |
| 0 to 5 | 0 to 0.34 | PX359-005AV | $320 | PX359-005A5V | PX359-005AI | $345 |
| 0 to 15 | 0 to 1 | PX359-015AV | 215 | PX359-015A5V | PX359-015AI | 265 |
| 0 to 30 | 0 to 2.1 | PX359-030AV | 215 | PX359-030A5V | PX359-030AI | 265 |
| 0 to 50 | 0 to 3.4 | PX359-050AV | 215 | PX359-050A5V | PX359-050AI | 265 |
| 0 to 100 | 0 to 6.9 | PX359-100AV | 215 | PX359-100A5V | PX359-100AI | 265 |
| 0 to 200 | 0 to 14 | PX359-150AV | 215 | PX359-150A5V | PX359-150AI | 265 |
| 0 to 300 | 0 to 21 | PX359-200AV | 215 | PX359-200A5V | PX359-200AI | 265 |
| **GAGE PRESSURE** | | | | | | |
| 0 to 1 | 0 to 0.07 | PX359-001GV | $320 | PX359-001G5V | PX359-001GI | $365 |
| 0 to 2 | 0 to 0.14 | PX359-002GV | 320 | PX359-002G5V | PX359-002GI | 345 |
| 0 to 5 | 0 to 0.34 | PX359-005GV | 320 | PX359-005G5V | PX359-005GI | 320 |
| 0 to 15 | 0 to 1 | PX359-015GV | 195 | PX359-015G5V | PX359-015GI | 245 |
| 0 to 30 | 0 to 2.1 | PX359-030GV | 195 | PX359-030G5V | PX359-030GI | 245 |
| 0 to 50 | 0 to 3.4 | PX359-050GV | 195 | PX359-050G5V | PX359-050GI | 245 |
| 0 to 100 | 0 to 6.9 | PX359-100GV | 195 | PX359-100G5V | PX359-100GI | 245 |
| 0 to 150 | 0 to 10.3 | PX359-150GV | 195 | PX359-150G5V | PX359-150GI | 245 |
| 0 to 200 | 0 to 14 | PX359-200GV | 195 | PX359-200G5V | PX359-200GI | 245 |
| 0 to 300 | 0 to 21 | PX359-300GV | 195 | PX359-300G5V | PX359-300GI | 245 |
| 0 to 500 | 0 to 34 | PX359-500GV | 195 | PX359-500G5V | PX359-500GI | 245 |
| 0 to 1000 | 0 to 69 | PX359-1KGV | 195 | PX359-1KG5V | PX359-1KGI | 245 |
| 0 to 2000 | 0 to 138 | PX359-2KGV | 195 | PX359-2KG5V | PX359-2KGI | 245 |
| 0 to 3000 | 0 to 207 | PX359-3KGV | 195 | PX359-3KG5V | PX359-3KGI | 245 |
| 0 to 5000 | 0 to 345 | PX359-5KGV | 195 | PX359-5KG5V | PX359-5KGI | 245 |
| 0 to 7500 | 0 to 517 | PX359-7.5KGV | 195 | PX359-7.5KG5V | PX359-7.5KGI | 245 |
| 0 to 10,000 | 0 to 690 | PX359-10KGV | 195 | PX359-10KG5V | PX359-10KGI | 245 |

*Comes complete with 5-point NIST traceable calibration. M12 cables sold separately, see accessories.*

*Note: Ranges 100 psi and above may be subjected to a vacuum on the process port without damage.*

*Ordering Examples: PX359-100GV, 100 psi gage pressure transducer 10 mV/V output and M12 connector termination, $195.*

*PX359-030A5V, 30 psi absolute pressure transducer 0 to 5 Vdc output and M12 connector termination, $265.*

*PX359-3KGI, 3000 psi gage pressure transducer 4 to 20 mA output and M12 connector termination, $245.*

*P002414-1, 2 m (6') vented cable for PX359, $100.*

ACCESSORIES

| MODEL NO. | PRICE | DESCRIPTION |
|---|---|---|
| DP25B-S | $245.00 | 4-digit strain meter for mV/V models |
| DP25B-E | 245.00 | 4-digit process meter for amplified models |
| PT06V-10-6S | 26.50 | Mating connector for PX359 |
| P002414-1 | 100.00 | 2 m (6') vented cable with M12 connector for PX359 for gage ranges >100 psi |
| P002414-2 | 150.00 | 5 m (16') vented cable with M12 connector for PX359 for gage ranges >100 psi |
| M12C-PVC-4-S-F-5 | 15.50 | 5 m (16') PVC cable, straight 4-pin M12 female connector one end, flying leads one end, for all PX359 absolute ranges and gage ranges >100 psi |
| CAL-3 | 150.00 | Recalibration with 5 pt NIST traceable documentation |

Manufacturer: Omega
Model: PX209-300G5V
Serial #: 96607
Range: 0-300 psig
Output: 0-5 V

| Omega | 96607 |
|---|---|
| psi | V |
| 0 | 0.007768 |
| 45 | 0.752937 |
| 85 | 1.41574 |
| 125 | 2.0842 |
| 165 | 2.75135 |
| 195 | 3.24126 |
| 225 | 3.74351 |
| 265 | 4.41035 |
| 285 | 4.74641 |
| 265 | 4.41414 |
| 225 | 3.74935 |
| 195 | 3.41325 |
| 165 | 2.74854 |
| 125 | 2.08291 |
| 85 | 1.41223 |
| 45 | 0.749362 |
| 0 | 0.003529 |

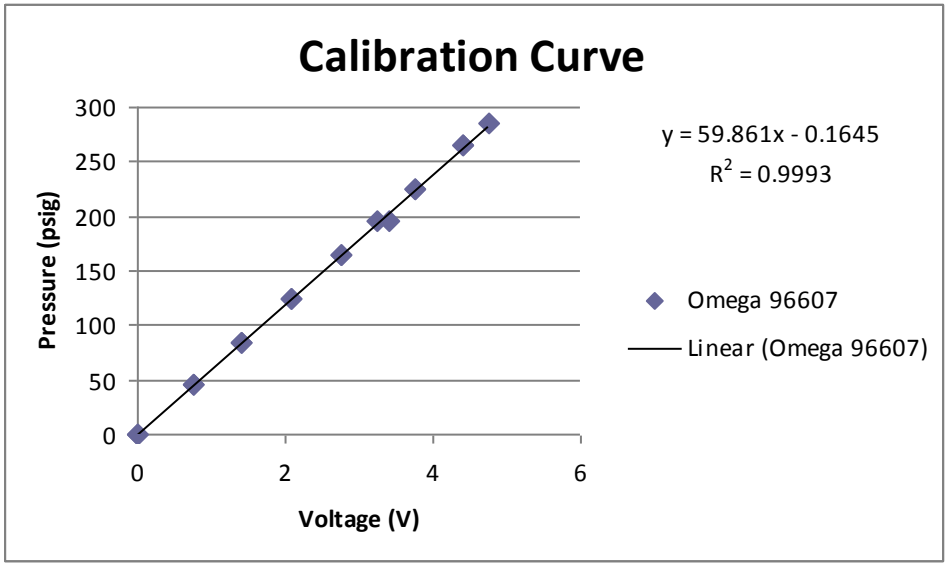

Manufacturer: Omega
Model: PX209-300G5V
Serial #: 96611
Range: 0-300 psig
Output: 0-5 V

| Omega | 96611 |
|---|---|
| psi | V |
| 0 | 0.016788 |
| 45 | 0.760901 |
| 85 | 1.42698 |
| 125 | 2.08748 |
| 165 | 2.75308 |
| 195 | 3.25389 |
| 225 | 3.75272 |
| 265 | 4.41966 |
| 285 | 4.75332 |
| 265 | 4.42015 |
| 225 | 3.75544 |
| 195 | 3.42255 |
| 165 | 2.75675 |
| 125 | 2.08668 |
| 85 | 1.42146 |
| 45 | 0.754826 |
| 0 | 0.00815 |

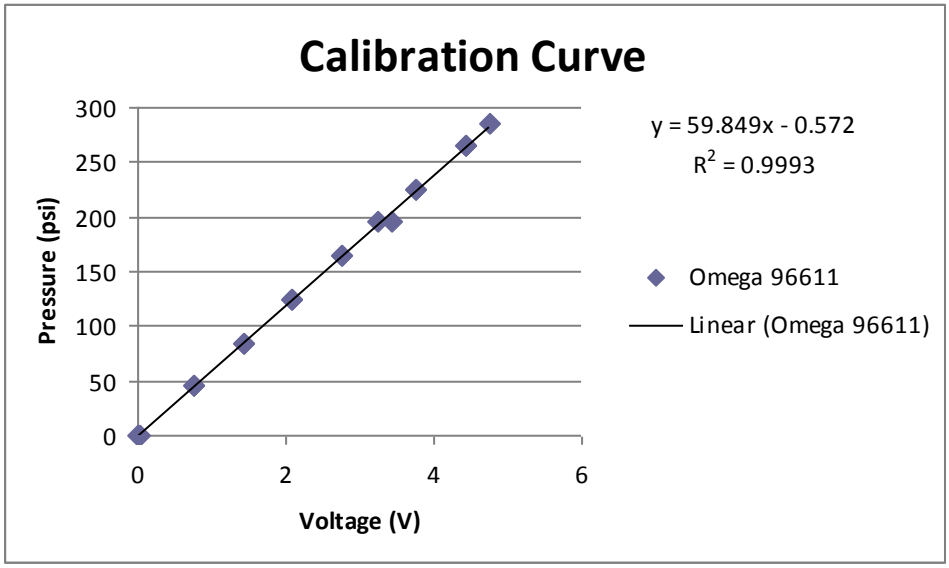

Manufacturer: Omega
Model: PX309-500G5V
Serial #: 103110D854
Range: 0-500 psig
Output: 0-5 V

| Omega | 103110D854 |
|---|---|
| psi | V |
| 0 | 0.00108 |
| 45 | 0.448694 |
| 85 | 0.845774 |
| 125 | 1.24397 |
| 165 | 1.64328 |
| 195 | 1.94213 |
| 225 | 2.2415 |
| 265 | 2.64023 |
| 285 | 2.83955 |
| 265 | 2.6403 |
| 225 | 2.24126 |
| 195 | 1.94184 |
| 165 | 1.64266 |
| 125 | 1.24356 |
| 85 | 0.845765 |
| 45 | 0.448766 |
| 0 | 0.002105 |

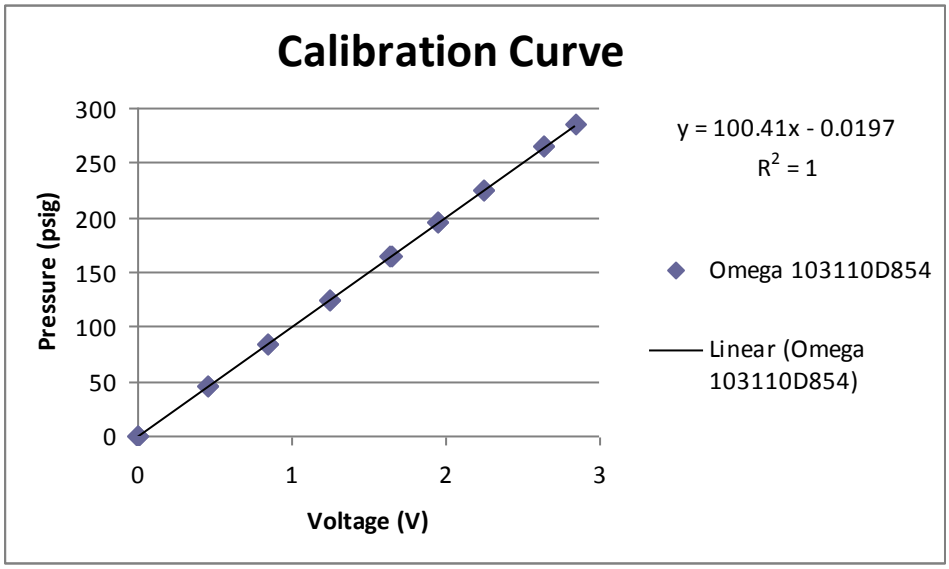

# Fox Venturi Products

Fox Valve Development Corp, 85 Franklin Road, Dover, NJ 07801 USA
973-328-1011 Fax: 973-328-6972
e-mail: mark@foxvalve.com www: foxvalve.com

**Attn: Matthew Hitt** November 14, 2011
**University of Alabama in Huntsville**
Huntsville, AL 35899

Tel: 256-824-2863
Email: mah0004@uah.edu

Ref: **Liquid Nitrogen Cavitating Venturi - 1" male AN**
**Fox PN: 610722-72**

Matthew,

Thanks for this inquiry.

Per your request, please see the following quote for the 1" AN cavitating venturi, as per Fox Valve P/N: 610722-72.

Per your request this part will not be calibrated by Fox Valve.

We are pleased to offer the following:

**Item #1: Liquid Nitrogen cavitating venturi; CT-1**
**Fox P/N: 610722-72 - 1" male AN Venturi**

| | |
|---|---|
| **Fluid Media :** | LN2, 47.17 lbs/ft3,<br>Vapor pressure = 46.72psia |
| **Line Size** | 1" (0.834" ID) |
| **Material** | 316ss |
| **Design Conditions:** | *Best Effort* - Approx. 3 lbs/sec at 250psia |
| **Throat Dia:** | Approx. = 0.26" |
| **Configuration:** | 1" male AN ends<br>NO Pressure tap connections |

| | |
|---|---|
| **Budget Cost:** | **$1,675 each**, FOB ship point |
| **Delivery:** | About 5-6 weeks, ARO - *for manufacture* |

**Calibration not included.**

**Delivery:** 5-6 weeks, ARO - *for manufacture*

# Fox Venturi Products

Fox Valve Development Corp, 85 Franklin Road, Dover, NJ 07801 USA
973-328-1011 Fax: 973-328-6972
e-mail: mark@foxvalve.com www: foxvalve.com

---

*The above quote is based on the following:*

1) *Does not include any calibration / flow testing, dye pentrant test, radiography of welds, Source Inspection, noise tests nor any procedures or submissions not explicitly stated in the above as included with this quotation.*
2) *No special cleaning, marking, or packaging .*
4) *Part will be shipped with standard commercial installation & Operating instructions (2 sets).*

**Fox terms - warranty and delivery ONLY apply:**

2. **Delivery:** (a) Fox will endeavor to fill all orders on time. All quoted deliveries or 'ship dates' are estimated ship dates made in **good faith.** ( b) Fox assumes no liability for loss or consequential damages resulting from non-delivery of goods by a specific date. Fox will not be responsible for delays beyond our control, such as fire, flood, strikes, accidents and carrier delays. (c) There are no circumstances where Fox is responsible for paying overnight, air-freight or rush delivery of equipment. This would constitute a 'de facto' penalty clause for late shipment, and penalty clauses for late shipment will never be accepted as part of a purchase order to Fox Valve. (d) All expedited orders - for which a special premium has been added to the cost of supplied equipment — are accepted on a "Best Effort Basis". Premium charges for shipments not meeting the expedited date are charged on a pro-rated basis by mutual agreement.

3. **Warranty**

a) All Fox products are warranted to be free from defects of workmanship or material. In the event Fox delivers non-conforming goods or parts, Fox will be liable only to repair or replace, at our option, such non-conforming goods/parts, FOB our shop, provided such items are proven to be non-conforming to Fox's satisfaction within one (1) year (60 days for solids conveying eductors) from the date of original shipment. Any item received deemed to be defective should be returned immediately.

b) Fox will not be liable for any indirect, special, consequential or liquidated damages, penalties or related costs with respect to performance of Fox equipment. Fox shall also not be liable for expenses relating to erection or disconnecting or losses resulting from any alleged defect or design inadequacy. Fox Valve's total financial liability from a purchase order is limited to the value of that purchase order, i.e. - the return of equipment for a refund of purchase price.

c) Fox does not make material selection decisions when handling corrosives. Material selection is made by Fox's customer. Fox therefore provides no warranty regarding the service life of Fox equipment when installed in corrosive applications.

Regards and thanks,

**Mark Edgar**
Application Engineering

*2*

**4700F-XXX-CS Series Full Port Valve**

**4700F-XXX-S6 Series Full Port Valve**

| Quick Spec | |
|---|---|
| **Product Scope** | |
| Size Range | 1/2" – 4", Full Port |
| Body Type | 3-pc, non swing-out w/FNPT ends (weld ends optional) |
| Pressure Rating | 1/2" to 2": 2000 psi WOG (138 bar)<br>2-1/2" to 4": 1000 psi WOG (69 bar) |
| Temperature Range / WSP | -20°F thru 450°F / 150 psi Steam<br>-29°C thru 232°C / 10.3 bar Steam |
| Body | Stainless or Carbon Steel Body |
| Ball & Stem | Stainless Steel, Anti-Static Design |
| Ball Seats | RPTFE |
| Stem Packing & Seals | Adjustable, Live Loaded Grafoil w/Viton o-ring Stem & Graphite body |
| Operator/Mounting Pad | Manual Locking Lever / ISO 5211 |
| **Design Standards** | |
| Design | ANSI B16.34, Class 600 |
| Thread Design | ASME B1.20.1 |
| **Testing Standards** | |
| Pressure Testing | API 598 |
| **Approvals** | |
| CRN#C2628.5 | |
| API 607, 5th Ed. | |

### Features

- Investment cast body construction
- ISO 5211 actuator mounting pad
- Blow-out proof stem
- Reinforced PTFE seats
- Adjustable, live loaded PTFE stem packing
- API 598 inspection and testing
- API 607 5th Edition fire tested
- Locking lever operator

**Durlon®700 Pressure/Temperature Ratings**

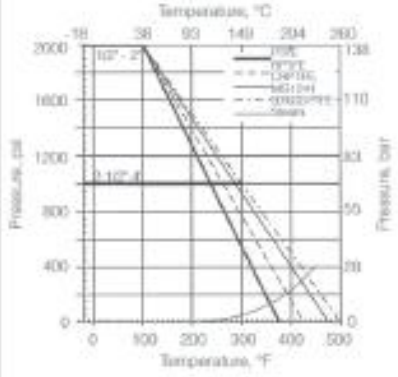


| Materials of Construction (1/2" - 2") | | |
|---|---|---|
| Part | Carbon Steel | Stainless Steel |
| Body | WCB | CF8M |
| End Cap | WCB | CF8M |
| Seat | RPTFE | |
| Ball | CF8M/316 | |
| Stem | AISI 316 | |
| Seal, Body | Graphite | |
| Thrust Washer | RPTFE | |
| Packing | Grafoil | |
| Belleville Spring Washer | AISI 301 | |
| Gland Ring | AISI 304 | |
| Handle, Locking | | |
| Nut, Stem | | |
| Stop Screw | | |
| Locking Tab | | |
| Cover, Handle | Vinyl | |
| Bolt, Body | A2-70 | B8 |
| O-Ring Stem | Viton | |
| Antistatic Ball | AISI 316 | |
| Antistatic Spring | | |
| Name Plate | SS | |

Refer to page 4 for 2-1/2" – 4" size Materials of Construction

| Technical Specifications | |
|---|---|
| Valve Size Inches | Flow Coefficient, Cv |
| 1/2" | 17 |
| 3/4" | 34 |
| 1" | 57 |
| 1-1/4" | 80 |
| 1-1/2" | 143 |
| 2" | 245 |
| 2-1/2" | 562 |
| 3" | 700 |
| 4" | 1200 |

| Technical Specifications, metric | |
|---|---|
| Valve Size NPS | Flow Coefficient, Kv |
| DN15 | 14.6 |
| DN20 | 29.2 |
| DN25 | 49.0 |
| DN32 | 68.8 |
| DN40 | 123 |
| DN50 | 211 |
| DN65 | 483 |
| DN80 | 602 |
| DN100 | 1032 |

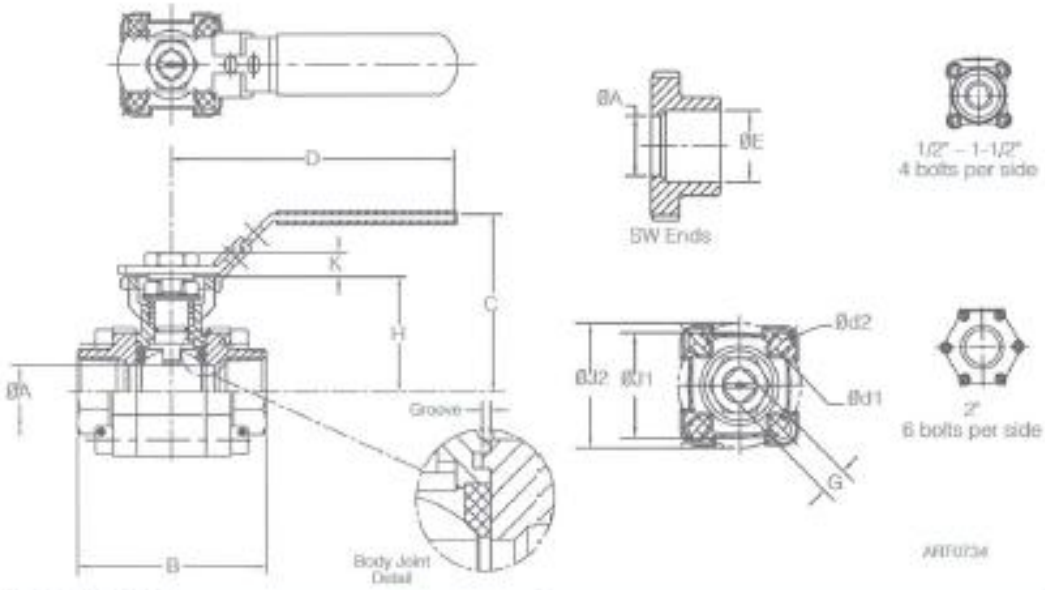


**Dimensions, Inches**

| Valve Size | Size Range 1/2" – 2" | | | | | | | | | | | | | | |
|---|---|---|---|---|---|---|---|---|---|---|---|---|---|---|---|
| Inches | ØA | B | C | D | ØE | G Sq. | H | K | ISO Pattern | ØJ1 (BC) | ØJ2 (BC) | Ød1 | Ød2 | ISO Pattern | Weight, lbs |
| 1/2" | 0.63 | 2.95 | 2.8 | 4.4 | 0.80 | 0.354 | 1.67 | 0.35 | F03 | 1.42 | 1.65 | 0.24 | 0.24 | F04 | 1.9 |
| 3/4" | 0.79 | 3.15 | 2.9 | 4.4 | 1.07 | 0.354 | 1.78 | 0.32 | F03 | 1.42 | 1.65 | 0.24 | 0.24 | F04 | 2.3 |
| 1" | 0.95 | 3.54 | 3.0 | 5.3 | 1.34 | 0.433 | 2.13 | 0.46 | F04 | 1.65 | 1.97 | 0.24 | 0.28 | F05 | 3.8 |
| 1-1/4" | 1.26 | 4.33 | 3.5 | 5.3 | 1.68 | 0.433 | 2.13 | 0.46 | F04 | 1.65 | 1.97 | 0.24 | 0.28 | F05 | 5.7 |
| 1-1/2" | 1.50 | 4.72 | 4.3 | 6.5 | 1.92 | 0.551 | 2.89 | 0.58 | F06 | 1.97 | 2.76 | 0.28 | 0.35 | F07 | 8.2 |
| 2" | 1.97 | 5.51 | 4.7 | 6.5 | 2.41 | 0.551 | 3.26 | 0.58 | F05 | 1.97 | 2.76 | 0.28 | 0.35 | F07 | 14.6 |

**Dimensions, mm**

| Valve Size | Size Range DN15 – DN50 | | | | | | | | | | | | | | |
|---|---|---|---|---|---|---|---|---|---|---|---|---|---|---|---|
| NPS | ØA | B | C | D | ØE | G Sq. | H | K | ISO Pattern | ØJ1 (BC) | ØJ2 (BC) | Ød1 | Ød2 | ISO Pattern | Weight, kgs |
| DN15 | 16,0 | 74,9 | 71 | 110 | 21,8 | 9 | 42,4 | 8,8 | F03 | 36,1 | 41,9 | 6,0 | 6,0 | F04 | 0,9 |
| DN20 | 20,1 | 80,0 | 74 | 110 | 27,2 | 9 | 44,7 | 8,8 | F03 | 36,1 | 41,9 | 6,0 | 6,0 | F04 | 1,0 |
| DN25 | 24,4 | 89,9 | 84 | 135 | 34,0 | 11 | 54,1 | 10,8 | F04 | 41,9 | 50,0 | 6,0 | 7,0 | F05 | 1,7 |
| DN32 | 32,0 | 110 | 90 | 135 | 42,7 | 11 | 59,2 | 10,8 | F04 | 41,9 | 50,0 | 6,0 | 7,0 | F05 | 2,6 |
| DN40 | 38,1 | 120 | 110 | 165 | 48,8 | 14 | 73,4 | 14,8 | F06 | 50,0 | 70,1 | 7,0 | 9,0 | F07 | 3,7 |
| DN50 | 50,0 | 140 | 119 | 135 | 61,2 | 14 | 82,8 | 14,8 | F05 | 50,0 | 70,1 | 7,0 | 9,0 | F07 | 6,6 |

**Technical Specifications**

| Valve Size | | Operating Torque, in-lb | | | | | |
|---|---|---|---|---|---|---|---|
| Inches | NPS | 0 – 1250 psi | 0 – 86,2 bar | 1500 psi | 103 bar | 2000 psi | 138 bar |
| 1/2" | DN15 | 45 | 5,1 | 45 | 5,1 | 45 | 5,1 |
| 3/4" | DN20 | 70 | 7,9 | 70 | 7,9 | 70 | 7,9 |
| 1" | DN25 | 130 | 14,7 | 130 | 14,7 | 130 | 14,7 |
| 1-1/4" | DN32 | 190 | 21,5 | 190 | 21,5 | 250 | 28 |
| 1-1/2" | DN40 | 250 | 28 | 350 | 40 | 550 | 62 |
| 2" | DN50 | 400 | 45 | 800 | 90 | 1600 | 181 |

Operating torques in table are for RPTFE seats. For PTFE seats, multiply by 0,87; for CRPTFE (15% Glass PTFE), and 60% SS PTFE, multiply by 1,09. Include an appropriate service factor for sizing actuators.

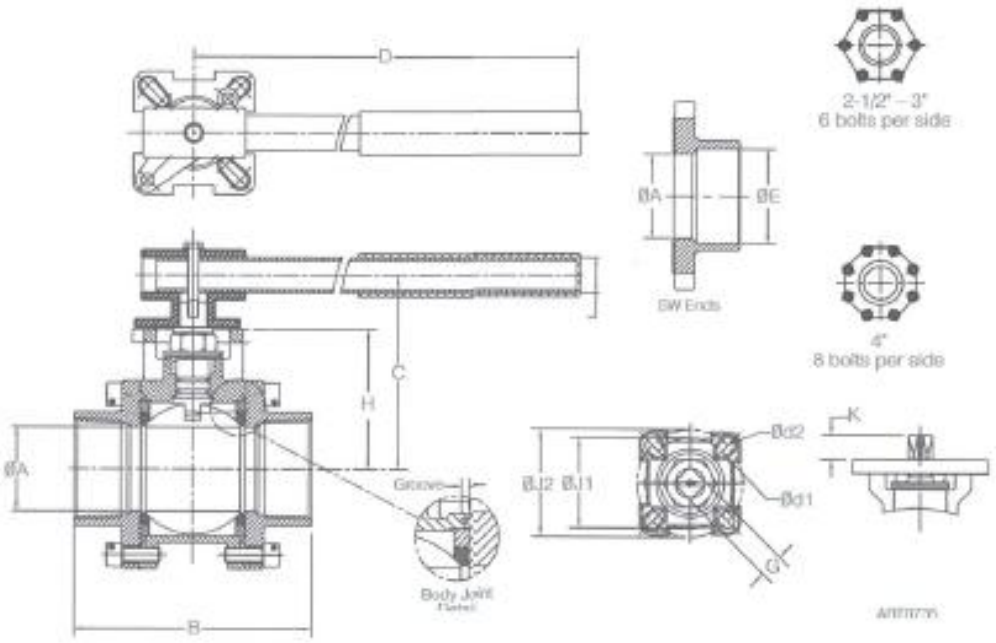


**Dimensions, Inches**

| Valve Size | Size Range 2-1/2" – 4" | | | | | | | | | | | | | | |
|---|---|---|---|---|---|---|---|---|---|---|---|---|---|---|---|
| Inches | ØA | B | C | D | E | G Sq. | H | ISO Pattern | ØJ1 (BC) | ØJ2 (BC) | Ød1 | Ød2 | ISO Pattern | K | Weight, lbs |
| 2-1/2" | 2.56 | 7.28 | 5.9 | 16.4 | 3.02 | 0.669 | 4.21 | F07 | 2.76 | 4.02 | 0.354 | 0.433 | F10 | 0.67 | 22.6 |
| 3" | 3.15 | 8.07 | 6.3 | 14.4 | 3.64 | 0.669 | 4.62 | F07 | 2.76 | 4.02 | 0.354 | 0.433 | F10 | 0.67 | 35.4 |
| 4" | 3.94 | 9.45 | 6.9 | 14.4 | 4.50 | 0.669 | 5.21 | F07 | 2.76 | 4.02 | 0.354 | 0.433 | F10 | 0.67 | 56.7 |

**Dimensions, mm**

| Valve Size | Size Range DN65 – DN100 | | | | | | | | | | | | | | |
|---|---|---|---|---|---|---|---|---|---|---|---|---|---|---|---|
| NPS | ØA | B | C | D | E | G Sq. | H | ISO Pattern | ØJ1 (BC) | ØJ2 (BC) | Ød1 | Ød2 | ISO Pattern | K | Weight, kgs |
| DN65 | 65.0 | 185 | 150 | 265 | 77.0 | 17 | 107 | F07 | 70.1 | 102 | 9.0 | 11.0 | F10 | 17.1 | 10.3 |
| DN80 | 80.0 | 205 | 160 | 365 | 89.9 | 17 | 117 | F07 | 70.1 | 102 | 9.0 | 11.0 | F10 | 17.1 | 16.1 |
| DN100 | 100 | 240 | 175 | 365 | 114 | 17 | 132 | F07 | 70.1 | 102 | 9.0 | 11.0 | F10 | 17.1 | 25.7 |

**Technical Specifications**

| Valve Size | | Operating Torque, in-lb | | | |
|---|---|---|---|---|---|
| Inches | NPS | 0 – 750 psi | 0 – 51.7 bar | 1000 psi | 68.9 bar |
| 2-1/2" | DN65 | 600 | 66 | 675 | 75 |
| 3" | DN80 | 800 | 90 | 925 | 105 |
| 4" | DN100 | 1450 | 164 | 1600 | 181 |

Operating torques in table are for RPTFE seats. For PTFE seats, multiply by 0.87; for CRPTFE (15% Glass PTFE), and 50% SS PTFE, multiply by 1.09. Include an appropriate service factor for sizing actuators.

| Materials of Construction (2-1/2" – 4") | | |
|---|---|---|
| Part | Carbon Steel | Stainless Steel |
| Body | WCB | CF8M |
| End Cap | WCB | CF8M |
| Seat | RPTFE | |
| Ball | CF8M/316 | |
| Stem | AISI 316 | |
| Seal, Body | Graphite | |
| Thrust Washer | RPTFE | |
| Packing | Grafoil | |
| Gland Ring | AISI 304 | |
| Belleville Spring Washer | AISI 301 | |
| Adaptor, Handle | CF8M | |
| Stem Nut | AISI 304 | |
| Stop Screw | AISI 304 | |
| Cover, Handle | Vinyl | |
| Bolt, Body | A2-70 | 8.8 |
| Centering Ring, Seat | AISI 316 | |
| O-Ring, Stem | Viton | |
| Locking Tab | AISI 304 | |
| Antistatic Ball | AISI 316 | |
| Antistatic Spring | AISI 316 | |
| Handle | AISI 304 | |
| Bolt, Handle | AISI 304 | |
| Name Plate | SS | |

Refer to page 1 for 1/2" – 2" size Materials of Construction

| How to Order | | | | | | |
|---|---|---|---|---|---|---|
| Valve Series | Port Design | Size | Body Material | Packing/Seat | Ends | Handle |
| 4700 | F = Full Port | 05A = 1/2" | CS = Carbon Steel | F = Grafoil/RPTFE (std) | A = FNPT (std) | HL = Lever (std) |
| | | 07A = 3/4" | S6 = Stainless Steel | A = PTFE/PTFE | B = FSW (std) | NN = None |
| | | 10A = 1" | | B = PTFE/RPTFE | | |
| | | 12A = 1-1/4" | | C = PTFE/CRPTFE | | |
| | | 15A = 1-1/2" | | D = PTFE/UHMWPE | | |
| | | 20A = 2" | | E = Grafoil/PTFE | | |
| | | 25A = 2-1/2" | | G = Grafoil/CRPTFE | | |
| | | 30A = 3" | | H = Grafoil/UHMWPE | | |
| | | 40A = 4" | | J = UHMWPE/UHMWPE | | |
| | | | | N = Grafoil/50% SS PTFE | | |

*Sample Ordering Schematic*

| | | | | | | |
|---|---|---|---|---|---|---|
| 4700 | F | 10A | S6 | B | A | HL |

Series 4700 valves are suitable for a wide range of automation and accessories, incouding UT-SR spring return pneumatic actuators, UT-DA double acting pneumatic actuators, ER electric actuators, fusible link, assemblies, etc. Available accessories include solenoid valves, position indicators / limit switches, valve positioners, etc.

**Marwin Valve**
A Division of Richards Industries, 3170 Wasson Road, Cincinnati, OH 45209
toll free. 800.543.7311, local. 513.533.5600, fax. 513.871.0105
www.marwinvalve.com

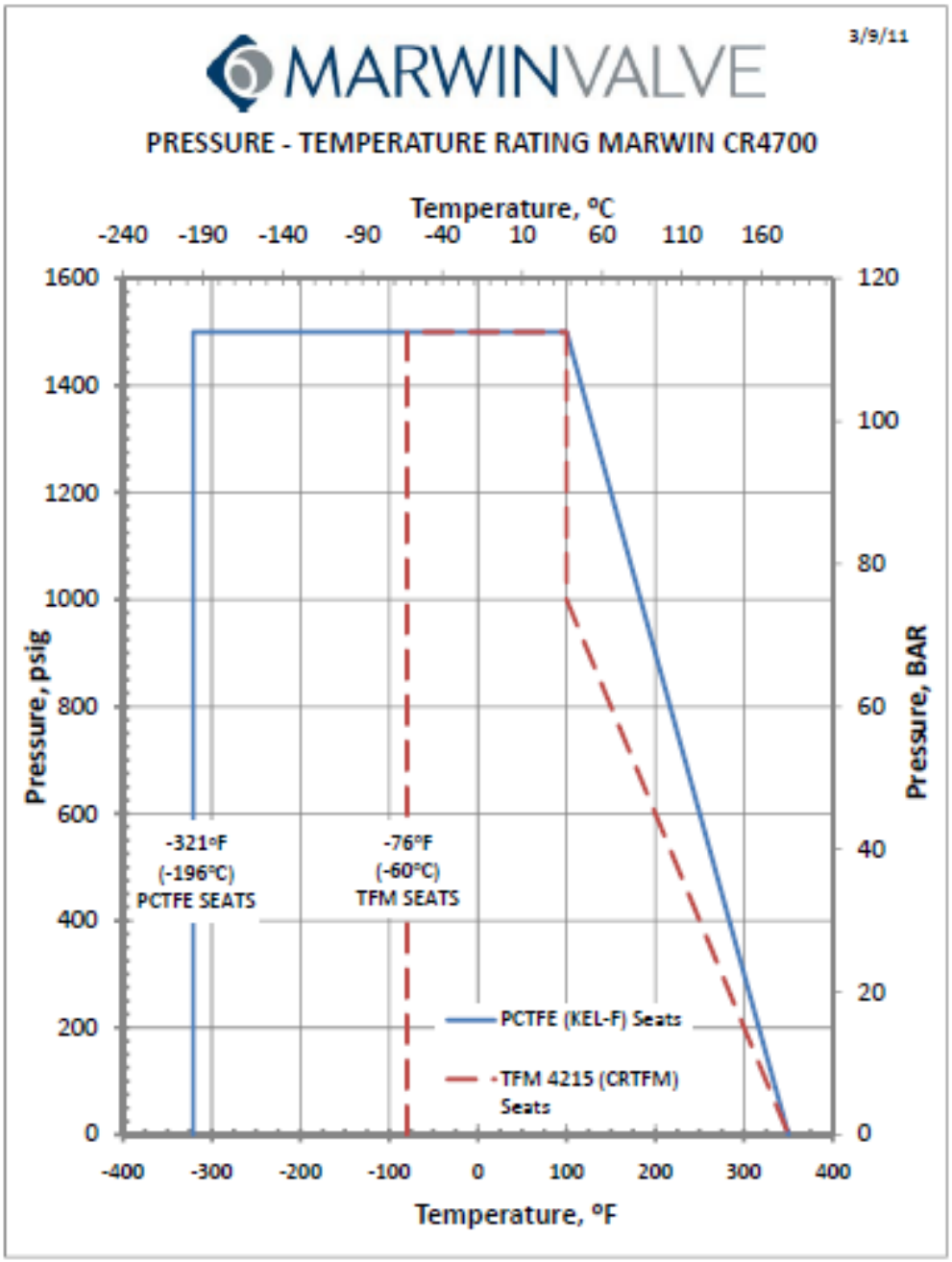
3/9/11
MARWINVALVE
PRESSURE - TEMPERATURE RATING MARWIN CR4700
Temperature, °C
-240 -190 -140 -90 -40 10 60 110 160
1600 1400 1200 1000 800 600 400 200 0
Pressure, psig
120 100 80 60 40 20 0
Pressure, BAR
-321°F
(-196°C)
PCTFE SEATS
-76°F
(-60°C)
TFM SEATS
PCTFE (KEL-F) Seats
TFM 4215 (CRTFM) Seats
-400 -300 -200 -100 0 100 200 300 400
Temperature, °F

# Extended Bonnet Cryogenic Globe Valves
# BK and BKA Series Valves

## Application

The BK and BKA Series valves are designed exclusively for the handling of cryogenic liquids on bulk storage tanks, transports, and pipelines. These globe valves provide positive shutoff and offer a long, low-maintenance service life. The valves are available with a variety of inlet and outlet connections and stem lengths. Certain BK valves are offered with brazed-in Sch 5 Stainless Steel Pipe Stubs.

## Features

- CTFE seat disc and swivel seat design offer positive shutoff, minimal seat wear, and a long service life.
- Unique spring-loaded upper packing provides extended service life without constant packing adjustment
- One piece slip-on seat assembly for easy replacement.
- Each valve is pressure tested to be leak free.
- Each valve is cleaned and packaged for oxygen service per CGA G-4.1.
- Maximum working pressure is 600 psig CWP.
- Working temperature range is -320°F to +165°F.
- 100% Factory Tested

## Materials

| | |
|---|---|
| Body | Bronze |
| Body and Bonnet | Brass |
| Seat Disc | CTFE |
| Seat Retainer Assembly | Brass |
| Stem and Bonnet Extension Tube | Stainless Steel |
| Packing Spring, Washer | Stainless Steel |
| Jam Ring and Pressure Seal Rings | PTFE |
| Upper Bonnet, Packing Gland | Brass |
| Handwheel | Aluminum for up to 1" valve size, Coated Malleable Iron for larger size |

## Bonnet Design

Union Bonnet for 1/2", 3/4", 1" valve sizes and on both the 1" model BKA8408S and 1 1/2" model BKA8412S angle valves. Bolted Bonnet design is used on the BK9410, BK9412, and BK9416 models.

BK 8408T

BK 9412S

BKA9408AA

BKA8412S



GODDARD REGO

APPENDIX B

Orifice Design

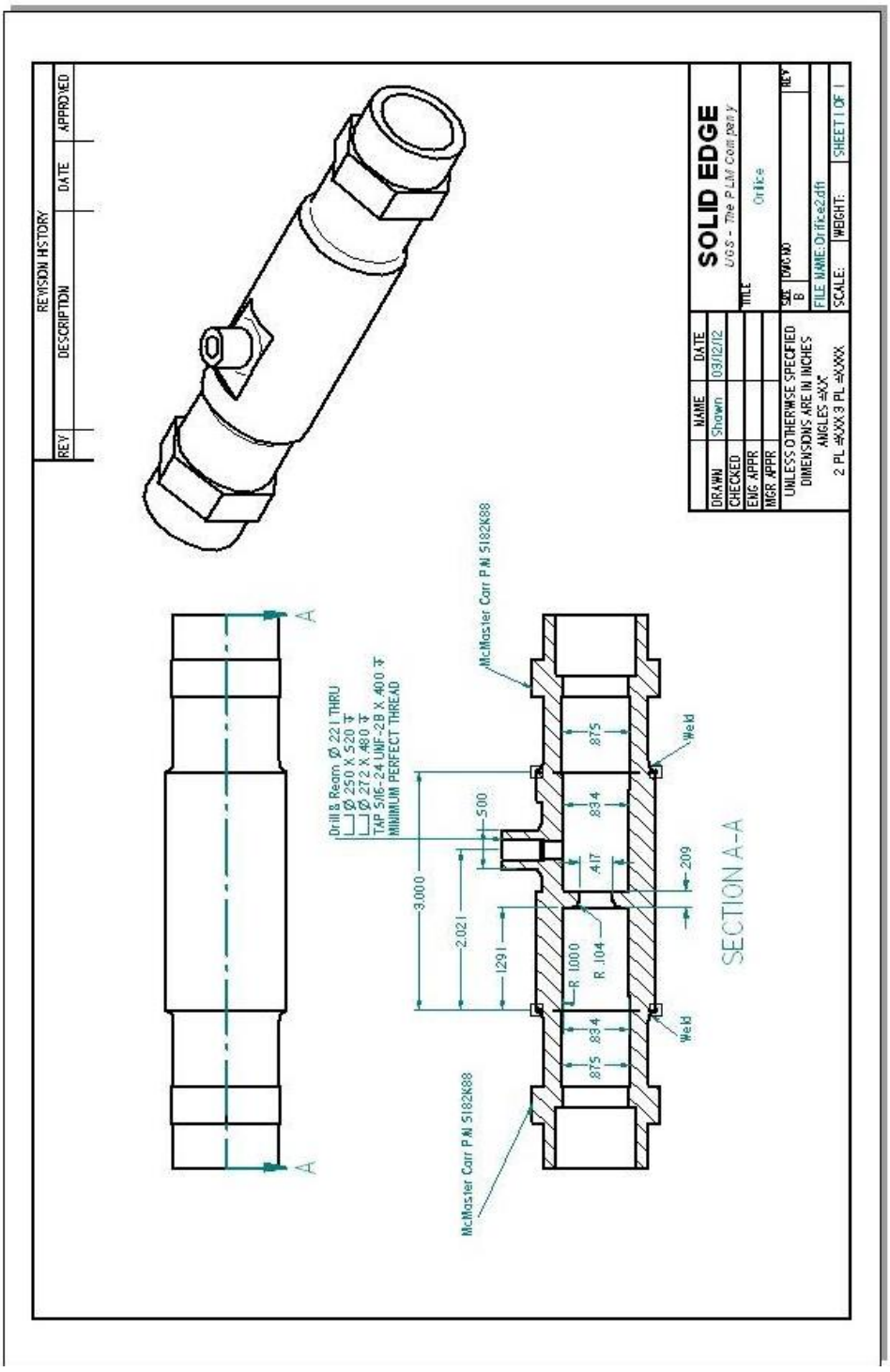

APPENDIX C

Set 166178-Test 42 Calculations

Set: 166178

Test: 42

## Conditions

Inlet pressure $p_1 := 94.12psi$

Outlet pressure $p_2 := 79.83psi$

Venturi pressure $p_{vent} := 241.12psi$

Inlet temperature $T_1 := 94.97K$

Venturi temperature $T_v := 93.58K$

Orifice diameter $d := 0.417in$

Venturi diameter $d_v := 0.26in$

Tubing diameter $D := 0.834in$

Orifice thickness $t := 0.209in$

Venturi Cd $C_d := 0.86$

Harmonic Frequency $f := 977Hz$

## Curve Fits

| | | | |
|---|---|---|---|
| $r_1 := 0$ | $m_1 := 0.00000000001892$ | $pv_1 := 0.00000425$ | |
| $r_2 := -0.000053$ | $m_2 := 0.00000001253179$ | $pv_2 := 0.0048597$ | |
| $r_3 := -0.031599$ | $m_3 := 0.00000312835654$ | $pv_3 := 1.9553483$ | $r_{v3} := -0.0025$ |
| $r_4 := -6.521386$ | $m_4 := 0.00034753578571$ | $pv_4 := 336.09391727$ | $r_{v4} := 0.1386$ |
| $r_5 := -413.56327$ | $m_5 := 0.01448495255839$ | $pv_5 := 21092.91410559$ | $r_{v5} := 54.613$ |

### Inlet Density

$$\rho(T_1) := \left[ r_2 \cdot \left( \frac{T_1}{K} - 273.15 \right)^3 + r_3 \cdot \left( \frac{T_1}{K} - 273.15 \right)^2 + r_4 \cdot \left( \frac{T_1}{K} - 273.15 \right) + r_5 \right] \cdot \frac{lbm}{ft^3}$$

### Venturi Density

$$\rho_{vent}(T_v) := \left[ r_{v3} \cdot \left( \frac{T_v}{K} \right)^2 + r_{v4} \cdot \left( \frac{T_v}{K} \right) + r_{v5} \right] \cdot \frac{lbm}{ft^3}$$

### Inlet Viscosity

$$\mu(T_1) := \left[ m_1 \cdot \left( \frac{T_1}{K} - 273.15 \right)^4 + m_2 \cdot \left( \frac{T_1}{K} - 273.15 \right)^3 + m_3 \cdot \left( \frac{T_1}{K} - 273.15 \right)^2 + m_4 \cdot \left( \frac{T_1}{K} - 273.15 \right) + m_5 \right] \cdot \frac{lbm}{ft \cdot s}$$

### Vapor Pressure

$$p_v(T_1) := \left[ pv_1 \cdot \left( \frac{T_1}{K} - 273.15 \right)^4 + pv_2 \cdot \left( \frac{T_1}{K} - 273.15 \right)^3 + pv_3 \cdot \left( \frac{T_1}{K} - 273.15 \right)^2 + pv_4 \cdot \left( \frac{T_1}{K} - 273.15 \right) + pv_5 \right] \cdot psi$$

$$\rho(T_1) = 45.023 \cdot \frac{lbm}{ft^3}$$

$$\mu(T_1) = 5.99 \times 10^{-5} \cdot \frac{lbm}{ft \cdot s}$$

$$p_v(T_1) = 79.34 \cdot psi$$

## Calculations

### Mass Flow Rate

$$mdot(C_d, d_v, p_{vent}, T_v, D) := C_d \cdot \left( \frac{\pi}{4} \cdot d_v^2 \right) \cdot \sqrt{\frac{2 \cdot (p_{vent} - p_v(T_v)) \cdot \rho_{vent}(T_v)}{1 - \left( \frac{d_v}{D} \right)^4}}$$

$$mdot(C_d, d_v, p_{vent}, T_v, D) = 2.701 \cdot \frac{lbm}{s}$$

### Reynolds Number

$$Re_D(C_d, d_v, p_{vent}, T_1, D, T_v) := \frac{4 \cdot \left[ C_d \cdot \left( \frac{\pi}{4} \cdot d_v^2 \right) \cdot \sqrt{\frac{2 \cdot (p_{vent} - p_v(T_v)) \cdot \rho_{vent}(T_v)}{1 - \left( \frac{d_v}{D} \right)^4}} \right]}{\pi \cdot \mu(T_1) \cdot D}$$

$$Re_D(C_d, d_v, p_{vent}, T_1, D, T_v) = 8.261 \times 10^5$$

### Orifice Throat Velocity

$$v(C_d, d_v, p_{vent}, T_v, D, d, T_1) := \frac{mdot(C_d, d_v, p_{vent}, T_v, D)}{\rho(T_1) \cdot \frac{\pi}{4} \cdot d^2}$$

### Cavitation Number

$$cav(C_d, d_v, p_{vent}, T_v, D, d, T_1) := \frac{p_1 - p_v(T_1)}{\frac{1}{2} \cdot \rho(T_1) \, v(C_d, d_v, p_{vent}, T_v, D, d, T_1)^2}$$

$$cav(C_d, d_v, p_{vent}, T_v, D, d, T_1) = 0.76$$

### Strouhal Number

$$St(f, t, C_d, d_v, p_{vent}, T_v, D, T_1, d) := \frac{f \cdot t}{\frac{mdot(C_d, d_v, p_{vent}, T_v, D)}{\rho(T_1) \cdot \frac{\pi}{4} \cdot d^2}}$$

$$St(f, t, C_d, d_v, p_{vent}, T_v, D, T_1, d) = 0.269$$

## Uncertainty

### Inlet Pressure

$$U_{p1} := \left[ 0.11 \cdot \left( \frac{\frac{p_1}{psi} - 14.7 + 0.57195}{59.84884} \right)^2 - 0.54 \cdot \left( \frac{\frac{p_1}{psi} - 14.7 + 0.57195}{59.84884} \right) + 2.734 \right] \cdot psi$$

$$U_{p1} = 2.209 \cdot psi$$

### Outlet Pressure

$$U_{p2} := \left[ 0.109 \cdot \left( \frac{\frac{p_2}{psi} - 14.7 + 0.16448}{59.86067} \right)^2 - 0.532 \cdot \left( \frac{\frac{p_2}{psi} - 14.7 + 0.16448}{59.86067} \right) + 2.705 \right] \cdot psi$$

$$U_{p2} = 2.254 \cdot psi$$

Venturi Pressure

$$U_{pvent} := \left[ 0.045 \cdot \left( \frac{\frac{p_{vent}}{psi} - 14.7 + 0.01968}{100.40592} \right)^2 - 0.116 \cdot \left( \frac{\frac{p_{vent}}{psi} - 14.7 + 0.01968}{100.40592} \right) + 1.14 \right] \cdot psi$$

$U_{pvent} = 1.107 \cdot psi$

Inlet Temperature

$U_{T1} := \left| 0.015 \cdot (T_1 - 273.15K) \right|$

$U_{T1} = 2.673\,K$

Venturi Temperature

$U_{Tv} := \left| 0.015 \cdot (T_v - 273.15K) \right|$

$U_{Tv} = 2.694\,K$

Venturi Throat Unc

$U_{dv} := 0.005in$

Orifice Unc

$U_d := 0.005in$

Tubing Diameter

$U_D := 0.005in$

Venturi Cd

$U_{Cd} := 0.05 \cdot C_d$

$U_{Cd} = 0.043$

Inlet Vapor pressure

$$U_{pv} := \sqrt{\left( \frac{d}{dT_1} p_v(T_1) \right)^2 \cdot {U_{T1}}^2}$$

$$U_{pv} = 15.977 \cdot psi$$

Inlet Density

$$U_\rho := \sqrt{\left(\frac{d}{dT_1}\rho(T_1)\right)^2 \cdot U_{T1}{}^2}$$

$$U_\rho = 0.825 \cdot \frac{lbm}{ft^3}$$

Inlet Viscosity

$$U_\mu := \sqrt{\left(\frac{d}{dT_1}\mu(T_1)\right)^2 \cdot U_{T1}{}^2 + (0.02 \cdot \mu(T_1))^2}$$

$$U_\mu = 4.999 \times 10^{-6} \cdot \frac{lbm}{ft \cdot s}$$

Frequency

$$U_f := 0.05 \cdot f$$

$$U_f = 48.85\,Hz$$

Orifice Thickness

$$U_t := 0.005in$$

Mass Flow Rate

$$U_{mdot} := \sqrt{\left[\frac{d}{dC_d}(mdot(C_d,d_v,P_{vent},T_v,D))\right]^2 \cdot U_{Cd}^2 + \left[\frac{d}{dd_v}(mdot(C_d,d_v,P_{vent},T_v,D))\right]^2 \cdot U_{dv}^2 + \left[\frac{d}{dp_{vent}}(mdot(C_d,d_v,P_{vent},T_v,D))\right]^2 \cdot U_{pvent}^2 + \left[\frac{d}{dT_v}(mdot(C_d,d_v,P_{vent},T_v,D))\right]^2 \cdot U_{Tv}^2 + \left[\frac{d}{dD}(mdot(C_d,d_v,P_{vent},T_v,D))\right]^2 \cdot U_D^2}$$

$U_{mdot} = 0.224 \frac{lbm}{s}$

Reynolds Number

$$U_{ReD} := \sqrt{\left[\frac{d}{dC_d}(Re_D(C_d,d_v,P_{vent},T_1,D,T_v))\right]^2 \cdot U_{Cd}^2 + \left[\frac{d}{dd_v}(Re_D(C_d,d_v,P_{vent},T_1,D,T_v))\right]^2 \cdot U_{dv}^2 + \left[\frac{d}{dT_v}(Re_D(C_d,d_v,P_{vent},T_1,D,T_v))\right]^2 \cdot U_{Tv}^2 + \left[\frac{d}{dp_{vent}}(Re_D(C_d,d_v,P_{vent},T_1,D,T_v))\right]^2 \cdot U_{pvent}^2 + \left[\frac{d}{dT_1}(Re_D(C_d,d_v,P_{vent},T_1,D,T_v))\right]^2 \cdot U_{T1}^2 + \left[\frac{d}{dD}(Re_D(C_d,d_v,P_{vent},T_1,D,T_v))\right]^2 \cdot U_D^2}$$

$U_{ReD} = 9.593 \times 10^4$

Cavitation Number

$$U_{cav} := \sqrt{\left[\frac{d}{dC_d}(cav(C_d,d_v,P_{vent},T_v,D,d,T_1))\right]^2 \cdot U_{Cd}^2 + \left[\frac{d}{dd}(cav(C_d,d_v,P_{vent},T_v,D,d,T_1))\right]^2 \cdot U_d^2 + \left[\frac{d}{dT_1}(cav(C_d,d_v,P_{vent},T_v,D,d,T_1))\right]^2 \cdot U_{T1}^2 + \left[\frac{d}{dd_v}(cav(C_d,d_v,P_{vent},T_v,D,d,T_1))\right]^2 \cdot U_{dv}^2 + \left[\frac{d}{dp_{vent}}(cav(C_d,d_v,P_{vent},T_v,D,d,T_1))\right]^2 \cdot U_{pvent}^2 + \left[\frac{d}{dT_v}(cav(C_d,d_v,P_{vent},T_v,D,d,T_1))\right]^2 \cdot U_{Tv}^2 + \left[\frac{d}{dD}(cav(C_d,d_v,P_{vent},T_v,D,d,T_1))\right]^2 \cdot U_D^2}$$

$U_{cav} = 0.846$

Strouhal Number

$$U_{St} := \sqrt{\left[\frac{d}{dC_d}(St(f,t,C_d,d_v,P_{vent},T_v,D,T_1,d))\right]^2 \cdot U_{Cd}^2 + \left[\frac{d}{df}(St(f,t,C_d,d_v,P_{vent},T_v,D,T_1,d))\right]^2 \cdot U_f^2 + \left[\frac{d}{dt}(St(f,t,C_d,d_v,P_{vent},T_v,D,T_1,d))\right]^2 \cdot U_t^2 + \left[\frac{d}{dd}(St(f,t,C_d,d_v,P_{vent},T_v,D,T_1,d))\right]^2 \cdot U_d^2 + \left[\frac{d}{dd_v}(St(f,t,C_d,d_v,P_{vent},T_v,D,T_1,d))\right]^2 \cdot U_{dv}^2 + \left[\frac{d}{dT_v}(St(f,t,C_d,d_v,P_{vent},T_v,D,T_1,d))\right]^2 \cdot U_{Tv}^2 + \left[\frac{d}{dp_{vent}}(St(f,t,C_d,d_v,P_{vent},T_v,D,T_1,d))\right]^2 \cdot U_{pvent}^2 + \left[\frac{d}{dT_1}(St(f,t,C_d,d_v,P_{vent},T_v,D,T_1,d))\right]^2 \cdot U_{T1}^2 + \left[\frac{d}{dD}(St(f,t,C_d,d_v,P_{vent},T_v,D,T_1,d))\right]^2 \cdot U_D^2}$$

$U_{St} = 0.028$

## Mass Flow Rate Contributors

### UMFs

$$UMFmdot_{Cd} := \frac{C_d}{mdot(C_d, d_v, p_{vent}, T_v, D)} \cdot \frac{d}{dC_d}\left(mdot(C_d, d_v, p_{vent}, T_v, D)\right)$$

$$UMFmdot_{Cd} = 1$$

$$UMFmdot_{dv} := \frac{d_v}{mdot(C_d, d_v, p_{vent}, T_v, D)} \cdot \frac{d}{dd_v}\left(mdot(C_d, d_v, p_{vent}, T_v, D)\right)$$

$$UMFmdot_{dv} = 2.019$$

$$UMFmdot_{pvent} := \frac{p_{vent}}{mdot(C_d, d_v, p_{vent}, T_v, D)} \cdot \frac{d}{dp_{vent}}\left(mdot(C_d, d_v, p_{vent}, T_v, D)\right)$$

$$UMFmdot_{pvent} = 0.71$$

$$UMFmdot_{Tv} := \frac{T_v}{mdot(C_d, d_v, p_{vent}, T_v, D)} \cdot \frac{d}{dT_v}\left(mdot(C_d, d_v, p_{vent}, T_v, D)\right)$$

$$UMFmdot_{Tv} = -1.86$$

$$UMFmdot_{D} := \frac{D}{mdot(C_d, d_v, p_{vent}, T_v, D)} \cdot \frac{d}{dD}\left(mdot(C_d, d_v, p_{vent}, T_v, D)\right)$$

$$UMFmdot_{D} = -0.019$$

### UPCs

$$UPCmdot_{Cd} := \frac{UMFmdot_{Cd}^{2} \cdot \left(\frac{U_{Cd}}{C_d}\right)^2}{\left(\frac{U_{mdot}}{mdot(C_d, d_v, p_{vent}, T_v, D)}\right)^2} \cdot 100$$

$$UPCmdot_{Cd} = 36.32$$

$$UPCmdot_{dv} := \frac{UMFmdot_{dv}^{2} \cdot \left(\frac{U_{dv}}{d_v}\right)^{2}}{\left(\frac{U_{mdot}}{mdot(C_d, d_v, p_{vent}, T_v, D)}\right)^{2}} \cdot 100$$

$UPCmdot_{dv} = 21.903$

$$UPCmdot_{pvent} := \frac{UMFmdot_{pvent}^{2} \cdot \left(\frac{U_{pvent}}{p_{vent}}\right)^{2}}{\left(\frac{U_{mdot}}{mdot(C_d, d_v, p_{vent}, T_v, D)}\right)^{2}} \cdot 100$$

$UPCmdot_{pvent} = 0.154$

$$UPCmdot_{Tv} := \frac{UMFmdot_{Tv}^{2} \cdot \left(\frac{U_{Tv}}{T_v}\right)^{2}}{\left(\frac{U_{mdot}}{mdot(C_d, d_v, p_{vent}, T_v, D)}\right)^{2}} \cdot 100$$

$UPCmdot_{Tv} = 41.622$

$$UPCmdot_{D} := \frac{UMFmdot_{D}^{2} \cdot \left(\frac{U_{D}}{D}\right)^{2}}{\left(\frac{U_{mdot}}{mdot(C_d, d_v, p_{vent}, T_v, D)}\right)^{2}} \cdot 100$$

$UPCmdot_{D} = 1.899 \times 10^{-4}$

## Reynolds Number Contributors

### UMFs

$$UMFRe_{Cd} := \frac{C_d}{Re_D(C_d, d_v, p_{vent}, T_1, D, T_v)} \cdot \frac{d}{dC_d}\left(Re_D(C_d, d_v, p_{vent}, T_1, D, T_v)\right)$$

$UMFRe_{Cd} = 1$

$$UMFRe_{dv} := \frac{d_v}{Re_D(C_d, d_v, p_{vent}, T_1, D, T_v)} \cdot \frac{d}{dd_v}\left(Re_D(C_d, d_v, p_{vent}, T_1, D, T_v)\right)$$

$UMFRe_{dv} = 2.019$

$$UMFRe_{pvent} := \frac{p_{vent}}{Re_D(C_d, d_v, p_{vent}, T_1, D, T_v)} \cdot \frac{d}{dp_{vent}} \left(Re_D(C_d, d_v, p_{vent}, T_1, D, T_v)\right)$$

$$UMFRe_{pvent} = 0.71$$

$$UMFRe_{Tv} := \frac{T_v}{Re_D(C_d, d_v, p_{vent}, T_1, D, T_v)} \cdot \frac{d}{dT_v} \left(Re_D(C_d, d_v, p_{vent}, T_1, D, T_v)\right)$$

$$UMFRe_{Tv} = -1.86$$

$$UMFRe_D := \frac{D}{Re_D(C_d, d_v, p_{vent}, T_1, D, T_v)} \cdot \frac{d}{dD} \left(Re_D(C_d, d_v, p_{vent}, T_1, D, T_v)\right)$$

$$UMFRe_D = -1.019$$

$$UMFRe_{T1} := \frac{T_1}{Re_D(C_d, d_v, p_{vent}, T_1, D, T_v)} \cdot \frac{d}{dT_1} \left(Re_D(C_d, d_v, p_{vent}, T_1, D, T_v)\right)$$

$$UMFRe_{T1} = 2.879$$

UPCs

$$UPCRe_{Cd} := \frac{UMFRe_{Cd}^2 \cdot \left(\frac{U_{Cd}}{C_d}\right)^2}{\left(\frac{U_{ReD}}{Re_D(C_d, d_v, p_{vent}, T_1, D, T_v)}\right)^2} \cdot 100$$

$$UPCRe_{Cd} = 18.539$$

$$UPCRe_{dv} := \frac{UMFRe_{dv}^2 \cdot \left(\frac{U_{dv}}{d_v}\right)^2}{\left(\frac{U_{ReD}}{Re_D(C_d, d_v, p_{vent}, T_1, D, T_v)}\right)^2} \cdot 100$$

$$UPCRe_{dv} = 11.18$$

$$UPCRe_{pvent} := \frac{UMFRe_{pvent}^{2} \cdot \left(\frac{U_{pvent}}{p_{vent}}\right)^{2}}{\left(\frac{U_{ReD}}{Re_D(C_d, d_v, p_{vent}, T_1, D, T_v)}\right)^{2}} \cdot 100$$

$UPCRe_{pvent} = 0.079$

$$UPCRe_{Tv} := \frac{UMFRe_{Tv}^{2} \cdot \left(\frac{U_{Tv}}{T_v}\right)^{2}}{\left(\frac{U_{ReD}}{Re_D(C_d, d_v, p_{vent}, T_1, D, T_v)}\right)^{2}} \cdot 100$$

$UPCRe_{Tv} = 21.245$

$$UPCRe_{D} := \frac{UMFRe_{D}^{2} \cdot \left(\frac{U_{D}}{D}\right)^{2}}{\left(\frac{U_{ReD}}{Re_D(C_d, d_v, p_{vent}, T_1, D, T_v)}\right)^{2}} \cdot 100$$

$UPCRe_{D} = 0.277$

$$UPCRe_{T1} := \frac{UMFRe_{T1}^{2} \cdot \left(\frac{U_{T1}}{T_1}\right)^{2}}{\left(\frac{U_{ReD}}{Re_D(C_d, d_v, p_{vent}, T_1, D, T_v)}\right)^{2}} \cdot 100$$

$UPCRe_{T1} = 48.681$

## Cavitation Number Contributors

### UMFs

$$UMFcav_{Cd} := \frac{C_d}{cav(C_d, d_v, p_{vent}, T_v, D, d, T_1)} \cdot \frac{d}{dC_d}\left(cav(C_d, d_v, p_{vent}, T_v, D, d, T_1)\right)$$

$UMFcav_{Cd} = -2$

$$UMFcav_{dv} := \frac{d_v}{cav(C_d, d_v, p_{vent}, T_v, D, d, T_1)} \cdot \frac{d}{dd_v}\left(cav(C_d, d_v, p_{vent}, T_v, D, d, T_1)\right)$$

$$UMFcav_{dv} = -4.038$$

$$UMFcav_{pvent} := \frac{p_{vent}}{cav(C_d, d_v, p_{vent}, T_v, D, d, T_1)} \cdot \frac{d}{dp_{vent}}\left(cav(C_d, d_v, p_{vent}, T_v, D, d, T_1)\right)$$

$$UMFcav_{pvent} = -1.42$$

$$UMFcav_{Tv} := \frac{T_v}{cav(C_d, d_v, p_{vent}, T_v, D, d, T_1)} \cdot \frac{d}{dT_v}\left(cav(C_d, d_v, p_{vent}, T_v, D, d, T_1)\right)$$

$$UMFcav_{Tv} = 3.719$$

$$UMFcav_{D} := \frac{D}{cav(C_d, d_v, p_{vent}, T_v, D, d, T_1)} \cdot \frac{d}{dD}\left(cav(C_d, d_v, p_{vent}, T_v, D, d, T_1)\right)$$

$$UMFcav_{D} = 0.038$$

$$UMFcav_{T1} := \frac{T_1}{cav(C_d, d_v, p_{vent}, T_v, D, d, T_1)} \cdot \frac{d}{dT_1}\left(cav(C_d, d_v, p_{vent}, T_v, D, d, T_1)\right)$$

$$UMFcav_{T1} = -39.064$$

$$UMFcav_{d} := \frac{d}{cav(C_d, d_v, p_{vent}, T_v, D, d, T_1)} \cdot \frac{d}{dd}\left(cav(C_d, d_v, p_{vent}, T_v, D, d, T_1)\right)$$

$$UMFcav_{d} = 4$$

UPCs

$$UPCcav_{Cd} := \frac{UMFcav_{Cd}^{2} \cdot \left(\frac{U_{Cd}}{C_d}\right)^2}{\left(\frac{U_{cav}}{cav(C_d, d_v, p_{vent}, T_v, D, d, T_1)}\right)^2} \cdot 100$$

$UPCcav_{Cd} = 0.807$

$$UPCcav_{dv} := \frac{UMFcav_{dv}^{2} \cdot \left(\frac{U_{dv}}{d_v}\right)^2}{\left(\frac{U_{cav}}{cav(C_d, d_v, p_{vent}, T_v, D, d, T_1)}\right)^2} \cdot 100$$

$UPCcav_{dv} = 0.487$

$$UPCcav_{pvent} := \frac{UMFcav_{pvent}^{2} \cdot \left(\frac{U_{pvent}}{p_{vent}}\right)^2}{\left(\frac{U_{cav}}{cav(C_d, d_v, p_{vent}, T_v, D, d, T_1)}\right)^2} \cdot 100$$

$UPCcav_{pvent} = 3.435 \times 10^{-3}$

$$UPCcav_{Tv} := \frac{UMFcav_{Tv}^{2} \cdot \left(\frac{U_{Tv}}{T_v}\right)^2}{\left(\frac{U_{cav}}{cav(C_d, d_v, p_{vent}, T_v, D, d, T_1)}\right)^2} \cdot 100$$

$UPCcav_{Tv} = 0.925$

$$UPCcav_{D} := \frac{UMFcav_{D}^{2} \cdot \left(\frac{U_{D}}{D}\right)^2}{\left(\frac{U_{cav}}{cav(C_d, d_v, p_{vent}, T_v, D, d, T_1)}\right)^2} \cdot 100$$

$UPCcav_{D} = 4.222 \times 10^{-6}$

$$UPCcav_{T1} := \frac{UMFcav_{T1}^{2} \cdot \left(\frac{U_{T1}}{T_1}\right)^2}{\left(\frac{U_{cav}}{cav(C_d, d_v, p_{vent}, T_v, D, d, T_1)}\right)^2} \cdot 100$$

$UPCcav_{T1} = 97.591$

$$UPCcav_{d} := \frac{UMFcav_{d}^{2} \cdot \left(\frac{U_{d}}{d}\right)^2}{\left(\frac{U_{cav}}{cav(C_d, d_v, p_{vent}, T_v, D, d, T_1)}\right)^2} \cdot 100$$

$UPCcav_{d} = 0.186$

## UPC Verification

$UPCmdot_{Cd} + UPCmdot_{dv} + UPCmdot_{pvent} + UPCmdot_{D} + UPCmdot_{Tv} = 100$

$UPCRe_{Cd} + UPCRe_{dv} + UPCRe_{pvent} + UPCRe_{D} + UPCRe_{Tv} + UPCRe_{T1} = 100$

$UPCcav_{Cd} + UPCcav_{dv} + UPCcav_{pvent} + UPCcav_{D} + UPCcav_{Tv} + UPCcav_{T1} + UPCcav_{d} = 100$

APPENDIX D

UMFs and UPCs

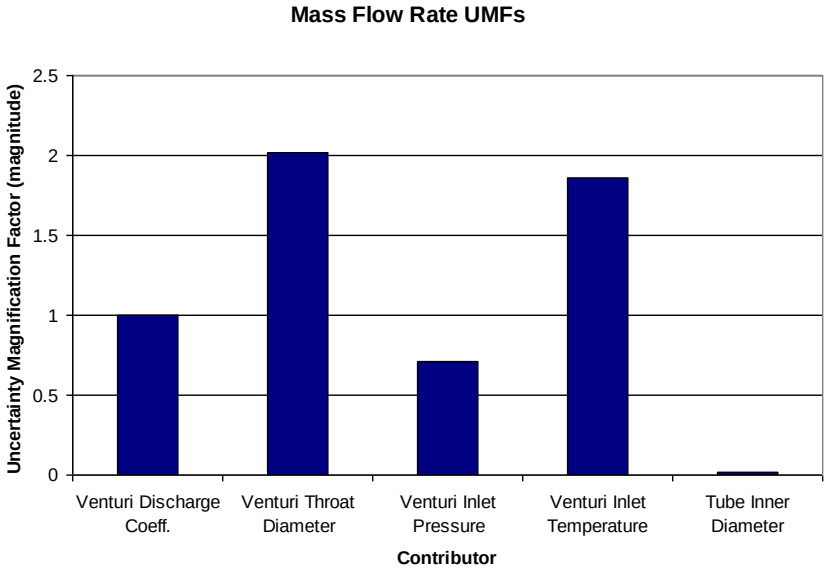


**Figure D.1: Mass Flow Rate UMFs**

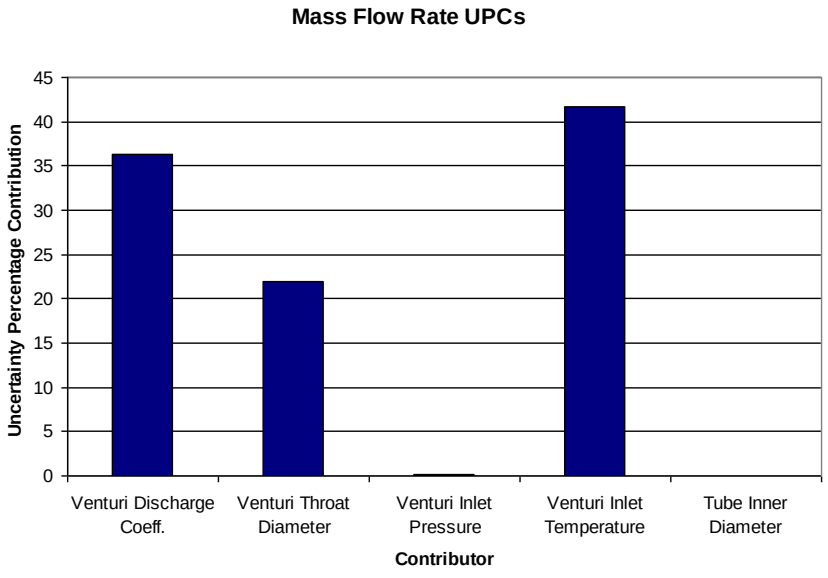


**Figure D.2: Mass Flow Rate UPCs**

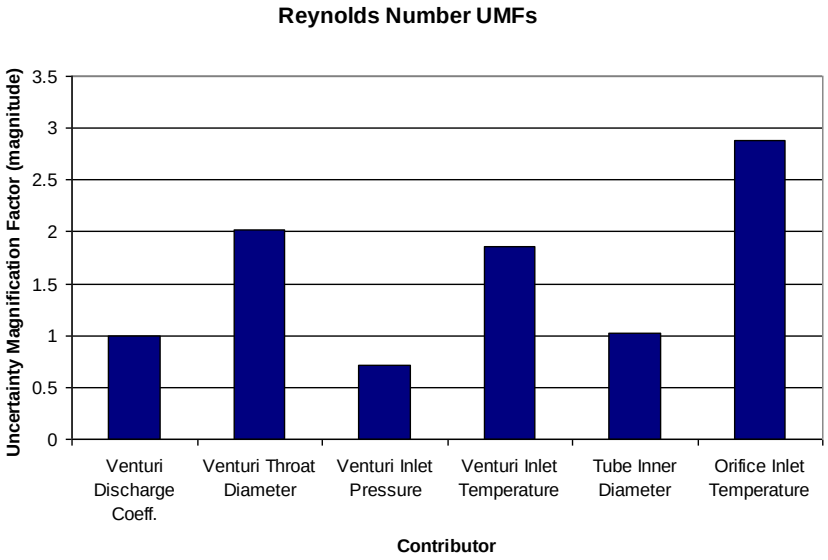


**Figure D.3: Reynolds Number UMFs**

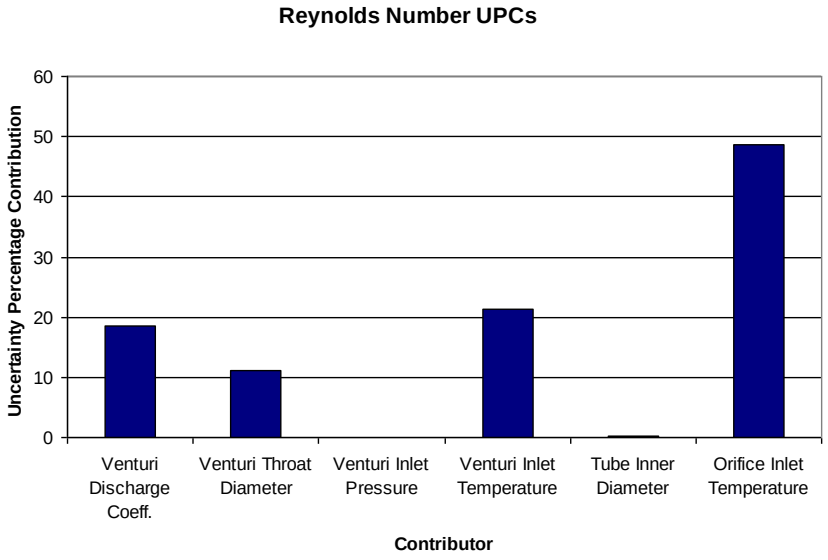


**Figure D.4: Reynolds Number UPCs**

APPENDIX E

Test Procedures

# $LN_2$ Orifice Test Procedure

## Red Team Members:

Dr. Lineberry _____

Tony Hall _____

Matthew Hitt _____

Ethan Wilson _____

_____

Other operators or Red Team Members not shown on this document must be certified by the Test Engineer or Dr. Lineberry

## Red Team Members Required Training:

1) AED/CPR
2) Attended or reviewed Chip Sauer's presentation from Orbital Technologies Corporation Cryogenic Safety and Hazards for Propulsion Systems
3) At least one Red Team Member must have participated in ASTM Certification in Fire Safety in Oxygen Systems

## Procedure Approval:

**Mr. Matthew Hitt:** _____ **date:**_____

**Mr. Ethan Wilson:** _____ **date:**_____

**Mr. Tony Hall:** _____ **date:**_____
**(Test Engineer)**

**Dr. Lineberry:** _____ **date:**_____

**Dr. Frederick:** _____ **date:**_____

## Foreword:

This procedure details the use of the PRC Cryogenic System for an investigation of the instabilities induced by the use of a cryogenic orifice. For this project, the PRC Cryogenic System was modified to utilize 1" OD tubing and be controlled by manually operated valves.

# $LN_2$ Orifice Test Sheet

**Date: _____**

**Red Team Members:**

Dr. Lineberry _____

Tony Hall _____

Matthew Hitt _____

Ethan Wilson _____

_____

Other operators or Red Team Members not shown on this document must be

## Test Conditions

Table 1: Test Conditions

| Operating Condition | Venturi Pressure [psig] | Orifice Inlet Pressure [psig] | Orifice Outlet Pressure [psig] |
|---|---|---|---|
| | | | |
| | | | |
| | | | |

## Filenames:

LabVIEW Operating Program: E:\Test Stand Data\Hitt\LN2_orifice_Rev*XX*.vi

LabVIEW Test Record: E:\Test Stand Data\Hitt*date**date*_test.lvm_____

CXOne PLC Program: C:\Control Room Computer\Eberhart\LN2_June17_rev1.cxp_____

Sensor Locations Sheet: E:\Test Stand Data\Hitt\Sensor Info and Locations.xls

## Experiment Positions

Experiment Operator _____

Range Safety Officer _____

Labview Operator _____

**Descriptions:**
Experiment Operator: Operates manual cryogenic valves
Range Safety Officer: Ensures safety and restricts outside access throughout experiment
Control Room Operator: Runs Labview and control board throughout experiment

**Table E.1: Emergency Contact Phone Numbers**

| | |
|---|---|
| **Police** | **911 or 256-824-6911 (6911 from campus phone)** |
| **Fire Department** | |
| **Hazardous Materials Incident** | |
| **Utility Failure** | |
| **PRC/UAH Contacts** | |
| **Tony Hall** | **Office : 256-824-2887** |
| **David Lineberry** | **Office : 256-824-2888**<br>**Cell : 256-348-8978** |
| **Robert Frederick** | **Office : 256-824-7200**<br>**Cell : 256-503-4909** |
| **PRC Main Office** | **256-824-7209** |
| **JRC Test Stand** | **256-824-1756 or 256-824-1759** |
| **Bobby Dempsey** | **256-824-2352** |
| **John Horack** | **256-824-6100** |
| **Other Emergency Numbers of Interest** | |
| **Huntsville Police Department** | **256-722-7100** |
| **Madison County Sheriff's Office** | **256-722-7181** |
| **Alabama State Troopers** | **256-533-4202** |
| **Crestwood Medical Center** | **256-882-3100** |
| **Huntsville Hospital Main** | **256-265-1000** |

# Pre-Test Certifications:

**Pre-Test Procedures:**
**This test procedure assumes the following:**

1. **All lines have been connected.**
2. **The facility is clean**
3. **The system has been leak checked to 275 psi in accordance with Appendix 1 (pg. 9) and all leaks corrected.**
4. **All instrumentation has been calibrated as required.**
5. **All Red Team members have reviewed and understand Cryogenic and Oxygen safety hazards in Appendix 2 (pg. 11) and additionally completed the required safety trainings stated on page 1 of this document.**
6. **High frequency pressure sensor is in upstream location**

Pre-Test Certifications: The undersigned certify that the pre-test procedures have been completed.

Tony Hall _____ (Test Engineer)

Dr. Lineberry _____

Matthew Hitt _____

## Test Stand Preparation

- ☐ Attach pressurization air to actuated fire valve air manifold on the back of the test stand (plastic tubing)
- ☐ Attach the pressurization air to the compressor in the instrumentation room and make sure that the compressor is on auto compress
- ☐ Ensure air compressor tank pressure is at least 80 psi
- ☐ Put up all blockades around the test facility
  - ➢ See JRC Test stand footprint for blockade location in Appendix 3 (pg 14)
- ☐ Close and Lock Security Fence

## Instrumentation

- ☐ Check the *Sensor Locations Sheet* located in Appendix 4 (pg 15) for proper set-up channels with correct pressure sensors and/or thermocouples
- ☐ Turn on LabView and open the *LabVIEW Operating Program*
- ☐ Press RUN and ensure program is running properly
- ☐ Type in the appropriate *LabVIEW Data Record* filename _____
- ☐ Press RECORD and press STOP after 5 seconds. This will record a zeros file
- ☐ Ensure LabVIEW recorded properly

## Control Room Settings

- ☐ Announce over intercom clear the test area
- ☐ Give key to Range Safety Officer
- ☐ Walk test stand area to make sure test facility is clear
- ☐ Check with Range Safety Officer to make sure test facility area is clear
- ☐ Insert key and toggle
  - LOX Fill
  - LOX Main Relief
  - LOX Dome
  - LOX Pressure Shutoff
  - 3-way diverter valve
- ☐ Check BRB functionality
- ☐ Press Reset on the control board
- ☐ Toggle all valves
- ☐ Press Reset on the control board
- ☐ Ensure the actuators are functioning properly
- ☐ Place 3 way diverter valve switch in the up (energized) position

**ONLY Red Team allowed in test cell area from this point forward**

Pressurized Lines – Safety Glasses/Crvo Gear Required

## LOX Run Tank Fill Procedure[1] – Only needed at beginning of testing series

- ☐ Reference Appendix 5 (Pg 16) for LOX Run Tank fill procedure

## Domeloader Pressurization

- ☐ With all Red Team members in the control room place key in control board
- ☐ Initiate DVR recording
- ☐ Use control board to
  - **Close LOX Tank Pressurization Shutoff Valve**
  - **Open LOX Dome**
- ☐ Remove the key from the control board
- ☐ Give experiment operator control key
- ☐ Open the nitrogen ball valves on the nitrogen manifold
- ☐ Crack open all k-bottle valves to slowly bleed in pressure
- ☐ Fully open all k-bottle valves then close ¼ turn
- ☐ Crack open nitrogen 12-pack valves
- ☐ Completely open nitrogen 12-pack valves then close ¼ turn
- ☐ Ensure that there is sufficient pressure in the manifold (at least 1.5 times operating pressure)
- ☐ Adjust LOX tank pressure setting to 240 psi; set all other pressures to 0 psig

[1] Familiarize yourself with Cryogenic and Oxygen safety hazards in Appendix 2 Cryogenic safety table mode and solutions before fill procedure

- ☐ Return to control room
- ☐ Close LOX Dome

## System Pressurization

- ☐ Give experiment operator control key
- ☐ Close LOX low pressure manual globe valve
- ☐ Open LOX Main Relief valve
- ☐ Open Run Valve
- ☐ Walk test stand area to make sure test facility is clear
- ☐ Check with Range Safety Officer to make sure test facility area is clear
- ☐ Go back to control room
- ☐ Check to make sure all Red Team members are in control room
- ☐ Close LOX Main Relief valve
- ☐ Open LOX Dome Loader and LOX Tank Pressure Shutoff to pressurize LOX Run Tank
- ☐ Ensure that there is sufficient pressure in the LOX Run Tank (orifice operating pressure) and pressure reading steady,
    - If LOX Tank Pressure is not steady
        - Close LOX Tank Pressure Shutoff
        - Announce Venting LOX Tank on Facility intercom
        - Open LOX Main Relief Valve to vent LOX Main tank
        - Call for a solution discussion and fix problem, or
        - Proceed to experimental shut-down sequence
    - Otherwise, continue
- ☐ Make sure test facility area is clear
- ☐ Check to make sure all Red Team members are in control room
- ☐ Ensure that all test stand pressures are correct in Labview

**Test cell must be evacuated if oxygen level drops below 19%**

## Orifice Testing

- ☐ Send out experiment operator (wearing cryogenic safety equipment, radio, and personal oxygen monitor)
- ☐ Press Reset
- ☐ Insert key into control panel and turn on
- ☐ Have experiment operator open backpressure valve
- ☐ Monitoring temperature measurements T venturi and T orifice and P orifice pressure measurement to establish liquid phase in line ( 30-60 seconds)

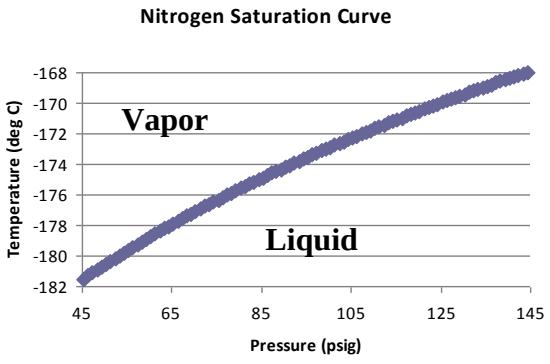

Pressurized Lines – Safety Glasses/Cryo Gear Required

- Verify test cell oxygen levels no less than 19% (see Appendix 2, Table 7)
- Adjust backpressure valve to match orifice inlet pressure setpoint **(Step Segno)**
  **********Repeat until desired orifice inlet pressure is attained**********
- If necessary, open $LN_2$ jacket atmospheric bypass valve to lower temperature
  ******If the tank runs out of $LN_2$, close Run Valve, open Line Vent, and******
  ******proceed to Shut-Down Sequence******
- When orifice inlet pressure reaches the setpoint and data is at steady state:
  - Initiate LabView data recording
  - Stop LabView data recording
- Close Run Valve
- Open Line vent
- Move high frequency pressure sensor to downstream location
- Close Line Vent
- Open Run Valve
- When data reaches steady state
  - Initiate LabView data recording
  - Stop LabView data recording **(Step Fine)**
- Adjust backpressure valve to make orifice inlet pressure match second setpoint
- When second setpoint is reached and data is at steady state:
  - Initiate LabView data recording
  - Stop LabView data recording
- Close Run Valve
- Open Line Vent
- Move high frequency pressure sensor to upstream location
- Close Line Vent
- Open Run Valve
- When data reaches steady state
  - Initiate LabView data recording
  - Stop LabView data recording
  - If third set point is desired, repeat steps **Segno** to **Fine**
- Close Run Valve
- Open Line Vent
- Stop DVR

## Shut-Down Sequence

- Fully open backpressure valve
- Ensure all Red Team members are in the control room
- Close LOX Dome Loader
- Announce Venting LOX Main Tank on Facility
- Vent LOX Main Relief
- Close LOX Tank Pressure Shutoff
- Open LOX Low Pressure Manual Globe Valve

Pressurized Lines – Safety Glasses Required

- Close all Domes and Mains
- Turn off all switches
    - If another test point is required, leave 3-way diverter valve switch in the up (energized) position, refill LOX tank, and return to Domeloader Pressurization sequence
    - Otherwise, proceed with Shut-Down Sequence
- Close all nitrogen k-bottles
- Vent Nitrogen manifold
- Close Nitrogen manifold ball valves and 12-pack valves
- Ensure all pressures are back to ambient with LabVIEW
- Open vents and cycle control board switches to relieve any remaining pressure if necessary
- Detach actuator air line from the compressor
- Detach instrumentation and store camera in instrumentation room
- Plug or cap holes according to oxygen safety protocols

# Appendix 1 – Propellant Line Leak Check

**LOX Main Line**

**Table E.2: Experimental Pressure Settings**

| Oxygen Main |
|---|
| 275 psi |

- ☐ Close backpressure valve
- ☐ Close run valve
- ☐ Turn on control board
- ☐ Turn on the:
  - LOX Primary Dome
- ☐ Go outside to the Oxygen & Nitrogen storage area
- ☐ Move nitrogen 12-pack to the nitrogen main manifold
- ☐ Close 12-pack valves
- ☐ Connect 12-pack to nitrogen main manifold
- ☐ Fully open nitrogen manifold ball valves
- ☐ Crack open k-bottle globe valves to slowly bleed in pressure
- ☐ Fully open all k-bottles then close ¼ turn
- ☐ Crack open nitrogen 12-pack valves on nitrogen main manifold to bleed in pressure
- ☐ Completely open nitrogen 12-pack valves to the nitrogen main manifold then close ¼ turn
- ☐ Adjust Oxygen Main hand regulator to pressure on Table 6
- ☐ Verify sufficient pressure in the manifold using the analog gauges
- ☐ Follow Steps on Table E.3

**Table E.3: LOX Main Leak Check Procedure**

| Step | Control Room | Test Cell |
|---|---|---|
| 1 | Replace key and turn on board | |
| 2 | Communication check with the intercom | |
| 3 | | Tell control room to open LOX Pressure Shutoff Valve |
| 4 | Open LOX Shutoff Valve | |
| 5 | | Open Run Valve |
| 6 | | Find leaks with bubble solution |
| 7 | | Tighten the appropriate fittings |
| 8 | Iterate Steps 6 & 7 until no leaks are present | |

- ☐ Close all nitrogen k-bottles globe valves

Pressurized Lines – Safety Glasses Required

- Close LOX Primary Dome
- Open nitrogen main manifold vent to vent nitrogen manifold
- Close nitrogen 12-pack valves on the nitrogen main manifold
- Close all nitrogen manifold ball valves
- Announce, “Venting LOX Main Tank” over the intercom
- Open LOX Main Relief
- When vented, close LOX Main Relief
- Close LOX Pressure Shutoff valve
- Close Run Valve

# Appendix 2 – Cryogenic Fluid Safety & Failure Modes

## Cryogenic Fluid Safety

Safety is a paramount concern when using cryogenic fluid systems. Cryogenic fluids can present severe safety concerns to the operators – most notably the risk of asphyxiation, superficial burns, and/or frostbite. These concerns often do not require direct physical contact with the fluid, and, as such, caution and consideration for safety should be taken in regards to all aspects of a cryogenic fluid system.

**TREAT CRYOGENIC SYSTEMS WITH RESPECT!**

**Table E.4: Normal Oxygen Atmosphere**

| Gas | % Volume |
|---|---|
| Nitrogen | 78 % |
| Oxygen | 21 % |
| Argon | 1 % |

**Table E.5: Health Effects of Reduced Oxygen Atmosphere**

| Percentage of Oxygen in the air (%) | Symptoms (effects noted below are time dependent) |
|---|---|
| 21 – 19 | None |
| > 19 - 15 | Reduced Reaction Times |
| > 15 - 12 | Heavy breathing, rapid pulse, lack of coordination |
| > 12 - 10 | Dizziness, unclear thinking, lips slightly blush |
| > 10 - 8 | Nausea, vomiting, loss of consciousness |
| > 8 - 6 | Death within 8 minutes, brain damage within 4-8 minutes |
| 4 | Coma within 40 seconds, respiratory failure, death |

## Table E.6: Cryogenic Physiological Hazards

| HAZARD | DEFINTION | MITIGATION | EFFECT |
|---|---|---|---|
| Contact Burn | Direct contact with cryogenic fluids, boiled off cryogenic vapor or surfaces cooled by cryogenic fluids | - Protective clothing as stated in Appendix 2<br>- Stay out of the path of all boil off vapor<br>- Ensure that all pressure relief valves and rupture disk vent paths are directed away from personnel<br>- Perform routine inspections of cryogenic system<br>- Buddy System | - Similar to heat burns; can locally freeze and tear or remove skin<br>- Due to decrease in feeling can lead to frostbite |
| Frostbite | Freezing of skin and body parts due to the exposure to low temperatures | - Protective clothing as stated in Appendix 2<br>- Stay out of the path of all boil off vapor<br>- Ensure that all pressure relief valves and rupture disk vent paths are directed away from personnel<br>- Perform routine inspections of cryogenic system<br>- Buddy System | - Can lead to permanent damage and discoloration up to loss of limb<br>- Prolonged exposure of cold vapor or gas can damage lungs and the eyes<br>- Exposure is on the order of seconds, not minutes |
| Hypothermia | Body not capable of maintaining normal temperature | - Protective clothing as stated in Appendix 2<br>- Stay out of the path of all boil off vapor<br>- Ensure that all pressure relief valves and rupture disk vent paths are directed away from personal<br>- Perform routine inspections of cryogenic system<br>- Buddy System<br>- Avoid long term exposure | - Fatigue<br>- Confusion<br>- Loss of coordination<br>- Unconsciousness<br>- Death |
| Oxygen Deficiency/ Asphyxiation | Extreme volume expansion from a liquid to a gas when warmed can reduce the amount of oxygen in the air | - Oxygen monitoring in the test area or on personnel<br>- Buddy System | See Table for Symptoms of rarefied oxygen atmosphere |

**Table E.7: Failure Modes and Mitigations**

| FAILURE MODE | MITIGATION | SOLUTION | EFFECT |
|---|---|---|---|
| Leaks in supply lines | Leak check before test | Leak Check | Possible oxygen depletion of test area |
| Power failure | Shut-down sequence when power returns | Fuel vent valve releases fuel to drainage.<br>Close Tanks and vent | |
| Pressure Buildup due to Vaporization | Ensure that all areas where cryogenic fluids could be trapped are equipped with relief valves. | Press BRB on the test stand control box and reset control switches.<br>Stop LabVIEW.<br>Check for damaged parts. | Damage to parts.<br>Oxygen depletion of test area. |
| Over Pressurization | Max test pressure is also lower than rated parts.<br>Vents used wherever cryogenic fluids could be trapped. | Press BRB on the test stand control box and reset control switches.<br>Stop LabVIEW.<br>Check for damaged parts. | Shut-down sequence and assess failure location and possible damage. |

# Appendix 3 – JRC Test Stand Footprint

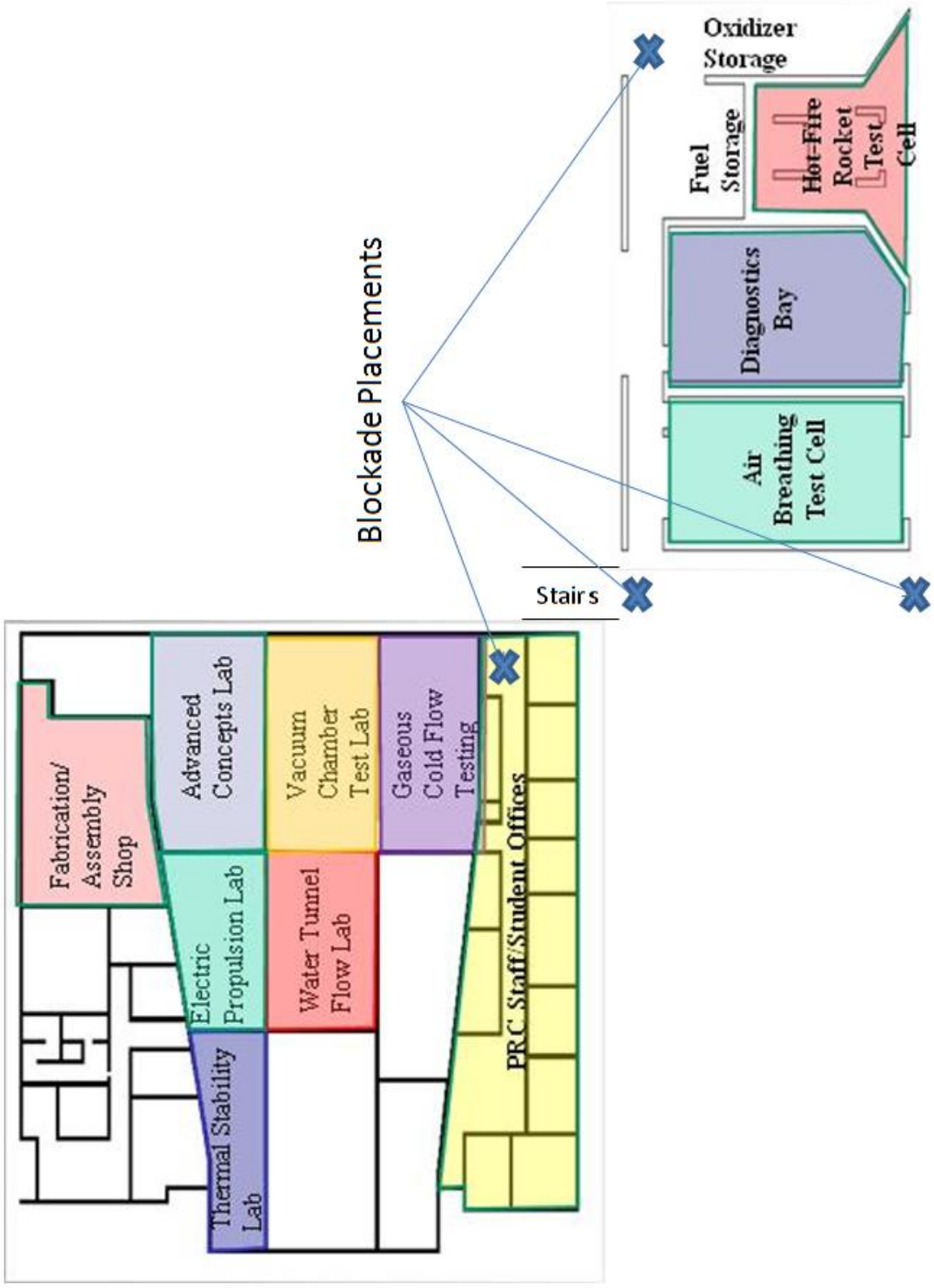


**Figure E.1: JRC Footprint**

# Appendix 4 – Sensor Locations Sheet

**Table E.8: Sensor Location Sheet**

| Sensor | Measurement | Nomenclature | Range | Voltage Range | Test Stand | CH # |
|---|---|---|---|---|---|---|
| | | | | | | **BNC-2095 SC1Mod2** |
| Omega 96611 | Orifice Inlet | P Orifice In | 0-300 psig | 0-5 V | B17 | 16 |
| Omega 96607 | Orifice Outlet | P Orifice Out | 0-300 psig | 0-5 V | B20 | 6 |
| Omega 103110D854 | Venturi | P Venturi | 0-500 psig | 0-5 V | B22 | 8 |
| HW 1196157 | LOX Main Dome | P LOX Dome | 0-3000 psig | 0-5 V | B11 | 25 |
| HW 1144308 | LOX Tank | P LOX Tank | 0-3000 psig | 0-5 V | B21 | 31 |
| HW 1195664 | $GN_2$ Manifold | P GN2 | 0-3000 psig | 0-5 V | B19 | 30 |
| PCB 30315 | High Freq | P High Freq | 0-5000 psia | ± 5V | BNC2 | BF2 |
| | | | | | | **TC-2095** |
| Type T | Orifice Inlet | T Orifice In | -200 – 350 °C | | 13 | 13 |
| Type T | Orifice Outlet | T Orifice Out | -200 – 350 °C | | 14 | 14 |
| Type T | Venturi | T Venturi | -200 – 350 °C | | 15 | 15 |
| Type T | Run Valve | T Run Valve | -200 – 350 °C | | 16 | 16 |

Crvogenic Temperatures – Protective Clothing Required

# Appendix 5 – LOX Run Tank Fill Procedure

Pre-Test Procedures:
PRC Red Team members performing the cryogenic fill procedure must be properly clothed in protective clothing. All of the cryogenic protective clothing is located in the lockers in the instrumentation room. Protective clothing includes the following:

1) Closed toe shoes – non-absorbent, non cloth (sneakers or boots, not provided by PRC).
2) Pants – No cuff, No Shorts (not provided by PRC)
3) Lab Coat – Nomex Flame Resistant (No Pockets Preferred)
4) Cryogenic Apron
5) Cryogenic Gloves – worn above sleeve for actions above head, and worn tucked in sleeve for actions below head.
6) Safety Glasses
7) Mask with Face Shield

This test procedure assumes the following:

1) All lines have been connected.
2) The system has been leak checked in accordance with Appendix 1and all leaks corrected.
3) The system is clean
4) All instrumentation has been calibrated as required.
5) $LN_2$ Dewars has been delivered to the Facility
6) Transfer hose has been cleaned/ and capped till service
7) Fill area is secure and area clear
8) Requisite tools accessible

## Facility Preparation

- Attach the pressurization air to the compressor in the instrumentation room and make sure that the compressor is on auto compress
- Ensure air compressor tank pressure is at least 80 psi
- Toggle all valves for functionality: LOX Fill, LOX Main, LOX Main Relief, LOX Fire, LOX Line Vent
- Turn on LOX Run Tank Level Sensor Monitor
- Put up all blockades around the test facility as illustrated in Appendix 3
- Close and Lock Security Fence

The liquid nitrogen (**$LN_2$**) fill takes approximately two hours to fill the liquid oxygen (**LOX**) run tank outer jacketed volume. The $LN_2$ fill of the LOX Run Tank takes approximately 30 minutes to fill the 23 gallon run tank volume completely. Monitor the LOX Run Tank Level Sensor to establish when the tank is full.

## $LN_2$ Fill

- Turn TV monitor on so that fill area is completely visible from control room
- Go out to fill area
- Uncap $LN_2$ fill transfer hose
- Connect $LN_2$ fill transfer hose to 1st $LN_2$ Dewar
- Manually close $LN_2$ fill line vent valve
- Open $LN_2$ Vent Bypass valve to Atmosphere
- Open $LN_2$ fill valve
- Slowly open 1st $LN_2$ Dewar valve
- Completely open 1st $LN_2$ Dewar valve
- Empty 1st $LN_2$ Dewar (≈ 45-70 minutes)
- Close $LN_2$ fill valve
- Crack $LN_2$ fill line vent valve
- Close 1st $LN_2$ Dewar valve
- Open $LN_2$ fill line vent valve to vent excess pressure (keep feet away from the discharge area)
- Disconnect $LN_2$ transfer hose from 1st $LN_2$ Dewar
- Move 1st $LN_2$ Dewar out of fill area
- Reconnect $LN_2$ transfer hose to 2nd $LN_2$ Dewar
- Manually close $LN_2$ fill line vent valve
- Open $LN_2$ fill valve
- Slowly open 2nd $LN_2$ Dewar valve
- Completely open 2nd $LN_2$ Dewar valve
- Empty 2nd $LN_2$ Dewar (≈ 45-70 minutes)
- Close $LN_2$ fill valve
- Crack $LN_2$ fill line vent valve
- Close 2nd $LN_2$ Dewar valve
- Open $LN_2$ fill line vent valve to vent excess pressure (keep feet away from the discharge area)
- Disconnect $LN_2$ transfer hose from 2nd $LN_2$ Dewar
- Move 2nd $LN_2$ Dewar out of fill area
- Close $LN_2$ Vent Bypass valve to Atmosphere ($LN_2$ tank jacket volume should be full and there should be a thick frost encompassing the LOX Run Tank) – leave slightly open to alleviate check valve chatter
  - If the Outer Jacket is not full then repeat the process emptying 3rd $LN_2$ Dewar into outer jacket
  - If full then go forward
- Reconnect $LN_2$ transfer hose to3rd $LN_2$ Dewar (this Dewar is to be utilized to replenish the $LN_2$ in the outer jackets for chilling the LN2 jacketed lines and additionally to hold the LOX at cryogenic temperatures)
- As needed replenish $LN_2$ Outer Jacket
  - Open $LN_2$ fill valve
  - Slowly open $LN_2$ Dewar valve
  - Completely open $LN_2$ Dewar valve

- Hold $LN_2$ Outer Jacket Tank with $LN_2$ from 3rd $LN_2$ Dewar

## $LN_2$ Fill of LOX Run Tank

- ☐ Close Run Valve
- ☐ Open LOX Main Relief valve
- ☐ Open LOX Fill valve
- ☐ Go out to fill area (at least two red team members)
- ☐ Wearing cleaning gloves: Uncap LOX fill transfer hose (place cap in clean baggy and seal)
- ☐ Connect the LOX fill transfer hose to $LN_2$ Dewar (need extra fitting)
- ☐ Manually close LOX Fill Line Vent valve
- ☐ Slowly open $LN_2$ Dewar valve
- ☐ Completely open $LN_2$ Dewar valve
- ☐ Fill LOX Main Tank (≈ 30 minutes)
  - Use the Dewar pressurization valve to adjust the $LN_2$ fill flow as needed
- ☐ Close LOX fill valve
- ☐ Crack LOX fill line vent valve
- ☐ Close $LN_2$ Dewar valve
- ☐ Open LOX fill line vent valve to relive any remaining pressure
- ☐ Close LOX Main Relief valve
- ☐ Open Low pressure manual globe valve
- ☐ Disconnect LOX fill transfer hose from $LN_2$ Dewar
- ☐ Take off baggy and cap LOX fill transfer hose
- ☐ Move $LN_2$ Dewar out of fill area

# Appendix 6: Facility Schematic

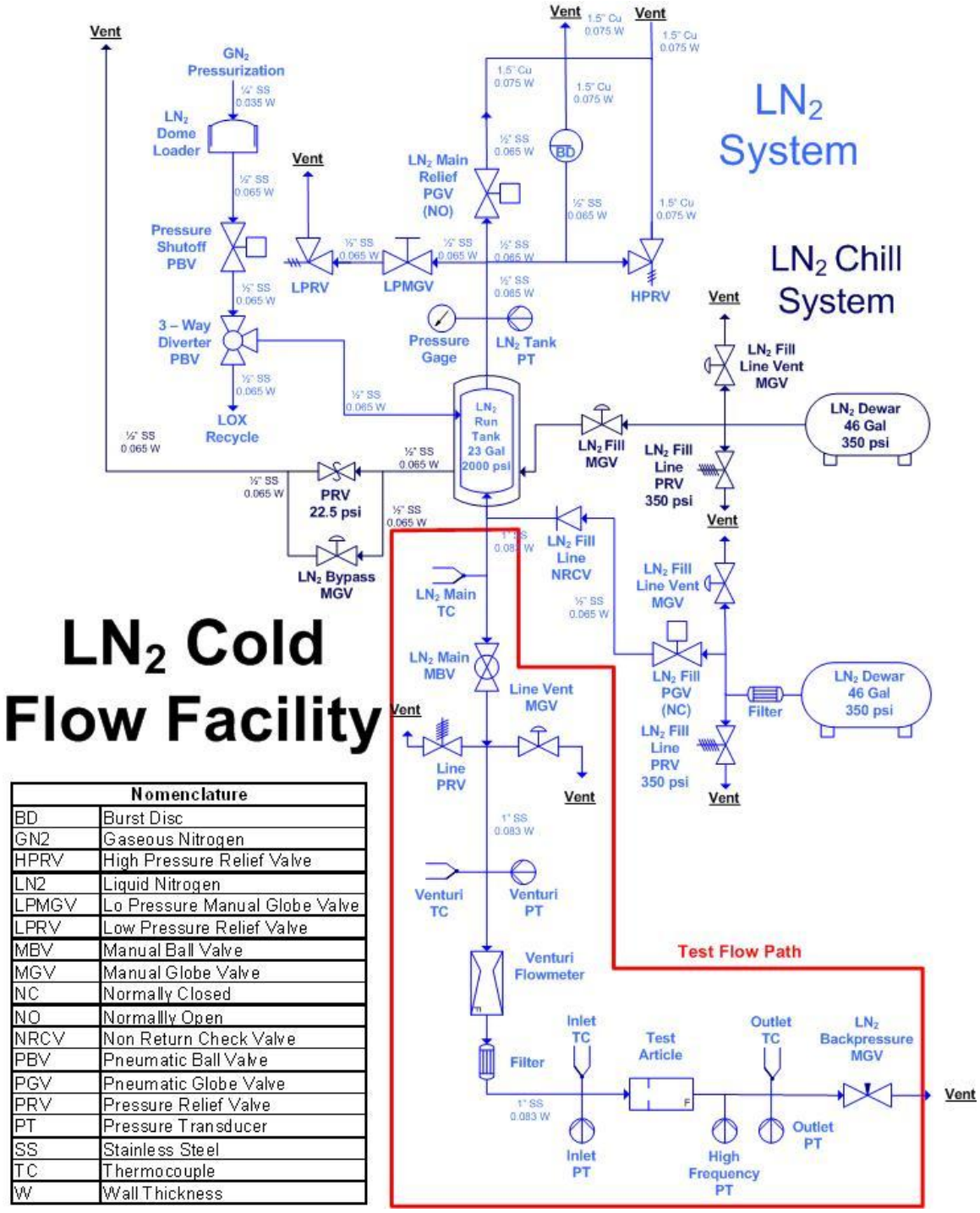


| Nomenclature | |
|---|---|
| BD | Burst Disc |
| GN2 | Gaseous Nitrogen |
| HPRV | High Pressure Relief Valve |
| LN2 | Liquid Nitrogen |
| LPMGV | Lo Pressure Manual Globe Valve |
| LPRV | Low Pressure Relief Valve |
| MBV | Manual Ball Valve |
| MGV | Manual Globe Valve |
| NC | Normally Closed |
| NO | Normallly Open |
| NRCV | Non Return Check Valve |
| PBV | Pneumatic Ball Valve |
| PGV | Pneumatic Globe Valve |
| PRV | Pressure Relief Valve |
| PT | Pressure Transducer |
| SS | Stainless Steel |
| TC | Thermocouple |
| W | Wall Thickness |

**Figure E.2: Orifice Test Facility**

APPENDIX F

Static Plots

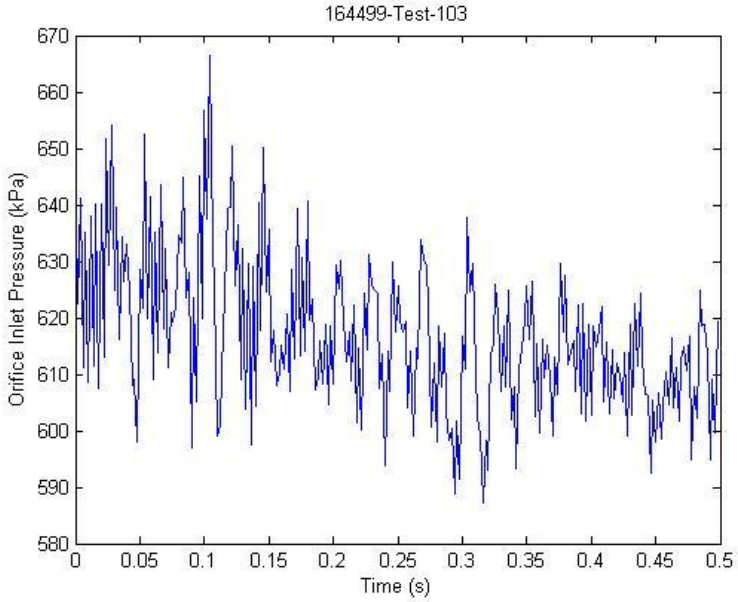


**Figure F.1: 164499-103 Orifice Inlet Pressure**

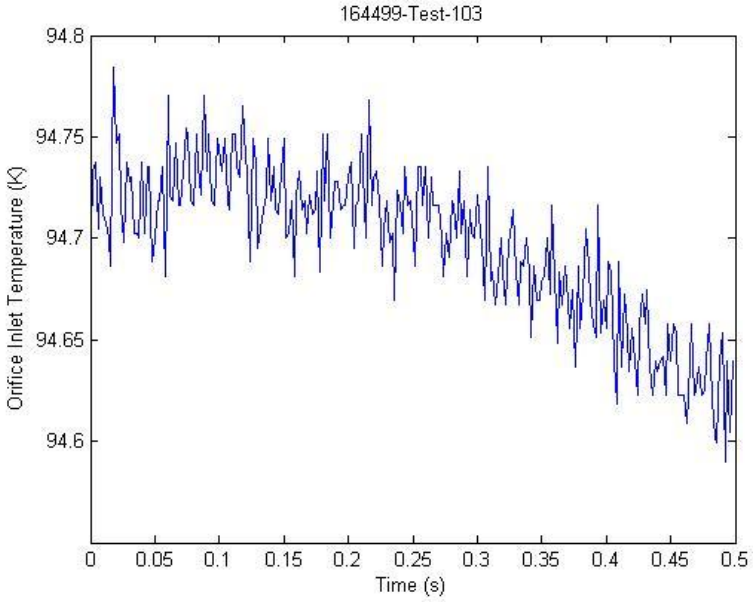


**Figure F.2: 164499-103 Orifice Inlet Temperature**

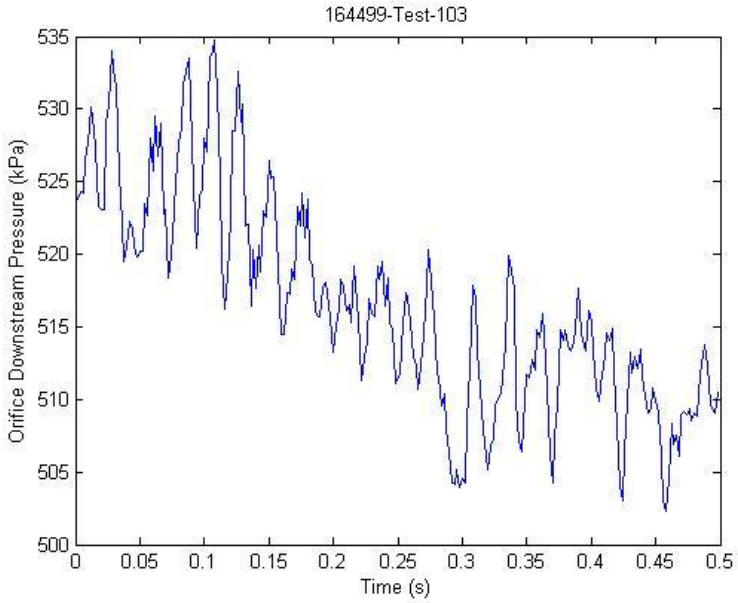


**Figure F.3: 164499-103 Orifice Outlet Pressure**

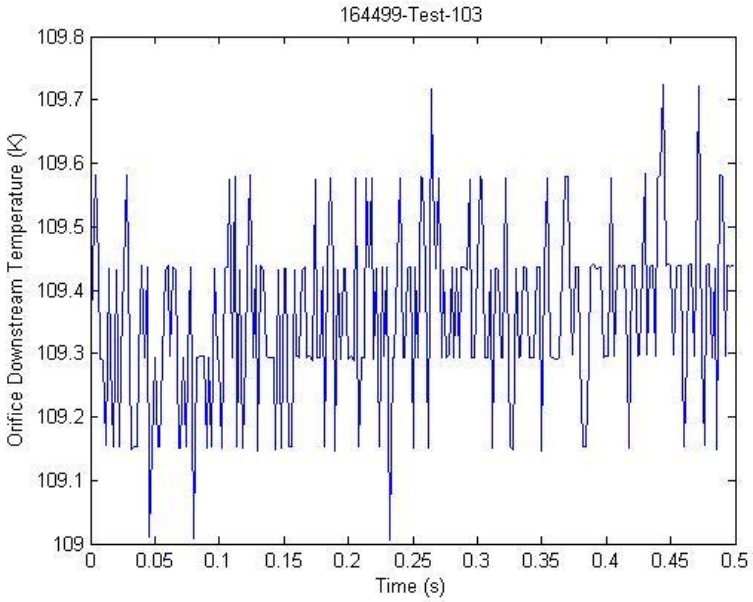


**Figure F.4: 164499-103 Orifice Outlet Temperature**

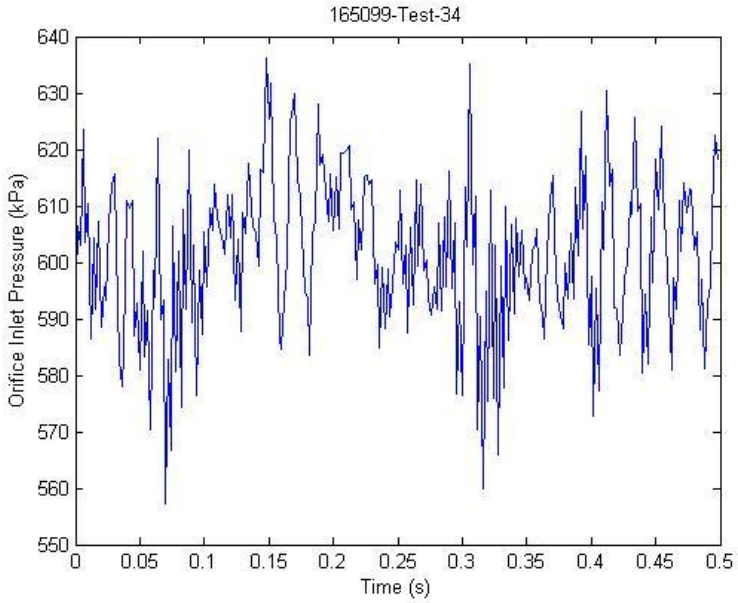


**Figure F.5: 165099-34 Orifice Inlet Pressure**

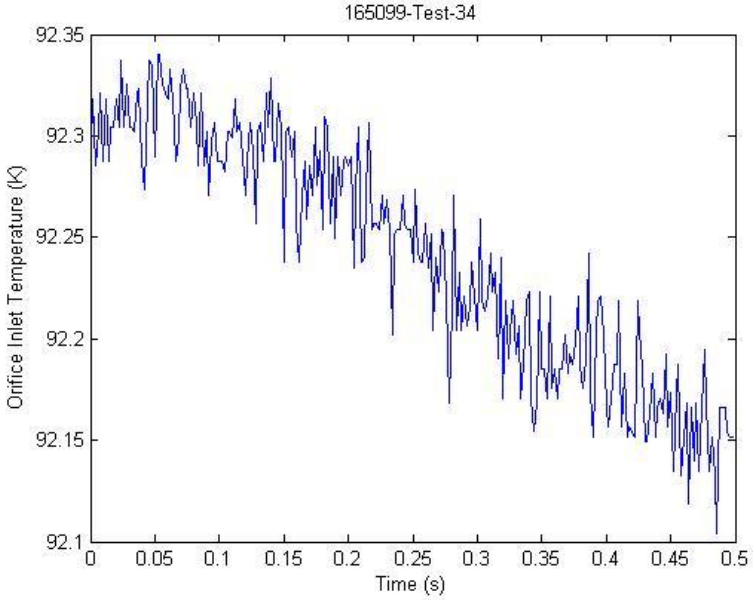


**Figure F.6: 165099-34 Orifice Inlet Temperature**

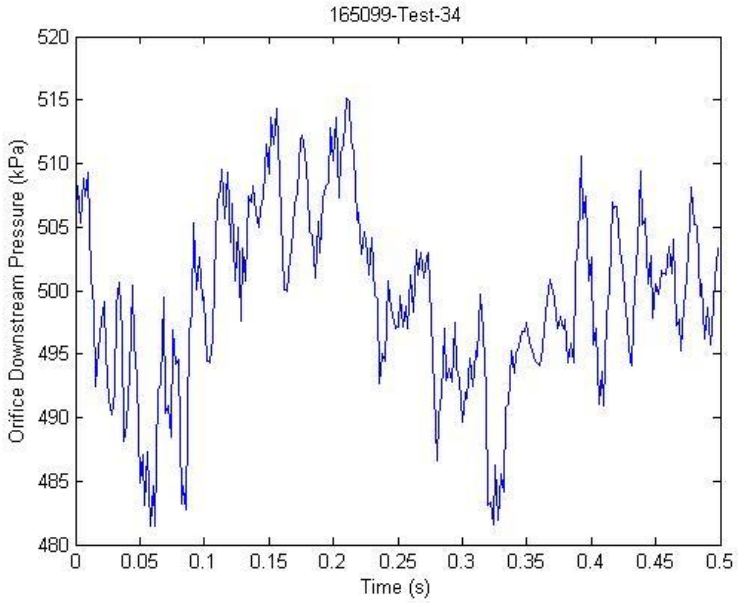


**Figure F.7: 165099-34 Orifice Outlet Pressure**

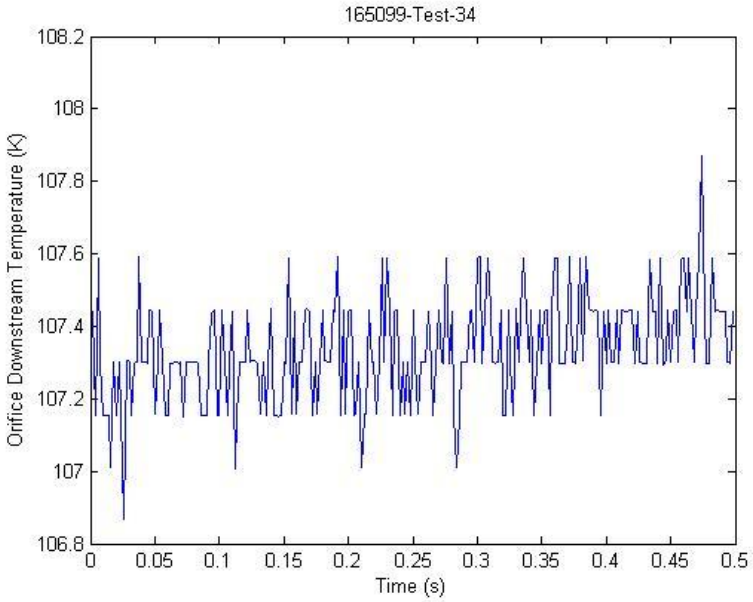


**Figure F.8: 165099-34 Orifice Outlet Temperature**

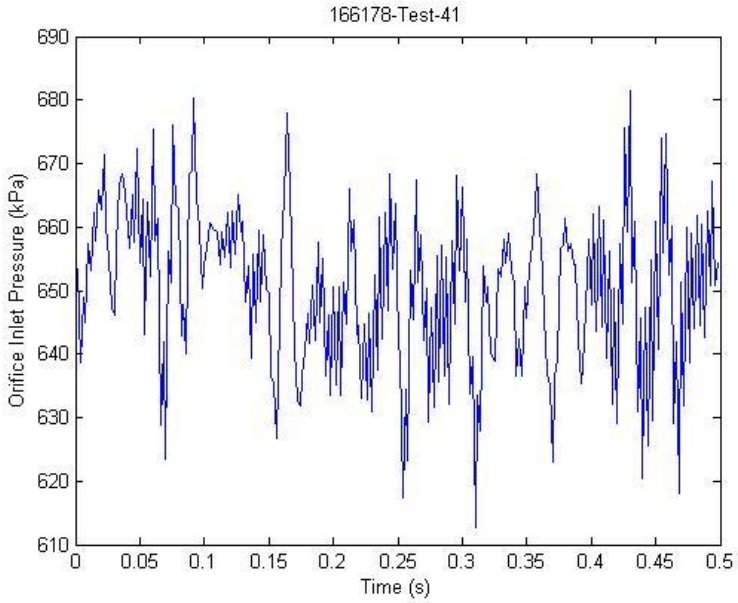


**Figure F.9: 166178-41 Orifice Inlet Pressure**

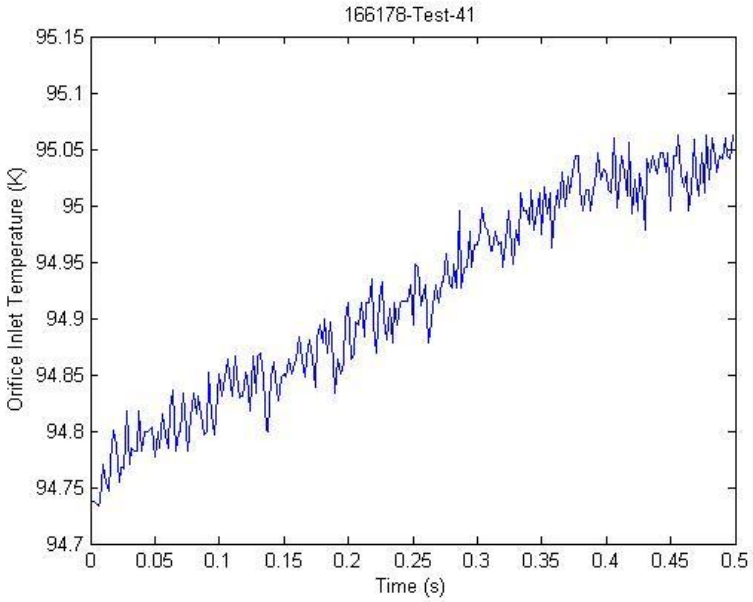


**Figure F.10: 166178-41 Orifice Inlet Temperature**

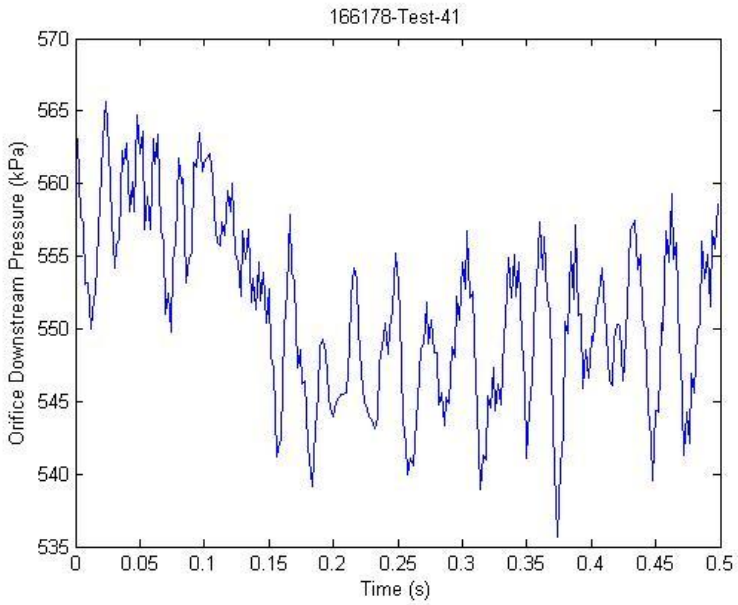


**Figure F.11: 166178-41 Orifice Outlet Pressure**

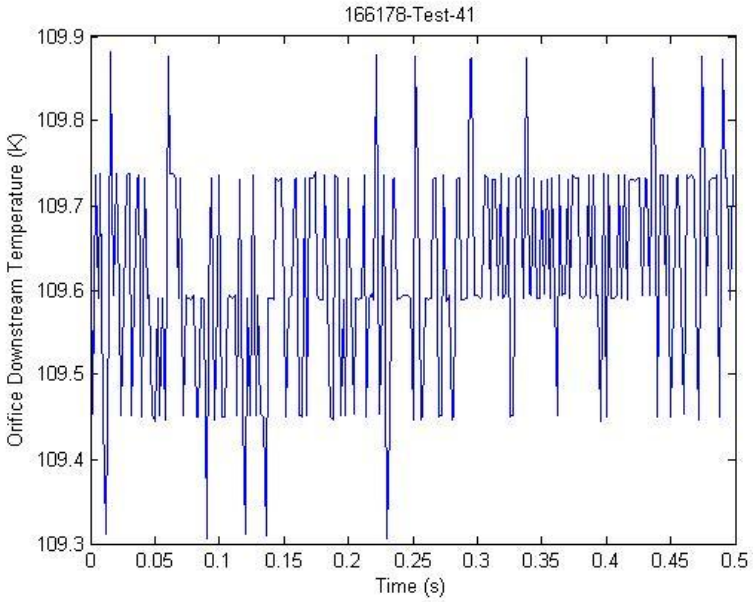


**Figure F.12: 166178-41 Orifice Outlet Temperature**

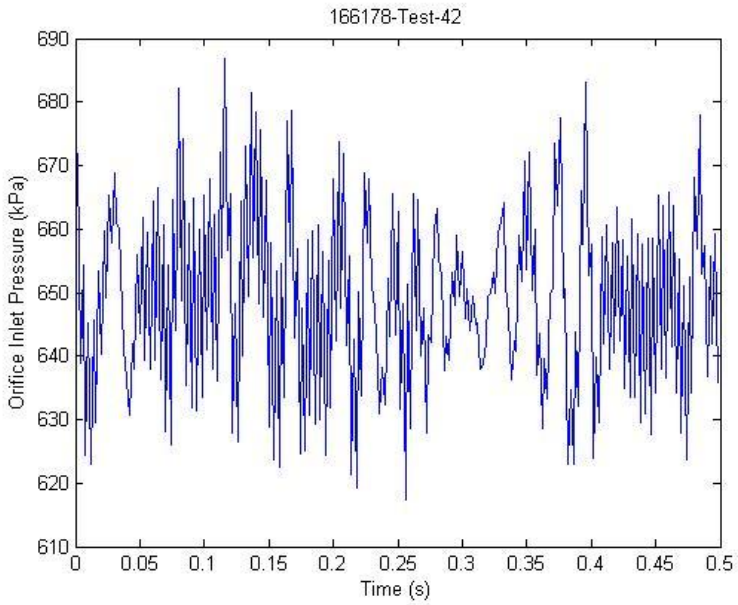


**Figure F.13: 166178-42 Orifice Inlet Pressure**

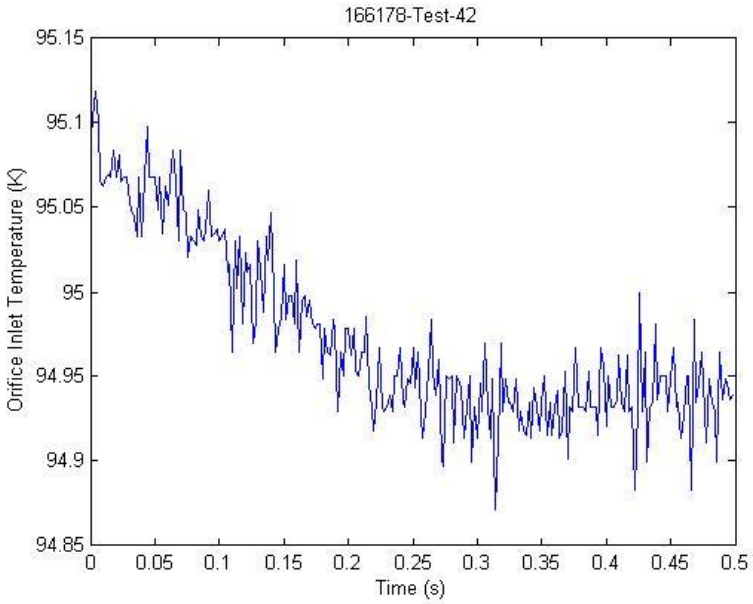


**Figure F.14: 166178-42 Orifice Inlet Temperature**

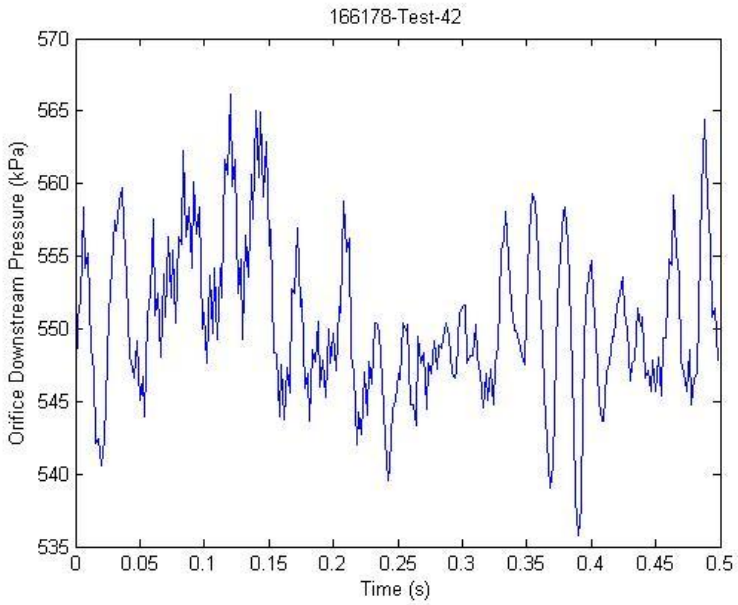


**Figure F.15: 166178-42 Orifice Outlet Pressure**

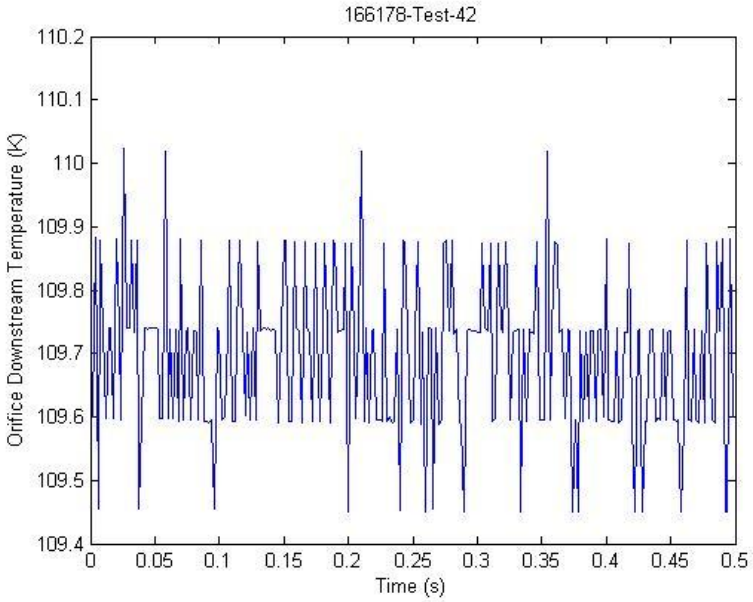


**Figure F.16: 166178-42 Orifice Outlet Temperature**

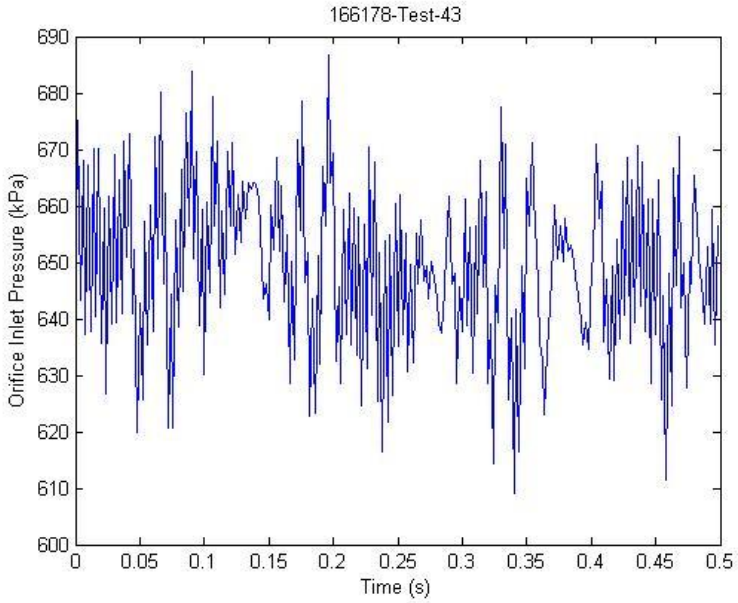


**Figure F.17: 166178-43 Orifice Inlet Pressure**

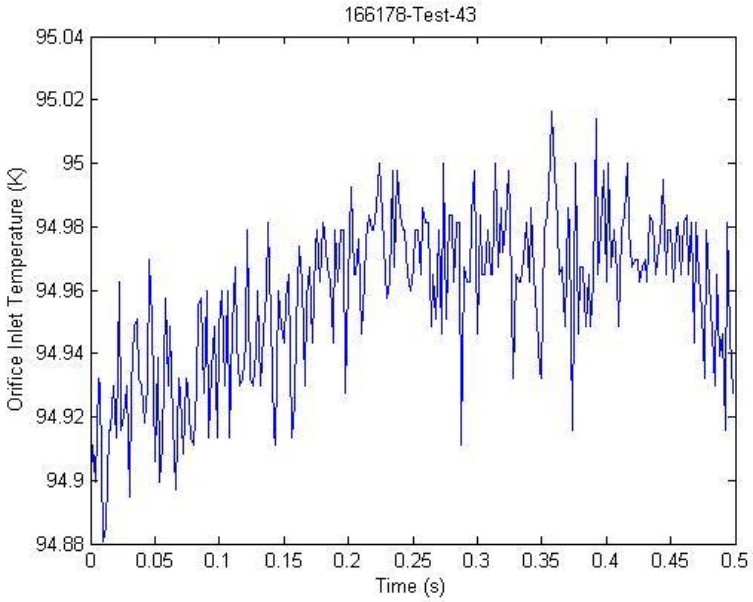


**Figure F.18: 166178-43 Orifice Inlet Temperature**

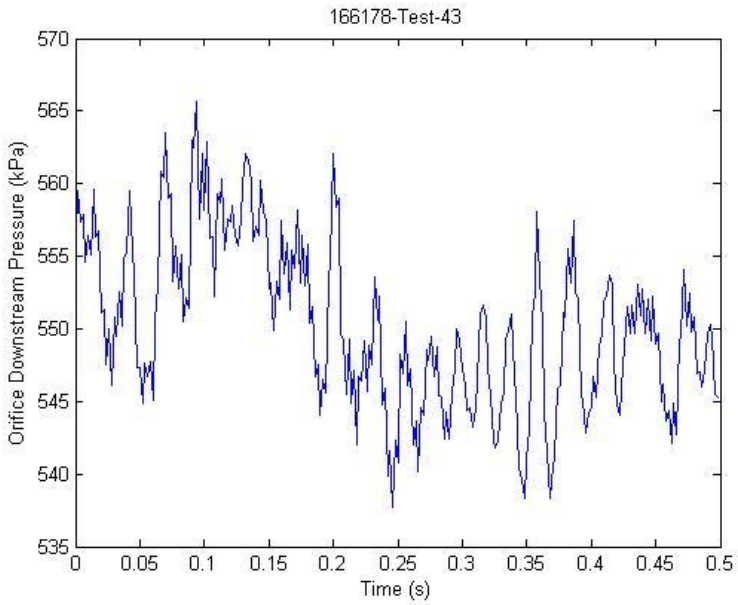


**Figure F.19: 166178-43 Orifice Outlet Pressure**

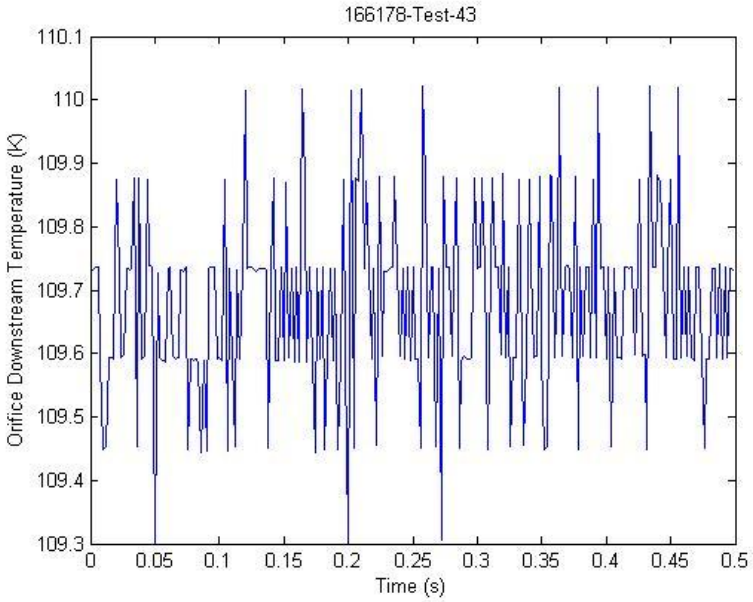


**Figure F.20: 166178-43 Orifice Outlet Temperature**

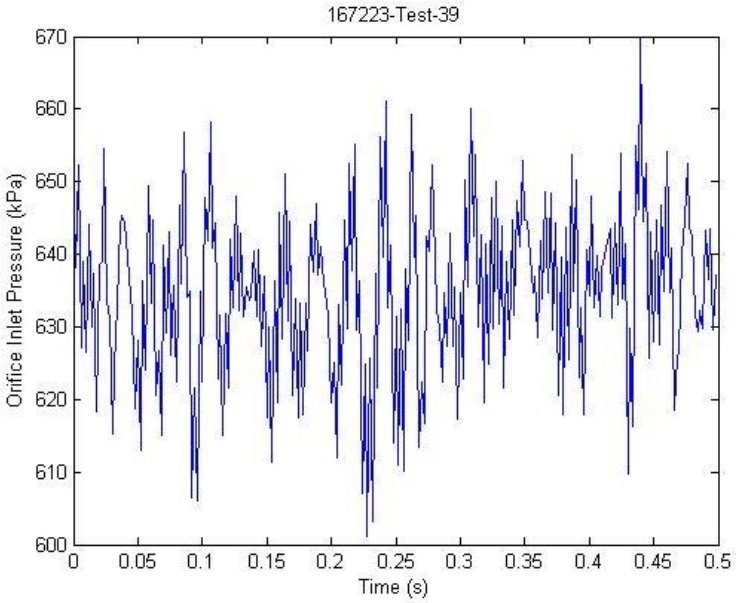


**Figure F.21: 167223-39 Orifice Inlet Pressure**

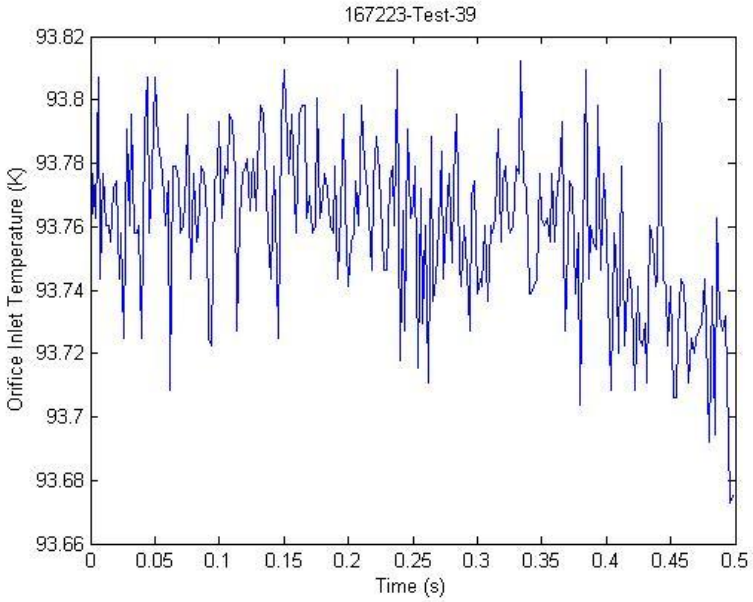


**Figure F.22: 167223-39 Orifice Inlet Temperature**

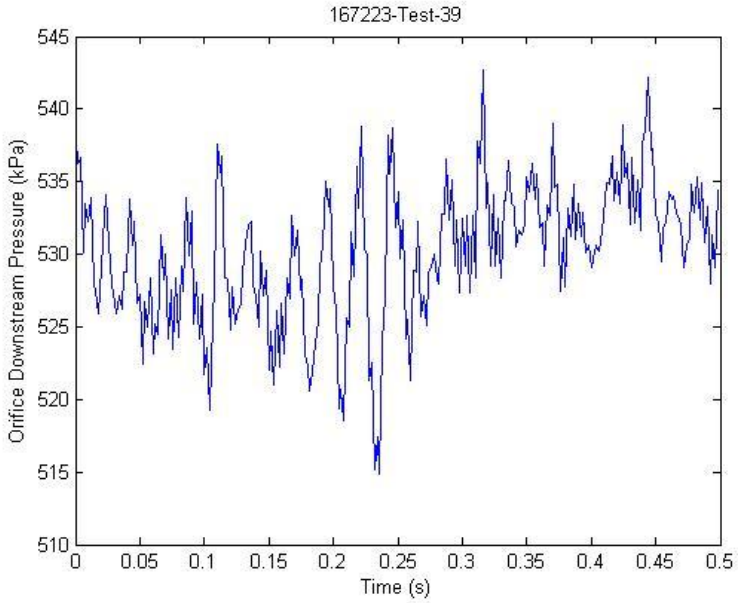


**Figure F.23: 167223-39 Orifice Outlet Pressure**

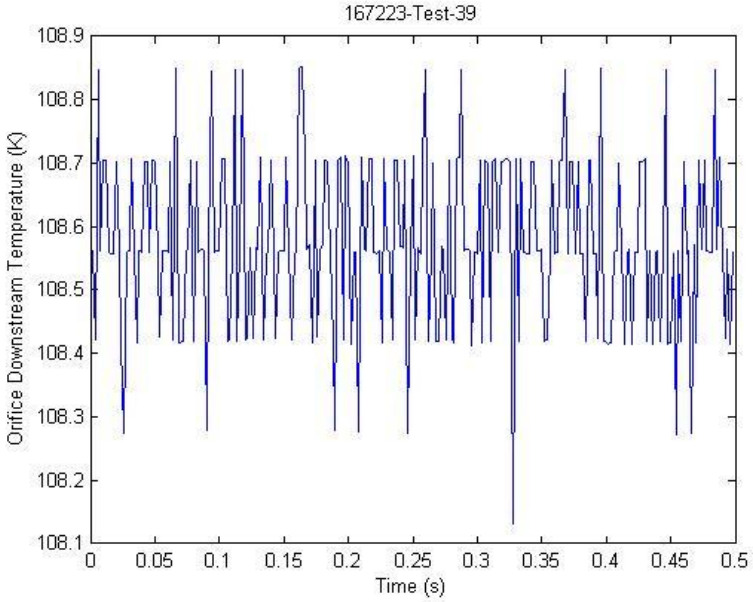


**Figure F.24: 167223-39 Orifice Outlet Temperature**

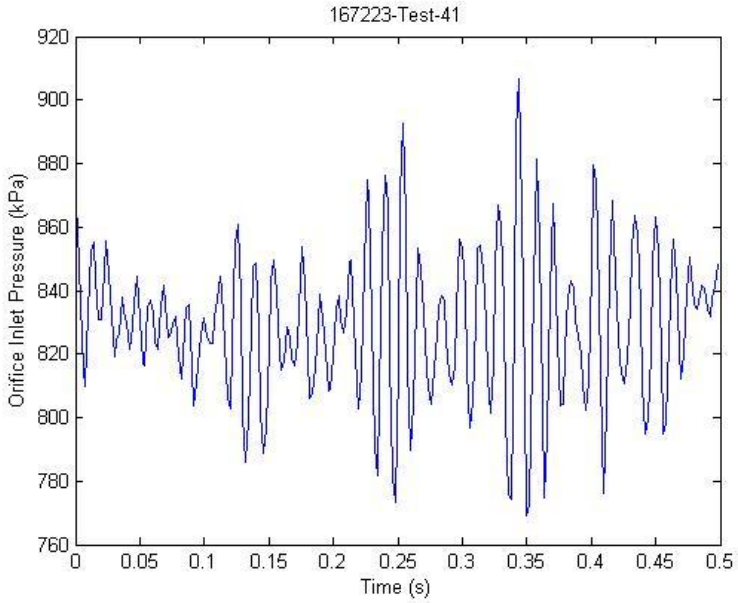


**Figure F.25: 167223-41 Orifice Inlet Pressure**

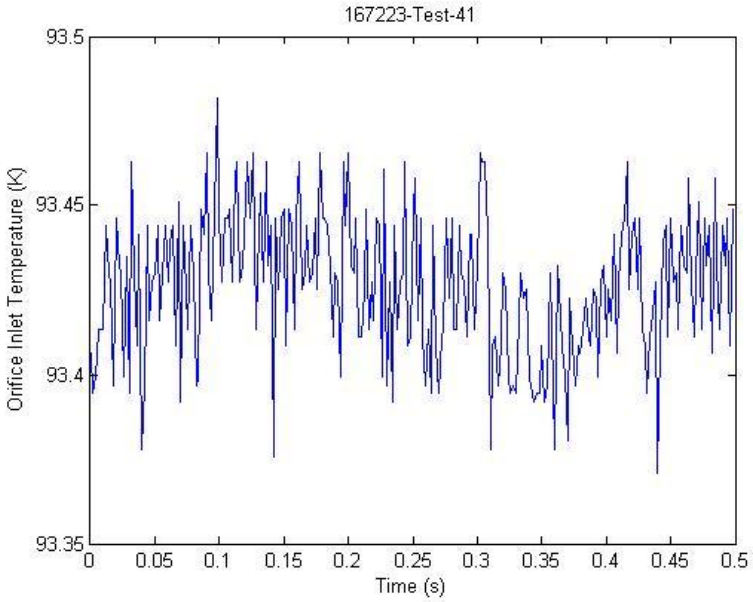


**Figure F.26: 167223-41 Orifice Inlet Temperature**

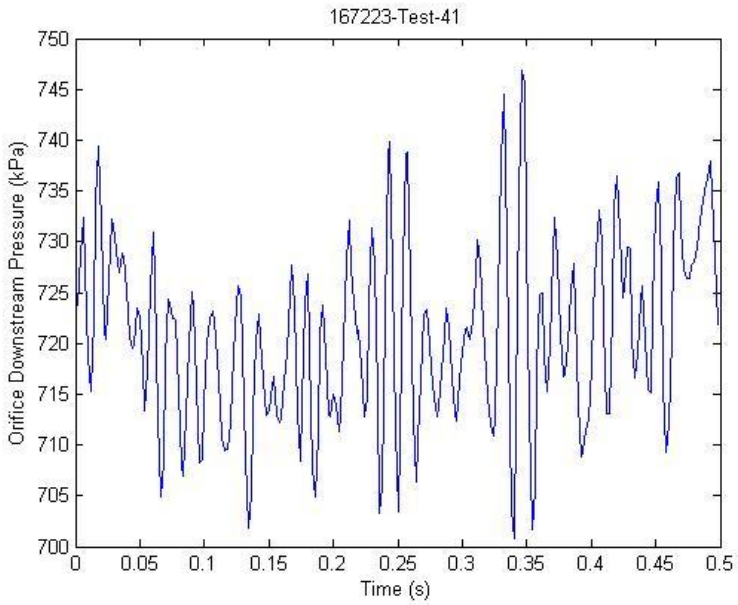


**Figure F.27: 167223-41 Orifice Outlet Pressure**

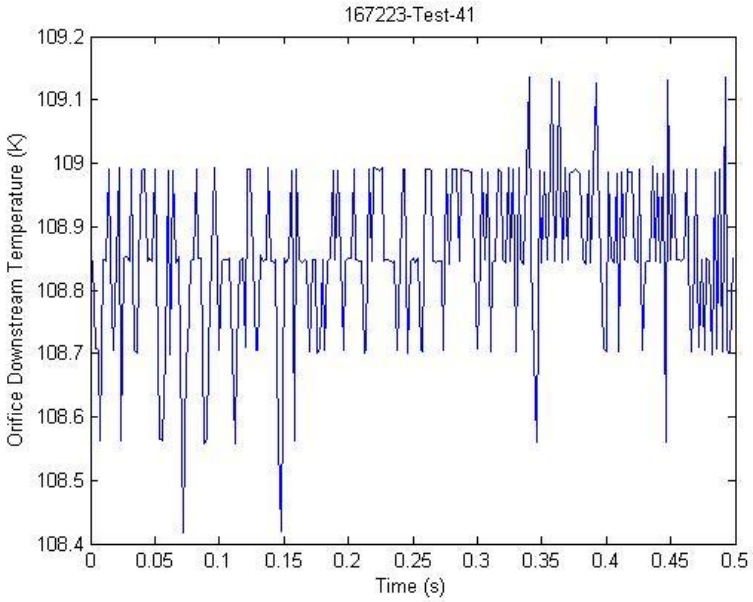


**Figure F.28: 167223-41 Orifice Outlet Temperature**

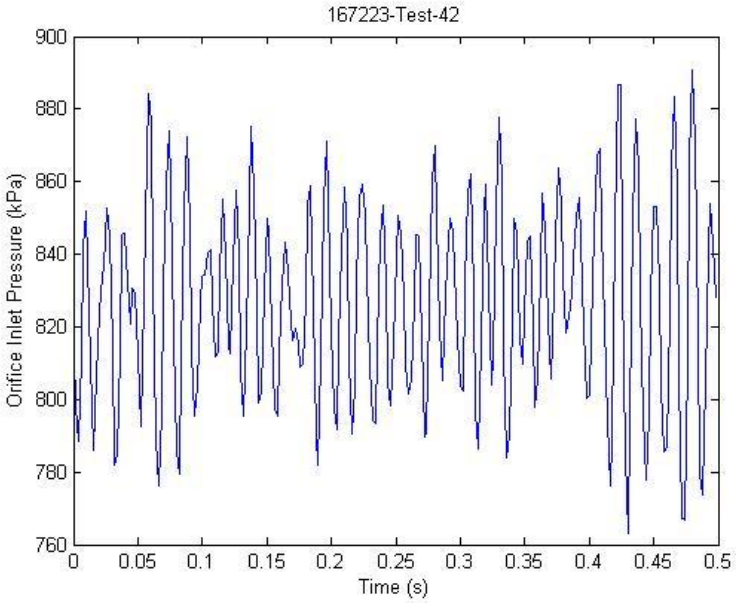


**Figure F.29: 167223-42 Orifice Inlet Pressure**

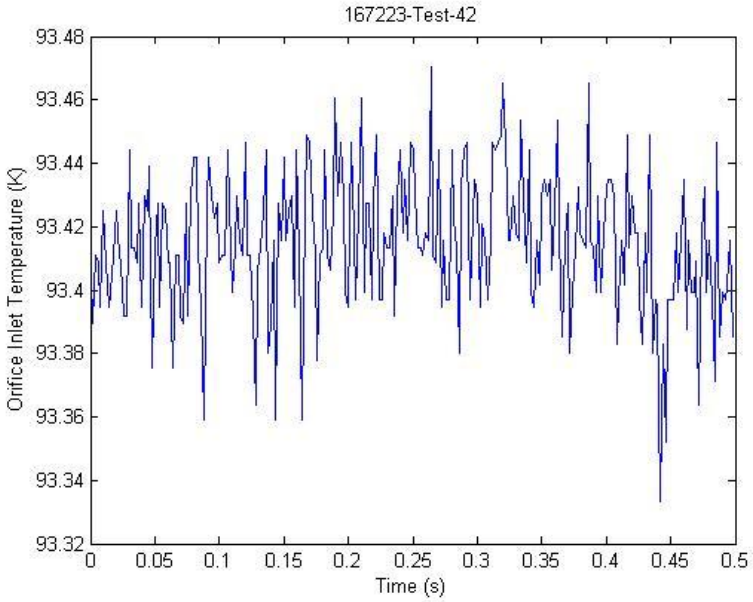


**Figure F.30: 167223-42 Orifice Inlet Temperature**

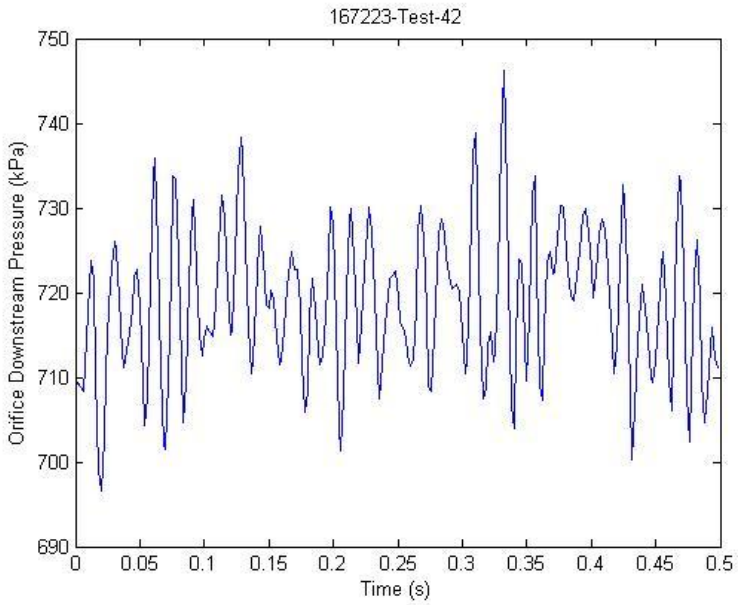


**Figure F.31: 167223-42 Orifice Outlet Pressure**

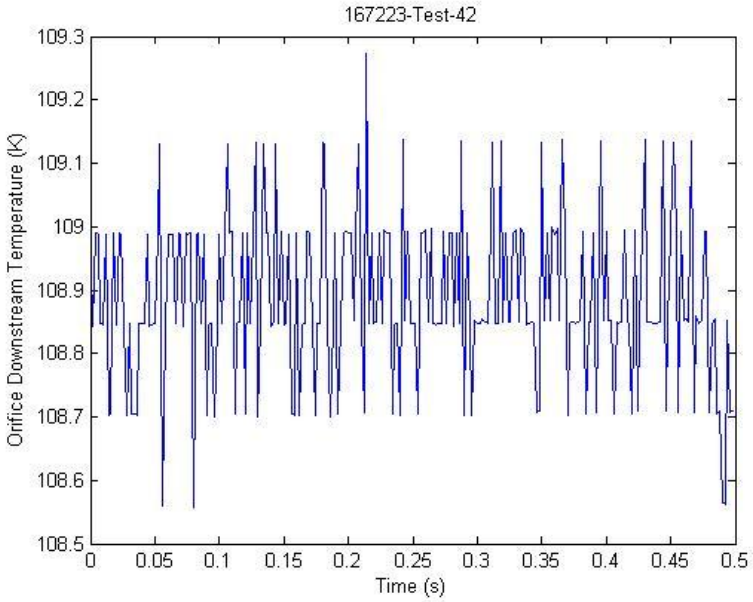


**Figure F.32: 167223-42 Orifice Outlet Temperature**

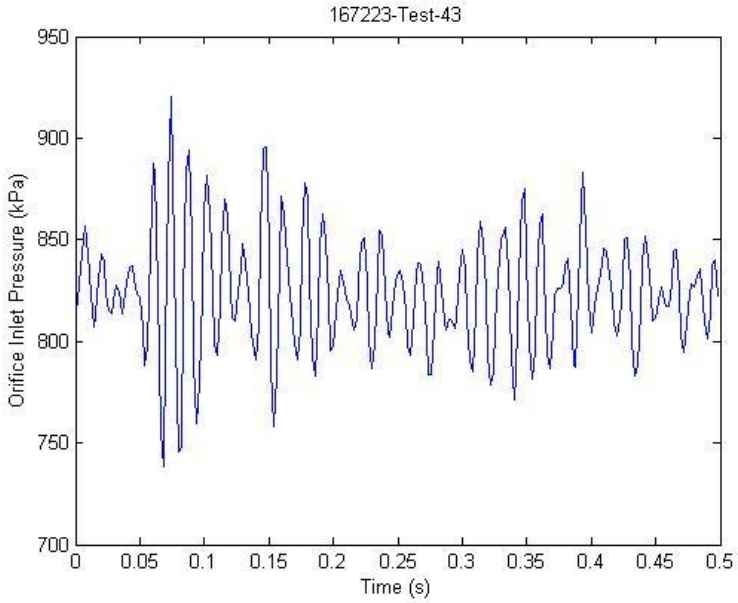


**Figure F.33: 167223-43 Orifice Inlet Pressure**

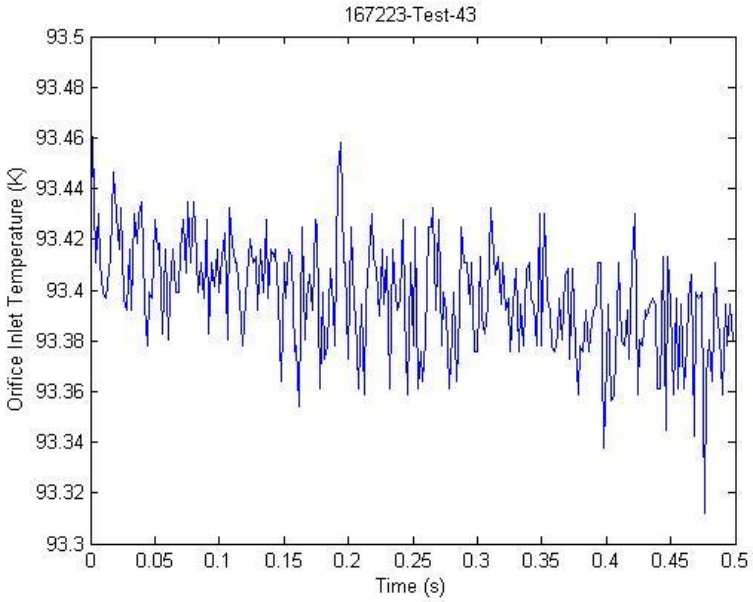


**Figure F.34: 167223-43 Orifice Inlet Temperature**

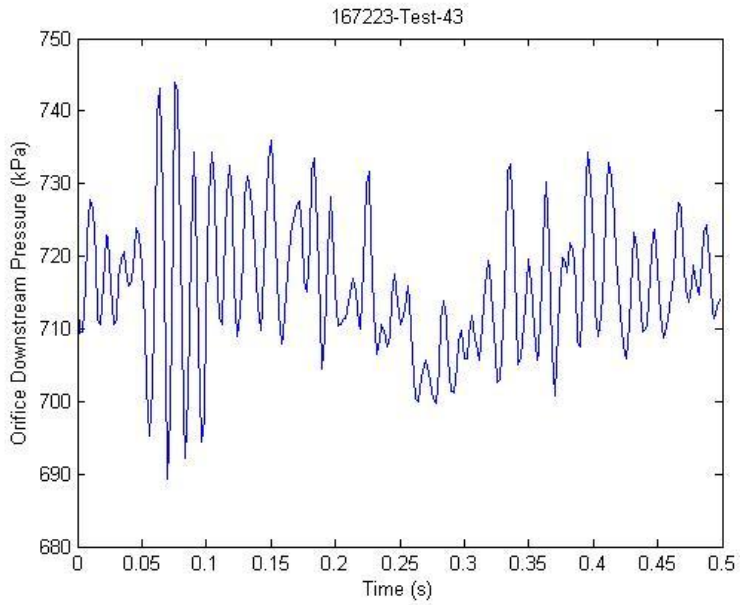


**Figure F.35: 167223-43 Orifice Outlet Pressure**

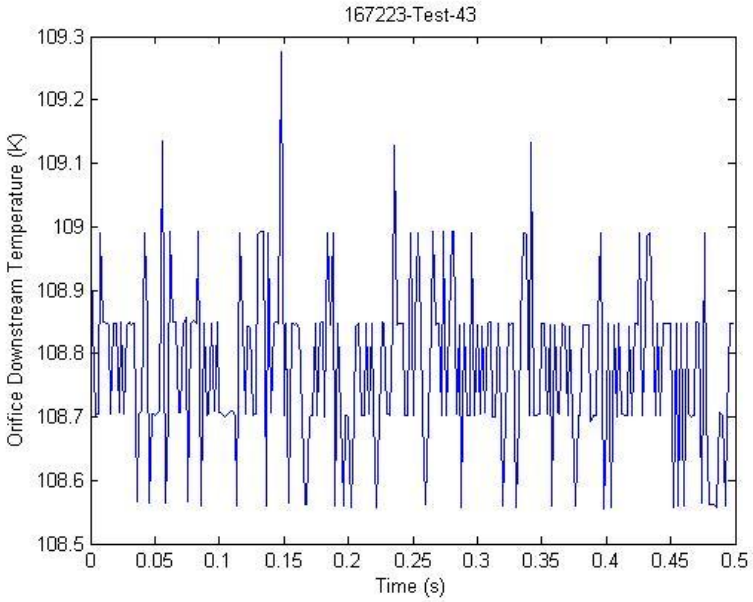


**Figure F.36: 167223-43 Orifice Outlet Temperature**

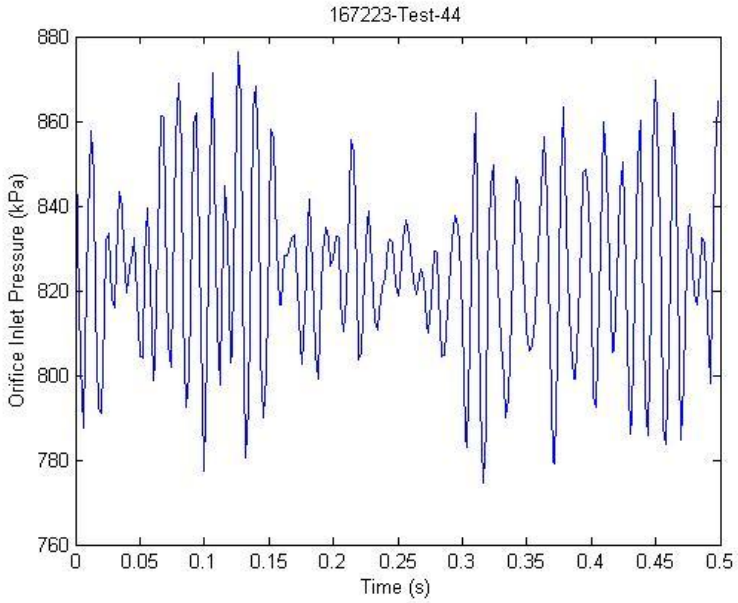


**Figure F.37: 167223-44 Orifice Inlet Pressure**

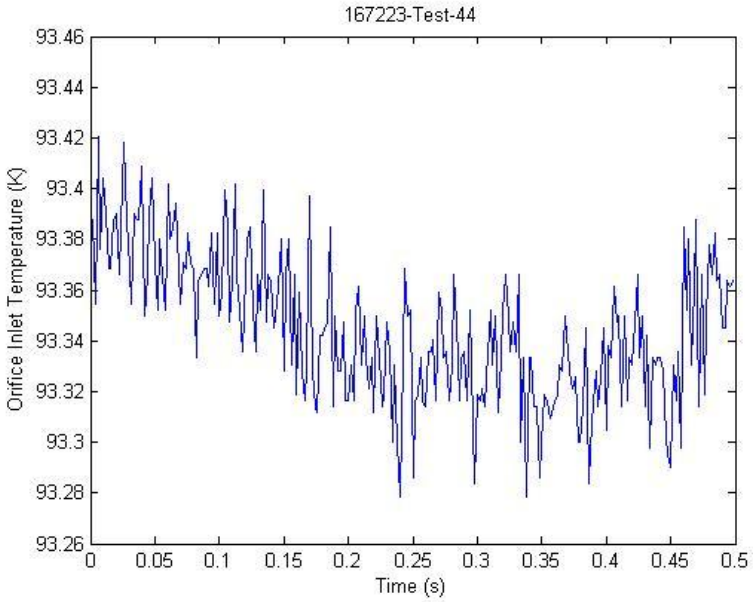


**Figure F.38: 167223-44 Orifice Inlet Temperature**

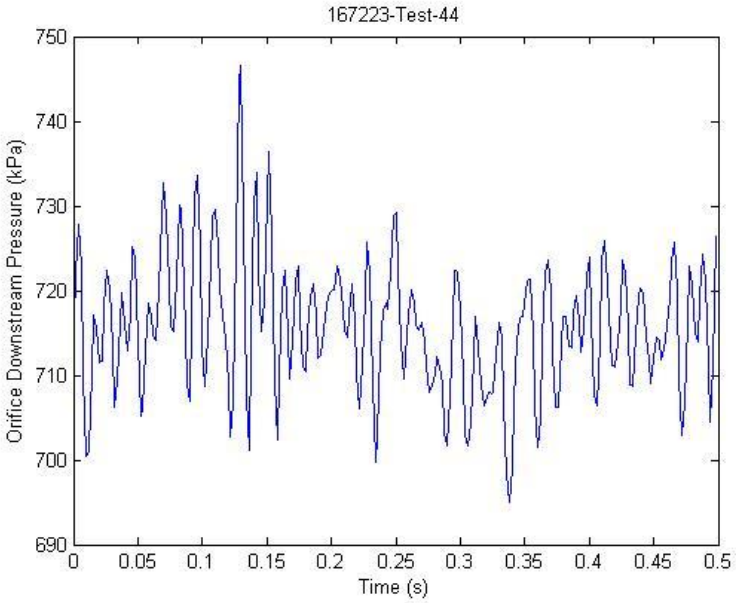


**Figure F.39: 167223-44 Orifice Outlet Pressure**

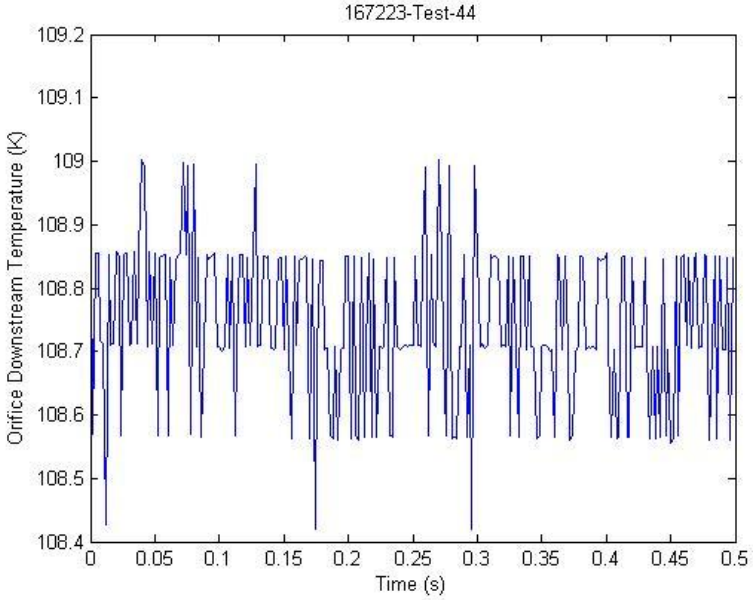


**Figure F.40: 167223-44 Orifice Outlet Temperature**

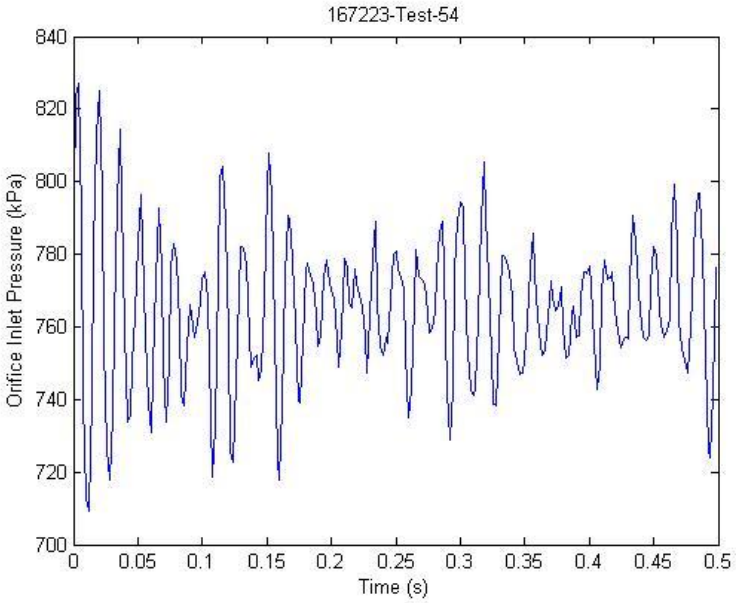


**Figure F.41: 167223-54 Orifice Inlet Pressure**

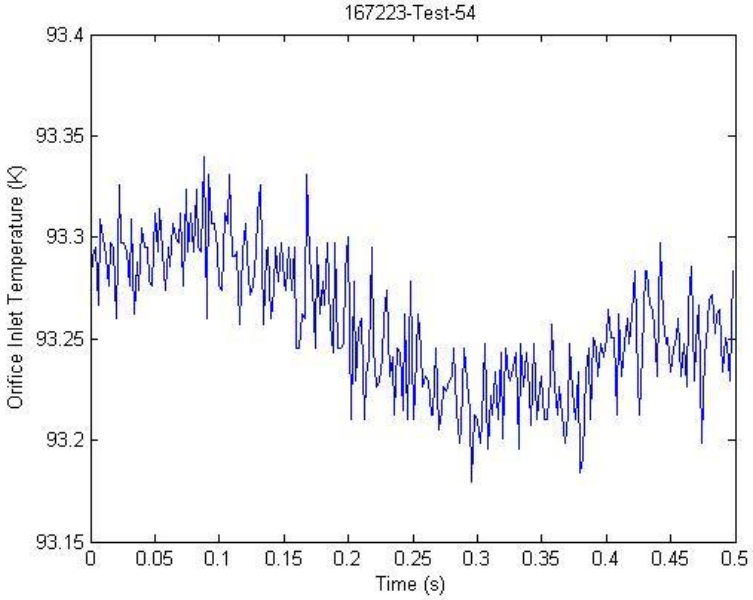


**Figure F.42: 167223-54 Orifice Inlet Temperature**

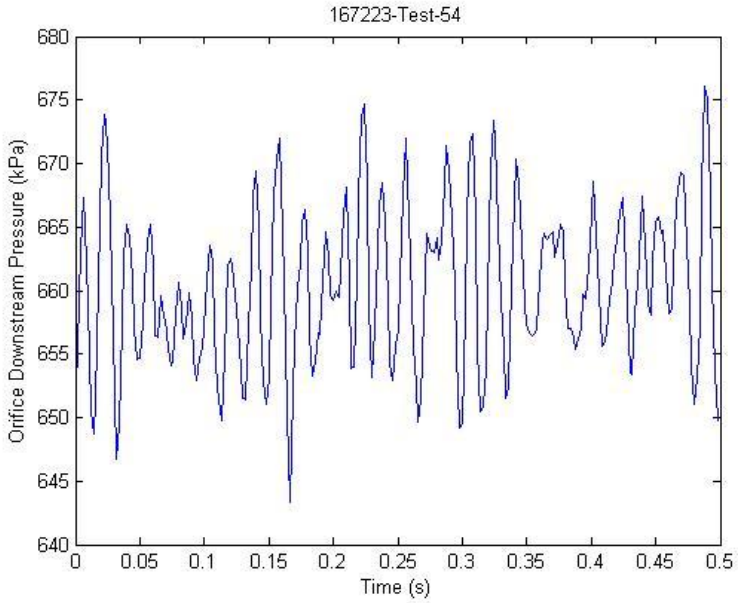


**Figure F.43: 167223-54 Orifice Outlet Pressure**

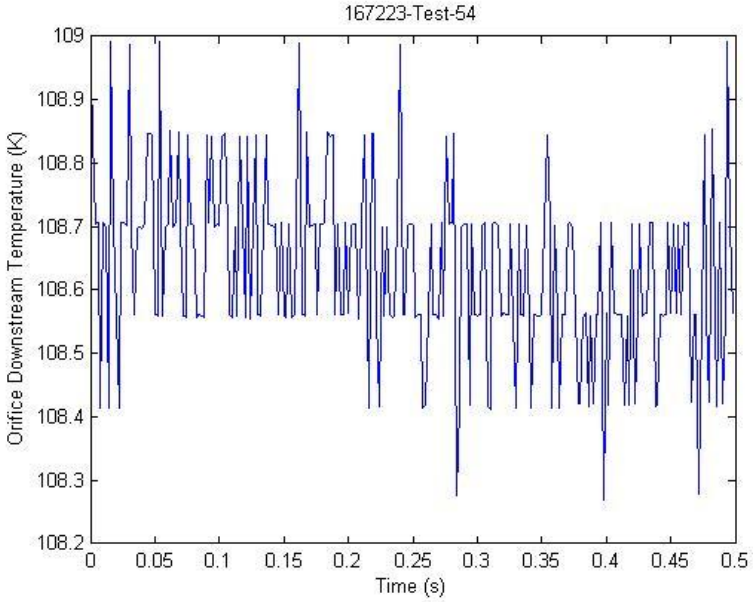


**Figure F.44: 167223-54 Orifice Outlet Temperature**

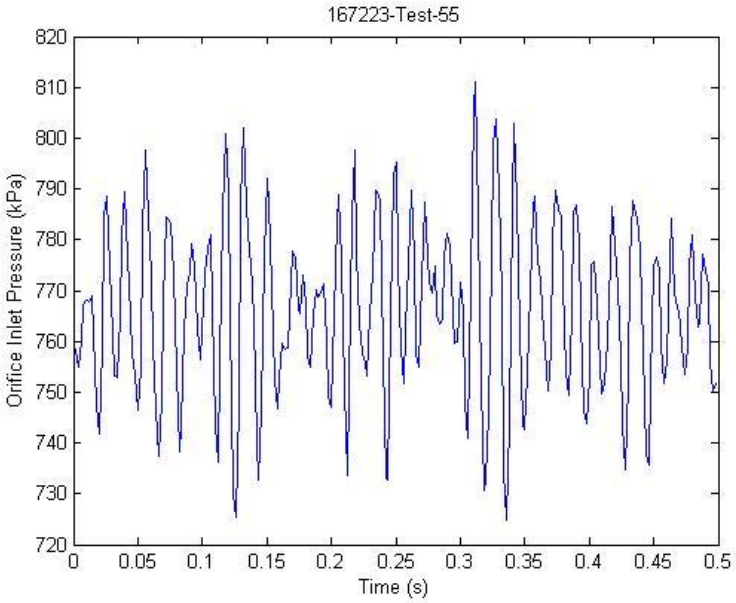


**Figure F.45: 167223-55 Orifice Inlet Pressure**

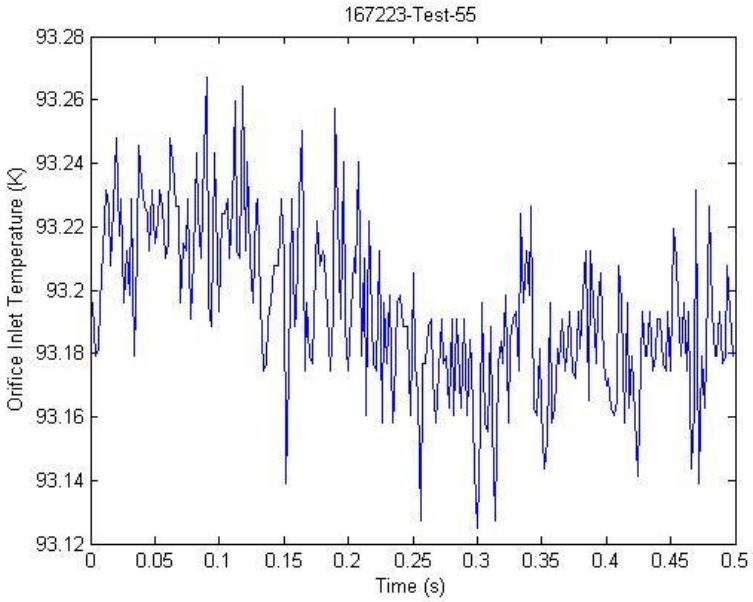


**Figure F.46: 167223-55 Orifice Inlet Temperature**

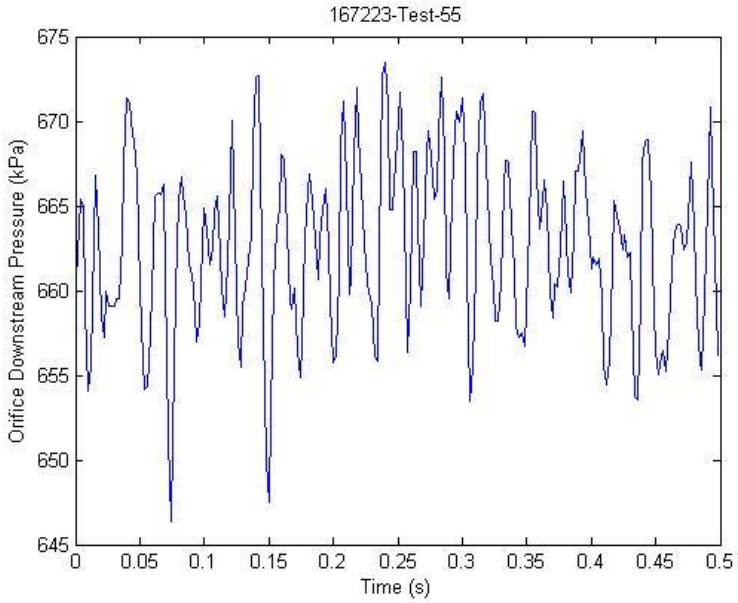


**Figure F.47: 167223-55 Orifice Outlet Pressure**

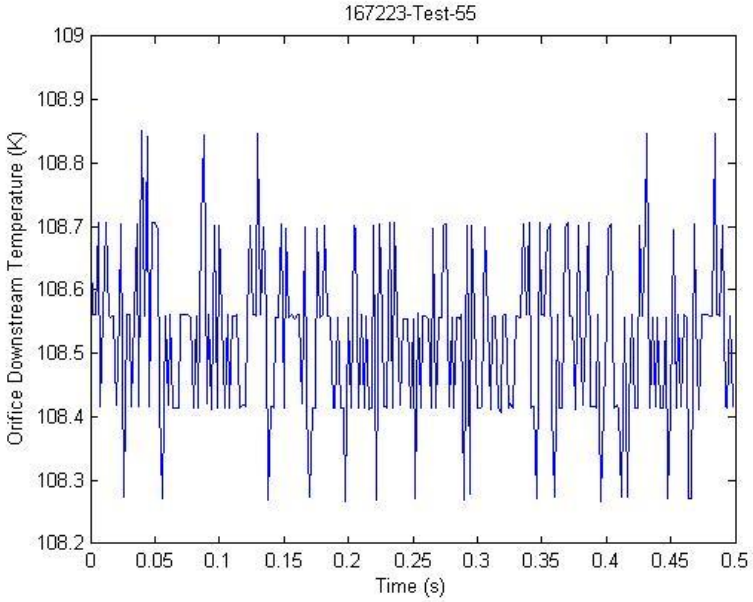


**Figure F.48: 167223-55 Orifice Outlet Temperature**

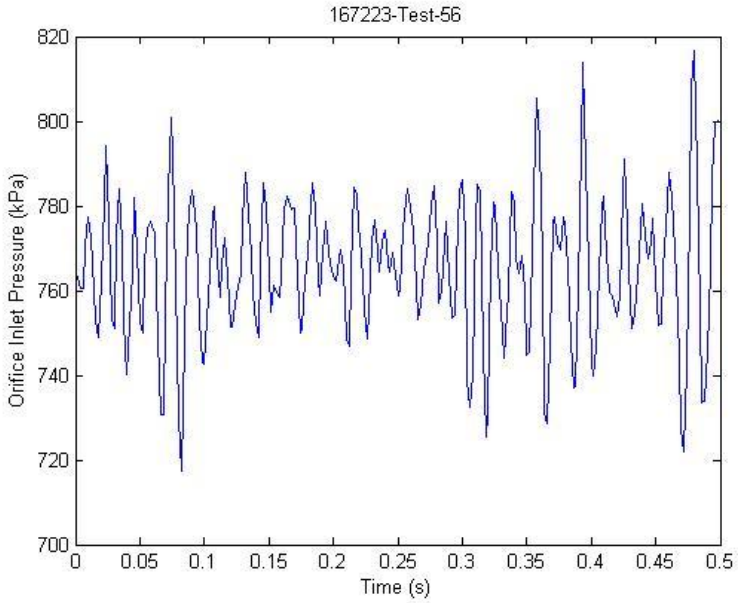


**Figure F.49: 167223-56 Orifice Inlet Pressure**

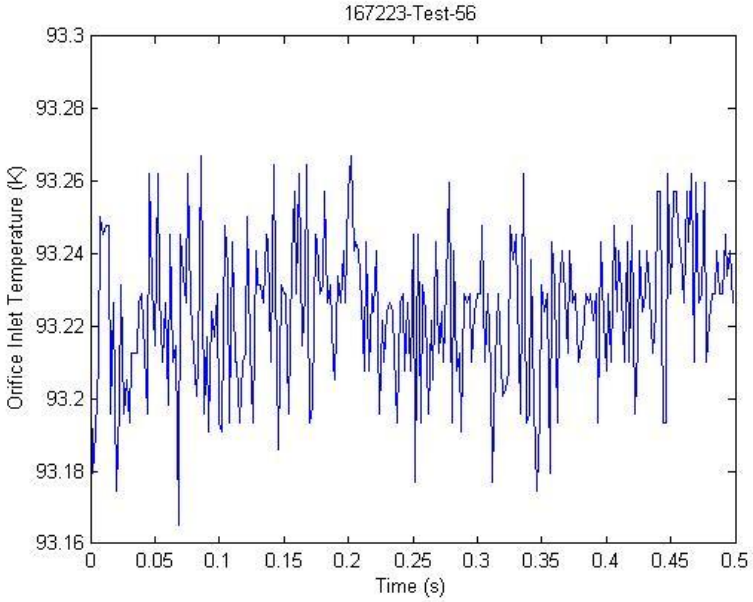


**Figure F.50: 167223-56 Orifice Inlet Temperature**

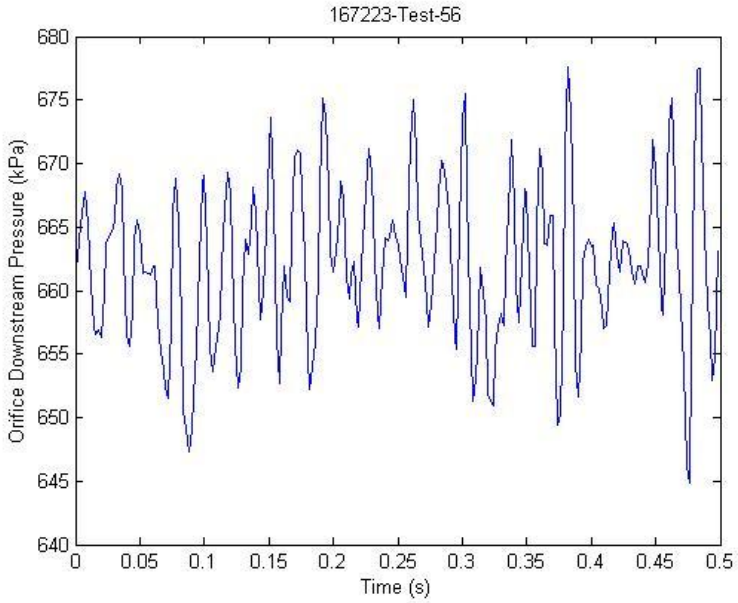


**Figure F.51: 167223-56 Orifice Outlet Pressure**

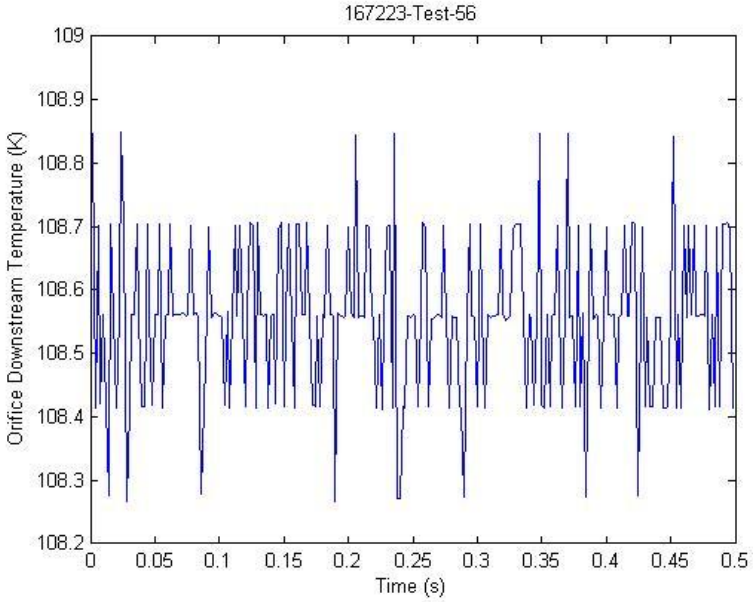


**Figure F.52: 167223-56 Orifice Outlet Temperature**

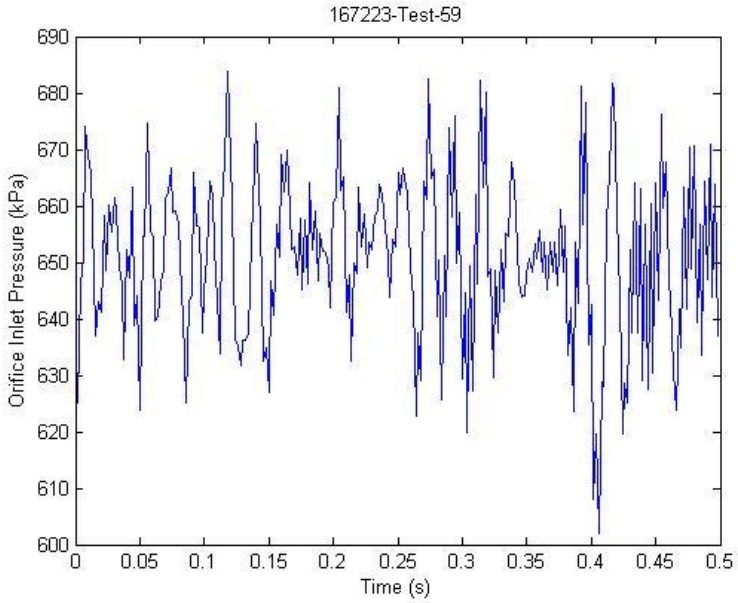


**Figure F.53: 167223-59 Orifice Inlet Pressure**

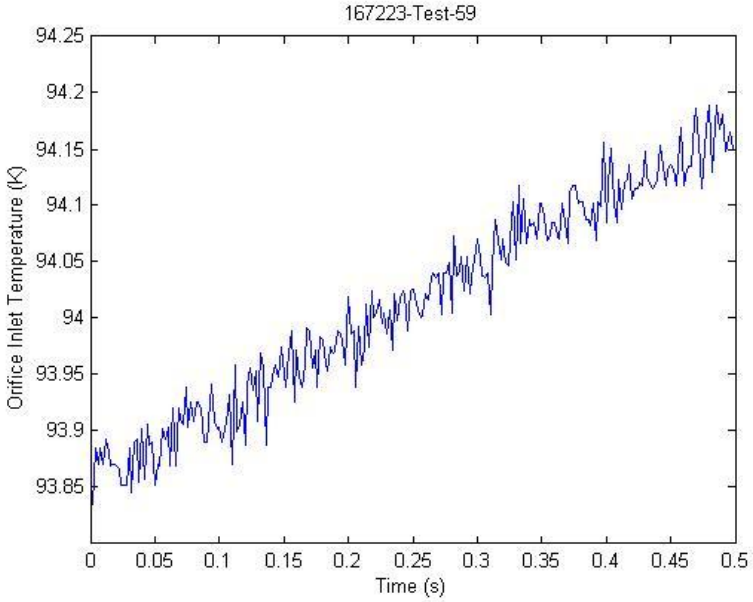


**Figure F.54: 167223-59 Orifice Inlet Temperature**

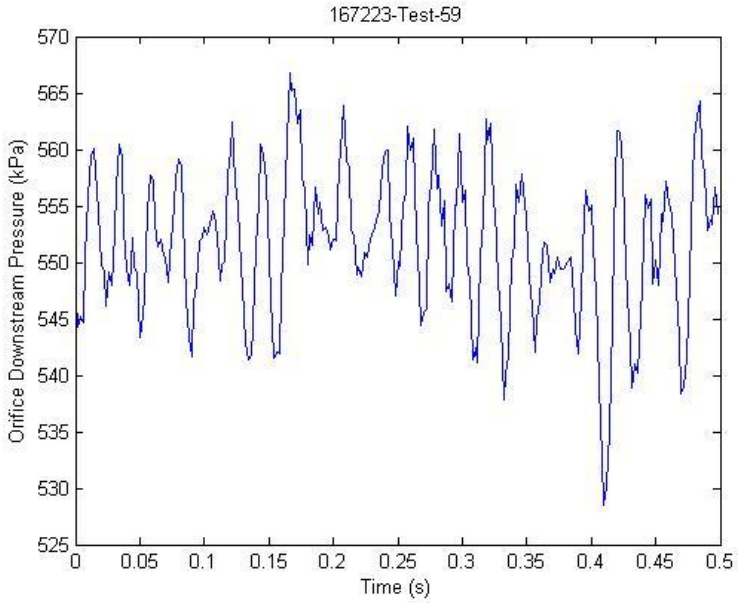


**Figure F.55: 167223-59 Orifice Outlet Pressure**

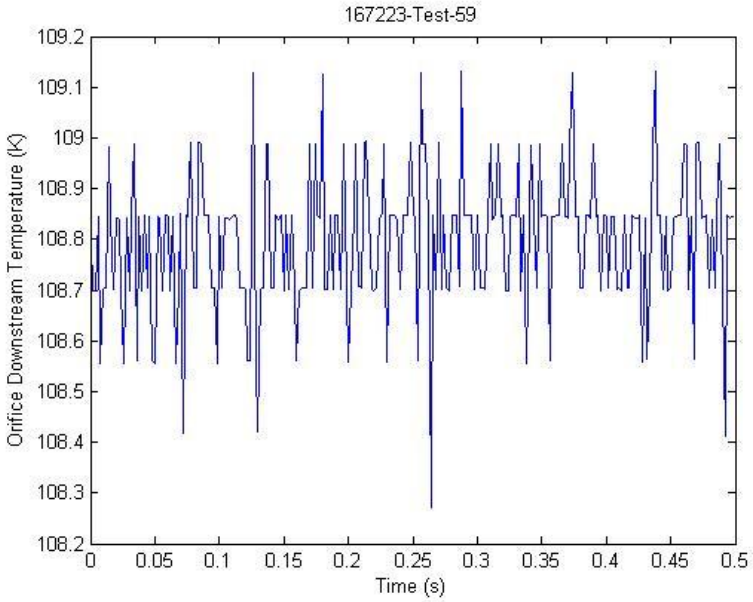


**Figure F.56: 167223-59 Orifice Outlet Temperature**

APPENDIX G

High Frequency Plots

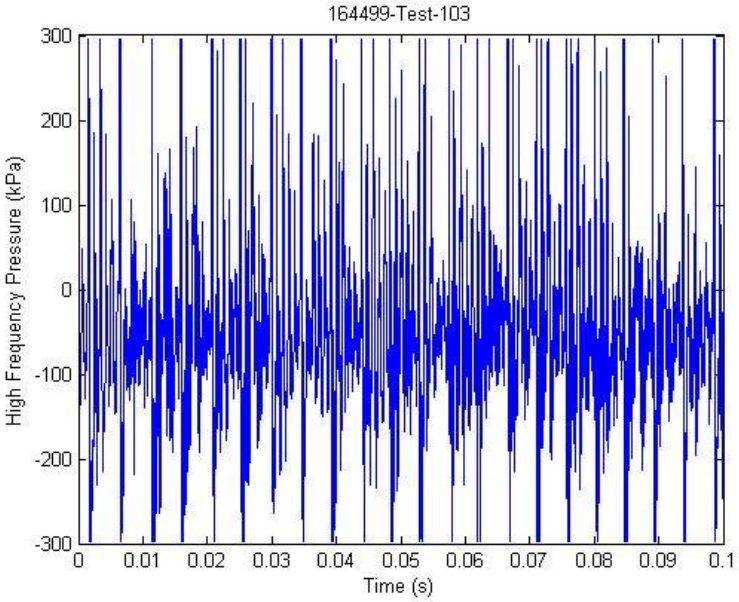


**Figure G.1: 164499-103 Raw High Frequency Signal**

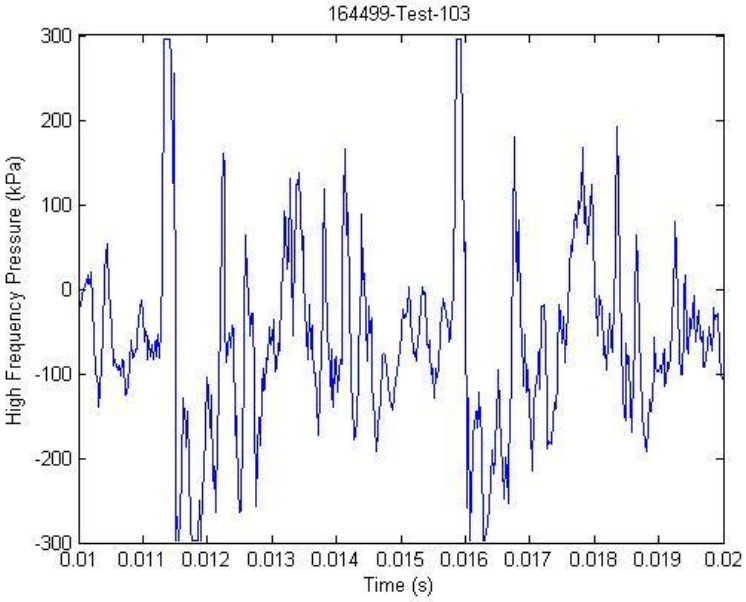


**Figure G.2: 164499-103 Magnified Raw High Frequency Signal**

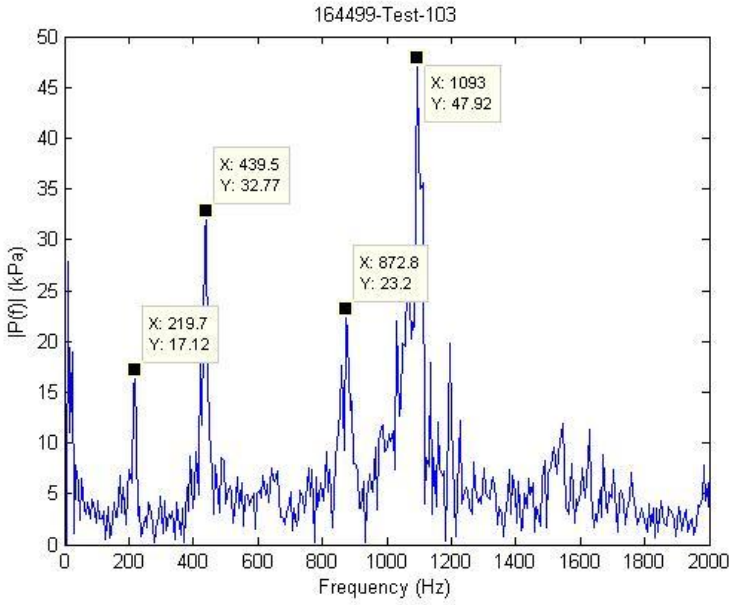


**Figure G.3: 164499-103 FFT**

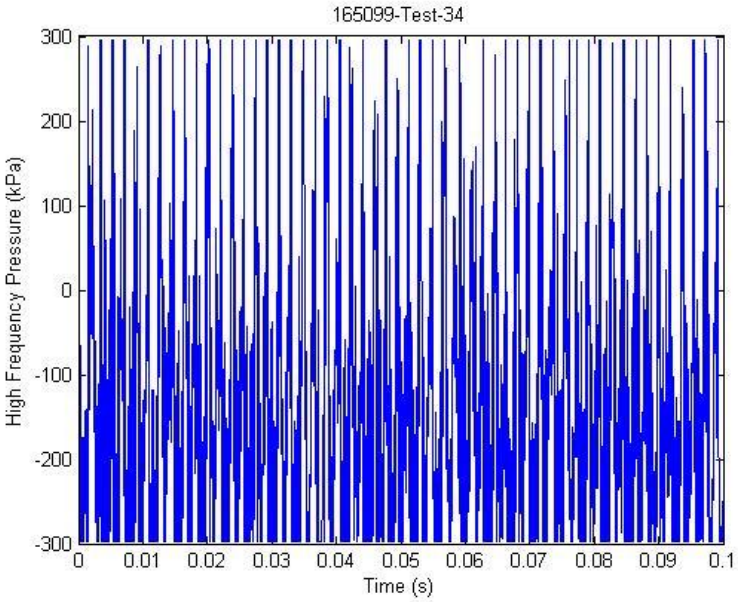


**Figure G.4: 165099-34 Raw High Frequency Signal**

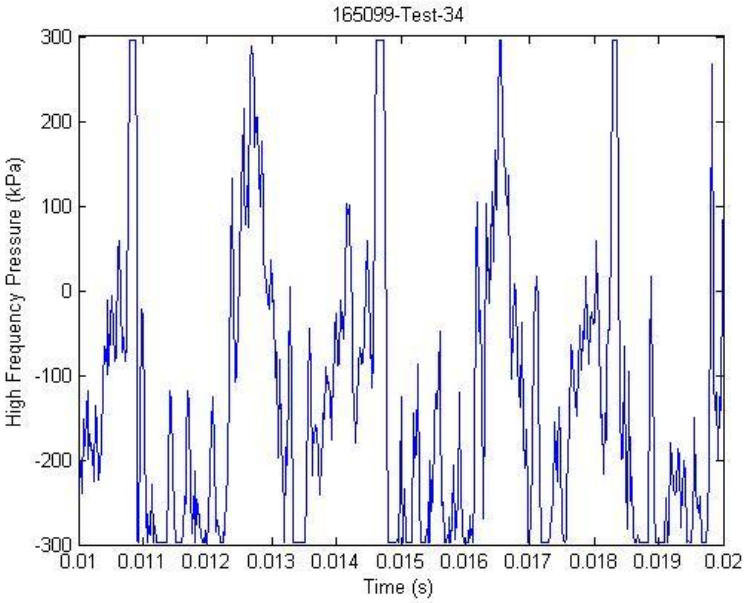


**Figure G.5: 165099-34 Magnified Raw High Frequency Signal**

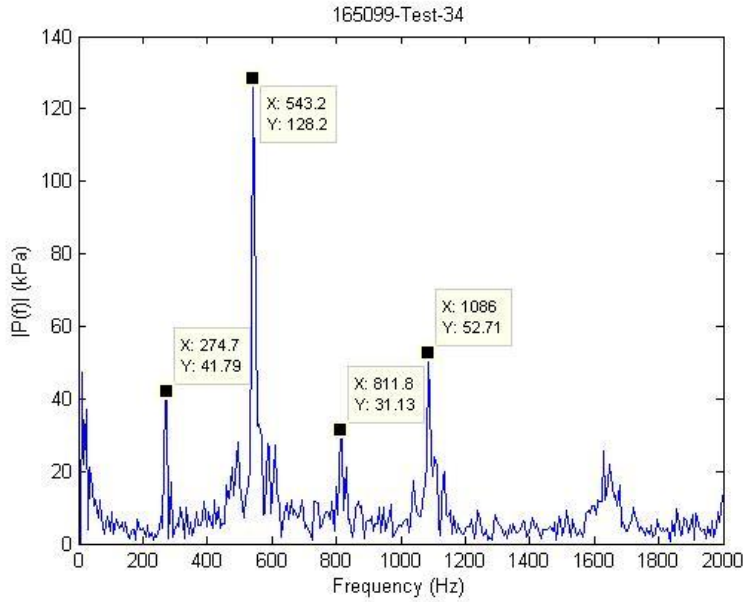


**Figure G.6: 165099-34 FFT**

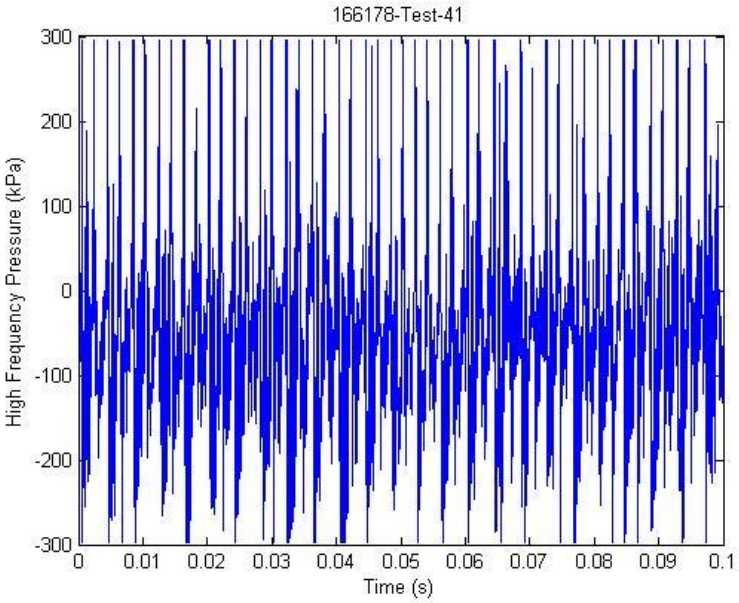


**Figure G.7: 166178-41 Raw High Frequency Signal**

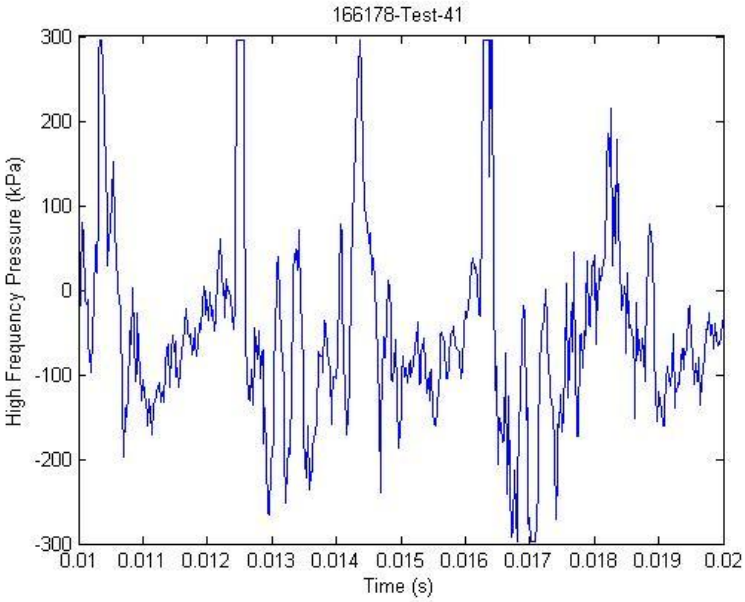


**Figure G.8: 166178-41 Magnified Raw High Frequency Signal**

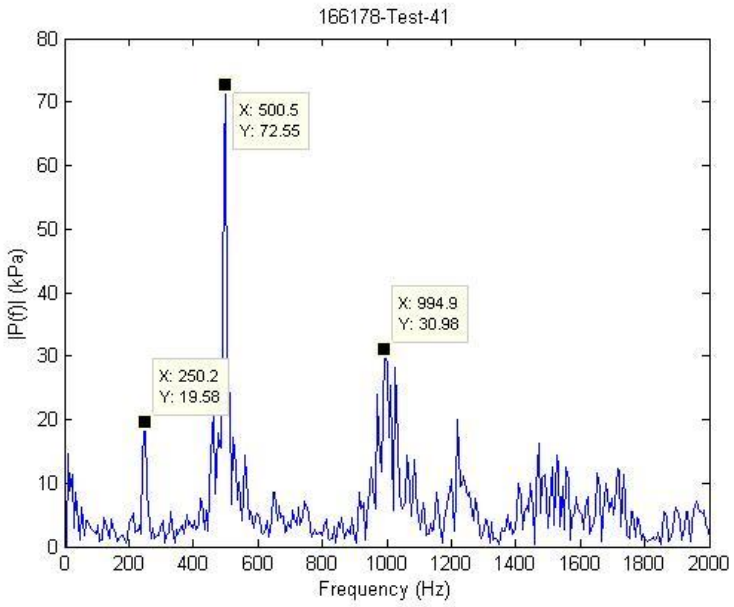


**Figure G.9: 166178-41 FFT**

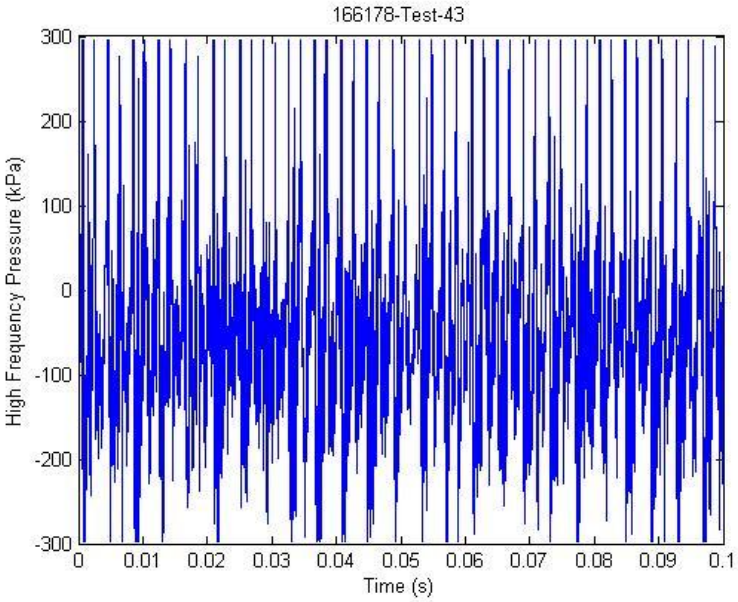


**Figure G.10: 166178-43 Raw High Frequency Signal**

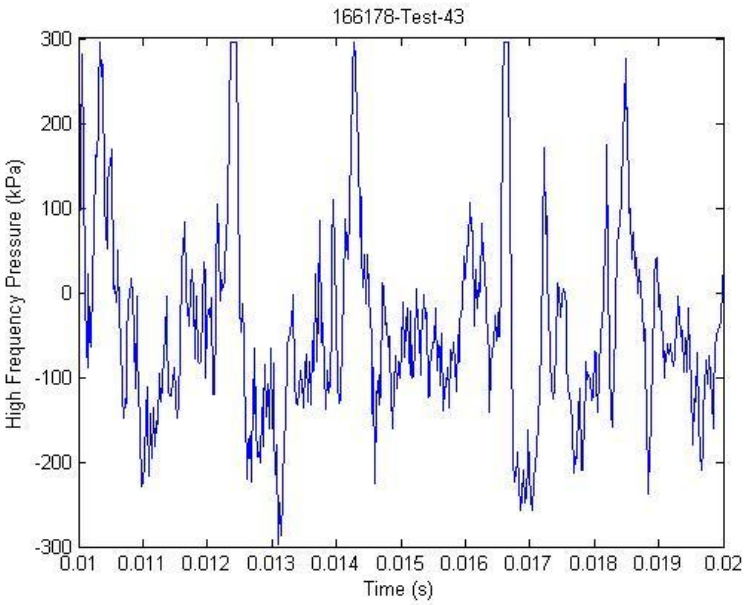


**Figure G.11: 166178-43 Magnified Raw High Frequency Signal**

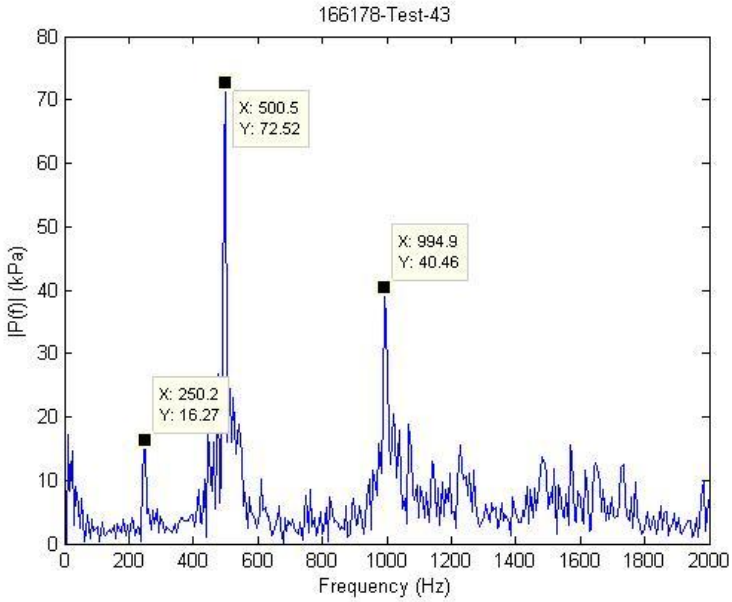


**Figure G.12: 166178-43 FFT**

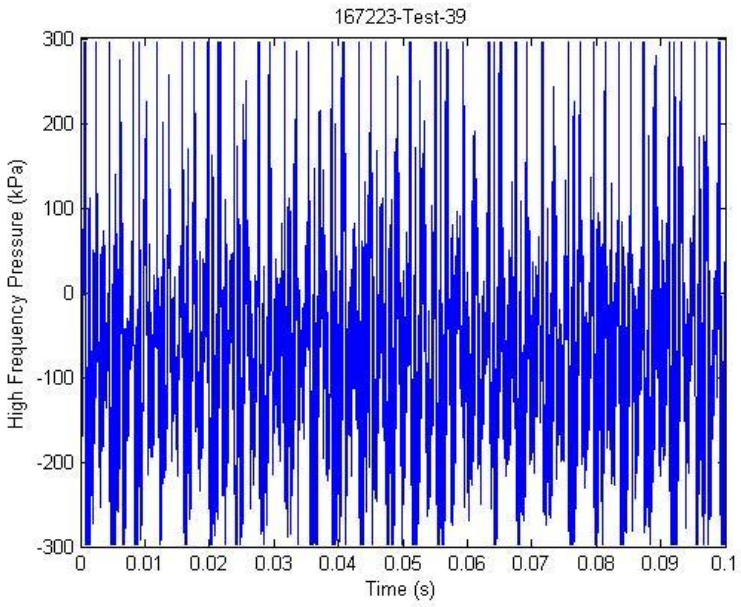


**Figure G.13: 167223-39 Raw High Frequency Signal**

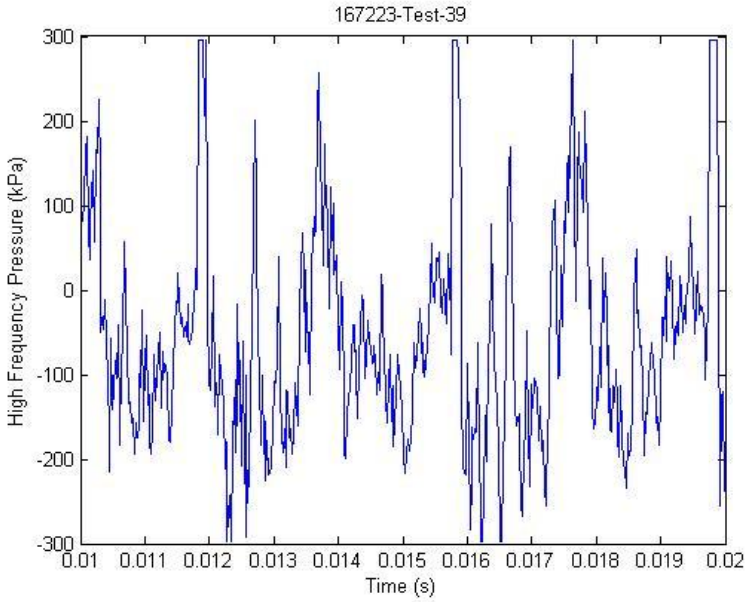


**Figure G.14: 167223-39 Magnified Raw High Frequency Signal**

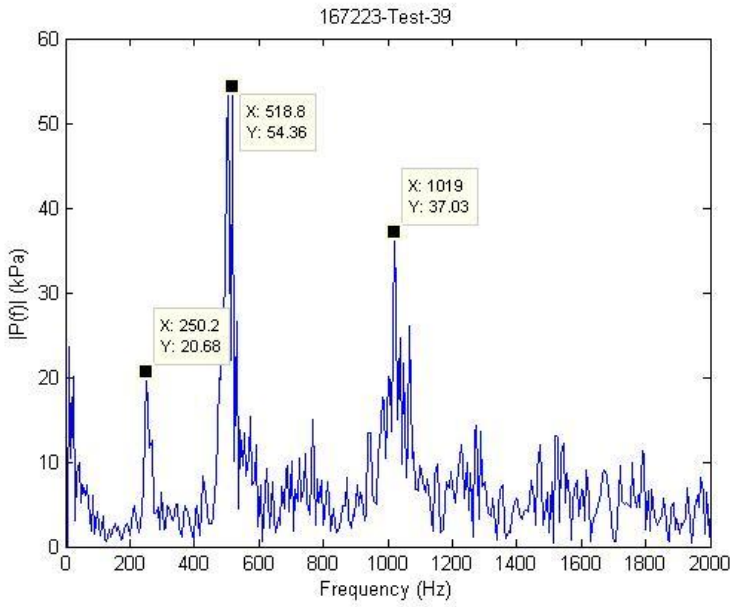


**Figure G.15: 167223-39 FFT**

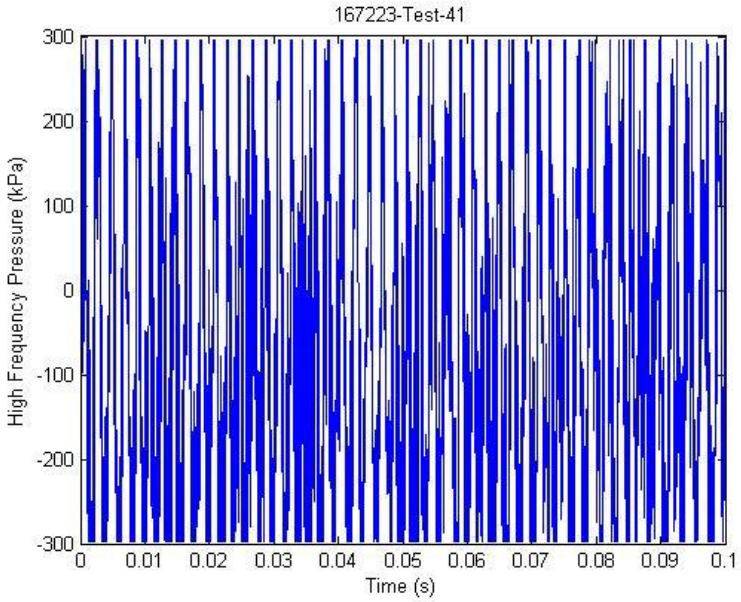


**Figure G.16: 167223-41 Raw High Frequency Signal**

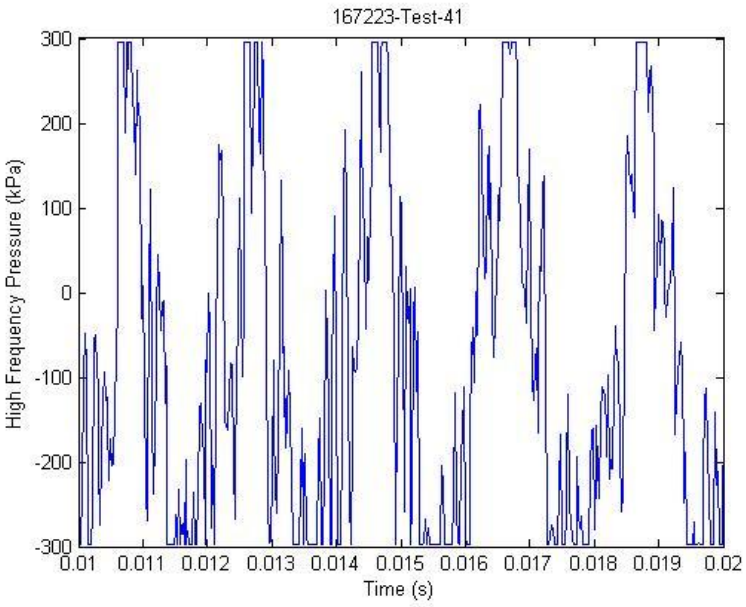


**Figure G.17: 167223-41 Magnified Raw High Frequency Signal**

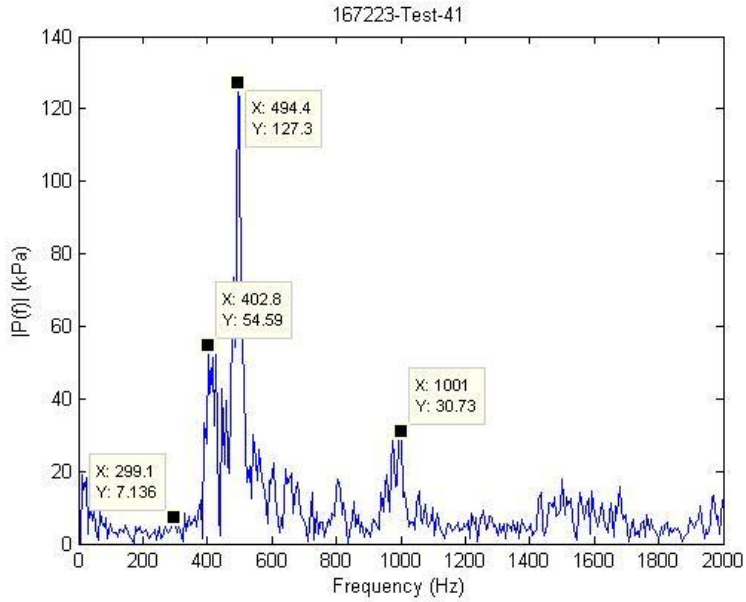


**Figure G.18: 167223-41 FFT**

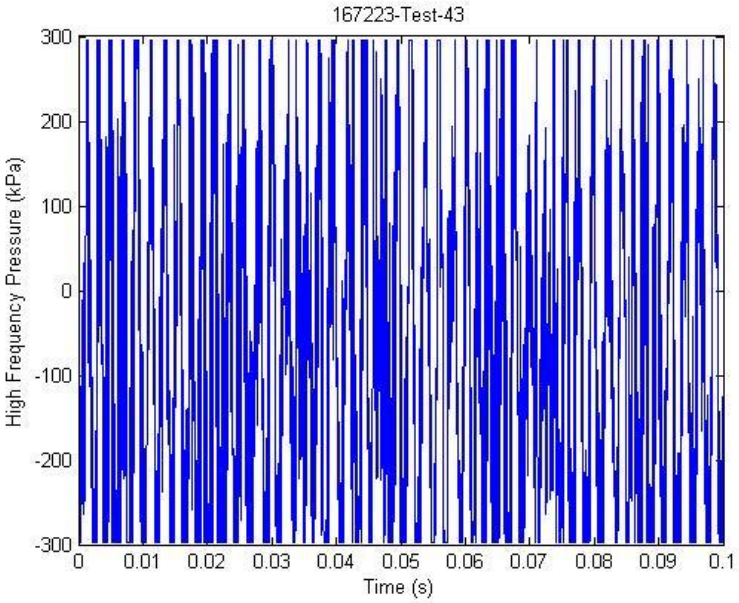


**Figure G.19: 167223-43 Raw High Frequency Signal**

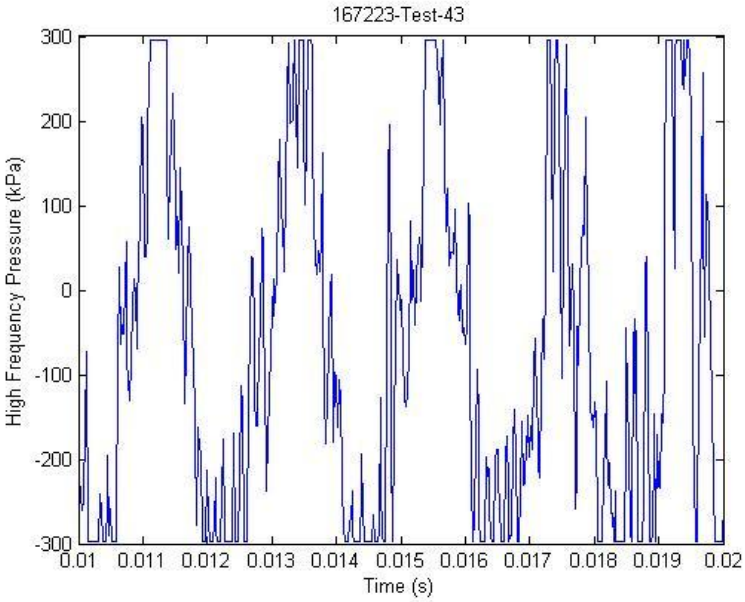


**Figure G.20: 167223-43 Magnified Raw High Frequency Signal**

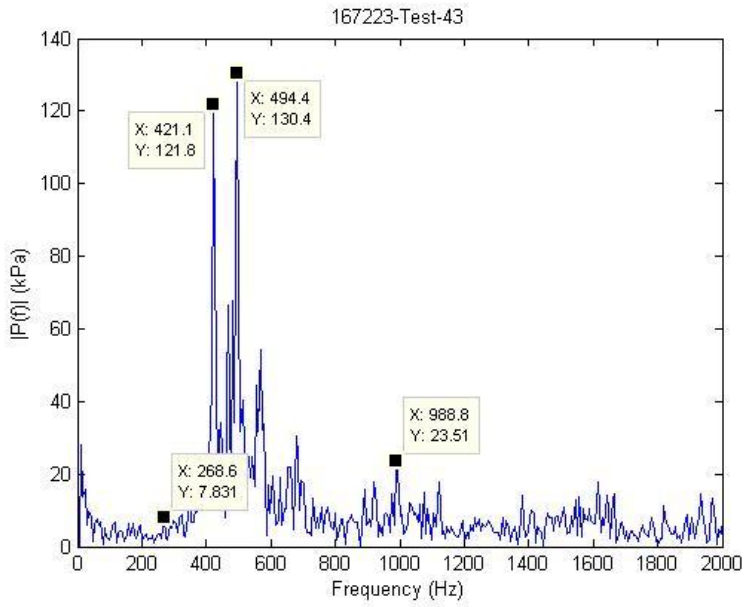


**Figure G.21: 167223-43 FFT**

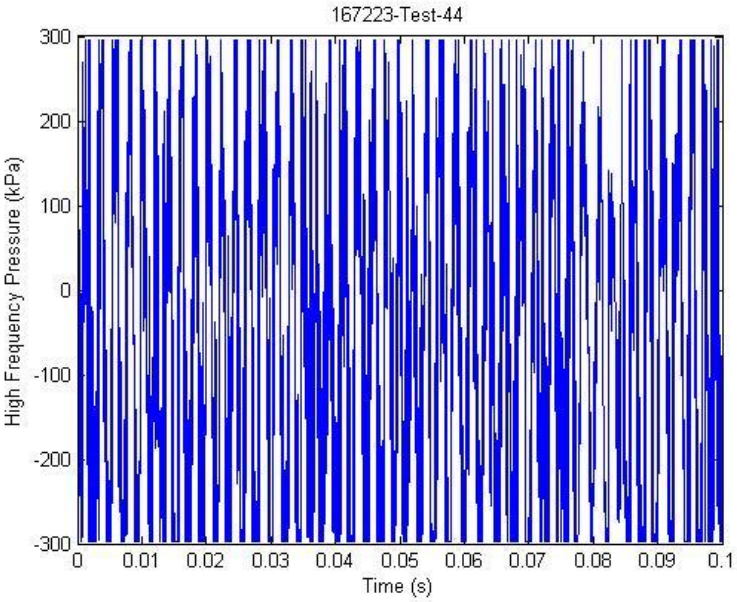


**Figure G.22: 167223-44 Raw High Frequency Signal**

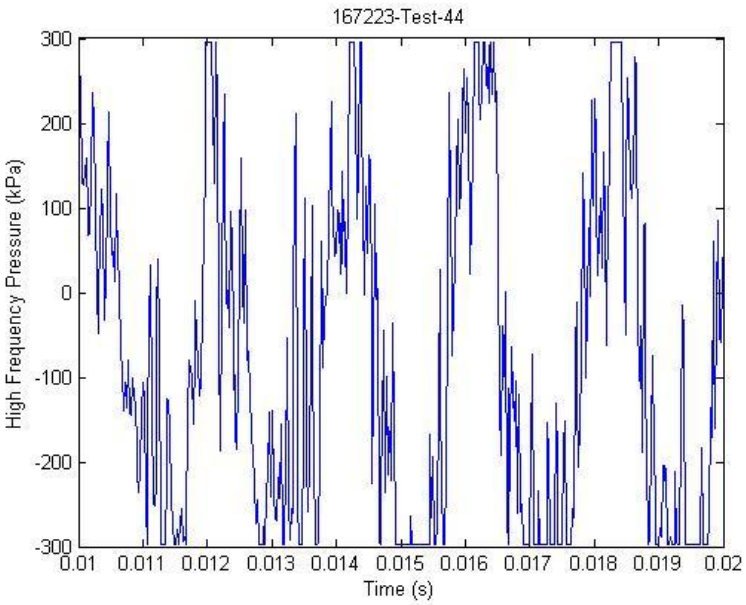


**Figure G.23: 167223-44 Magnified Raw High Frequency Signal**

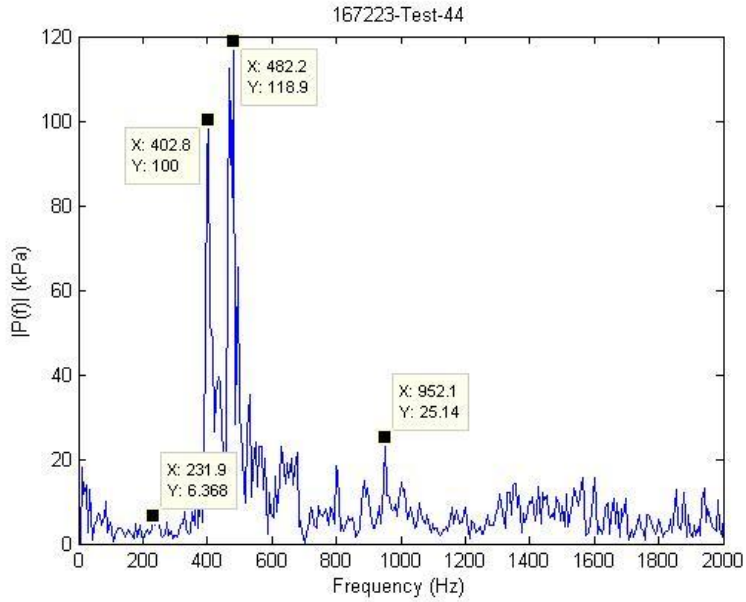


**Figure G.24: 167223-44 FFT**

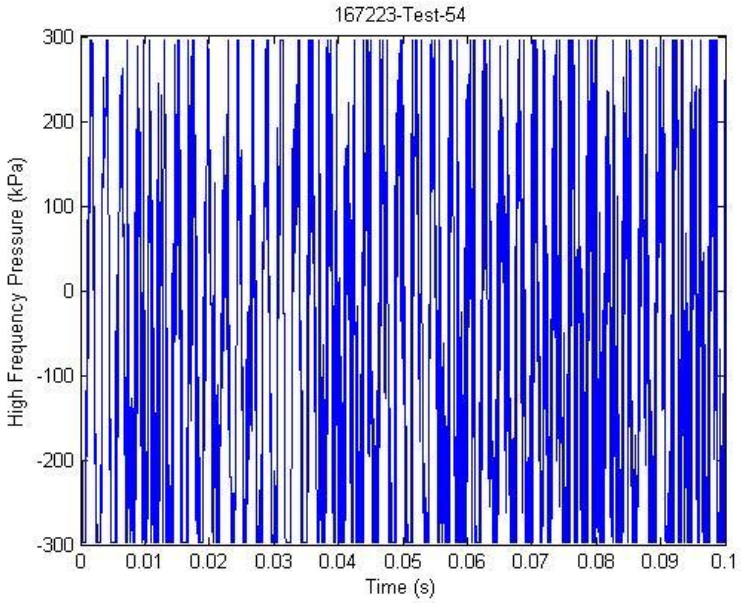


**Figure G.25: 167223-54 Raw High Frequency Signal**

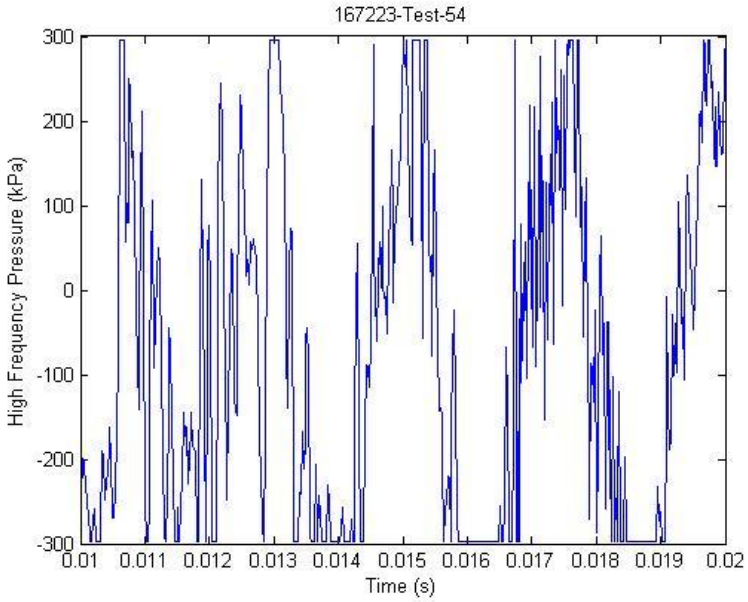


**Figure G.26: 167223-54 Magnified Raw High Frequency Signal**

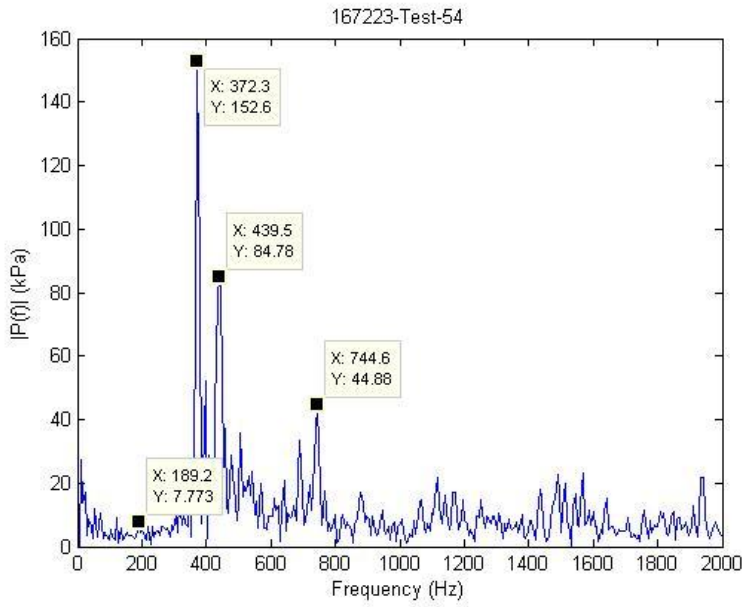


**Figure G.27: 167223-54 FFT**

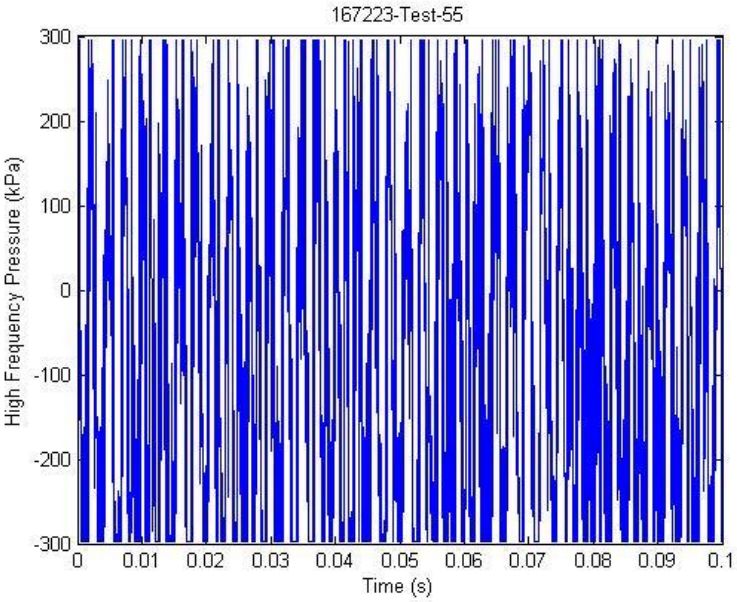


**Figure G.28: 167223-55 Raw High Frequency Signal**

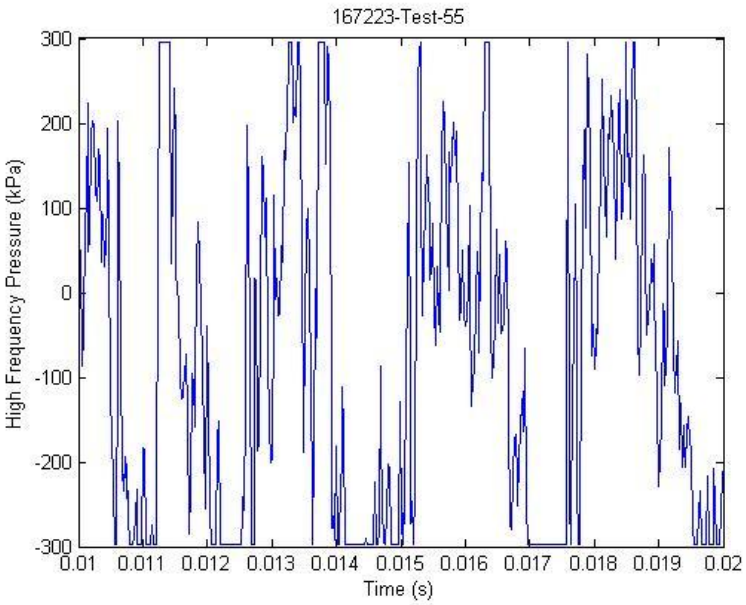


**Figure G.29: 167223-55 Magnified Raw High Frequency Signal**

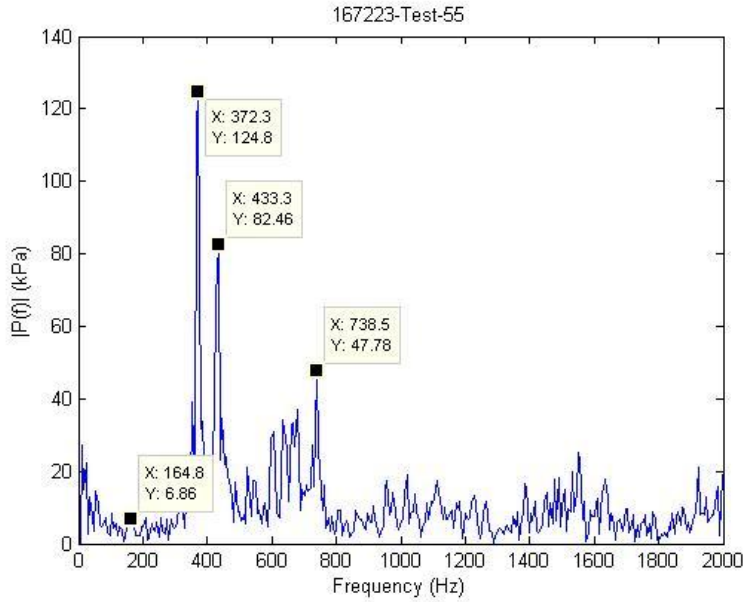


**Figure G.30: 167223-55 FFT**

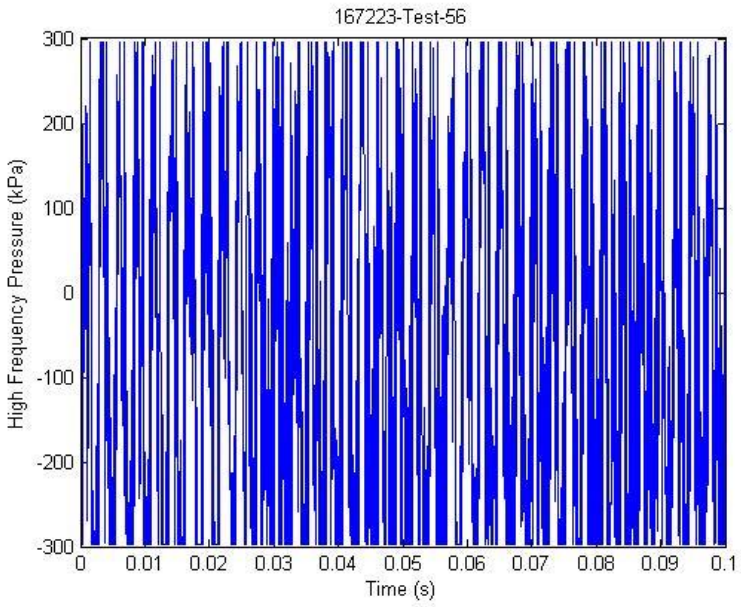


**Figure G.31: 167223-56 Raw High Frequency Signal**

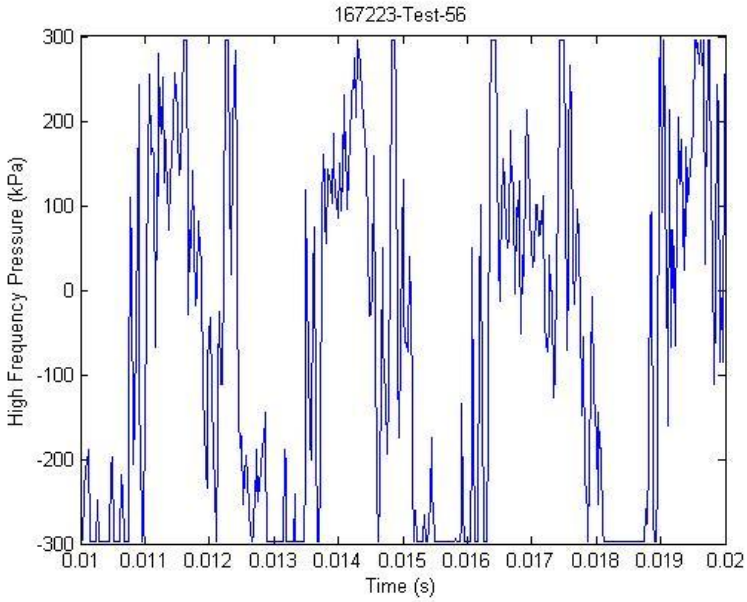


**Figure G.32: 167223-56 Magnified Raw High Frequency Signal**

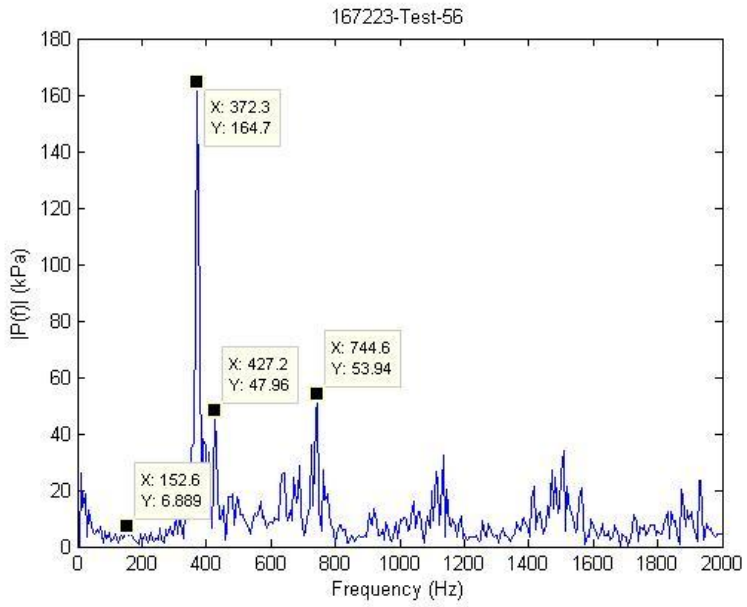


**Figure G.33: 167223-56 FFT**

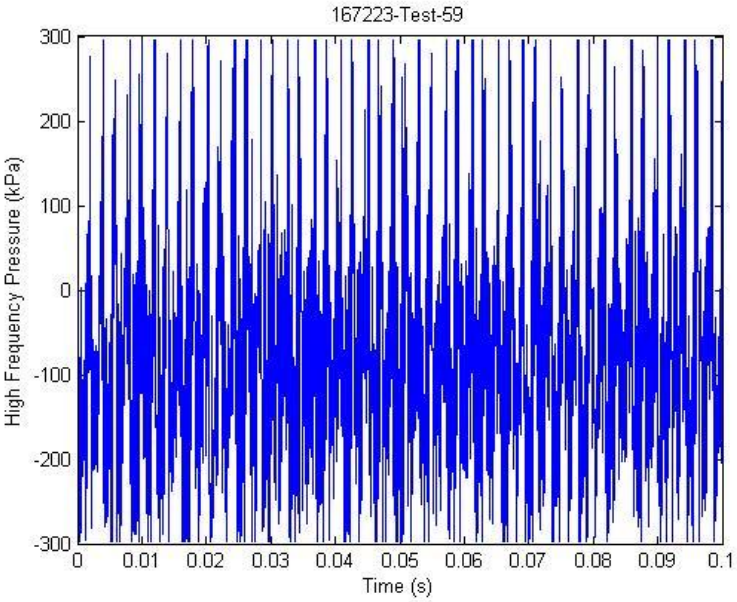


**Figure G.34: 167223-59 Raw High Frequency Signal**

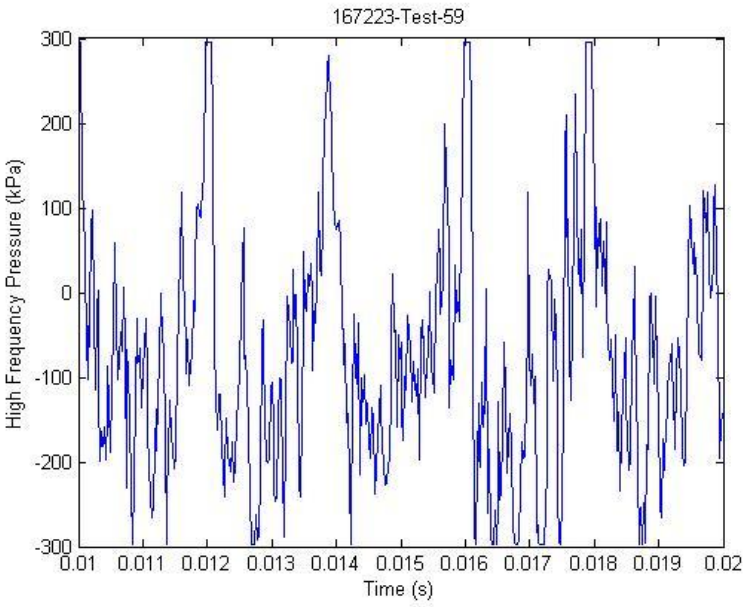


**Figure G.35: 167223-59 Magnified Raw High Frequency Signal**

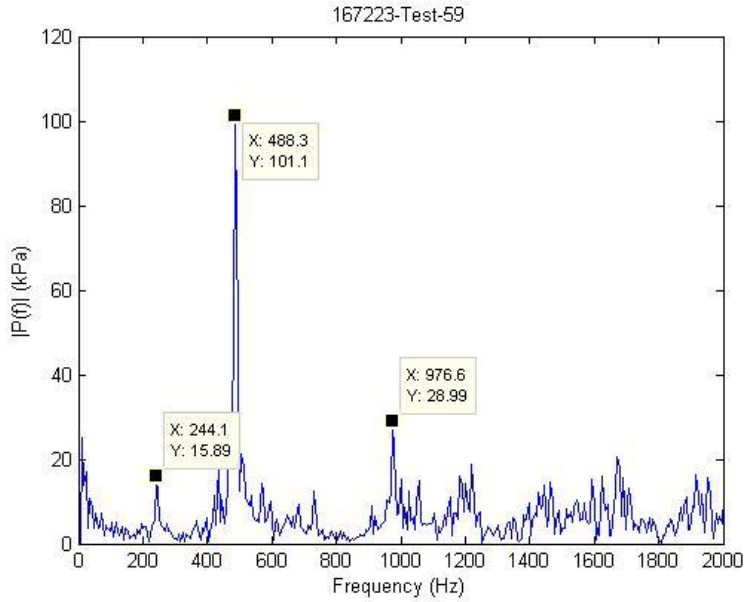


**Figure G.36: 167223-59 FFT**

APPENDIX H

Frequency Shift Calculations

## Conditions

Inlet pressure $p_1 := 80psi$

Inlet temperature $T_1 := 88.75K$

Orifice diameter $d := 0.4in$

Tubing diameter $D := 0.8in$

Orifice thickness $t := 0.209in$

Mass Flow Rate $mdot := 3\frac{lbm}{s}$

## Curve Fits

$r_1 := 0$ $m_1 := 0.00000000001892$ $pv_1 := 0.00000425$

$r_2 := -0.000053$ $m_2 := 0.00000001253179$ $pv_2 := 0.0048597$

$r_3 := -0.031599$ $m_3 := 0.00000312835654$ $pv_3 := 1.9553483$ $r_{v3} := -0.0025$

$r_4 := -6.521386$ $m_4 := 0.00034753578571$ $pv_4 := 336.09391727$ $r_{v4} := 0.1386$

$r_5 := -413.56327$ $m_5 := 0.01448495255839$ $pv_5 := 21092.91410559$ $r_{v5} := 54.613$

### Inlet Density

$$\rho(T_1) := \left[r_2\cdot\left(\frac{T_1}{K} - 273.15\right)^3 + r_3\cdot\left(\frac{T_1}{K} - 273.15\right)^2 + r_4\cdot\left(\frac{T_1}{K} - 273.15\right) + r_5\right]\cdot\frac{lbm}{ft^3}$$

### Venturi Density

$$\rho_{vent}(T_v) := \left[r_{v3}\cdot\left(\frac{T_v}{K}\right)^2 + r_{v4}\cdot\left(\frac{T_v}{K}\right) + r_{v5}\right]\cdot\frac{lbm}{ft^3}$$

### Inlet Viscosity

$$\mu(T_1) := \left[ m_1 \cdot \left( \frac{T_1}{K} - 273.15 \right)^4 + m_2 \cdot \left( \frac{T_1}{K} - 273.15 \right)^3 + m_3 \cdot \left( \frac{T_1}{K} - 273.15 \right)^2 + m_4 \cdot \left( \frac{T_1}{K} - 273.15 \right) + m_5 \right] \cdot \frac{lbm}{ft \cdot s}$$

### Vapor Pressure

$$p_v(T_1) := \left[ pv_1 \cdot \left( \frac{T_1}{K} - 273.15 \right)^4 + pv_2 \cdot \left( \frac{T_1}{K} - 273.15 \right)^3 + pv_3 \cdot \left( \frac{T_1}{K} - 273.15 \right)^2 + pv_4 \cdot \left( \frac{T_1}{K} - 273.15 \right) + pv_5 \right] \cdot psi$$

$$\rho(T_1) = 46.83 \cdot \frac{lbm}{ft^3}$$

$$\mu(T_1) = 7.276 \times 10^{-5} \cdot \frac{lbm}{ft \cdot s}$$

$$p_v(T_1) = 48.193 \cdot psi$$

## Calculations

### Reynolds Number

$$Re_D(T_1, D) := \frac{4 \cdot mdot}{\pi \cdot \mu(T_1) \cdot D}$$

$$Re_D(T_1, D) = 7.875 \times 10^5$$

### Orifice Throat Velocity

$$v(d, T_1) := \frac{mdot}{\rho(T_1) \cdot \frac{\pi}{4} \cdot d^2}$$

### Cavitation Number

$$cav(d, T_1) := \frac{p_1 - p_v(T_1)}{\frac{1}{2} \cdot \rho(T_1) \, v(d, T_1)^2}$$

$$cav(d, T_1) = 1.168$$

Strouhal Number

Assuming constant Strouhal number with experimental comparison $St := 0.28$

$$f := \frac{St \cdot \frac{mdot}{\rho(T_1) \cdot \frac{\pi}{4} \cdot d^2}}{t}$$

$f = 1.18 \times 10^3\ Hz$

APPENDIX I

Additional Data Points

**Table I.1: Additional Data Points**

| Set | Test | Inlet Pressure (kPa) | Inlet Temperature (K) | Outlet Pressure (kPa) |
|---|---|---|---|---|
| 169232 | 55 | 504.1 | 92.0 | 401.5 |
| 169232 | 56 | 509.1 | 92.1 | 407.2 |
| 169232 | 57 | 510.4 | 92.2 | 408.7 |
| 169232 | 58 | 519.0 | 92.5 | 418.9 |

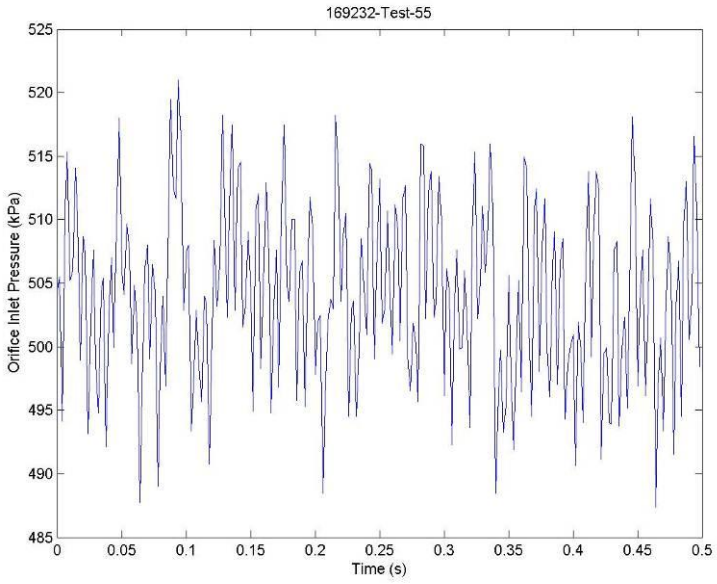


**Figure I.1: 169232-55 Orifice Inlet Pressure**

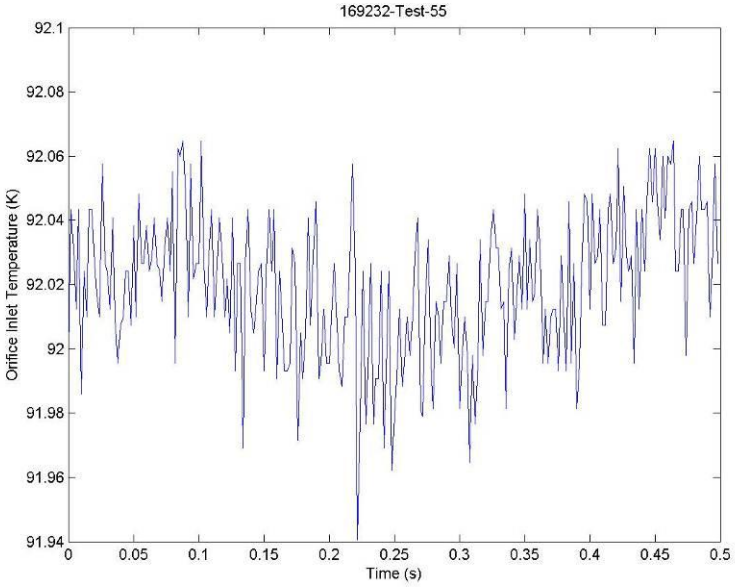


**Figure I.2: 169232-55 Orifice Inlet Temperature**

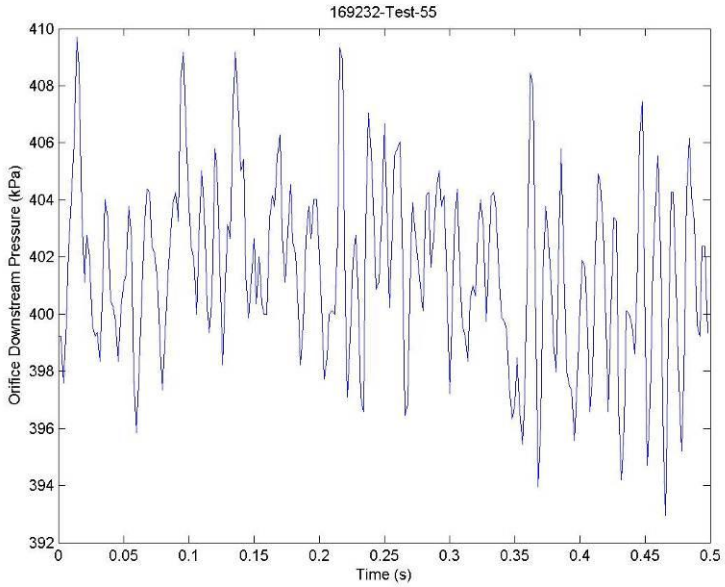


**Figure I.3: 169232-55 Orifice Outlet Pressure**

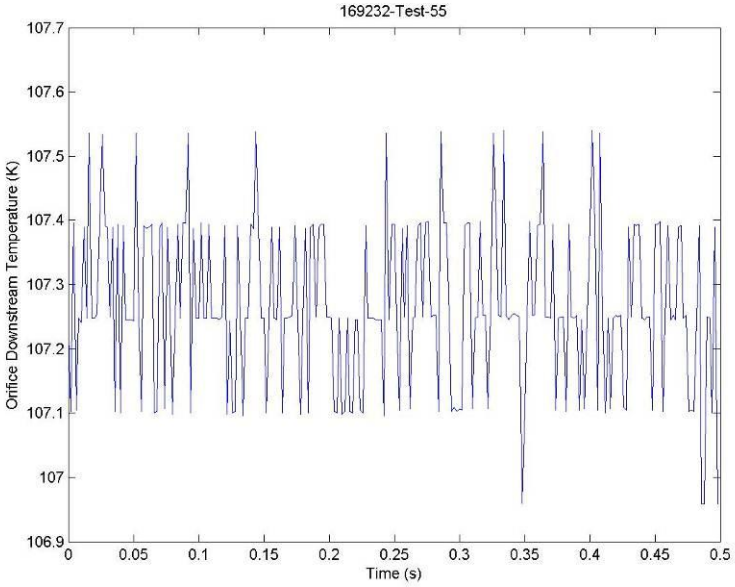


**Figure I.4: 169232-55 Orifice Outlet Temperature**

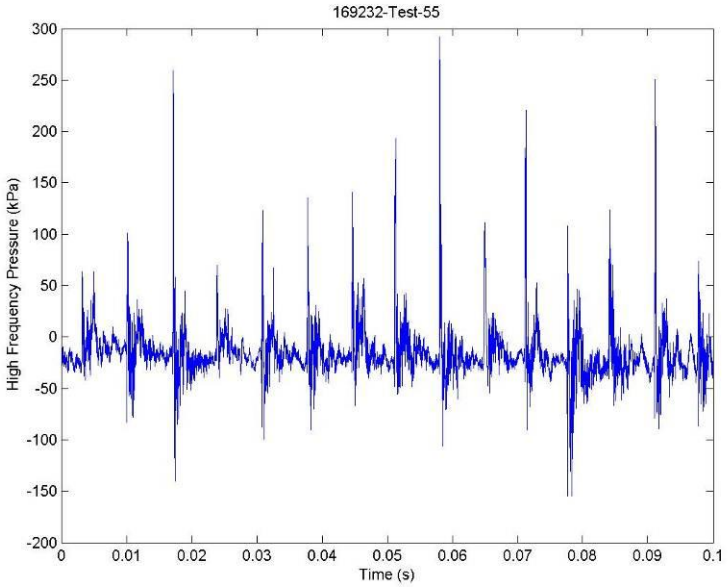


**Figure I.5: 169232-55 Raw High Frequency Signal**

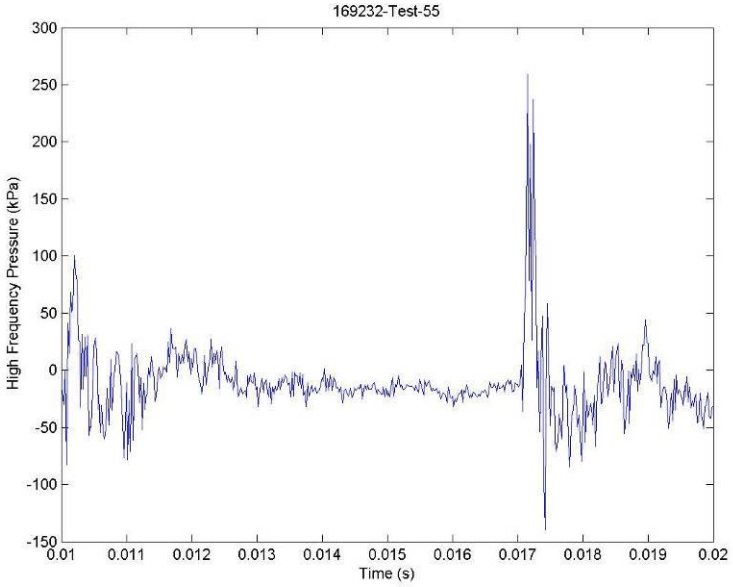


**Figure I.6: 169232-55 Magnified Raw High Frequency Signal**

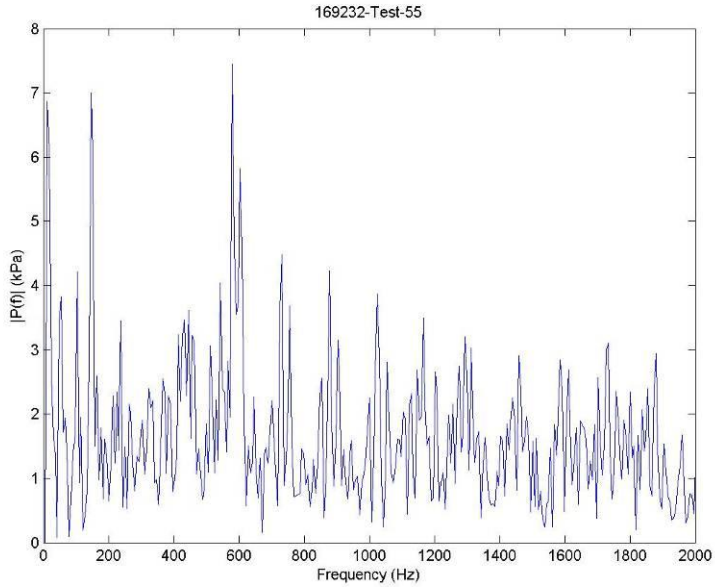


**Figure I.7: 169232-55 FFT**

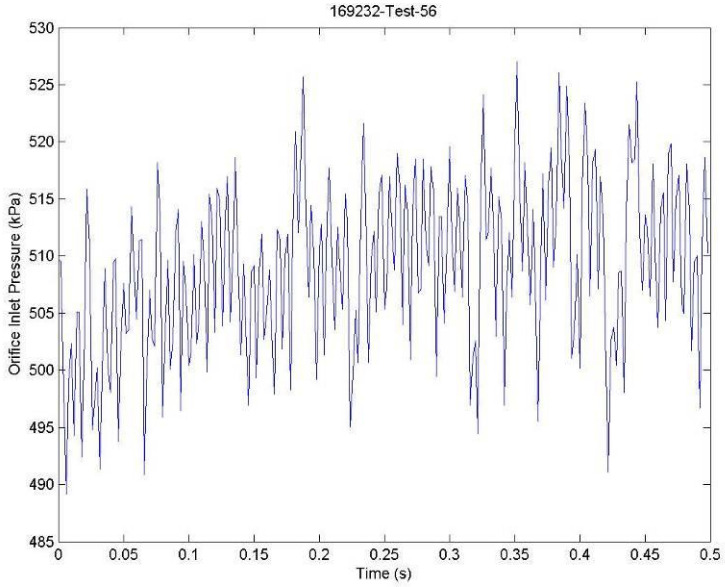


**Figure I.8: 169232-56 Orifice Inlet Pressure**

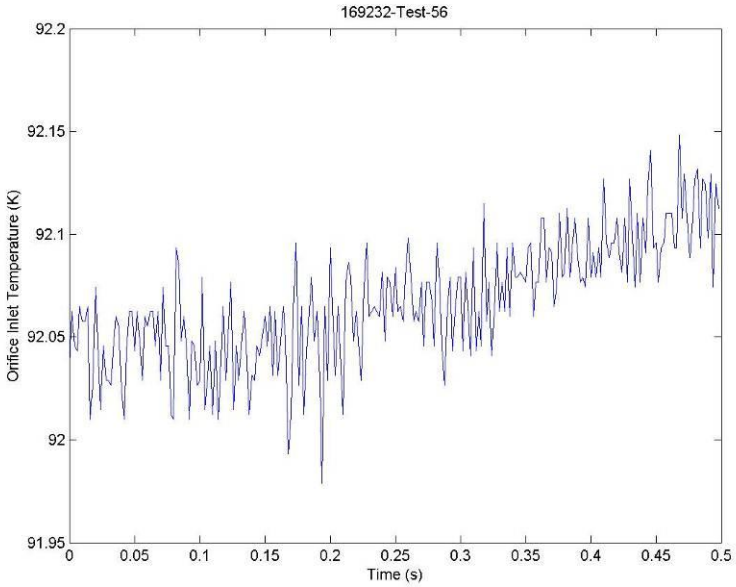


**Figure I.9: 169232-56 Orifice Inlet Temperature**

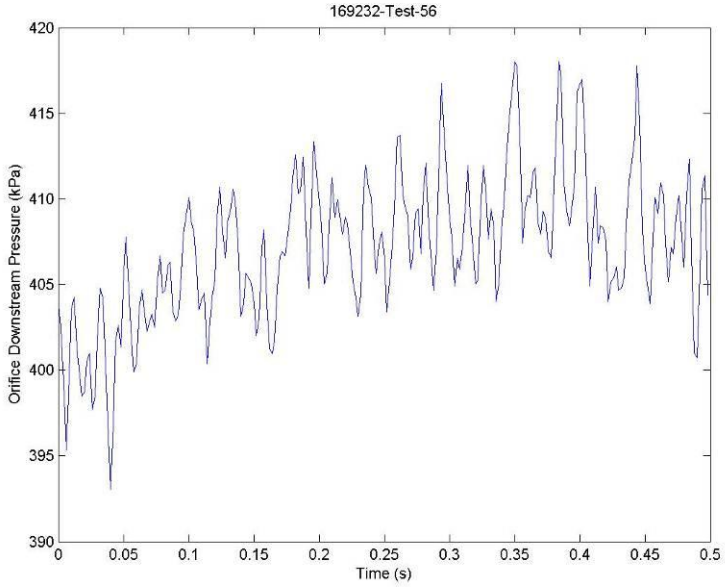


**Figure I.10: 169232-56 Orifice Outlet Pressure**

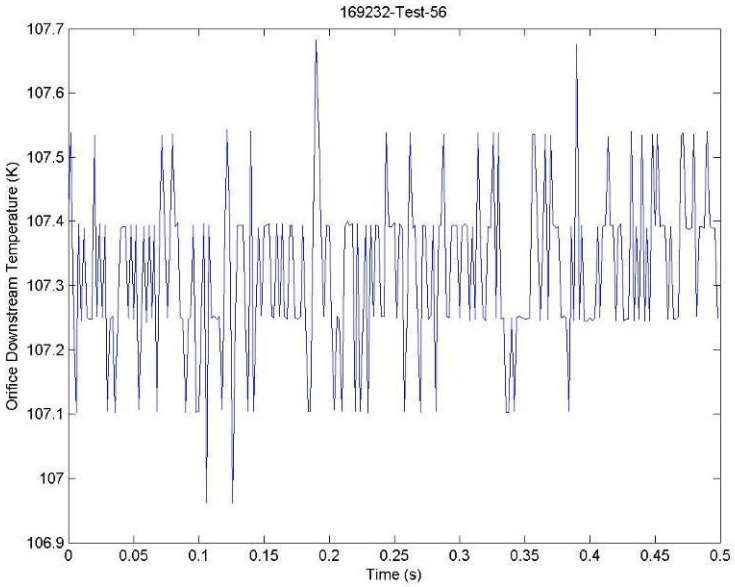


**Figure I.11: 169232-56 Orifice Outlet Temperature**

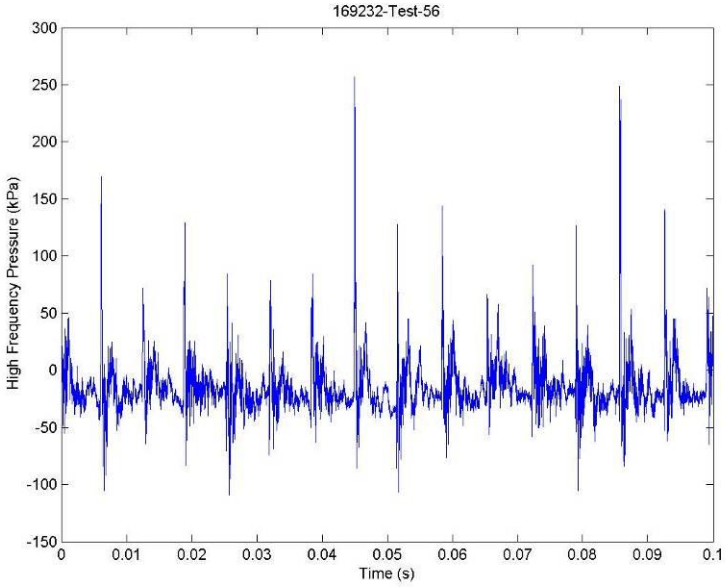


**Figure I.12: 169232-56 Raw High Frequency Signal**

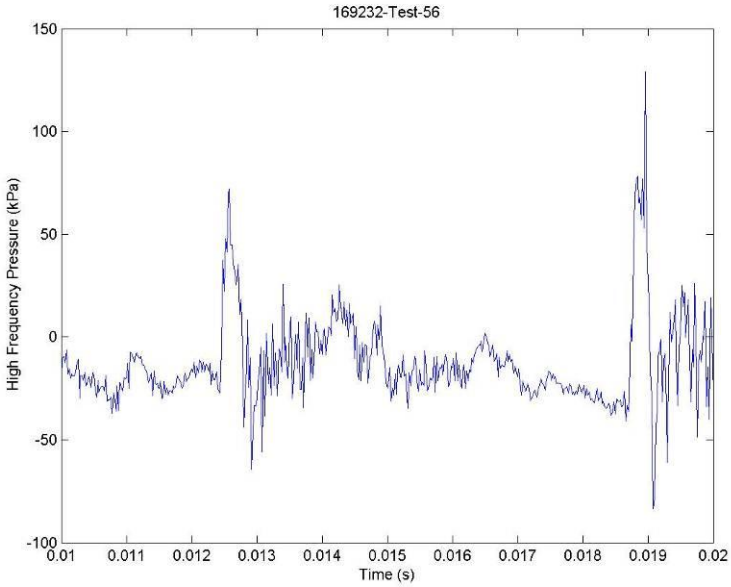


**Figure I.13: 169232-56 Magnified Raw High Frequency Signal**

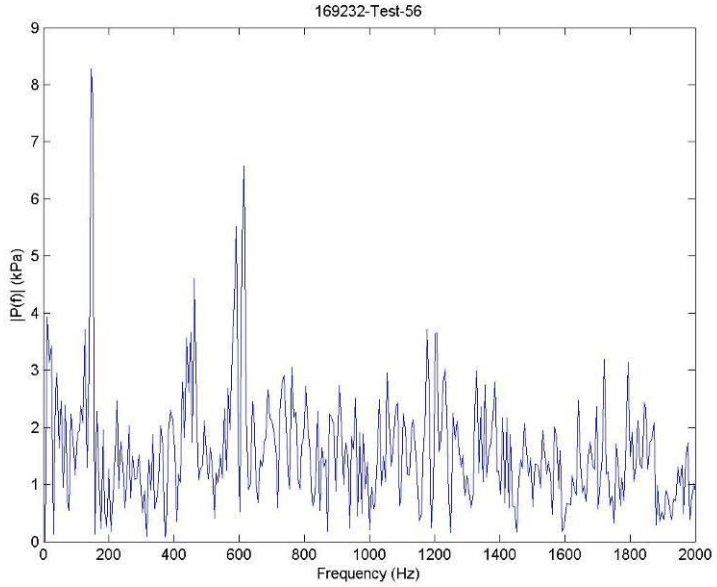


**Figure I.14: 169232-56 FFT**

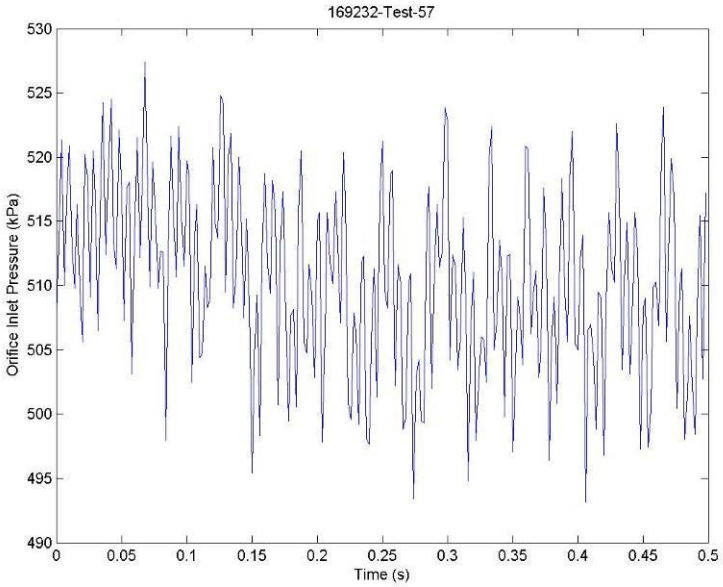


**Figure I.15: 169232-57 Orifice Inlet Pressure**

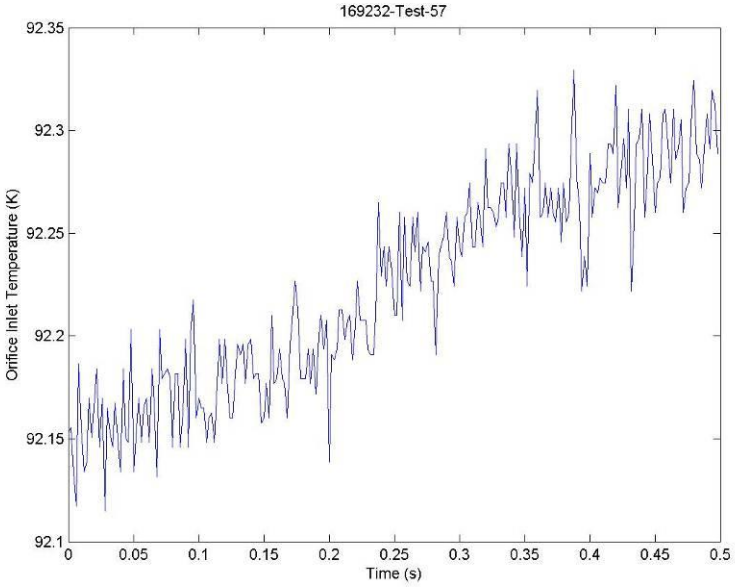


**Figure I.16: 169232-57 Orifice Inlet Temperature**

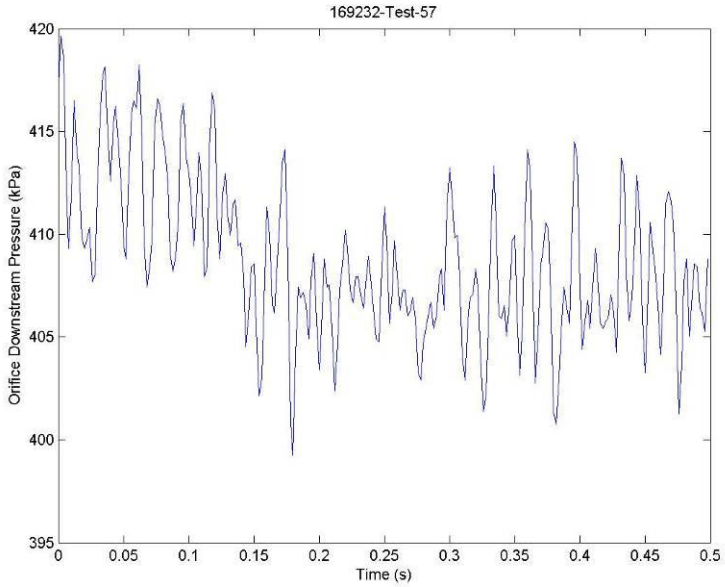


**Figure I.17: 169232-57 Orifice Outlet Pressure**

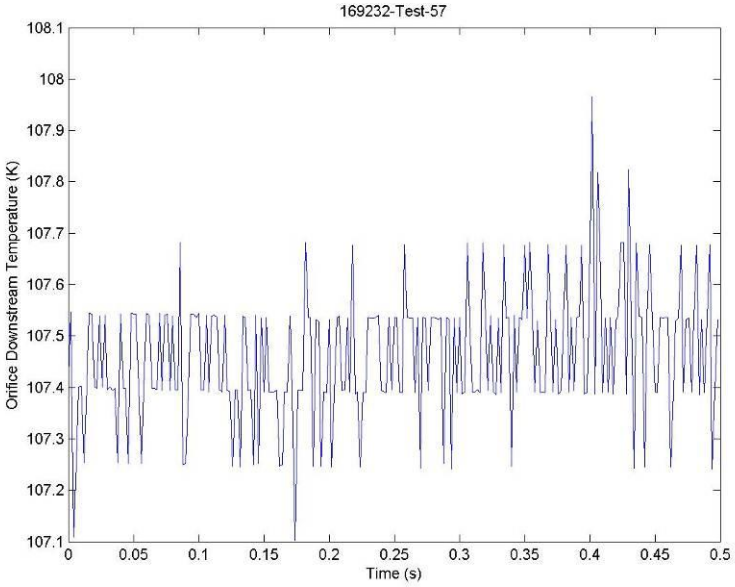


**Figure I.18: 169232-57 Orifice Outlet Temperature**

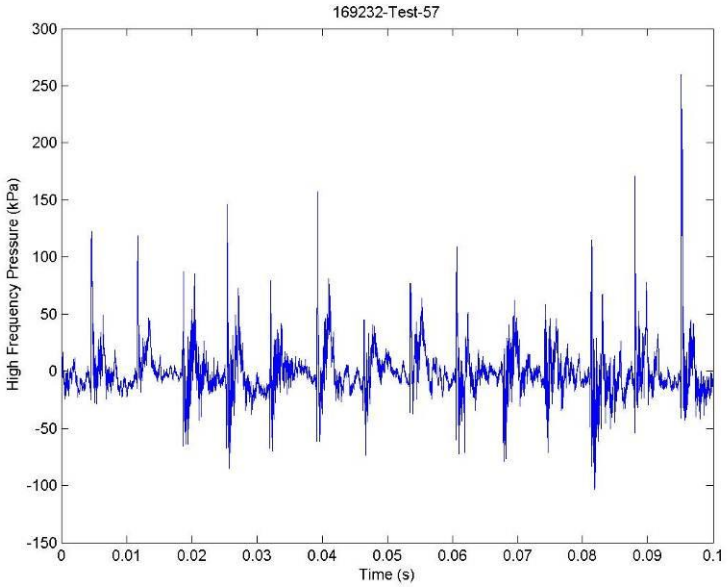


**Figure I.19: 169232-57 Raw High Frequency Signal**

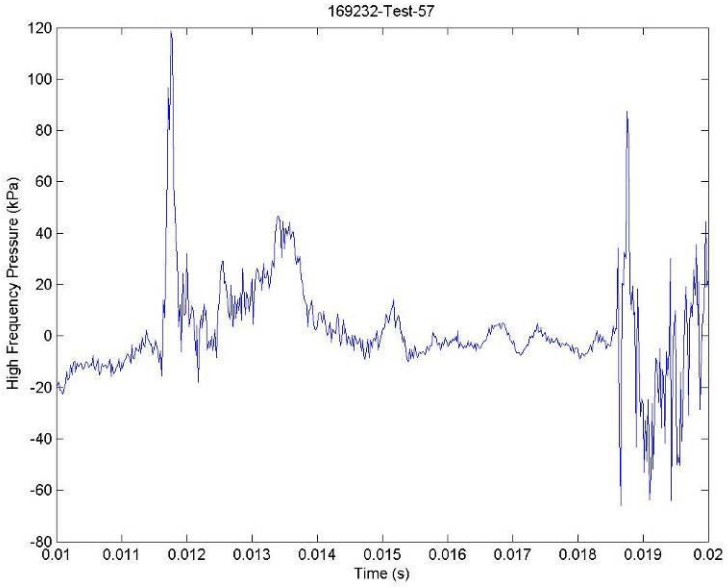


**Figure I.20: 169232-57 Magnified Raw High Frequency Signal**

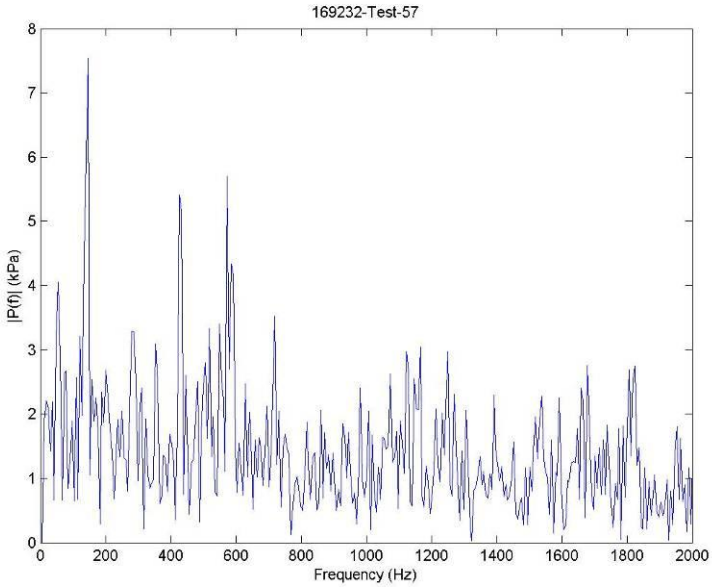


**Figure I.21: 169232-57 FFT**

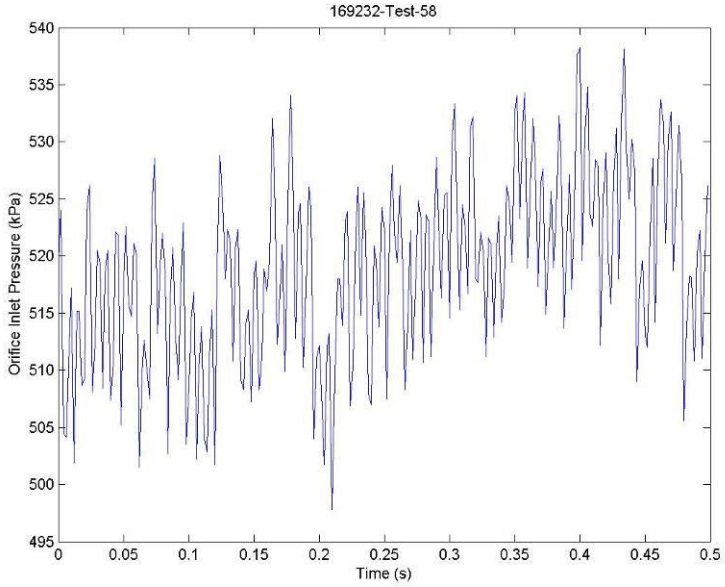


**Figure I.22: 169232-58 Orifice Inlet Pressure**

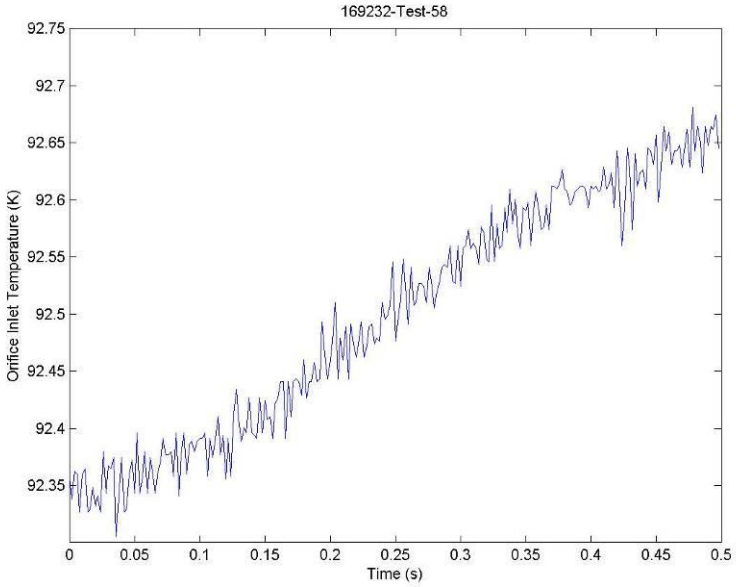


**Figure I.23: 169232-58 Orifice Inlet Temperature**

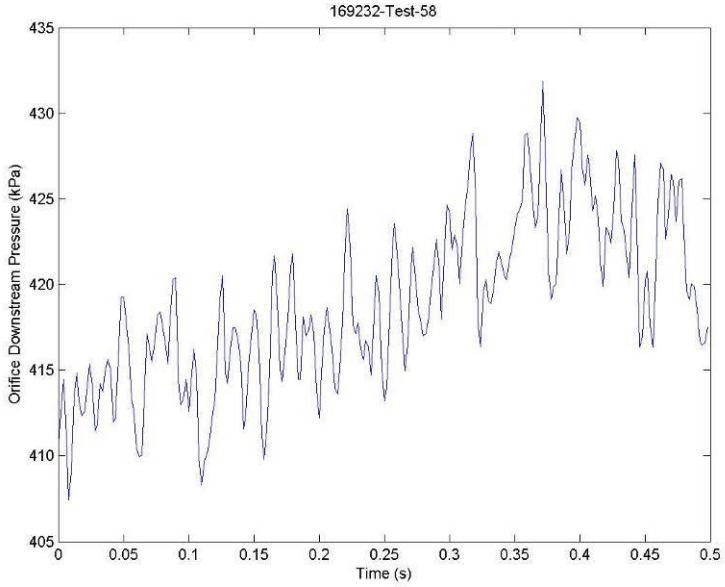


**Figure I.24: 169232-58 Orifice Outlet Pressure**

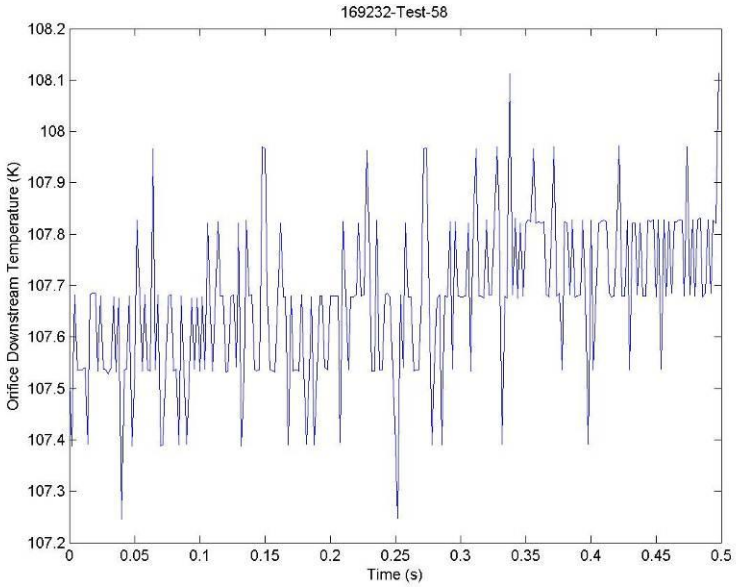


**Figure I.25: 169232-58 Orifice Outlet Temperature**

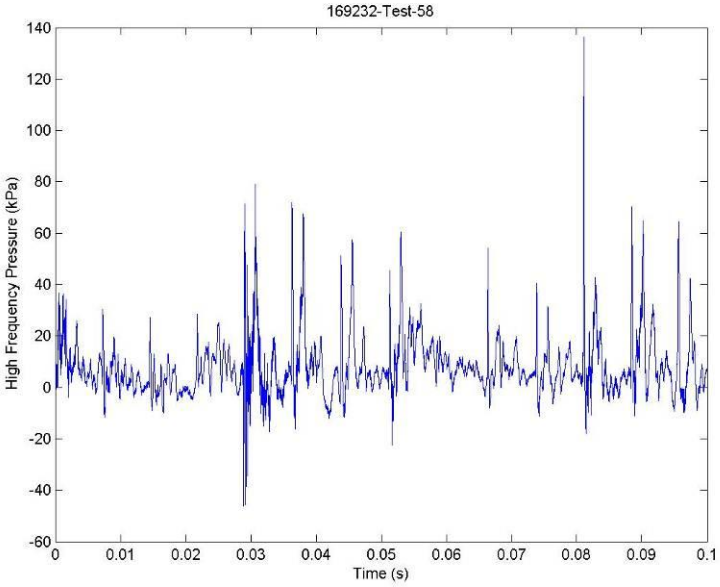


**Figure I.26: 169232-58 Raw High Frequency Signal**

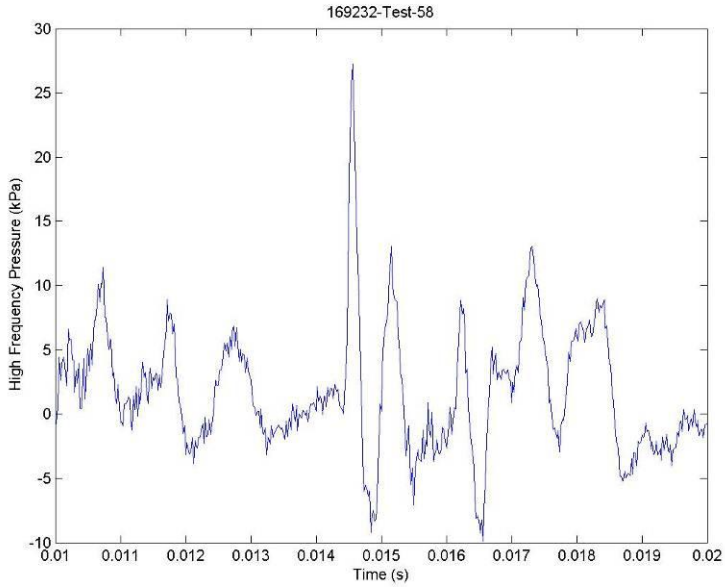


**Figure I.27: 169232-58 Magnified Raw High Frequency Signal**

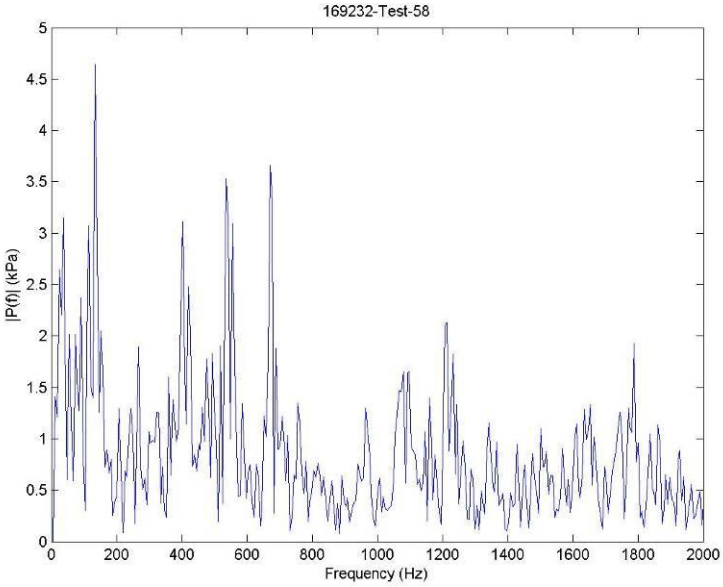


**Figure I.28: 169232-58 FFT**

## REFERENCES


[1] Broerman, E. L., Smolik, M. A., and Scrivner, C. M., "Helmholtz Absorbers: Experiments in Controlling Resonant Pulsation Without the Use of Orifice Plates," PVP2007-26246, 2007 ASME Pressure Vessels and Piping Division Conference, San Antonio, Texas, 22-26 July 2007.

[2] Adams, J. C., Ezekoye, L. I., Smith, S. M., and Swantner S. R., "An Application of Computational Fluid Dynamics (CFD) Code to the Design of a Multi-Stage Breakdown Orifice in Support of GSI-191 Evaluations," PVP2007-26208, 2007 ASME Pressure Vessels and Piping Division Conference, San Antonio, Texas, 22-26 July 2007.

[3] Sutton, G. P., and Biblarz, O., *Rocket Propulsion Elements*, 8th ed., John Wiley & Sons, Inc., Hoboken, New Jersey, 2010, Chap. 9, 11.

[4] Dotson, K., "Mitigating Pogo on Liquid-Fueled Rockets," *Crosslink*, Vol. 5, No. 1, 2003/2004, pp. 26-29.

[5] Lee, C., and Roh, T., "Flow Instability due to Cryogenic Cavitation in the Downstream of Orifice," *Journal of Mechanical Science and Technology*, Vol. 23, No. 3, 2009, pp. 643-649.

[6] Harrje, D., and Reardon, F. (ed.), "Liquid Propellant Rocket Combustion Instability," NASA SP-194, 1972.

[7] Skousen, P.., *Valve Handbook*, 3rd ed., McGraw Hill, New York, 2011, Chap. 9.

[8] Dabiri, S., Sirignano, W. A., and Joseph, D. D., "Cavitation in an Orifice Flow," *Physics of Fluids*, Vol. 19, No. 7, 2007.

[9] White, F. M., *Fluid Mechanics*, 6nd ed., McGraw Hill, New York, 2006.

[10] Stutz, B., and Reboud, J.-L., "Measurements within Unsteady Cavitation," *Experiments in Fluids*, Vol. 29, No. 6, 2000, pp. 545-552.

[11] Testud, P., Moussou, P., Hirschberg, A., and Auregan, Y., "Noise Generated by Cavitating Single-hole and Multi-hole Orifices in a Water Pipe," *Journal of Fluids and Structures*, Vol. 23, No. 2, 2007, pp. 163-189.

[12] Kelly, S., and Segal, C., "Simulation of Cryogenics Cavitation," AIAA-2011-0808, 49th AIAA Aerospace Sciences Meeting and Exhibit, Orlando, Florida, 4-7 January 2011.

[13] Koivula, T., "On Cavitation in Fluid Power," *Proc. Of 1st FPNI-PhD Symp.*, Hamburg, 2000, pp. 371-382.

[14] Ahuja, V. and Hosangadi, A., "Simulations of Cavitation in Orifice and Venturis," PVP2007-26639, 2007 ASME Pressure Vessels and Piping Division Conference, San Antonio, Texas, 22-26 July 2007.

[15] Testud, P., Moussou, P., Auregan, Y., and Hirschberg, A., "An Acoustic Criterion for the Whistling of Orifices in Pipes," PVP2007-26157, 2007 ASME Pressure Vessels and Piping Division Conference, San Antonio, Texas, 22-26 July 2007.

[16] White, F. M., *Viscous Fluid Flow*, 3rd ed., McGraw Hill, New York, 2006, Chap. 1.

[17] Testud, P., Auregan, Y., and Hirschberg, A., "Experimental Validation of a Whistling Criterion for Orifices in Air Pipe Flow," 8th French Congress of Acoustics, Tours, France, 24-27 April 2006.

[18] Mulkey, H. W., "Development of a Liquid Oxygen Facility for Rocket Engine Injector Performance Testing," M.S.E. Thesis, Mechanical and Aerospace Engineering Department, University of Alabama in Huntsville, Huntsville, AL, 2010.

[19] Coleman, H. W., and Steele, W. G., *Experimentation, Validation, and Unceratinty Analysis for Engineers*, 3rd ed., John Wiley & Sons, Inc., Hoboken, New Jersey, 2009, Chap. 3-4.

[20] Ahuja, V., "Novel Design of Orifice Type Control Element for Mitigating Instabilities," Combustion Research and Flow Technology, Inc., CRAFT Tech Report No. CRAFTR-02.2012.005, Pipersville, PA, Feb. 2012.